

CONFORMATIONAL BEHAVIOR AND STRUCTURAL PARAMETERS  
OF SOME CYCLIC AND CHAIN MOLECULES

A DISSERTATION IN  
Chemistry  
and  
Molecular Biology and Biochemistry (MBB)

Presented to the Faculty of the University  
of Missouri-Kansas City in partial fulfillment of  
the requirements for the degree

DOCTOR OF PHILOSOPHY

by

Dattatray Kisan Sawant

B. Tech (dyes), University of Mumbai, 2004

M.S., University of Kentucky, 2010

Kansas City, Missouri

2017

© 2017  
DATTATRAY KISAN SAWANT  
ALL RIGHTS RESERVED

CONFORMATIONAL BEHAVIOR AND STRUCTURAL PARAMETERS  
OF SOME CYCLIC AND CHAIN MOLECULES

Dattatray Kisan Sawant, Candidate for the Doctor of Philosophy Degree

University of Missouri-Kansas City, 2017

ABSTRACT

The physicochemical properties of a molecule derive from its molecular structure, and that structure often involves the orientation of one part of the molecule about a particular bond with respect to the rest of the molecule. Additionally, the way the molecule will react chemically and its available reaction pathways are often critically dependent upon the architecture of the reactant molecule. The energy differences of various conformations generally result from non-bonded interactions which, even though they are individually too weak to determine any single geometric feature by themselves, may nevertheless act together to uniquely determine the spatial structures of large and complicated molecules such as proteins and even DNA. Therefore, conformational analysis can lead to significant improvements in the understanding of more complex systems.

The mid-infrared ( $3100\text{-}400\text{ cm}^{-1}$ ) and Raman spectra ( $3200\text{-}20\text{ cm}^{-1}$ ) of a number of substituted ring and straight chain molecules were recorded in the gaseous, liquid and solid phases. Additionally, variable temperature studies of the infrared spectra of the sample dissolved in liquid xenon have been carried out. From these spectral data, the possible stable conformers have been identified and the enthalpy differences are given

among the various forms for each molecule. By utilizing microwave determined rotational constants for isotopomers, combined with structural parameters predicted from MP2(full)/6-311+G(d,p) calculations, adjusted  $r_0$  structural parameters have been obtained for the stable forms of some of the aforementioned molecules. Complete vibrational assignments are proposed for the stable conformers of each molecule. To support the vibrational assignments, normal coordinate calculations with scaled force constants from MP2(full)/6-31G(d) calculations were carried out to predict the fundamental vibrational frequencies, infrared intensities, Raman activities, depolarization values and infrared band contours.

The abovementioned spectroscopic and computational methods have been successfully applied for the determination of the enthalpy difference(s) between two or more conformers and  $r_0$  structural parameters of 2-methylbutane, isocyanocyclopentane, cyanocyclopentane, cyclopropylcyanosilane, and (chloromethyl)fluorosilane. In the study of 2-methylbutane, both the *trans* and *gauche* conformers have been identified and the enthalpy difference between conformers has been determined to be  $161 \pm 5 \text{ cm}^{-1}$  ( $1.93 \pm 0.06 \text{ kJ/mol}$ ) with the *trans* conformer the more stable form. The percentage of the *gauche* conformer is estimated to be  $18 \pm 1\%$  at ambient temperature.

For isocyanocyclopentane, the *axial* (*Ax*) and *envelope-equatorial* (*Eq*) conformers have been identified. The enthalpy difference between these two conformers has been determined to be  $102 \pm 10 \text{ cm}^{-1}$  ( $1.21 \pm 0.11 \text{ kJ mol}^{-1}$ ) with the *Ax* conformer the more stable form. The percentage of the *Eq* conformer is estimated to be  $38 \pm 1\%$  at ambient temperature.

Similar to isocyanocyclopentane, the *Eq* and *Ax* conformers have been identified for cyanocyclopentane. The enthalpy difference between these two rotamers has been determined to be  $55 \pm 12 \text{ cm}^{-1}$  ( $0.66 \pm 0.14 \text{ kJ/mol}$ ) with the *Eq* conformer the more stable form in this case. The percentage of the *Ax* conformer is estimated to be  $45 \pm 1\%$  at ambient temperature.

For cyclopropylcyanosilane, the enthalpy difference between the *cis* and *gauche* conformers has been determined to be  $123 \pm 13 \text{ cm}^{-1}$  ( $1.47 \pm 0.16 \text{ kJ mol}^{-1}$ ) with the *cis* conformer as the more stable form. Approximately  $48 \pm 2\%$  of the *cis* form is present at ambient temperature.

Both *trans* and *gauche* conformers are predicted and observed for (chloromethyl)fluorosilane. The enthalpy difference between the *trans* and *gauche* conformers in xenon solutions has been determined to be  $109 \pm 15 \text{ cm}^{-1}$  ( $1.47 \pm 0.16 \text{ kJ mol}^{-1}$ ) and in krypton solution the enthalpy difference has been determined to be  $97 \pm 16 \text{ cm}^{-1}$  ( $1.16 \pm 0.19 \text{ kJ mol}^{-1}$ ) with the *trans* conformer as the more stable form in both cases. Approximately  $46 \pm 2\%$  of the *trans* form is present at ambient temperature.

For all aforementioned molecules,  $r_0$  structural parameters have been determined for heavy-atom bond lengths, bond angles, and dihedral angles. In addition, comparisons with the conformations and  $r_0$  structural parameters of related molecules have been made and are discussed.

The faculty listed below, appointed by the Dean of the School of Graduate Studies have examined a thesis titled “Conformational Behavior and Structural Parameters of Some Cyclic and Chain Molecules” presented by Dattatray Kisan Sawant, candidate for the Doctor of Philosophy, and certify that in their opinion it is worthy of acceptance.

Supervisory Committee

Kathleen V. Kilway, Ph.D., Committee Chair  
Department of Chemistry

Charles J. Wurrey, Ph.D.  
Department of Chemistry

James R. Durig, Ph.D. (honorary)  
Department of Chemistry

Keith R. Buszek, Ph.D.  
Department of Chemistry

Jerry R. Dias, Ph.D.  
Department of Chemistry

Edward Gogol, Ph.D.  
School of Biological Sciences

Ashim K. Mitra, Ph.D.  
School of Pharmacy

## CONTENTS

ABSTRACT.....	iii
LIST OF TABLES.....	viii
LIST OF ILLUSTRATIONS.....	xii
ACKNOWLEDGMENTS.....	xvi
CHAPTER	
1. INTRODUCTION.....	1
2. EXPERIMENTAL AND THEORETICAL METHODS.....	9
3. $r_0$ STRUCTURAL PARAMETERS, CONFORMATIONAL EQUILIBRIUM, VIBRATIONAL SPECTRA AND <i>AB INITIO</i> CALCULATIONS STUDIES OF 2-METHYLBUTANE.....	12
4. $r_0$ STRUCTURAL PARAMETERS, CONFORMATIONAL, VIBRATIONAL STUDIES AND <i>AB INITIO</i> CALCULATIONS OF CYANOCYCLOPENTANE.....	52
5. $r_0$ STRUCTURAL PARAMETERS, CONFORMATIONAL, VIBRATIONAL STUDIES AND <i>AB INITIO</i> CALCULATIONS OF ISOCYANOCYCLOPENTANE.....	89
6. MICROWAVE, $r_0$ STRUCTURAL PARAMETERS, CONFORMATIONAL STABILITY AND VIBRATIONAL ASSIGNMENT STUDIES OF CYCLOPROPYLCYANOSILANE.....	130
7. MICROWAVE, $r_0$ STRUCTURAL PARAMETERS, CONFORMATIONAL STABILITY AND VIBRATIONAL ASSIGNMENT STUDIES OF (CHLOROMETHYL)FLUOROSILANE.....	180
8. CONCLUSION.....	224

## TABLES

Table	Page
1.	Observed and calculated frequencies ( $\text{cm}^{-1}$ ) and potential energy distributions (P.E.D.s) for the <i>trans</i> ( $C_1$ ) conformer of 2-methylbutane. ....21
2.	Observed and calculated frequencies ( $\text{cm}^{-1}$ ) and potential energy distributions (P.E.D.s) for the <i>gauche</i> ( $C_s$ ) conformer of 2-methylbutane .....23
3.	Calculated electronic energies (Hartrees, H) and energy differences ( $\text{cm}^{-1}$ ) for 2-methylbutane.....25
4.	Symmetry coordinates for 2-methylbutane.....26
5.	Temperature and intensity ratios of the conformational bands of 2-methylbutane from the infrared spectra of the liquid xenon solution phase. ....37
6.	Comparison of rotational constants (MHz) obtained from <i>ab initio</i> MP2(full)/6-311+G(d,p) predictions, experimental values from microwave spectra, and from the adjusted $r_0$ structural parameters for the <i>trans</i> and <i>gauche</i> conformers of 2-methylbutane. ....40
7.	Structural parameters ( $\text{\AA}$ and degrees), rotational constants (MHz) and dipole moment (Debye) for 2-methylbutane.....41
8.	Observed and calculated frequencies ( $\text{cm}^{-1}$ ) and potential energy distributions (P.E.D.s) for the <i>Eq</i> ( $C_s$ ) conformer of cyanocyclopentane.....60
9.	Observed and calculated frequencies ( $\text{cm}^{-1}$ ) and potential energy distributions (P.E.D.s) for the <i>Ax</i> ( $C_s$ ) conformer of cyanocyclopentane .....62
10.	Calculated electronic energies (Hartrees, H) for the <i>Ax</i> ( $C_s$ ) and energy differences ( $\text{cm}^{-1}$ ) for <i>Eq</i> ( $C_s$ ), <i>Twist</i> ( $C_1$ ) and <i>Planar</i> ( $C_s$ ) forms of cyanocyclopentane. ....64
11.	Symmetry coordinates for cyanocyclopentane .....65
12.	Temperature and intensity ratios of the <i>Eq</i> and <i>Ax</i> bands of cyanocyclopentane. ....76
13.	Structural parameters ( $\text{\AA}$ and degrees), rotational constants (MHz) and dipole moment (Debye) for cyanocyclopentane <i>Eq</i> and <i>Ax</i> ( $C_s$ ) Forms .....80

14.	Rotational transition frequencies (MHz) of the ground vibrational state of the <i>Ax</i> form of isocyanocyclopentane. ....	94
15.	Experimental rotational and centrifugal distortion constants of the <i>Ax</i> form of isocyanocyclopentane. ....	95
16.	Observed and calculated frequencies ( $\text{cm}^{-1}$ ) and potential energy distributions (P.E.D.s) for the <i>Ax</i> ( $C_s$ ) conformer of isocyanocyclopentane. ....	99
17.	Observed and calculated frequencies ( $\text{cm}^{-1}$ ) and potential energy distributions (P.E.D.s) for the <i>Eq</i> ( $C_s$ ) conformer of isocyanocyclopentane. ....	101
18.	Calculated electronic energies (Hartrees, H) for the <i>Ax</i> ( $C_s$ ) and energy differences ( $\text{cm}^{-1}$ ) for <i>Eq</i> ( $C_s$ ), <i>Twist</i> ( $C_1$ ), and <i>Planar</i> ( $C_s$ ) forms of isocyanocyclopentane. ....	103
19.	Structural parameters ( $\text{\AA}$ and degrees), rotational constants (MHz) and dipole moment (Debye) for isocyanocyclopentane <i>Ax</i> and <i>Eq</i> ( $C_s$ ) forms .....	104
20.	Symmetry coordinates for isocyanocyclopentane.....	105
21.	Comparison of frequencies ( $\text{cm}^{-1}$ ) of ring fundamentals for the <i>Ax</i> conformer of molecules of the form <i>c</i> - $C_5H_9$ -X.....	109
22.	Temperature and intensity ratios of the <i>Ax</i> and <i>Eq</i> bands of isocyanocyclopentane .....	117
23.	Comparison of select structural parameters ( $\text{\AA}$ and degrees) of molecules of the form $C\equiv N$ -R.....	124
24.	Comparison of select structural parameters ( $\text{\AA}$ and degrees) for the <i>Ax</i> conformer of molecules of the form <i>c</i> - $C_5H_9$ - $X\equiv Y$ .....	125
25.	Rotational transition frequencies (MHz) of the ground vibrational state of <i>cis</i> -cyclopropylcyanosilane, <i>c</i> - $C_3H_5SiH_2CN$ . ....	136
26.	Rotational transition frequencies (MHz) of the ground vibrational state of six isotopomers of <i>cis</i> -cyclopropylcyanosilane, <i>c</i> - $C_3H_5^{29}SiH_2CN$ . ....	138
27.	Rotational transition frequencies (MHz) of the ground vibrational state of <i>gauche c</i> - $C_3H_5SiH_2CN$ .....	142
28.	Rotational transition frequencies (MHz) of the ground vibrational state of seven isotopomers of <i>gauche</i> -cyclopropylcyanosilane, <i>c</i> - $C_3H_5SiH_2CN$ .....	143

29.	Calculated and observed frequencies ( $\text{cm}^{-1}$ ) for <i>cis</i> -cyclopropylcyanosilane, $c\text{-C}_3\text{H}_5\text{SiH}_2\text{CN}$ .....	148
30.	Calculated and observed frequencies ( $\text{cm}^{-1}$ ) for <i>gauche</i> -cyclopropylcyanosilane, $c\text{-C}_3\text{H}_5\text{SiH}_2\text{CN}$ .....	150
31.	Calculated electronic energies (Hartrees, H) and energy differences ( $\text{cm}^{-1}$ ) for cyclopropylcyanosilane, $c\text{-C}_3\text{H}_5\text{SiH}_2\text{CN}$ .....	152
32.	Symmetry coordinates for cyclopropylcyanosilane, $c\text{-C}_3\text{H}_5\text{SiH}_2\text{CN}$ . .....	152
33.	Experimental and predicted rotational and centrifugal distortion constants of cyclopropylcyanosilane isotopomers, $c\text{-C}_3\text{H}_5\text{SiH}_2\text{CN}$ .....	158
34.	Structural parameters ( $\text{\AA}$ and degrees), rotational constants (MHz) and dipole moments for <i>cis</i> and <i>gauche</i> rotamers of cyclopropylcyanosilane, $c\text{-C}_3\text{H}_5\text{SiH}_2\text{CN}$ .....	161
35.	Comparison of rotational constants (MHz) obtained from <i>ab initio</i> MP2(full)/6-311+G(d,p) predictions, experimental values from microwave spectra, and from the adjusted $r_0$ structural parameters for cyclopropylcyanosilane, $c\text{-C}_3\text{H}_5\text{SiH}_2\text{CN}$ .....	163
36.	Temperature and intensity ratios of the conformational bands of cyclopropylcyanosilane, $c\text{-C}_3\text{H}_5\text{SiH}_2\text{CN}$ from the infrared spectra of the liquid xenon solution phase .....	172
37.	Comparison of select structural parameters ( $\text{\AA}$ and degrees) of molecules of the form $c\text{-C}_3\text{H}_5\text{SiH}_2\text{X}$ .....	176
38.	Rotational transition frequencies (MHz) of the ground vibrational state for parent species and isotopologues of <i>trans</i> (chloromethyl)fluorosilane .....	185
39.	Calculated and observed frequencies ( $\text{cm}^{-1}$ ) for the <i>trans</i> form of (chloromethyl)fluorosilane .....	195
40.	Calculated and observed frequencies ( $\text{cm}^{-1}$ ) for the <i>gauche</i> form of (chloromethyl)fluorosilane.....	196
41.	Calculated electronic energies (Hartrees) and energy differences ( $\text{cm}^{-1}$ ) for (chloromethyl)fluorosilane .....	197
42.	Symmetry coordinates for the <i>trans</i> conformer of (chloromethyl)fluorosilane .....	198

43.	Experimental and predicted rotational constants including centrifugal distortion constants for the <i>trans</i> conformer of (chloromethyl)fluorosilane .....	201
44.	Nuclear quadrupole coupling constants for the parent species and isotopologues of <i>trans</i> (chloromethyl)fluorosilane.....	201
45.	Comparison of rotational constants (MHz) obtained from <i>ab initio</i> MP2(full)/6-311+G(d,p) predictions, experimental values from microwave spectra, and from the adjusted $r_0$ structural parameters for the <i>trans</i> form of (chloromethyl)fluorosilane (ClCH <sub>2</sub> SiH <sub>2</sub> F).....	203
46.	Structural parameters (Å and degrees), rotational constants (MHz) and dipole moment (Debye) for (chloromethyl)fluorosilane.....	204
47.	The three planar moments ( <i>Paa</i> , <i>Pbb</i> , <i>Pcc</i> ) for parent species and isotopologues of <i>trans</i> (chloromethyl)fluorosilane with the <i>ab initio</i> values for the parent species .....	206
48.	Temperature and intensity ratios of the conformational bands of (chloromethyl)fluorosilane from the infrared spectra of the liquid xenon solution phase.....	213
49.	Temperature and intensity ratios of the conformational bands of (chloromethyl)fluorosilane from the Raman spectra of the liquid krypton solution phase.....	214
50.	Natural population analysis for (halomethyl)halosilane derivatives .....	222

## ILLUSTRATIONS

Figure	Page
1. Structure of (A) maleic acid; (B) fumaric acid .....	5
2. Resonance structures of peptide bond.....	6
3. Conformers of 2-methylbutane (A) <i>trans</i> ; (B) <i>gauche</i> .....	15
4. Comparison of experimental and calculated infrared spectra of 2-methylbutane: (A) observed spectrum of the gas; (B) observed spectrum of the Xe solution at -70 °C; (C) simulated spectrum of a mixture of <i>trans</i> and <i>gauche</i> conformers ( $\Delta H = 161 \text{ cm}^{-1}$ ) at 25 °C; (D) simulated spectrum of the <i>gauche</i> conformer; (E) simulated spectrum of the <i>trans</i> conformer.....	17
5. Comparison of experimental and calculated infrared spectra of 2-methylbutane: (A) observed spectrum of the amorphous solid; (B) observed spectrum of the annealed solid; (C) simulated spectrum of a mixture of <i>trans</i> and <i>gauche</i> conformers ( $\Delta H = 161 \text{ cm}^{-1}$ ) at 25 °C; (D) simulated spectrum of the <i>gauche</i> conformer; (E) simulated spectrum of the <i>trans</i> conformer. ....	18
6. Temperature (-100 to -55 °C) dependent infrared spectrum of 2-methylbutane dissolved in liquid xenon solution. ....	19
7. Comparison of experimental and calculated Raman spectra of 2-methylbutane: (A) observed spectrum of the liquid; (B) simulated spectrum of a mixture of <i>trans</i> and <i>gauche</i> conformers ( $\Delta H = 161 \text{ cm}^{-1}$ ) at 25 °C; (C) simulated spectrum of the <i>gauche</i> conformer; (D) simulated spectrum of the <i>trans</i> conformer. ....	20
8. Potential energy function (MP2(full)) governing the internal rotation of 2-methylbutane from the <i>gauche</i> (57.4°) to the <i>trans</i> (-65.0 and 180°) forms .....	50
9. Conformers of cyanocyclopentane (A) <i>Eq</i> ; (B) <i>Ax</i> .....	54
10. Comparison of experimental and calculated infrared spectra of cyanocyclopentane: (A) observed spectrum of the gas; (B) observed spectrum of the Xe solution at -70 °C; (C) simulated spectrum of a mixture of <i>Eq</i> and <i>Ax</i> conformers ( $\Delta H = 55 \text{ cm}^{-1}$ ) at 25 °C; (D) simulated spectrum of the <i>Ax</i> conformer; (E) simulated spectrum of the <i>Eq</i> conformer.....	57
11. Comparison of experimental and calculated infrared spectra of cyanocyclopentane: (A) observed spectrum of the amorphous solid; (B)	

observed spectrum of the annealed solid; (C) simulated spectrum of the <i>Eq</i> conformer; (D) simulated spectrum of the <i>Ax</i> conformer.....	58
12. Comparison of experimental and calculated Raman spectra of cyanocyclopentane: (A) observed spectrum of the liquid; (B) simulated spectrum of a mixture of <i>Eq</i> and <i>Ax</i> conformers ( $\Delta H = 55 \text{ cm}^{-1}$ ) at 25 °C; (C) simulated spectrum of the <i>Ax</i> conformer; (D) simulated spectrum of the <i>Eq</i> conformer. ....	59
13. Infrared spectra of cyanocyclopentane (A) gas; (B) Xe solution at -70 °C.....	73
14. Temperature (-70 to -100 °C) dependent infrared spectrum of cyanocyclopentane dissolved in liquid xenon solution.....	75
15. Band contour predictions for the <i>Eq</i> and <i>Ax</i> conformers of cyanocyclopentane .....	83
16. Conformers of isocyanocyclopentane (A) <i>Eq</i> ; (B) <i>Ax</i> .....	91
17. Comparison of experimental and calculated infrared spectra of isocyanocyclopentane: (A) observed spectrum of the gas; (B) observed spectrum of the Xe solution at -70 °C; (C) observed spectrum of the solid; (D) simulated spectrum of a mixture of <i>Ax</i> and <i>Eq</i> conformers ( $\Delta H = 102 \text{ cm}^{-1}$ ) at 25 °C; (E) simulated spectrum of the <i>Eq</i> conformer; (F) simulated spectrum of the <i>Ax</i> conformer.....	97
18. Comparison of experimental and calculated Raman spectra of isocyanocyclopentane: (A) observed spectrum of the liquid; (B) simulated spectrum of a mixture of <i>Ax</i> and <i>Eq</i> conformers ( $\Delta H = 102 \text{ cm}^{-1}$ ) at 25 °C; (C) simulated spectrum of the <i>Eq</i> conformer; (D) simulated spectrum of the <i>Ax</i> conformer .....	98
19. Infrared spectra of isocyanocyclopentane (A) gas; (B) Xe solution at -70 °C.....	114
20. Temperature (-70 to -100 °C) dependent infrared spectrum of isocyanocyclopentane dissolved in liquid xenon solution.....	115
21. Band contour predictions for the <i>Ax</i> and <i>Eq</i> conformers of isocyanocyclopentane. ....	121
22. Synthesis of cyclopropylcyanosilane.....	133
23. Comparison of experimental and calculated infrared spectra of cyclopropylcyanosilane: (A) observed spectrum of the gas; (B) observed spectrum in the xenon solution at -70 °C; (C) simulated spectrum of a mixture of <i>gauche</i> and <i>cis</i> conformers at -100 °C with $\Delta H = 123 \text{ cm}^{-1}$ ; (D) simulated	

	spectrum of the <i>gauche</i> conformer; (E) simulated spectrum of the <i>cis</i> conformer .....	146
24.	Comparison of experimental and calculated Raman spectra of cyclopropylcyanosilane: (A) observed spectrum of the liquid; (B) simulated spectrum of a mixture of <i>gauche</i> and <i>cis</i> conformers at 25 °C with $\Delta H = 123 \text{ cm}^{-1}$ ; (C) simulated spectrum of <i>gauche</i> ; (D) simulated spectrum of <i>cis</i> .....	147
25.	<i>Gauche</i> and <i>cis</i> conformers of cyclopropylcyanosilane showing atom numbering and internal coordinates .....	154
26.	Mid-infrared spectra of cyclopropylcyanosilane: (A) gas in transmittance; (B) liquid xenon solution at -70 °C in absorbance .....	170
27.	Temperature (- 60 to -100 °C) dependent mid-infrared spectrum of cyclopropylcyanosilane dissolved in liquid xenon.....	171
28.	Potential energy function (MP2(full)) governing the internal rotation of the -SiH <sub>2</sub> CN moiety from the <i>gauche</i> to the <i>cis</i> form for cyclopropylcyanosilane .....	178
29.	Conformers of (chloromethyl)fluorosilane (A) <i>trans</i> ; (B) <i>gauche</i> .....	183
30.	Synthesis of (chloromethyl)fluorosilane.....	184
31.	Comparison of experimental and calculated infrared spectra of (chloromethyl)fluorosilane: (A) observed spectrum of the gas; (B) observed spectrum of the Xe solution at -70 °C; (C) simulated spectrum of a mixture of <i>trans</i> and <i>gauche</i> conformers ( $\Delta H = 109 \text{ cm}^{-1}$ ) at 25 °C; (D) simulated spectrum of the <i>gauche</i> conformer; (E) simulated spectrum of the <i>trans</i> conformer. (Peaks assigned for impurities were marked with star '★' symbol).....	191
32.	Comparison of experimental and calculated infrared spectra of (chloromethyl)fluorosilane: (A) observed spectrum of the amorphous solid; (B) observed spectrum of the annealed solid; (C) simulated spectrum of a mixture of <i>trans</i> and <i>gauche</i> conformers ( $\Delta H = 109 \text{ cm}^{-1}$ ) at 25 °C; (D) simulated spectrum of the <i>gauche</i> conformer; (E) simulated spectrum of the <i>trans</i> conformer (Peaks assigned for impurities were marked with star '★' symbol). .....	192
33.	Temperature (-133 to -153 °C) dependent Raman spectrum of (chloromethyl)fluorosilane dissolved in liquid krypton solution.....	193
34.	Comparison of experimental and calculated Raman spectra of (chloromethyl)fluorosilane: (A) observed spectrum of the sample dissolved in liquid krypton at 153°C; (B) simulated spectrum of a mixture of <i>trans</i> and <i>gauche</i> conformers ( $\Delta H = 97 \text{ cm}^{-1}$ ) at 25 °C; (C) simulated spectrum of the	

	<i>gauche</i> conformer; (D) simulated spectrum of the <i>trans</i> conformer (Peaks assigned for impurities were marked with star ‘★’ symbol). .....	194
35.	Internal coordinates for (chloromethyl)fluorosilane .....	197
36.	Infrared spectra of (chloromethyl)fluorosilane (A) gas; (B) Xe solution at -70 °C .....	211
37.	Temperature (-60 to -100 °C) dependent infrared spectrum of (chloromethyl)fluorosilane dissolved in liquid xenon solution .....	212
38.	Potential energy function (MP2(full)) governing the internal rotation of (chloromethyl)fluorosilane from the <i>gauche</i> to the <i>trans</i> form .....	218
39.	Potential energy function (MP2(full)) governing the internal rotation of (fluoromethyl)fluorosilane from the <i>trans</i> to the <i>gauche</i> form.....	219
40.	Potential energy function (MP2(full)) governing the internal rotation of (chloromethyl)chlorosilane from the <i>trans</i> to the <i>gauche</i> form.....	220
41.	Potential energy function (MP2(full)) governing the internal rotation of (chloromethyl)bromosilane from the <i>trans</i> to the <i>gauche</i> form .....	220
42.	Potential energy function (MP2(full)) governing the internal rotation of (bromomethyl)fluorosilane from the <i>trans</i> to the <i>gauche</i> form.....	221

## ACKNOWLEDGMENTS

This dissertation is dedicated to my parents, Kisan and Sunanda Sawant, who taught me that with perseverance, curiosity, honesty, and care for others everything is possible. In addition, this research work would not have been possible without the personal and professional collaboration and support of a vast number of people; people who have helped me over the years to become who I am.

I owe my deepest gratitude to my supervisor Professor James R. Durig, who gave me the incredible opportunity to work in his research laboratory. Without his continuous optimism concerning this work, enthusiasm, encouragement, and support this study would hardly have been completed. I also express my warmest gratitude to my other supervisors, Professor Charles J. Wurrey and Professor Kathleen V. Kilway, for their help and support particularly after Prof. Durig's retirement. Professor Wurrey always helped and guided me whenever I had any problem. Additionally, Professor Wurrey helped to expand my critical and logical thinking horizon. Professor Kilway readily took care of appropriate paperwork, and she also arranged for the Chemistry Department to support me as a GTA even after retirement of Professor Durig. I am deeply grateful to my committee members Professor Jerry R. Dias, Professor Keith R. Buszek, Professor Edward Gogol, and Professor Ashim Mitra for serving on my research supervisory committee.

Outside UMKC, Professor Gamil Guirgis from the College of Charleston synthesized compounds required for my projects. I would also like to thank Professor Guirgis for his support and help with other aspects of this research. In addition, I would

like to express my gratitude to Professor Brooks H. Pate and Dr. Nathan Seifert (University of Virginia), and Professor Michael Tubergen (Kent State University) for providing microwave spectra of samples. It is also my pleasure to thank Professor Wouter A. Herrebout (Universitair Centrum Antwerpen, Belgium) for providing Raman spectra of samples dissolved in liquefied krypton.

Working and learning from some of the finest Professors at UMKC has not only been a great honor but also a fascinating experience. I could spend several pages mentioning some of the supervisors, mentors, and friends at UMKC who have guided me through the different steps of my professional journey. People like Professor Mark Meir, Professor Fitzgerald Bramwell, Dr. Todor Gounev, Dr. Andrea Drew, Dr. Savitha Panikar, Dr. Bhushan Deodhar, Dr. Tanmoy Dutta, Dr. Sudhanshu Purohit, Dr. Alok Nerurkar, Dr. Nilesh Raut, Dr. Smita Joel, Dr. Manjiri Patwardhan, Mr. Kuldeep Shetye, Mr. John Whitchurch, Mrs. Maningat, Mrs. Florence Middleton, Miss Kathy Garrison, Miss. Asia Williams, and Mr. Michael Sykora are only some of those that have helped and guided me. Every one taught me something special, and I had great experiences working with them. I truly admire each of them for their dedication, leadership, and genuine desire to create a positive influence beyond themselves. Thanks to all of you for your support, teaching, and this incredible journey. You all know why.

UMKC is a place where I have great memories and friends, for which I will remember fondly for the rest of my life. I would like to express my deepest gratitude to the Department of Chemistry, School of Biological Sciences (SBS), and School of Graduate Studies (SGS) for their help and support.

Personally, I would like once again to thanks to my parents, Kisan and Sunanda Sawant, for their love, strength, and humble nature. There are no words and acts to thank them enough. Thanks to the late Leela Joshi - my high school teacher - for unconditional support, and for an inspirational and optimistic approach to life. Also thanks to the late Marlene Durig for her help and support. Thanks also to my sisters, Minaxi, Harsha, and Rina, for their patience, inspiration, and love. My acknowledgement will always be incomplete, and I would like to offer my special thanks with humble apologies to people who have helped me in this wonderful journey but who I may have forgotten to mention herein.

## CHAPTER 1

### INTRODUCTION

The infrared region of the electromagnetic spectrum is subdivided into the near-infrared (14000 – 4000  $\text{cm}^{-1}$ ), mid-infrared (4000 – 400  $\text{cm}^{-1}$ ), and far-infrared (400 – 40  $\text{cm}^{-1}$ ) sub-regions. Out of these three sub-regions, the mid-infrared region has been the most extensively studied and used by researchers. For many different applications, absorption bands observed in the mid-infrared spectra of molecules are the result of different vibrational modes of molecules; hence, mid-infrared spectroscopy is included as one method of vibrational spectroscopy. The number of fundamental vibrational modes a molecule will exhibit can be calculated by using the formula  $3N - 6$  for nonlinear molecules and  $3N - 5$  for linear molecules, where N is number of atoms in the molecule. Mid-infrared spectra have provided valuable information about functional groups present in molecules, and thus organic chemists commonly use mid-infrared spectra for qualitative identification of functional groups. Data obtained from the vibrational spectra of samples has been used in different fields such as materials science, biochemistry, pharmaceutical chemistry, and medical sciences. Recently, vibrational spectroscopy has been successfully utilized for the diagnosis of thyroid carcinoma.<sup>1</sup>

Overtone and combination bands of fundamental peaks are mainly observed in the near-infrared sub-region. Some low energy fundamental modes such as torsions, deformations of bonds between heavy atoms, and ring deformations of cyclic molecules are observed in the far-infrared sub-region. Furthermore, for solid samples, fundamental modes associated with lattice structures, termed as librations, are also observed in the same sub-region. Librations are useful for determining crystal structures and

polymorphism in solid samples. Another interesting application of vibrational spectroscopy is the determination of different conformers of the same molecule in the gaseous, liquid, and solid phases.

In addition to infrared spectroscopy, Raman spectroscopy is another method of vibrational spectroscopy, which is useful for the determination of the possible conformations of molecules in different states of matter. Peaks observed in Raman spectroscopy are due to inelastic scattering of photons by molecules and occur for approximately one out of a million photons sent in to the sample. For many years, the use of Raman spectroscopy was fairly limited due to the weak signals produced. However, the invention of the laser, development of different techniques such as Coherent Anti-stokes Raman Spectroscopy (CARS), Surface Enhanced Raman Spectroscopy (SERS), and other instrumental developments have helped to make the use of Raman spectroscopy in various fields more common. Similar to infrared spectroscopy, Raman spectroscopy is also useful for determining molecular and lattice vibrations, and the polymorphic structures of samples in the solid state. Raman spectroscopy has also been used for diagnoses of cancer in adipose tissues, where diagnostic information is mainly based on changes in the Raman peaks associated with the *cis/trans* isomers of fatty acids.<sup>2</sup>

Conformers of molecules have also been identified by utilizing microwave spectroscopy in which the molecule's rotational constants are determined by fitting the peaks observed in the experimental spectra. Values obtained for the A, B, and C rotational constants are useful for calculating detailed structural parameters of molecules. In microwave spectroscopy, peaks are observed due to the rotation of molecules about the three principal axes; hence, microwave spectroscopy is also known as one method of

rotational spectroscopy. In addition, inter- and intramolecular interactions of weakly bound complexes in the gaseous form have been determined by using microwave spectroscopy. Another application of microwave spectroscopy is for chemical analysis of gaseous mixtures. In comparison to gas chromatography/mass spectrometry (GC/MS), microwave spectroscopy has advantages of higher selectivity and faster response.<sup>3</sup> The sample requirement of the gaseous phase, however, limits the applications of microwave spectroscopy in other fields. However, in the last ten years, microwave spectra of amino acids and biological molecules have been recorded using heating and laser desorption technologies.<sup>3</sup>

Changes in peak intensities with respect to changes in temperatures, functional groups, and crystal structures in infrared and Raman spectra have been utilized for both quantitative and qualitative analysis. The degree of unsaturation of fatty acids has been calculated by using intensities of absorption peaks at 3015 and 967  $\text{cm}^{-1}$ , which were assigned to the *cis* =C-H group stretching and the *trans* -C=C-H deformations respectively.<sup>4</sup> The intensities of these two bands were observed to increase with respect to the increase of unsaturation degree of fatty acids. The quantity of the plasticizer, 2-ethylhexylphthalate, in poly(vinylchloride) (PVC) has been successfully determined by using vibrational spectroscopy.<sup>5</sup> The carbonyl (C=O) stretching frequency observed at 1729  $\text{cm}^{-1}$  for the ester group of 2-ethylhexylphthalate was used for this quantitative analysis of the plasticizer in PVC after baseline correction. Similarly, poly(ethylene glycol) (PEG) and ethoxylated polyethyleneimine (PEI) concentrations have been determined by using a similar vibrational spectroscopic method. Peak intensities of bands observed at 1109 and 843  $\text{cm}^{-1}$  increase as the concentration of PEG increases, whereas

the peak intensity of the band observed at  $1044\text{ cm}^{-1}$  decreases as the concentration of PEI decreases.<sup>5</sup> In both cases — analysis of 2-ethylhexylphthalate in PVC and PEG in PEI — the plots of peak intensities with respect to concentrations of compounds followed a linear regression model. For the quantitative analysis of styrene-butadiene and polystyrene resins, bands observed at  $967\text{ cm}^{-1}$  and  $699\text{ cm}^{-1}$  were utilized. These bands were assigned to *trans* unsaturation and to the aromatic ring vibration fundamental modes, respectively. However, the same method (plots of peak intensities with respect to concentrations of compounds) did not fit appropriately during quantitative analysis, whereas the use of the *ratio* of the intensities of absorbance bands showed a meaningful relationship.<sup>5</sup> Similarly, changes in the ratios of peak intensities with respect to temperature have been successfully utilized for the determination of enthalpy differences between two or more conformers of the same molecule.<sup>5</sup>

The conformational stabilities and detailed structural parameters of molecules are important, for example, in many areas of chemistry, including organic, inorganic, biochemistry, and pharmaceutical chemistry. Maleic acid and fumaric acid have the same molecular formula ( $\text{C}_4\text{H}_4\text{O}_4$ ) but different conformational structures. Maleic acid is a *cis* conformer where carboxylic acid groups are on the same side of the carbon-carbon double bond ( $\text{C}=\text{C}$ ). On the other hand, fumaric acid is a *trans* conformer where carboxylic acid groups are on opposite sides (Fig. 1). Maleic acid is highly soluble in water whereas fumaric acid is sparingly soluble in the same solvent. Melting points of maleic acid and fumaric acid are  $135^\circ\text{C}$  and  $298^\circ\text{C}$ , respectively.<sup>6</sup> The pKa value for maleic acid is 1.90 whereas the pKa value for fumaric acid is 3.03.<sup>7</sup> Additionally, fumaric acid is used as a drug for the treatment of psoriasis while maleic acid is ineffective as a

drug for the same disease.<sup>8</sup> Thus a simple change in the conformational structure highly affects the physical, chemical, and pharmaceutical properties of maleic and fumaric acid.

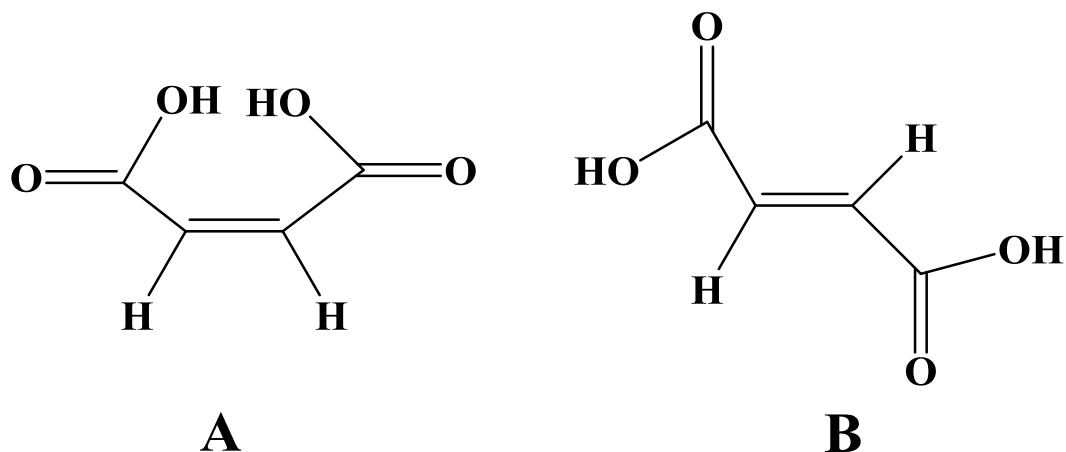


**Fig. 1** Structure of (A) maleic acid (B) fumaric acid.

Amino acid structures comprise a good example to explain the importance of detailed structural parameters. After the discovery of the formation of amino acid sequences in proteins, the next question that arose related to the nature of the peptide bond linking the amino acids together. As shown in Fig. 2, the peptide bond can involve a single bond (C-N) or double bond (C=N). If the peptide bond involves a single bond C-N, then there can be internal rotation along the amide bond and the formation of an amide plane will not be possible. On the other hand, if the amide bond is the double bond C=N, then there will not be any internal rotation along the carbon to nitrogen bond and the

formation of an amide plane is favored. During the study of other similar molecules, the bond length of C-N and C=N bonds were determined to be 1.49 and 1.27 Å, respectively.<sup>9</sup> However, in the study of proteins the C-N bond distance of the peptide bond was determined to be 1.33 Å.<sup>9</sup> This indicates that the peptide bond has substantial double bond character. Based on these experimental observations, the possibility of internal rotation along the C-N bond is eliminated, and, the formation of the amide plane in proteins was confirmed.

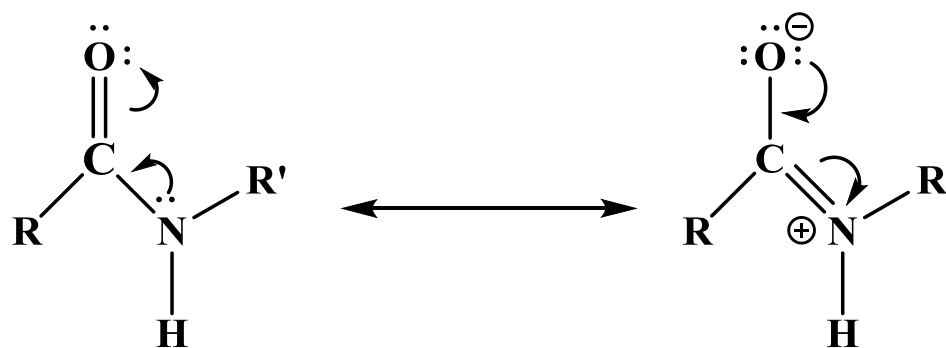


**Fig. 2** Resonance structures of peptide bond.

Utilization of a “lock and key” model is a very common method in the drug discovery process. Accurate structural and conformational data of both enzymes and drug molecules are important for successfully using a “lock and key” model. The Cyclooxygenase enzyme has two isoforms: Cyclooxygenase-I (COX-I) and

Cyclooxygenase-II (COX-II). As a result, molecular weights, amino acid sequences, and the catalytic site of COX-I and COX-II enzymes are almost the same.<sup>10</sup> Aspirin is a medicine commonly used to treat fever, pain, and inflammatory diseases. Aspirin mainly binds to the COX-I enzyme. However, due to there being too much similarity with the COX-I enzyme, aspirin also binds to the COX-II enzyme, which, however, results in the side effects of aspirin.<sup>11</sup> All these examples elaborate how structural parameters and conformation stability of molecules can have far reaching effects in different branches of chemistry.

In this dissertation, the different structures of the molecules under study were analyzed by infrared and Raman spectroscopy, which have been shown in the literature to be widely applicable for accurate determinations of conformer stability. These two techniques provide information about molecular vibrations, vibrational frequencies, band intensities, and Raman depolarization ratios; gas phase infrared band contours can also provide useful information. This data enables the investigator to assign unique fingerprints to the molecules and, in addition, valuable information is obtained about the symmetry and structure of the possible conformers under study. Infrared and Raman spectral investigations can be carried out on molecules in the vapor, liquid, solution, amorphous and crystalline solids states, and in inert matrices at high pressure or low temperatures. The different molecules, which are presented in this dissertation, are ones which contain one or more elements of symmetry and are capable of producing different conformations upon internal rotation.

The main focus of this dissertation is the determination of conformational stabilities of several straight chain and ring compounds with different functional groups

(cyanide, isocyanide, and silane). We have combined experimental and theoretical results to obtain more accurate structural parameters compared to those reported in previous investigations. Additionally, in some cases, this dissertation is unique, as one of the experimental methods used in this study is variable cryogenic temperature vibrational spectra in rare gas solutions. Also, this type of low temperature study has many advantages and benefits over conventional vibrational spectroscopy methods.

The research being reported in this dissertation thus includes a series of theoretical and experimental studies of rotational constants, vibrational assignments, molecular structure, and enthalpy determinations. The experimental methods include Raman spectra of the liquid phase of target compounds and infrared spectroscopy of the vapor and solid phases, rare gas solutions, microwave spectroscopy of the vapor, and far-infrared spectroscopy of the vapor and solid. Theoretical methods include the Møller-Plesset perturbation method<sup>12</sup> to the second order (MP2) with full electron correlation, and density functional theory by the B3LYP method using the Gaussian computational program.<sup>13</sup> The results of these studies are reported and discussed herein.

## CHAPTER 2

### EXPERIMENTAL AND THEORETICAL METHODS

The mid-infrared spectra of the gas and solid samples were obtained from 3200 to 400  $\text{cm}^{-1}$  using a Perkin-Elmer model 2000 Fourier transform spectrometer equipped with a Ge/CsI beamsplitter and a DTGS detector. Atmospheric water vapor was removed from the spectrometer housing by purging with dry nitrogen. The gas and solid spectra are obtained with a theoretical resolution of 0.5  $\text{cm}^{-1}$  for the gas and 2  $\text{cm}^{-1}$  for the solid with 128 interferograms added and truncated. Multiple annealings are required to obtain satisfactory spectra of the solid.

The mid-infrared spectra (3500 to 400  $\text{cm}^{-1}$ ) of samples dissolved in liquefied xenon at ten different temperatures (-60 C to -100 °C) were recorded on a Bruker model IFS-66 Fourier transform spectrometer equipped with a globar source, a Ge/KBr beamsplitter, and a DTGS detector. In all cases, 100 interferograms were collected at 1.0  $\text{cm}^{-1}$  resolution, averaged, and transformed with a boxcar truncation function. For these studies, a specially designed cryostat cell was used. It consisted of a copper cell with a path length of 4 cm with wedged silicon windows sealed to the cell with indium gaskets. The temperature was maintained with boiling liquid nitrogen and monitored by two Pt thermoresistors. After cooling to the designated temperature, a small amount of the sample was condensed into the cell, and the system was then pressurized with the noble gas, which condensed in the cell, allowing the compound to dissolve.

The Raman spectra of the liquid were recorded from 3200 to 40  $\text{cm}^{-1}$  on a Spex model 1403 spectrophotometer equipped with a Spectra-Physics model 2017 argon ion laser operating on the 514.5 nm line. The laser power used is 1.5 W with a spectral

band pass of  $3 \text{ cm}^{-1}$ . The spectra of the liquid are recorded with the sample sealed in a Pyrex glass capillary. The measurements of the Raman frequencies are expected to be accurate to  $\pm 2 \text{ cm}^{-1}$ .

*Ab initio* and density functional theory (DFT) calculations were performed with the Gaussian 03 program<sup>14</sup> by using Gaussian-type basis functions. The energy minima with respect to nuclear coordinates were obtained by the simultaneous relaxation of all geometric parameters by the gradient method of Pulay.<sup>15</sup> A variety of basis sets, as well as corresponding ones with diffuse functions were employed with the Møller-Plesset perturbation method<sup>12</sup> to the second order (MP2) with full electron correlation, as well as with density functional theory by the B3LYP method.

The predicted scaled frequencies are used together with a Lorentzian function to obtain the simulated spectra. Infrared intensities are obtained based on the dipole moment derivatives with respect to Cartesian coordinates. The derivatives are transformed with respect to normal coordinates by  $(\partial\mu_u/\partial Q_i) = \sum_j (\partial\mu_u/\partial X_j)L_{ij}$ , where  $Q_i$  is the  $i^{\text{th}}$  normal coordinate,  $X_j$  is the  $j^{\text{th}}$  Cartesian displacement coordinate, and  $L_{ij}$  is the transformation matrix between the Cartesian displacement coordinates and the normal coordinates. The infrared intensities are then calculated by  $(N\pi)/(3c^2) [(\partial\mu_x/\partial Q_i)^2 + (\partial\mu_y/\partial Q_i)^2 + (\partial\mu_z/\partial Q_i)^2]$ . A comparison may then be made of the experimental infrared spectra of the gas and simulated infrared spectra where the predictions for the isolated molecule are normally close to the values in the gas phase.

Additional support for the vibrational assignments is obtained from the simulated Raman spectra. The evaluation of Raman activity by using the analytical gradient methods has been developed<sup>16-19</sup> and the activity  $S_j$  can be expressed as:  $S_j = g_j(45\alpha_j^2 +$

$7\beta_j^2$ ), where  $g_j$  is the degeneracy of the vibrational mode  $j$ ,  $\alpha_j$  is the derivative of the isotropic polarizability, and  $\beta_j$  is the derivative of the anisotropic polarizability. To obtain the Raman scattering cross sections, the polarizabilities are incorporated into  $S_j$  by multiplying  $S_j$  with  $(1-\rho_j)/(1+\rho_j)$  where  $\rho_j$  is the depolarization ratio of the  $j^{\text{th}}$  normal mode. The Raman scattering cross sections and calculated wavenumbers obtained from the Gaussian 03 program are used together with a Lorentzian function to obtain the simulated Raman spectra. The average difference in band center due to going from gas to liquid is usually less than  $3 \text{ cm}^{-1}$ , where there is little interaction between molecules in the liquid phase, which is true for the majority of the molecules studied herein. A comparison may therefore be made of the experimental Raman spectra of the liquid and predicted Raman spectra.

## CHAPTER 3

### r<sub>0</sub> STRUCTURAL PARAMETERS, CONFORMATIONAL EQUILIBRIUM, VIBRATIONAL SPECTRA AND *AB INITIO* CALCULATIONS STUDIES OF 2-METHYLBUTANE

#### **Introduction**

Vibrational assignments of straight chain and branched chain hydrocarbons have been reported in the literature for an extensive time.<sup>20</sup> In related work, infrared and Raman spectra of six different hydrocarbons in the solid phase were studied to determine the rotational isomerism of these molecules.<sup>21</sup> In this latter study, the authors found that rotational isomers of hydrocarbons can be easily and conveniently determined using Raman spectra rather than infrared spectra.<sup>21</sup> The enthalpy difference between two different conformers of normal paraffins like n-butane, n-pentane, and n-hexane were determined by utilizing Raman spectra of samples in the liquid and solid states.<sup>22</sup> For n-butane, n-pentane, and n-hexane, enthalpy differences between the two major conformers were determined to be  $760 \pm 100$  cal/mol ( $266 \pm 35$  cm<sup>-1</sup>,  $3.18 \pm 0.42$  kJ/mol),  $520 \pm 70$  cal/mol ( $182 \pm 24$  cm<sup>-1</sup>;  $2.18 \pm 0.29$  kJ/mol) and  $470 \pm 60$  cal/mol ( $164 \pm 21$  cm<sup>-1</sup>;  $1.97 \pm 0.25$  kJ/mol), respectively.<sup>22</sup> As a continuation of this study, researchers further studied branched chain molecules such as 2-methylbutane. When infrared and Raman spectra of 2-methylbutane in solid and liquid forms were compared, no major changes in peaks were observed as the sample solidified from the liquid to the solid phase.<sup>20</sup> Using variable temperature liquid phase Raman spectra and Raman spectra of the solid phase, authors concluded that the enthalpy difference between the two conformers should be either less than 100 cal/mol ( $35$  cm<sup>-1</sup>;  $0.42$  kJ/mol) or 1600 cal/mol

(560  $\text{cm}^{-1}$ ; 6.69 kJ/mol) .<sup>23</sup> In another Raman spectroscopic study of 2-methylbutane in gaseous and solid forms, the enthalpy difference between the *trans* and *gauche* conformers was determined to be  $809 \pm 50$  cal/mol ( $283 \pm 17$   $\text{cm}^{-1}$ ;  $3.38 \pm 0.81$  kJ/mol) with the *trans* conformer as the most abundant form.<sup>24</sup> The latter study is believed to be more accurate than the previous study due to improved Raman instrumentation and the use of curve fitting software. However, the authors used only one band pair for determining the enthalpy difference between the two conformers, which calls into question the reliability of their results. Another method to determine the enthalpy difference between two or more conformers is to record variable temperature infrared spectra of the sample dissolved in liquid xenon. Durig and co-authors have used this method for several years, and it has consistently proved to be a more accurate and reliable method. Recently, rotational constants for the *trans* and *gauche* conformers of 2-methylbutane were calculated with the help of microwave spectra. However, the authors of that study did not determine structural parameters for the molecule.<sup>25</sup>

The aim of this present study is to determine a more definitive enthalpy difference between the *trans* and *gauche* conformers of 2-methylbutane, along with identifying the most stable conformer. Additionally, we have also determined the  $r_0$  structural parameters for both conformers of 2-methylbutane by utilizing previously reported rotational constants. For identifying the fundamental vibrational modes of 2-methylbutane, the Raman spectrum of the liquid and infrared spectra of the gas, amorphous and annealed solid were investigated. The enthalpy difference between the two possible conformers was investigated by utilizing the infrared spectra of the sample dissolved in xenon

solution at different temperatures between -100 to -55 °C. To support the vibrational study, *ab initio* calculations with basis sets up to aug-cc-pVTZ, as well as those with diffuse functions, *i.e.*, 6-311+G(2df,2pd), have been carried out. Density functional theory (DFT) calculations by the B3LYP method with the same basis sets have also been utilized. Optimized geometries, conformational stabilities, harmonic force fields, infrared intensities, Raman activities and depolarization ratios were also calculated. The results of these spectroscopic, structural, and theoretical studies of 2-methylbutane are reported herein.

### Methods

The sample of 2-methylbutane was purchased from Sigma-Aldrich with a stated purity of  $\geq 99.7\%$ . The sample was further purified using a low-temperature, low-pressure fractionation column. The purity of the sample was checked and verified by its infrared spectrum. Structures of the *trans* and *gauche* conformers of 2-methylbutane are shown in Fig. 3.

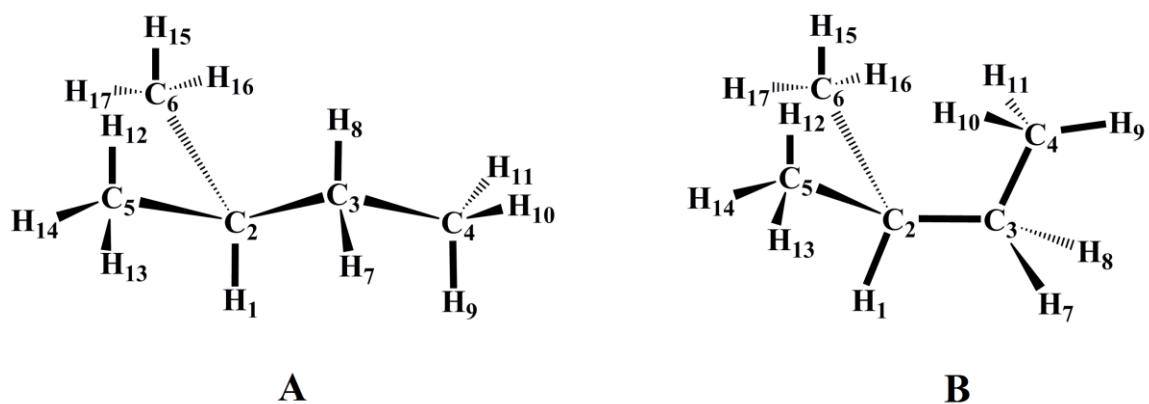


**Fig. 3** Conformers of 2-methylbutane (A) *trans* (B) *gauche*.

The mid-infrared spectra of 2-methylbutane in the gas, solid state (Fig. 4 and 5) were obtained from 3200 to 400  $\text{cm}^{-1}$  using a Perkin-Elmer 2000 Fourier transform spectrometer. Similarly, mid-infrared spectra of 2-methylbutane dissolved in liquefied xenon (Fig. 6) at ten different temperatures (-100 to  $-55^\circ\text{C}$ ) were recorded on a Bruker model IFS-66 Fourier transform spectrometer. The Raman spectrum of 2-methylbutane in the liquid state (Fig. 7) was recorded on a Spex model 1403 spectrophotometer. All of the observed bands in the Raman spectrum of the liquid, along with their proposed assignments and depolarization values, are listed in Tables 1 and 2. The predicted conformational energy differences calculated from *ab initio* calculations by using the Møller-Plesset perturbation method to the second order (MP2) with full electron correlation, as well as with density functional theory by the B3LYP method with different basis sets are listed in Table 3. The experimental methods of recording the infrared and Raman spectra are provided in detail in Chapter 2.

In order to obtain descriptions of the molecular motions involved in the

fundamental modes of 2-methylbutane, a normal coordinate analysis was carried out. The force field in Cartesian coordinates was obtained with the Gaussian 03 program at the MP2(full) level with the 6-31G(d) basis set (see chapter 2). The internal coordinates used to calculate the G and B matrices are given for the *trans* and *gauche* conformers in Table 4. By using the B matrix,<sup>26</sup> the force field in Cartesian coordinates was converted to force constants in internal coordinates. Subsequently, a scaling factor of 0.88 was used for the CH stretches and deformations, and a scaling factor of 0.90 was used for all other modes except for the heavy atom bends to obtain the fixed scaled force constants and resultant wavenumbers. A set of symmetry coordinates was used (Table 4) to determine the corresponding potential energy distributions (P.E.D.s). A comparison between the observed and calculated wavenumbers, along with the calculated infrared intensities, Raman activities, depolarization ratios and potential energy distributions for the *trans* and *gauche* conformers of 2-methylbutane, are given in Tables 1 and 2, respectively.

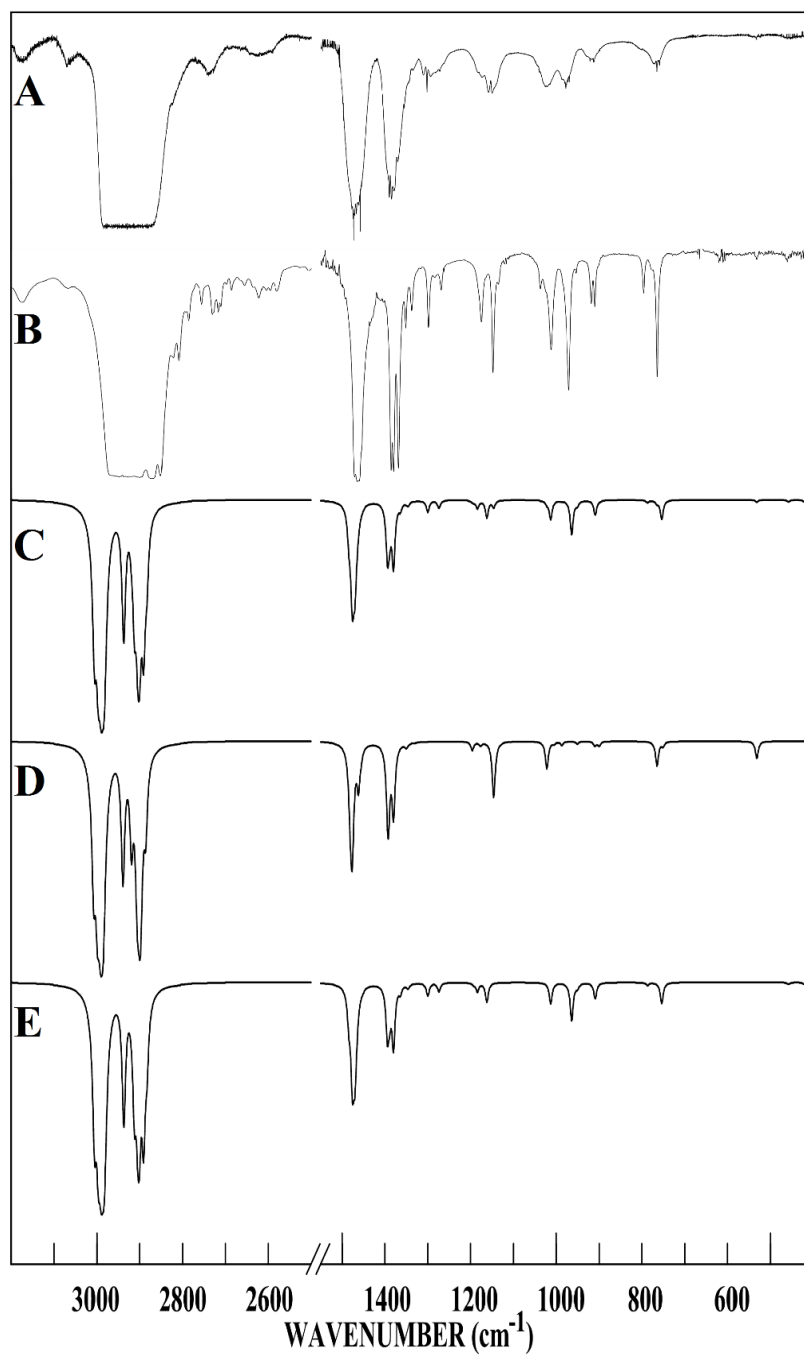


**Fig. 4** Comparison of experimental and calculated infrared spectra of 2-methylbutane: (A) observed spectrum of the gas; (B) observed spectrum of the Xe solution at -70 °C; (C) simulated spectrum of a mixture of *trans* and *gauche* conformers ( $\Delta H = 161 \text{ cm}^{-1}$ ) at 25 °C; (D) simulated spectrum of the *gauche* conformer; (E) simulated spectrum of the *trans* conformer.

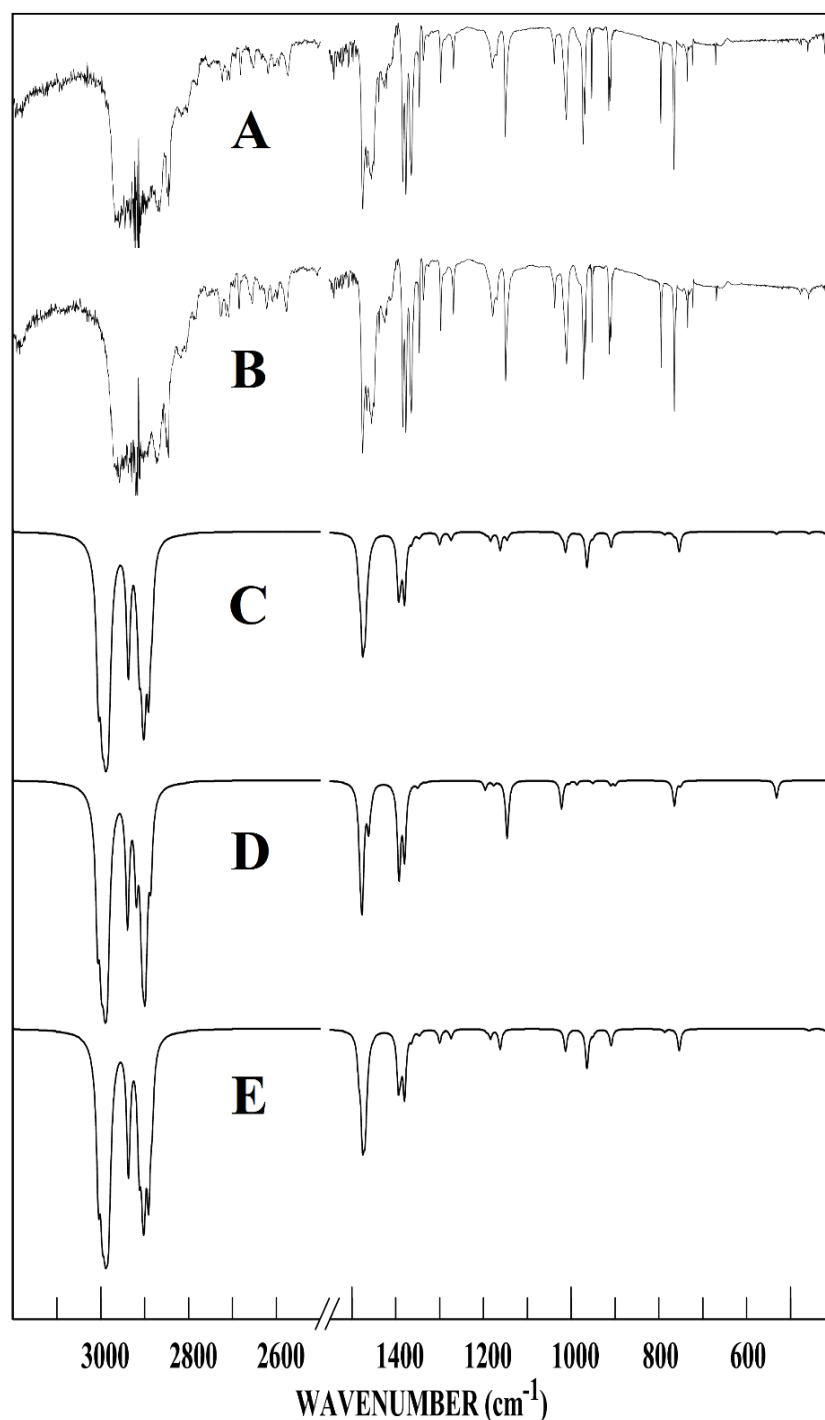


**Fig. 5** Comparison of experimental and calculated infrared spectra of 2-methylbutane: (A) observed spectrum of the amorphous solid; (B) observed spectrum of the annealed solid; (C) simulated spectrum of a mixture of *trans* and *gauche* conformers ( $\Delta H = 161 \text{ cm}^{-1}$ ) at 25 °C; (D) simulated spectrum of the *gauche* conformer; (E) simulated spectrum of the *trans* conformer.

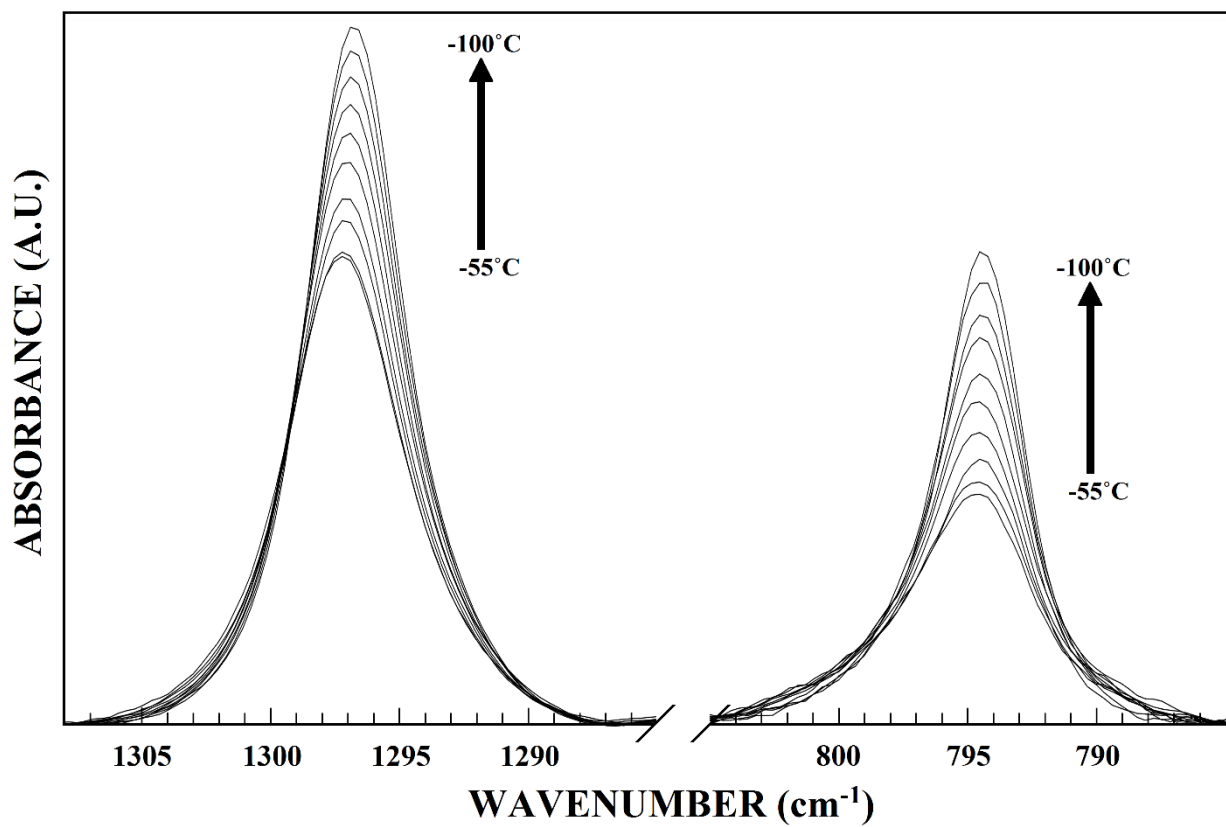


**Fig. 6** Temperature (-100 to -55 °C) dependent infrared spectrum of 2-methylbutane dissolved in liquid xenon solution.

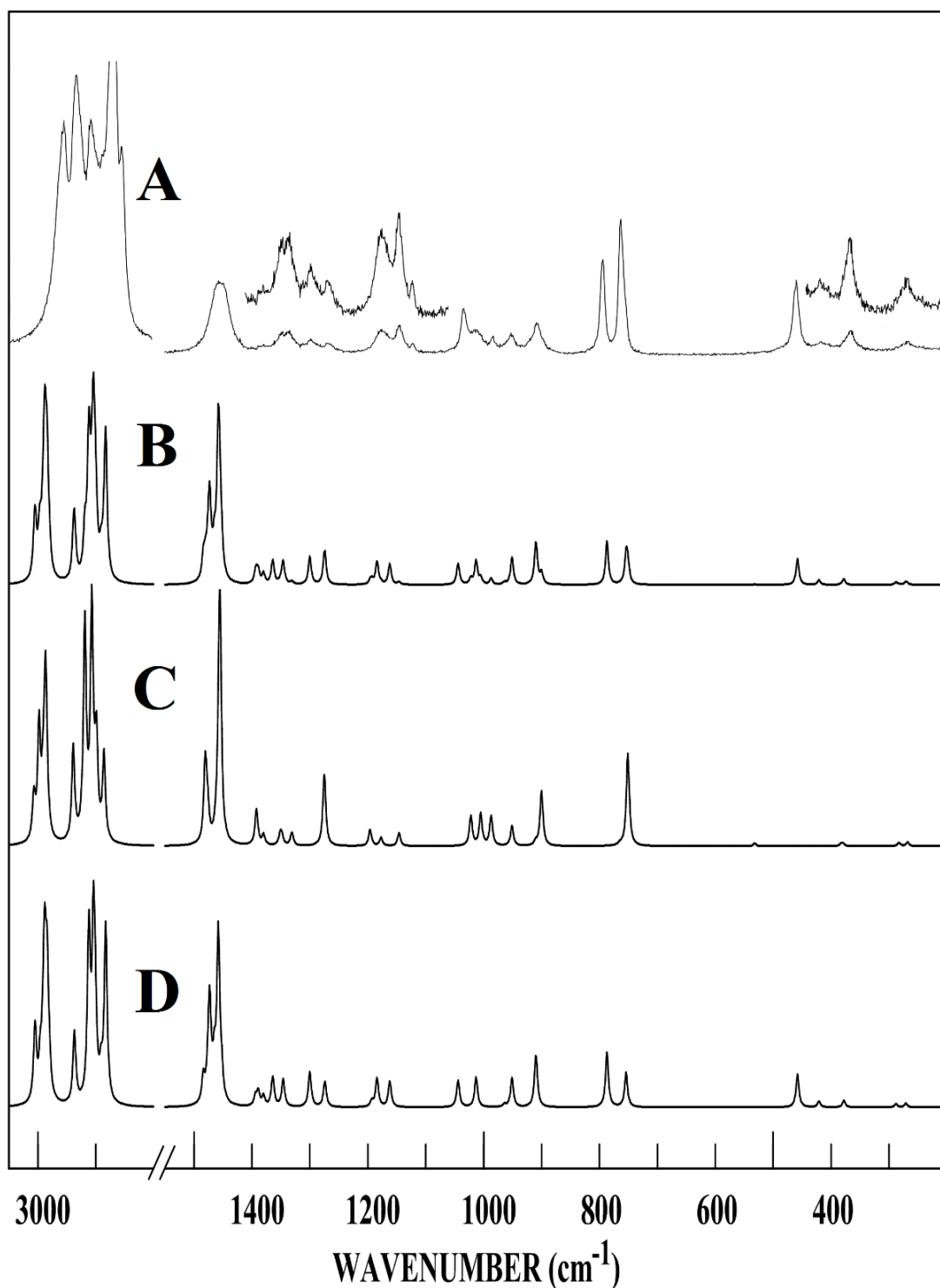


**Fig. 7** Comparison of experimental and calculated Raman spectra of 2-methylbutane: (A) observed spectrum of the liquid; (B) simulated spectrum of a mixture of *trans* and *gauche* conformers ( $\Delta H = 161 \text{ cm}^{-1}$ ) at 25 °C; (C) simulated spectrum of the *gauche* conformer; (D) simulated spectrum of the *trans* conformer.

**Table 1.** Observed and calculated<sup>a</sup> frequencies (cm<sup>-1</sup>) and potential energy distributions (P.E.D.s) for the *trans* (C<sub>1</sub>) conformer of 2-methylbutane.

Vib. No.	Approx. description	<i>ab initio</i>	Fixed scaled <sup>b</sup>	IR int.	Raman act.	dp ratio	Infrared				Raman	P.E.D. <sup>c</sup>	Band Contour		
							gas	Xe soln.	amorphous solid	annealed solid	liquid		A	B	C
v <sub>1</sub>	CH <sub>3</sub> antisymmetric stretch	3204	3005	27.2	55.6	0.74	2974	2970	2971	2971	2966	55S <sub>11</sub> ,15S <sub>3</sub> ,12S <sub>4</sub> ,11S <sub>2</sub>	6	88	6
v <sub>2</sub>	C <sub>(5,6)</sub> H <sub>3</sub> antisymmetric stretch	3194	2996	38.1	25.9	0.67	2974	2970	2971	2971	2966	38S <sub>2</sub> ,22S <sub>1</sub> ,22S <sub>4</sub>	71	9	20
v <sub>3</sub>	CH <sub>3</sub> antisymmetric stretch	3188	2990	36.4	50.0	0.69	2974	2970	2971	2971	2966	77S <sub>3</sub> ,21S <sub>1</sub>	20	6	74
v <sub>4</sub>	C <sub>(5,6)</sub> H <sub>3</sub> antisymmetric stretch	3185	2988	27.1	78.6	0.74	2974	2970	2971	2971	2966	48S <sub>4</sub> ,48S <sub>2</sub>	27	68	5
v <sub>5</sub>	C <sub>(5,6)</sub> H <sub>3</sub> antisymmetric stretch	3181	2984	46.6	88.1	0.64	2974	2970	2971	2971	2956	85S <sub>5</sub>	7	1	92
v <sub>6</sub>	C <sub>(5,6)</sub> H <sub>3</sub> antisymmetric stretch	3177	2980	2.9	11.5	0.71	2974	2970	2971	2971	2956	87S <sub>6</sub> ,10S <sub>4</sub>	7	85	8
v <sub>7</sub>	CH <sub>2</sub> antisymmetric stretch	3131	2937	22.7	50.9	0.64	2924	2936	2935	2937	2934	95S <sub>7</sub>	2	43	55
v <sub>8</sub>	CH <sub>3</sub> symmetric stretch	3105	2912	18.8	119.7	0.02	2907	2904	2898	2902	2909	97S <sub>8</sub>	77	17	6
v <sub>9</sub>	C <sub>(5,6)</sub> H <sub>3</sub> symmetric stretch	3096	2904	20.3	121.1	0.00	2907	2904	2898	2902	2900	79S <sub>9</sub> ,15S <sub>10</sub>	42	17	41
v <sub>10</sub>	CH <sub>3</sub> symmetric stretch	3092	2901	26.4	40.2	0.01	2907	2904	2898	2902	2900	82S <sub>10</sub> ,15S <sub>9</sub>	38	59	3
v <sub>11</sub>	CH <sub>2</sub> symmetric stretch	3082	2891	29.5	17.7	0.34	2886	2876	2871	2872	2888	82S <sub>11</sub> ,13S <sub>12</sub>	-	45	55
v <sub>12</sub>	CH stretch	3073	2883	7.7	122.5	0.28	2886	2876	2871	2872	2868	83S <sub>12</sub> ,14S <sub>11</sub>	3	16	81
v <sub>13</sub>	C <sub>(5,6)</sub> H <sub>3</sub> antisymmetric deformation	1580	1484	3.6	6.7	0.74	1476	1476	1474	1474	1478	31S <sub>13</sub> ,30S <sub>14</sub> ,15S <sub>15</sub> ,12S <sub>12</sub>	1	54	45
v <sub>14</sub>	CH <sub>3</sub> antisymmetric deformation	1572	1476	12.8	5.2	0.75	1470	1471	1472	1472	1478	32S <sub>14</sub> ,25S <sub>13</sub> ,14S <sub>19</sub> ,11S <sub>16</sub>	28	10	62
v <sub>15</sub>	C <sub>(5,6)</sub> H <sub>3</sub> antisymmetric deformation	1568	1473	2.6	24.5	0.75	1466	1464	1465	1465	1470	27S <sub>15</sub> ,16S <sub>13</sub> ,14S <sub>18</sub> ,13S <sub>16</sub>	14	7	79
v <sub>16</sub>	CH <sub>3</sub> antisymmetric deformation	1565	1470	10.9	1.7	0.70	1466	1464	1465	1465	1470	39S <sub>16</sub> ,18S <sub>15</sub> ,16S <sub>14</sub> ,10S <sub>17</sub>	-	35	65
v <sub>17</sub>	C <sub>(5,6)</sub> H <sub>3</sub> antisymmetric deformation	1560	1465	1.5	9.2	0.75	1459	1459	1460	1460	1463	32S <sub>17</sub> ,25S <sub>19</sub> ,21S <sub>16</sub> ,10S <sub>18</sub>	58	21	21
v <sub>18</sub>	C <sub>(5,6)</sub> H <sub>3</sub> antisymmetric deformation	1553	1458	0.2	43.3	0.75	1452	1452	1454	1453	1453	34S <sub>18</sub> ,22S <sub>17</sub> ,11S <sub>15</sub> ,10S <sub>14</sub> ,10S <sub>19</sub>	-	34	65
v <sub>19</sub>	CH <sub>2</sub> deformation	1545	1452	0.2	5.7	0.74	1448	1448	1449	1448	1453	38S <sub>19</sub> ,19S <sub>18</sub> ,18S <sub>15</sub>	1	88	11
v <sub>20</sub>	C <sub>(5,6)</sub> H <sub>3</sub> symmetric deformation	1477	1394	6.5	2.4	0.73	1389	1384	1387	1387	-	91S <sub>20</sub>	51	21	28
v <sub>21</sub>	CH <sub>3</sub> deformation	1472	1389	2.9	3.4	0.74	1389	1384	1387	1387	-	87S <sub>21</sub>	79	6	15
v <sub>22</sub>	C <sub>(5,6)</sub> H <sub>3</sub> symmetric deformation	1461	1380	8.3	2.4	0.75	1381	1378	1382	1382	1378	73S <sub>22</sub>	17	83	0
v <sub>23</sub>	CH in-plane bend	1437	1364	0.9	6.8	0.75	1363	1367	1363	1363	-	24S <sub>23</sub> ,32S <sub>25</sub>	42	57	1
v <sub>24</sub>	C <sub>5</sub> C <sub>2</sub> C <sub>6</sub> wag	1418	1346	0.5	6.2	0.74	1349	1349	1345	1345	1347	27S <sub>24</sub> ,18S <sub>22</sub> ,12S <sub>26</sub>	1	86	13
v <sub>25</sub>	CH <sub>2</sub> rock	1370	1300	1.5	7.6	0.75	1300	1297	1296	1296	1297	29S <sub>25</sub> ,14S <sub>23</sub> ,13S <sub>24</sub> ,13S <sub>41</sub>	99	1	-

**Table 1.**--Continued.

Vib. No.	Approx. description	<i>ab initio</i>	Fixed scaled <sup>b</sup>	IR int.	Raman act.	dp ratio	Infrared				Raman liquid	P.E.D. <sup>c</sup>	Band Contour		
							gas	Xe soln.	amorphous solid	annealed solid			A	B	C
v <sub>26</sub>	CH <sub>2</sub> twist	1342	1274	1.0	5.4	0.73	1270	1267	1267	1267	1267	54S <sub>26</sub> ,11S <sub>32</sub>	83	6	11
v <sub>27</sub>	C <sub>(5,6)</sub> H <sub>3</sub> rock	1252	1193	0.2	1.1	0.47	1193	-	1192	1190	1197	24S <sub>27</sub> ,21S <sub>37</sub> ,19S <sub>32</sub> ,10S <sub>23</sub>	96	1	3
v <sub>28</sub>	C <sub>(5,6)</sub> H <sub>3</sub> wag	1242	1184	1.0	5.5	0.75	1181	1175	1178	1177	~1184	28S <sub>28</sub> ,11S <sub>27</sub> ,11S <sub>36</sub> ,11S <sub>40</sub>	93	7	-
v <sub>29</sub>	C <sub>5</sub> C <sub>2</sub> C <sub>6</sub> antisymmetric stretch	1215	1162	2.3	4.9	0.69	1157	1153	1157	1157	1174	23S <sub>29</sub> ,17S <sub>41</sub> ,13S <sub>31</sub>	92	-	7
v <sub>30</sub>	C <sub>3</sub> C <sub>4</sub> stretch	1099	1044	0.0	4.4	0.41	-	-	-	-	1034	59S <sub>30</sub> ,12S <sub>29</sub>	29	68	4
v <sub>31</sub>	CH <sub>3</sub> wag	1067	1013	2.5	4.7	0.75	1012	1012	1009	1009	1012	28S <sub>31</sub> ,19S <sub>29</sub> ,10S <sub>36</sub>	54	45	1
v <sub>32</sub>	CH <sub>3</sub> rock	1016	964	4.7	0.4	0.64	968	970	966	966	983	28S <sub>32</sub> ,18S <sub>27</sub> ,14S <sub>23</sub> ,12S <sub>26</sub>	55	10	35
v <sub>33</sub>	C <sub>(5,6)</sub> H <sub>3</sub> wag	1003	951	0.5	4.3	0.70	954	953	951	951	951	57S <sub>33</sub> ,21S <sub>29</sub>	56	27	17
v <sub>34</sub>	C <sub>5</sub> C <sub>2</sub> C <sub>6</sub> symmetric stretch	959	910	0.4	4.6	0.74	910	909	910	910	908	22S <sub>34</sub> ,29S <sub>35</sub> ,10S <sub>28</sub>	24	14	62
v <sub>35</sub>	C <sub>(5,6)</sub> H <sub>3</sub> rock	959	909	1.5	2.8	0.73	910	909	908	908	908	38S <sub>35</sub> ,18S <sub>34</sub> ,10S <sub>28</sub>	42	53	5
v <sub>36</sub>	C <sub>2</sub> C <sub>3</sub> stretch	829	787	0.3	6.3	0.28	-	-	-	-	793	18S <sub>36</sub> ,21S <sub>37</sub> ,21S <sub>32</sub> ,14S <sub>34</sub> ,12S <sub>27</sub>	3	81	16
v <sub>37</sub>	CH <sub>2</sub> wag	794	754	2.5	3.8	0.12	756	760	759	759	762	36S <sub>37</sub> ,20S <sub>34</sub> ,16S <sub>31</sub> ,14S <sub>36</sub>	17	50	33
v <sub>38</sub>	C <sub>2</sub> C <sub>3</sub> C <sub>4</sub> deformation	470	458	0.2	1.9	0.13	460	459	458	458	460	24S <sub>38</sub> ,15S <sub>40</sub> ,11S <sub>39</sub>	37	40	23
v <sub>39</sub>	C <sub>5</sub> C <sub>2</sub> C <sub>6</sub> rock	431	421	0.2	0.3	0.51	-	-	418	418	417	31S <sub>39</sub> ,13S <sub>41</sub>	18	12	69
v <sub>40</sub>	C <sub>5</sub> C <sub>2</sub> C <sub>6</sub> deformation	381	378	0.0	0.3	0.21	-	-	-	-	366	55S <sub>40</sub> ,18S <sub>39</sub>	40	58	2
v <sub>41</sub>	C <sub>5</sub> C <sub>2</sub> C <sub>6</sub> twist	289	288	0.0	0.1	0.59	-	-	-	-	-	8S <sub>41</sub> ,24S <sub>44</sub> ,17S <sub>43</sub> ,16S <sub>38</sub> ,14S <sub>43</sub> ,13S <sub>24</sub>	18	68	15
v <sub>42</sub>	C <sub>(5,6)</sub> H <sub>3</sub> torsion	272	271	0.0	0.1	0.38	-	-	-	-	268	53S <sub>42</sub> ,15S <sub>38</sub>	90	3	7
v <sub>43</sub>	C <sub>(5,6)</sub> H <sub>3</sub> torsion	240	238	0.0	0.0	0.36	-	-	-	-	-	43S <sub>43</sub> ,16S <sub>38</sub> ,11S <sub>41</sub> ,10S <sub>44</sub>	9	83	8
v <sub>44</sub>	CH <sub>3</sub> torsion	228	227	0.0	0.0	0.55	-	-	-	-	-	51S <sub>44</sub> ,32S <sub>43</sub> ,13S <sub>42</sub>	55	45	-
v <sub>45</sub>	CH out-of-plane bend	100	95	0.0	0.0	0.75	-	-	-	-	-	89S <sub>45</sub>	-	58	42

<sup>a</sup>MP2(full)/6-31G(d) *ab initio* calculations, scaled frequencies, infrared intensities (km/mol), Raman activities ( $\text{\AA}^4/\text{u}$ ) and potential energy distributions (P.E.D.s)

<sup>b</sup>Scaled *ab initio* calculations with factors of 0.88 for CH stretches and CH deformations, 0.90 for all other modes except torsions and heavy atom bends.

<sup>c</sup>Symmetry coordinates with P.E.D. contributions less than 10% are omitted.

**Table 2.** Observed and calculated<sup>a</sup> frequencies (cm<sup>-1</sup>) and potential energy distributions (P.E.D.s) for the *gauche* (C<sub>s</sub>) conformer of 2-methylbutane.

Vib. No.	Approx. description	<i>ab initio</i>	Fixed scaled <sup>b</sup>	IR int.	Raman act.	dp ratio	Infrared				Raman	P.E.D. <sup>c</sup>	Band Contour		
							gas	Xe soln.	amorphous solid	annealed solid	liquid		A	B	C
A' v <sub>3</sub>	CH <sub>3</sub> antisymmetric stretch	3195	2998	38.2	84.0	0.71	2974	2970	2971	2971	2966	63S <sub>3</sub> ,36S <sub>2</sub>	3	-	97
v <sub>2</sub>	C <sub>(5,6)</sub> H <sub>3</sub> antisymmetric stretch	3189	2991	49.6	27.7	0.75	2974	2970	2971	2971	2966	63S <sub>2</sub> ,36S <sub>3</sub>	83	-	17
v <sub>5</sub>	C <sub>(5,6)</sub> H <sub>3</sub> antisymmetric stretch	3184	2987	36.9	102.3	0.74	2974	2970	2971	2971	2966	99S <sub>5</sub>	81	-	19
v <sub>8</sub>	CH <sub>3</sub> symmetric stretch	3111	2919	13.7	153.8	0.02	2924	2926	2935	2937	2966	96S <sub>8</sub>	44	-	56
v <sub>9</sub>	C <sub>(5,6)</sub> H <sub>3</sub> symmetric stretch	3098	2907	5.7	163.5	0.00	2907	2904	2898	2902	2909	92S <sub>9</sub>	99	-	1
v <sub>11</sub>	CH <sub>2</sub> symmetric stretch	3090	2899	51.1	67.2	0.15	2886	2876	2871	2872	2900	70S <sub>11</sub> ,25S <sub>12</sub>	2	-	98
v <sub>12</sub>	CH stretch	3076	2886	10.3	59.6	0.73	2886	2876	2871	2872	2868	72S <sub>12</sub> ,26S <sub>11</sub>	84	-	16
v <sub>13</sub>	C <sub>(5,6)</sub> H <sub>3</sub> antisymmetric deformation	1577	1481	5.0	9.7	0.75	1476	1476	1474	1474	1478	68S <sub>13</sub> ,10S <sub>17</sub> ,10S <sub>14</sub>	14	-	86
v <sub>17</sub>	C <sub>(5,6)</sub> H <sub>3</sub> antisymmetric deformation	1573	1477	11.4	2.3	0.72	1474	1473	1474	1474	1478	56S <sub>17</sub> ,18S <sub>13</sub> ,15S <sub>14</sub>	71	-	29
v <sub>14</sub>	CH <sub>3</sub> antisymmetric deformation	1571	1476	5.9	4.7	0.67	1470	1471	1472	1472	1478	52S <sub>14</sub> ,29S <sub>19</sub> ,10S <sub>17</sub>	34	-	66
v <sub>19</sub>	CH <sub>2</sub> deformation	1549	1456	0.7	32.4	0.75	1457	1457	1457	1457	1453	67S <sub>19</sub> ,14S <sub>17</sub> ,14S <sub>14</sub>	85	-	15
v <sub>20</sub>	C <sub>(5,6)</sub> H <sub>3</sub> deformation	1480	1393	6.3	1.6	0.67	1389	1384	1387	1387	-	85S <sub>20</sub>	50	-	50
v <sub>21</sub>	CH <sub>3</sub> symmetric deformation	1475	1392	7.2	7.1	0.74	1389	1384	1387	1387	-	78S <sub>21</sub>	59	-	41
v <sub>25</sub>	CH <sub>2</sub> rock	1426	1351	0.4	2.6	0.75	1349	1349	1345	1345	1347	39S <sub>25</sub> ,24S <sub>23</sub> ,18S <sub>21</sub> ,11S <sub>20</sub>	53	-	47
v <sub>23</sub>	CH in-plane bend	1400	1331	0.1	2.9	0.68	1334	1336	1336	1336	1336	19S <sub>23</sub> ,21S <sub>25</sub> ,15S <sub>39</sub> ,14S <sub>36</sub>	98	-	2
v <sub>27</sub>	C <sub>(5,6)</sub> H <sub>3</sub> rock	1255	1196	1.0	3.2	0.58	1193	-	1192	1190	1196	29S <sub>27</sub> ,17S <sub>28</sub> ,13S <sub>40</sub> ,12S <sub>34</sub>	61	-	39
v <sub>32</sub>	CH <sub>3</sub> rock	1120	1146	7.2	2.4	0.68	1149	1148	1149	1149	1146	19S <sub>32</sub> ,16S <sub>27</sub> ,15S <sub>23</sub> ,12S <sub>28</sub> ,11S <sub>30</sub>	93	-	7
v <sub>28</sub>	C <sub>(5,6)</sub> H <sub>3</sub> wag	1077	1022	3.3	4.7	0.73	1022	1037	1037	1036	1027	18S <sub>28</sub> ,22S <sub>32</sub> ,18S <sub>36</sub> ,14S <sub>25</sub> ,14S <sub>30</sub>	80	-	20
v <sub>30</sub>	C <sub>3</sub> C <sub>4</sub> stretch	1040	987	0.4	4.5	0.41	976	970	971	971	971	37S <sub>30</sub> ,16S <sub>32</sub> ,15S <sub>27</sub> ,13S <sub>23</sub> ,12S <sub>28</sub>	95	-	5
v <sub>34</sub>	C <sub>5</sub> C <sub>2</sub> C <sub>6</sub> symmetric stretch	949	900	0.5	7.5	0.74	901	900	-	-	908	38S <sub>34</sub> ,18S <sub>30</sub> ,16S <sub>32</sub> ,13S <sub>28</sub>	99	-	1
v <sub>36</sub>	C <sub>2</sub> C <sub>3</sub> stretch	791	751	0.5	10.1	0.08	-	-	-	-	762	42S <sub>36</sub> ,37S <sub>34</sub>	1	-	99
v <sub>39</sub>	C <sub>5</sub> C <sub>2</sub> C <sub>6</sub> rock	548	532	2.0	0.2	0.62	530	531	-	-	-	38S <sub>39</sub> ,28S <sub>38</sub> ,12S <sub>27</sub>	95	-	5
v <sub>40</sub>	C <sub>5</sub> C <sub>2</sub> C <sub>6</sub> deformation	383	379	0.1	0.1	0.36	-	-	-	-	366	78S <sub>40</sub>	27	-	73
v <sub>38</sub>	C <sub>2</sub> C <sub>3</sub> C <sub>4</sub> deformation	287	283	0.1	0.1	0.06	-	-	-	-	-	45S <sub>38</sub> ,19S <sub>42</sub> ,19S <sub>39</sub>	1	-	99

**Table 2.** --Continued.

Vib. No.	Approx. description	<i>ab initio</i>	Fixed scaled <sup>b</sup>	IR int.	Raman act.	dp ratio	Infrared				Raman	P.E.D. <sup>c</sup>	Band Contour		
							gas	Xe soln.	amorphous solid	annealed solid			A	B	C
v <sub>42</sub>	C <sub>(5,6)</sub> H <sub>3</sub> torsion	269	268	0.2	0.1	0.06	-	-	-	-	268 77S <sub>42</sub>	82	-	18	
A'' v <sub>1</sub>	CH <sub>3</sub> antisymmetric stretch	3205	3007	23.8	32.3	0.75	2974	2970	2971	2971	2971 91S <sub>1</sub>	-	100	-	
v <sub>4</sub>	C <sub>(5,6)</sub> H <sub>3</sub> antisymmetric stretch	3186	2989	19.6	7.2	0.75	2974	2970	2971	2971	2971 91S <sub>4</sub>	-	100	-	
v <sub>6</sub>	C <sub>(5,6)</sub> H <sub>3</sub> antisymmetric stretch	3182	2985	8.1	29.3	0.75	2974	2970	2971	2971	2971 97S <sub>6</sub>	-	100	-	
v <sub>7</sub>	CH <sub>2</sub> antisymmetric stretch	3133	2939	22.6	67.6	0.75	2924	2926	2935	2937	2934 98S <sub>7</sub>	-	100	-	
v <sub>10</sub>	CH <sub>3</sub> symmetric stretch	3096	2904	27.0	3.9	0.75	2907	2904	2898	2902	2900 100S <sub>10</sub>	-	100	-	
v <sub>16</sub>	CH <sub>3</sub> antisymmetric deformation	1576	1480	2.1	11.9	0.75	1476	1476	1474	1474	1478 62S <sub>16</sub> ,25S <sub>15</sub>	-	100	-	
v <sub>15</sub>	C <sub>(5,6)</sub> H <sub>3</sub> antisymmetric deformation	1556	1462	5.1	2.0	0.75	1462	1464	1465	1465	1463 36S <sub>15</sub> ,29S <sub>16</sub> ,25S <sub>18</sub>	-	100	-	
v <sub>18</sub>	C <sub>(5,6)</sub> H <sub>3</sub> antisymmetric deformation	1551	1455	0.2	34.8	0.75	1457	1457	1457	1457	1453 62S <sub>18</sub> ,32S <sub>15</sub>	-	100	-	
v <sub>22</sub>	C <sub>(5,6)</sub> H <sub>3</sub> symmetric deformation	1461	1380	9.8	2.4	0.75	1381	1384	1382	1382	1378 71S <sub>22</sub> ,10S <sub>24</sub>	-	100	-	
v <sub>24</sub>	C <sub>5</sub> C <sub>2</sub> C <sub>6</sub> wag	1422	1348	0.2	1.8	0.75	1349	1349	1345	1345	1347 34S <sub>24</sub> ,25S <sub>22</sub> ,13S <sub>26</sub> ,12S <sub>41</sub>	-	100	-	
v <sub>26</sub>	CH <sub>2</sub> twist	1344	1275	0.0	15.1	0.75	-	-	-	-	1267 57S <sub>26</sub> ,15S <sub>31</sub> ,10S <sub>41</sub>	-	100	-	
v <sub>31</sub>	CH <sub>3</sub> wag	1235	1177	0.4	1.6	0.75	1172	-	1168	1168	1174 19S <sub>31</sub> ,24S <sub>37</sub> ,20S <sub>41</sub> ,19S <sub>21</sub> ,18S <sub>29</sub>	-	100	-	
v <sub>29</sub>	C <sub>5</sub> C <sub>2</sub> C <sub>6</sub> antisymmetric stretch	1060	1005	0.2	5.0	0.75	-	-	-	-	~1002 43S <sub>29</sub> ,20S <sub>26</sub> ,20S <sub>31</sub>	-	100	-	
v <sub>33</sub>	C <sub>(5,6)</sub> H <sub>3</sub> wag	1002	951	0.3	2.9	0.75	954	953	951	951	951 60S <sub>33</sub> ,18S <sub>29</sub> ,11S <sub>35</sub>	-	100	-	
v <sub>35</sub>	C <sub>(5,6)</sub> H <sub>3</sub> rock	960	910	0.5	0.5	0.75	912	917	912	912	~908 66S <sub>35</sub> ,14S <sub>33</sub>	-	100	-	
v <sub>37</sub>	CH <sub>2</sub> wag	806	765	2.9	0.2	0.75	766	763	764	764	~762 56S <sub>37</sub> ,34S <sub>31</sub>	-	100	-	
v <sub>41</sub>	C <sub>5</sub> C <sub>2</sub> C <sub>6</sub> twist	386	383	0.0	0.1	0.75	-	-	-	-	366 37S <sub>41</sub> ,34S <sub>24</sub>	-	100	-	
v <sub>43</sub>	C <sub>(5,6)</sub> H <sub>3</sub> torsion bend	281	280	0.0	0.0	0.75	-	-	-	-	- 44S <sub>43</sub> ,34S <sub>44</sub>	-	100	-	
v <sub>44</sub>	CH <sub>3</sub> torsion	220	220	0.0	0.0	0.75	-	-	-	-	- 48S <sub>44</sub> ,50S <sub>43</sub>	-	100	-	
v <sub>45</sub>	CH out-of-plane	84	80	0.0	0.1	0.75	-	-	-	-	- 84S <sub>45</sub>	-	100	-	

<sup>a</sup>MP2(full)/6-31G(d) *ab initio* calculations, scaled frequencies, infrared intensities (km/mol), Raman activities ( $\text{\AA}^4/\text{u}$ ) and potential energy distributions (P.E.D.s)

<sup>b</sup>Scaled *ab initio* calculations with factors of 0.88 for CH stretches and CH deformations, 0.90 for all other modes except torsions and heavy atom bends.

<sup>c</sup>Symmetry coordinates with P.E.D. contributions less than 10% are omitted.

**Table 3.** Calculated electronic energies (Hartrees, H) and energy differences (cm<sup>-1</sup>) for 2-methylbutane.

Basis set	MP2(full)		B3LYP	
	<i>trans</i> <sup>a</sup>	<i>gauche</i> <sup>b</sup>	<i>trans</i> <sup>a</sup>	<i>gauche</i> <sup>b</sup>
6-31G(d)	0.0172877	281	0.7711159	318
6-31+G(d)	0.0258378	320	0.7772217	349
6-31G(d,p)	0.1172421	263	0.7878779	317
6-31+G(d,p)	0.1241809	293	0.7933396	351
6-311G(d,p)	0.2531102	230	0.8286250	318
6-311+G(d,p)	0.2556536	261	0.8292772	323
6-311G(2d,2p)	0.3154857	252	0.8381162	330
6-311+G(2d,2p)	0.3169061	254	0.8386901	335
6-311G(2df,2pd)	0.3982405	255	0.8427384	335
6-311+G(2df,2pd)	0.3993899	260	0.8432313	341
aug-cc-pVTZ	-	-	0.8484421	345

<sup>a</sup> Energy of *trans* conformer is given as  $-(E + 197)$  H.

<sup>b</sup> Energy of *gauche* conformer is relative to *trans* form

**Table 4.** Symmetry coordinates for 2-methylbutane.

Description	Symmetry Coordinate <sup>a</sup>
CH <sub>3</sub> antisymmetric stretch	S <sub>1</sub> = r <sub>5</sub> - r <sub>6</sub>
C <sub>(5,6)</sub> H <sub>3</sub> antisymmetric stretch	S <sub>2</sub> = r <sub>8</sub> - r <sub>9</sub> + r <sub>11</sub> - r <sub>12</sub>
CH <sub>3</sub> antisymmetric stretch	S <sub>3</sub> = -2r <sub>4</sub> + r <sub>5</sub> + r <sub>6</sub>
C <sub>(5,6)</sub> H <sub>3</sub> antisymmetric stretch	S <sub>4</sub> = r <sub>8</sub> - r <sub>9</sub> - r <sub>11</sub> + r <sub>12</sub>
C <sub>(5,6)</sub> H <sub>3</sub> antisymmetric stretch	S <sub>5</sub> = -2r <sub>7</sub> + r <sub>8</sub> + r <sub>9</sub> - 2r <sub>10</sub> + r <sub>11</sub> + r <sub>12</sub>
C <sub>(5,6)</sub> H <sub>3</sub> antisymmetric stretch	S <sub>6</sub> = -2r <sub>7</sub> + r <sub>8</sub> + r <sub>9</sub> + 2r <sub>10</sub> - r <sub>11</sub> - r <sub>12</sub>
CH <sub>2</sub> antisymmetric stretch	S <sub>7</sub> = r <sub>2</sub> - r <sub>3</sub>
CH <sub>3</sub> symmetric stretch	S <sub>8</sub> = r <sub>4</sub> + r <sub>5</sub> + r <sub>6</sub>
C <sub>(5,6)</sub> H <sub>3</sub> symmetric stretch	S <sub>9</sub> = r <sub>7</sub> + r <sub>8</sub> + r <sub>9</sub> + r <sub>10</sub> + r <sub>11</sub> + r <sub>12</sub>
CH <sub>3</sub> symmetric stretch	S <sub>10</sub> = r <sub>7</sub> + r <sub>8</sub> + r <sub>9</sub> - r <sub>10</sub> - r <sub>11</sub> - r <sub>12</sub>
CH <sub>2</sub> symmetric stretch	S <sub>11</sub> = r <sub>2</sub> + r <sub>3</sub>
CH stretch	S <sub>12</sub> = r <sub>1</sub>
C <sub>(5,6)</sub> H <sub>3</sub> antisymmetric deformation	S <sub>13</sub> = π <sub>1</sub> - π <sub>2</sub> + π <sub>4</sub> - π <sub>6</sub>
CH <sub>3</sub> antisymmetric deformation	S <sub>14</sub> = δ <sub>1</sub> + δ <sub>2</sub> - 2δ <sub>3</sub>
C <sub>(5,6)</sub> H <sub>3</sub> antisymmetric deformation	S <sub>15</sub> = π <sub>1</sub> + π <sub>2</sub> - 2π <sub>3</sub> - π <sub>4</sub> + 2π <sub>5</sub> - π <sub>6</sub>
CH <sub>3</sub> antisymmetric deformation	S <sub>16</sub> = δ <sub>1</sub> - δ <sub>2</sub>
C <sub>(5,6)</sub> H <sub>3</sub> antisymmetric deformation	S <sub>17</sub> = π <sub>1</sub> + π <sub>2</sub> - 2π <sub>3</sub> + π <sub>4</sub> - 2π <sub>5</sub> + π <sub>6</sub>
C <sub>(5,6)</sub> H <sub>3</sub> antisymmetric deformation	S <sub>18</sub> = π <sub>1</sub> - π <sub>2</sub> - π <sub>4</sub> + π <sub>6</sub>
CH <sub>2</sub> deformation	S <sub>19</sub> = φ <sub>1</sub>
C <sub>(5,6)</sub> H <sub>3</sub> symmetric deformation	S <sub>20</sub> = π <sub>1</sub> + π <sub>2</sub> + π <sub>3</sub> + π <sub>4</sub> + π <sub>5</sub> + π <sub>6</sub>
CH <sub>3</sub> deformation	S <sub>21</sub> = δ <sub>1</sub> + δ <sub>2</sub> + δ <sub>3</sub>
C <sub>(5,6)</sub> H <sub>3</sub> symmetric deformation	S <sub>22</sub> = π <sub>1</sub> + π <sub>2</sub> + π <sub>3</sub> - π <sub>4</sub> - π <sub>5</sub> - π <sub>6</sub>
CH in-plane bend	S <sub>23</sub> = θ <sub>1</sub>
C <sub>5</sub> C <sub>2</sub> C <sub>6</sub> wag	S <sub>24</sub> = σ <sub>2</sub> + θ <sub>2</sub> - σ <sub>3</sub> - θ <sub>3</sub>
CH <sub>2</sub> rock	S <sub>25</sub> = Ψ <sub>1</sub> + Ψ <sub>2</sub> - Ψ <sub>3</sub> - Ψ <sub>4</sub>
CH <sub>2</sub> twist	S <sub>26</sub> = Ψ <sub>1</sub> - Ψ <sub>2</sub> - Ψ <sub>3</sub> + Ψ <sub>4</sub>
C <sub>(5,6)</sub> H <sub>3</sub> rock	S <sub>27</sub> = -2β <sub>1</sub> + β <sub>2</sub> + β <sub>3</sub> - 2β <sub>4</sub> + β <sub>5</sub> + β <sub>6</sub>
C <sub>(5,6)</sub> H <sub>3</sub> wag	S <sub>28</sub> = β <sub>2</sub> - β <sub>3</sub> + β <sub>5</sub> - β <sub>6</sub>
C <sub>5</sub> C <sub>2</sub> C <sub>6</sub> antisymmetric stretch	S <sub>29</sub> = R <sub>3</sub> - R <sub>4</sub>
C <sub>3</sub> C <sub>4</sub> stretch	S <sub>30</sub> = R <sub>2</sub>
CH <sub>3</sub> wag	S <sub>31</sub> = λ <sub>2</sub> - λ <sub>3</sub>
CH <sub>3</sub> rock	S <sub>32</sub> = -2λ <sub>1</sub> + λ <sub>2</sub> + λ <sub>3</sub>
C <sub>(5,6)</sub> H <sub>3</sub> wag	S <sub>33</sub> = β <sub>2</sub> - β <sub>3</sub> - β <sub>5</sub> + β <sub>6</sub>
C <sub>5</sub> C <sub>2</sub> C <sub>6</sub> symmetric stretch	S <sub>34</sub> = R <sub>3</sub> + R <sub>4</sub>
C <sub>(5,6)</sub> H <sub>3</sub> rock	S <sub>35</sub> = -2β <sub>1</sub> + β <sub>2</sub> + β <sub>3</sub> + 2β <sub>4</sub> - β <sub>5</sub> - β <sub>6</sub>
C <sub>2</sub> C <sub>3</sub> stretch	S <sub>36</sub> = R <sub>1</sub>
CH <sub>2</sub> wag	S <sub>37</sub> = Ψ <sub>1</sub> - Ψ <sub>2</sub> + Ψ <sub>3</sub> - Ψ <sub>4</sub>
C <sub>2</sub> C <sub>3</sub> C <sub>4</sub> deformation	S <sub>38</sub> = σ <sub>1</sub>
C <sub>5</sub> C <sub>2</sub> C <sub>6</sub> rock	S <sub>39</sub> = σ <sub>2</sub> - θ <sub>2</sub> + σ <sub>3</sub> - θ <sub>3</sub>

**Table 4.** --Continued.

Description	Symmetry Coordinate <sup>a</sup>
C <sub>5</sub> C <sub>2</sub> C <sub>6</sub> deformation	S <sub>40</sub> = $\sigma_4$
C <sub>5</sub> C <sub>2</sub> C <sub>6</sub> twist	S <sub>41</sub> = $\sigma_2 - \theta_2 - \sigma_3 + \theta_3$
C <sub>(5,6)</sub> H <sub>3</sub> torsion	S <sub>42</sub> = $\tau_2 - \tau_3$
C <sub>(5,6)</sub> H <sub>3</sub> torsion	S <sub>43</sub> = $\tau_2 + \tau_3$
CH <sub>3</sub> torsion	S <sub>44</sub> = $\tau_1$
CH out-of-plane bend	S <sub>45</sub> = T <sub>4</sub>

<sup>a</sup> Not normalized

Comparisons of experimental and simulated infrared spectra of 2-methylbutane are shown in Fig. 4 and 5. The infrared spectrum of the gas, along with the predicted infrared spectra of the individual *trans* and *gauche* conformers and the mixture of the two conformers with relative concentrations calculated for the equilibrium mixture at 25 °C by using the experimentally determined enthalpy difference, are shown in Fig. 4(A-E). The predicted spectrum of the isolated molecule should be comparable to the spectrum of the gaseous phase. The predicted spectrum is in good agreement with the experimental spectrum, which shows the utility of the scaled predicted frequencies for supporting the vibrational assignment.

The Raman spectrum of the liquid, predicted Raman spectra for the pure *trans* and *gauche* conformers, as well as, the mixture of both conformers with their relative concentrations, are obtained by using the experimentally determined enthalpy difference (161 cm<sup>-1</sup>) and are shown in Fig. 7 (A-D). The predicted spectrum should be comparable to that of the room temperature liquid as frequency shifts due to the intermolecular

interactions in the liquid phase are relatively small, with an average value of  $3 \text{ cm}^{-1}$ .<sup>27-31</sup> The predicted spectrum is in reasonable agreement with the experimental spectrum.

### Vibrational Assignment

Establishing conformational stability is dependent on making confident and accurate vibrational assignments for the *trans* and *gauche* conformers of 2-methylbutane. The scaled frequencies, infrared intensities, Raman activities and band contours from the MP2(full)/6-31G(d) *ab initio* calculation were used to assist in making the vibrational assignment for both conformers (Tables 1 and 2). Additionally, the depolarization ratio and potential energy distributions (P. E. D.) were also used. Vibrational modes have been assigned in the infrared spectra of the gas, amorphous, and annealed solid, and dilute sample of 2-methylbutane dissolved in liquefied xenon. Assignments have also been made with the aid of the Raman spectrum of the liquid phase. The *trans* conformer of 2-methylbutane has  $C_1$  point group symmetry and therefore its 45 vibrational modes belong to one symmetry block. The *gauche* conformer of 2-methylbutane has  $C_s$  symmetry and therefore its 45 vibrational modes are split into two different blocks; the  $A'$  symmetry block contains 25 vibrational modes and  $A''$  symmetry block contains 19 vibrational modes.

The labeling of the vibrational modes,  $\nu_1$ - $\nu_{45}$ , for the *trans* conformer (Table 1) are sorted from highest to lowest wavenumbers. The same labeling of the vibrational modes from the *trans* conformer is used for the *gauche* conformer (Table 2) to maintain consistency. Due to the large number of vibrations, our discussion will be limited to vibrational modes below  $1500 \text{ cm}^{-1}$  for the Infrared spectra of the gas, xenon solution and amorphous and annealed solid, as well as for the Raman spectrum of the liquid.

Therefore, there will be no further discussion of any methyl or other CH stretching modes. The 33 remaining vibrational modes have been split into four different categories: deformations; rocks & wags; twists, bends & torsions; and skeletal (heavy atom) vibrations.

### Deformations

For the *trans* conformer, the  $C_{(5,6)}H_3$  antisymmetric deformation ( $\nu_{13}$ ) mode was predicted to have low to medium intensity at  $1484\text{ cm}^{-1}$  and observed as a strong peak at  $1476\text{ cm}^{-1}$  in the infrared spectra of the gas and xenon solution and at  $1474\text{ cm}^{-1}$  for the amorphous and annealed solid. The  $CH_3$  antisymmetric deformation ( $\nu_{14}$ ) mode was predicted at  $1476\text{ cm}^{-1}$  and observed as a shoulder peak at  $1470\text{ cm}^{-1}$  in the infrared spectrum of the gas but was more clearly resolved in the xenon spectrum and observed at  $1471\text{ cm}^{-1}$ . The  $C_{(5,6)}H_3$  antisymmetric deformation ( $\nu_{15}$ ) mode predicted at  $1473\text{ cm}^{-1}$  and  $CH_3$  antisymmetric deformation ( $\nu_{16}$ ) mode predicted at  $1470\text{ cm}^{-1}$  were observed as a single peak at  $1466\text{ cm}^{-1}$  in the infrared spectrum gas phase and  $1470\text{ cm}^{-1}$  in the Raman spectrum of the liquid. These two vibrations were also indistinguishable and taken as a single peak in all other recorded infrared spectra. The  $C_{(5,6)}H_3$  antisymmetric deformation ( $\nu_{17}$ ) mode was predicted at  $1465\text{ cm}^{-1}$  and observed at  $1459\text{ cm}^{-1}$  in the infrared spectrum of the gas and xenon solution, respectively. The  $C_{(5,6)}H_3$  antisymmetric deformation ( $\nu_{18}$ ) mode was predicted with low intensity at  $1458\text{ cm}^{-1}$  but observed as a strong peak at  $1452\text{ cm}^{-1}$  in the infrared spectrum of the gas and xenon solution and  $1453\text{ cm}^{-1}$  for the amorphous and annealed solid. Similarly, the  $CH_2$  deformation ( $\nu_{19}$ ) mode was predicted at  $1452\text{ cm}^{-1}$ , with low infrared intensity and high Raman activity, but observed as a strong peak at  $1448\text{ cm}^{-1}$  in the infrared spectrum of the gas, xenon solution and annealed

solid. Both the  $\nu_{18}$  and  $\nu_{19}$  modes were assigned to the same peak at  $1453\text{ cm}^{-1}$  in the Raman spectrum of the liquid. The  $C_{(5,6)}H_3$  symmetric deformation ( $\nu_{20}$ ) and  $CH_3$  deformation ( $\nu_{21}$ ) modes predicted at  $1394$  and  $1389\text{ cm}^{-1}$ , respectively, were observed as a single peak at  $1389\text{ cm}^{-1}$  in the infrared spectrum of the gas and taken as one peak for all other infrared spectra. The same mode was not observed in the Raman spectrum of the liquid even though it was predicted to have a nonzero activity. The  $C_{(5,6)}H_3$  symmetric deformation ( $\nu_{22}$ ) mode was predicted at  $1380\text{ cm}^{-1}$  and observed as sharp strong peak at  $1381\text{ cm}^{-1}$  and  $1378\text{ cm}^{-1}$  in the infrared spectrum of the gas and xenon solution, respectively.

For the  $A'$  symmetry block of the *gauche* conformer, the  $C_{(5,6)}H_3$  antisymmetric deformation ( $\nu_{13}$ ) mode was assigned to the same band for the same mode ( $\nu_{13}$ ) for the *trans* conformer. The  $C_{(5,6)}H_3$  antisymmetric deformation ( $\nu_{17}$ ) mode was predicted at  $1477\text{ cm}^{-1}$  and observed at  $1474$  in the infrared spectrum of the gas and  $1473\text{ cm}^{-1}$  for the xenon solution. The assignment for the  $CH_3$  antisymmetric deformation ( $\nu_{14}$ ) mode was assigned for the same ( $\nu_{14}$ ) mode for the *trans* conformer. The  $CH_2$  deformation ( $\nu_{19}$ ) was observed at  $1457\text{ cm}^{-1}$  for all infrared spectra and at  $1453\text{ cm}^{-1}$  for the Raman spectrum of the liquid. The  $C_{(5,6)}H_3$  symmetric deformation ( $\nu_{20}$ ) and  $CH_3$  deformation ( $\nu_{21}$ ) modes were assigned to the same peaks for the same modes that occur in the *trans* conformer and all were assigned as one peak in all infrared spectra.

For the  $A''$  symmetry block of the *gauche* conformer, the  $CH_3$  antisymmetric deformation ( $\nu_{16}$ ) mode was assigned to the same peaks corresponding to the ( $\nu_{13}$ ) mode for the *trans* conformer. In the Raman spectrum of the liquid, The  $C_{(5,6)}H_3$  antisymmetric deformation ( $\nu_{15}$ ) mode predicted at  $1462\text{ cm}^{-1}$  was assigned to a strong peak observed at

1462  $\text{cm}^{-1}$  in the infrared spectrum of the gas, but can be more clearly seen in the infrared spectrum of the xenon solution at 1464  $\text{cm}^{-1}$  and the amorphous and annealed solid at 1465  $\text{cm}^{-1}$ , which were assigned to the same peak as the ( $\nu_{16}$ ) mode for the *trans* conformer. The  $\text{C}_{(5,6)}\text{H}_3$  antisymmetric deformation ( $\nu_{18}$ ) mode predicted at 1455  $\text{cm}^{-1}$  was observed at 1457  $\text{cm}^{-1}$  in all infrared spectra. Similarly, the  $\text{C}_{(5,6)}\text{H}_3$  symmetric deformation ( $\nu_{22}$ ) mode was predicted at 1380  $\text{cm}^{-1}$  and observed at 1381  $\text{cm}^{-1}$  in the infrared spectrum of the gas and 1378  $\text{cm}^{-1}$  and assigned to the same peak for the same mode for the *trans* conformer.

#### Rocks and Wags

For the *trans* conformer, the  $\text{C}_5\text{C}_2\text{C}_6$  wag ( $\nu_{24}$ ) mode was predicted with low intensity at 1346  $\text{cm}^{-1}$  but was observed as a medium sharp peak at a slightly higher vibrational frequency of 1349  $\text{cm}^{-1}$  in the infrared spectra of the xenon solution and 1345  $\text{cm}^{-1}$  for the annealed solid. The  $\text{CH}_2$  rock ( $\nu_{25}$ ) mode was predicted at 1300  $\text{cm}^{-1}$  and observed at the same vibration frequency for the infrared spectrum of the gas and at 1297  $\text{cm}^{-1}$  for the xenon solution. The  $\text{C}_{(5,6)}\text{H}_3$  rocking ( $\nu_{27}$ ) mode predicted at 1193  $\text{cm}^{-1}$  was only observed as a weak shoulder at 1192  $\text{cm}^{-1}$  and 1190  $\text{cm}^{-1}$  in the infrared spectrum of the amorphous and annealed solid and 1197  $\text{cm}^{-1}$  in the Raman spectrum of the liquid. The  $\text{C}_{(5,6)}\text{H}_3$  wagging ( $\nu_{28}$ ) mode was observed at 1181  $\text{cm}^{-1}$  in the infrared of the gas and at a lower vibrational frequency of 1175  $\text{cm}^{-1}$  in the xenon solution. The  $\text{CH}_3$  wag ( $\nu_{31}$ ) mode predicted at 1013  $\text{cm}^{-1}$  was observed at 1012  $\text{cm}^{-1}$  in the infrared spectrum of the xenon solution, which was then used to help make the assignment at the same vibrational frequency of the gas. Similarly for the  $\text{CH}_3$  rock ( $\nu_{32}$ ) mode, the assignment at 970  $\text{cm}^{-1}$  in the infrared spectrum of the xenon solution was used to help determine the same mode

in the gas phase at  $968\text{ cm}^{-1}$ . Interestingly, the Raman spectrum shows a peak assigned to the same mode at a significantly higher vibrational frequency of  $983\text{ cm}^{-1}$ . The  $\text{C}_{(5,6)}\text{H}_3$  wag ( $\nu_{33}$ ) mode predicted at  $951\text{ cm}^{-1}$  was observed as a weak shoulder at  $954\text{ cm}^{-1}$  in the infrared of the gas and xenon solution but as a sharp medium peak at  $951\text{ cm}^{-1}$  for the amorphous and annealed solid. The same mode is clearly observed in the Raman spectrum at  $951\text{ cm}^{-1}$ . The  $\text{CH}_2$  wag ( $\nu_{37}$ ) mode was observed as a shoulder in the infrared spectrum of the gas and xenon solution at  $756\text{ cm}^{-1}$  and  $760\text{ cm}^{-1}$ , respectively.

For the  $A'$  symmetry block of the *gauche* conformer, the  $\text{CH}_2$  rock ( $\nu_{25}$ ) mode was observed as an obscured shoulder peak at  $1349\text{ cm}^{-1}$  in the infrared spectrum of the gas and xenon solution. The  $\text{C}_{(5,6)}\text{H}_3$  rock ( $\nu_{27}$ ) mode was observed as a shoulder at  $1192\text{ cm}^{-1}$  in the infrared of the annealed solid. The  $\text{CH}_3$  rocking ( $\nu_{32}$ ) mode predicted at  $1146\text{ cm}^{-1}$  was observed slightly higher at  $1149\text{ cm}^{-1}$  in the infrared spectrum of the gas. The  $\text{C}_{(5,6)}\text{H}_3$  wag ( $\nu_{28}$ ) mode was predicted and observed at  $1022\text{ cm}^{-1}$  in the infrared of the gas; however, the infrared spectrum of the xenon solution as well as the amorphous and annealed solid were observed to be much higher at  $1037\text{ cm}^{-1}$  and  $1036\text{ cm}^{-1}$  respectively.

For the  $A''$  symmetry block of the *gauche* conformer, the  $\text{CH}_3$  wag ( $\nu_{31}$ ) mode predicted at  $1177\text{ cm}^{-1}$  was observed at  $1172\text{ cm}^{-1}$  in the infrared spectrum of the gas at  $1168\text{ cm}^{-1}$  for the amorphous and annealed solid spectra and at  $1174\text{ cm}^{-1}$  in the Raman spectrum of the liquid. The  $\text{C}_{(5,6)}\text{H}_3$  wag ( $\nu_{33}$ ) mode was assigned to the same peaks for the same mode ( $\nu_{33}$ ) for the *trans* conformer. The  $\text{C}_{(5,6)}\text{H}_3$  rock ( $\nu_{35}$ ) predicted at  $910\text{ cm}^{-1}$  was observed at  $912\text{ cm}^{-1}$  in the infrared spectrum of the gas, and this assignment was confirmed by the assignments made at the same position for the infrared spectra of the

amorphous and annealed solid. The CH<sub>2</sub> wag ( $\nu_{37}$ ) mode predicted at 765 cm<sup>-1</sup> was observed as a small shoulder at 766 cm<sup>-1</sup> in the infrared spectrum of the gas and confirmed by the annealed spectrum of the solid at 759 cm<sup>-1</sup>.

#### Twists, Bends and Torsions

For the *trans* conformer, the CH in-plane bend ( $\nu_{23}$ ) mode was observed as a shoulder peak at 1364 cm<sup>-1</sup> in the infrared spectrum of the gas and has been predicted to have low intensity at 1364 cm<sup>-1</sup>. The same mode was not observed in the Raman spectrum of the liquid despite having a higher predicted activity. The CH<sub>2</sub> twist ( $\nu_{26}$ ) mode was observed at 1267 cm<sup>-1</sup> in the infrared of the gas and xenon solution. For the A' symmetry block of the *gauche* conformer, the CH in-plane bend ( $\nu_{23}$ ) mode was predicted to have low intensity at 1331 cm<sup>-1</sup> and observed as a very broad and weak peak in the infrared spectrum of the gas at 1334 cm<sup>-1</sup>. However, the band associated with the same ( $\nu_{23}$ ) mode is very apparent in the infrared spectra of the xenon solution, amorphous and annealed solid, as well as the Raman spectrum of the liquid – all of which are observed at 1336 cm<sup>-1</sup>.

#### Skeletal (Heavy Atom) Vibrations

For the *trans* conformer, the C<sub>5</sub>C<sub>2</sub>C<sub>6</sub> antisymmetric stretch ( $\nu_{29}$ ) mode was observed at 1157 cm<sup>-1</sup> in the infrared gas phase spectrum, but observed significantly higher at 1174 cm<sup>-1</sup> in the Raman spectrum of the liquid. According to the predictions, the C<sub>3</sub>C<sub>4</sub> stretch ( $\nu_{30}$ ) mode is predicted to have no intensity and is not observed in any of the infrared spectra. However, the same mode was observed as a medium intensity peak at 1034 cm<sup>-1</sup> in the Raman spectrum of the liquid. The C<sub>5</sub>C<sub>2</sub>C<sub>6</sub> symmetric stretch ( $\nu_{34}$ )

mode and  $C_{(5,6)}H_3$  rock ( $\nu_{35}$ ) were observed as a single peak in the infrared spectrum of the gas and xenon solution at  $910\text{ cm}^{-1}$  and  $909\text{ cm}^{-1}$ , respectively, and at  $908\text{ cm}^{-1}$  in the Raman spectrum of the liquid. The infrared spectra of the amorphous and annealed solid, however, showed two distinct peaks at  $910\text{ cm}^{-1}$  ( $\nu_{34}$ ) and  $908\text{ cm}^{-1}$  ( $\nu_{35}$ ), respectively. The  $C_2C_3$  stretch ( $\nu_{36}$ ) mode predicted at  $787\text{ cm}^{-1}$  was observed at  $793\text{ cm}^{-1}$  in the Raman spectrum of the liquid but not observed in any infrared spectra. The  $C_2C_3C_4$  deformation ( $\nu_{38}$ ) mode was observed as a broad and weak peak in the infrared spectrum of the gas at  $459\text{ cm}^{-1}$  but was more readily apparent at  $458\text{ cm}^{-1}$  in the amorphous and annealed solid spectra. The  $C_5C_2C_6$  rock ( $\nu_{39}$ ) mode was only observed in the infrared spectrum of the solid at  $418\text{ cm}^{-1}$  and Raman spectrum of the liquid at  $417\text{ cm}^{-1}$ . The  $C_5C_2C_6$  deformation ( $\nu_{40}$ ) and  $C_{(5,6)}H_3$  torsion ( $\nu_{42}$ ) modes were observed in the Raman spectrum of the liquid at  $366\text{ cm}^{-1}$  and  $268\text{ cm}^{-1}$ , respectively.

For the  $A'$  symmetry block of the *gauche* conformer, the  $C_3C_4$  stretch ( $\nu_{30}$ ) mode was observed lower in frequency in all spectra than its prediction at  $987\text{ cm}^{-1}$ . The ( $\nu_{30}$ ) mode was observed at  $976\text{ cm}^{-1}$  in the infrared spectrum of the gas and confirmed by the spectrum of the amorphous and annealed solid at  $971\text{ cm}^{-1}$ . The  $C_5C_2C_6$  symmetric stretch ( $\nu_{34}$ ) mode predicted at  $900\text{ cm}^{-1}$  was observed as a shoulder peak at  $901\text{ cm}^{-1}$ . The  $C_2C_3$  stretch ( $\nu_{36}$ ) mode was not observed in any of the infrared spectra, but, in the Raman spectrum of the liquid, the ( $\nu_{36}$ ) mode is assigned to the same peak at  $366\text{ cm}^{-1}$  as the ( $\nu_{37}$ ) mode for the *trans* conformer. The  $C_5C_2C_6$  rock ( $\nu_{39}$ ) mode predicted at  $532\text{ cm}^{-1}$  was only observed as a weak peak at  $530\text{ cm}^{-1}$  and  $531\text{ cm}^{-1}$  in the infrared spectra of the gas and xenon solution. No peaks in the infrared spectra were observed for the  $C_5C_2C_6$  deformation ( $\nu_{40}$ ) and  $C_{(5,6)}H_3$  torsion ( $\nu_{42}$ ) modes, but were assigned to the same

peaks in the Raman spectrum of the liquid for the same ( $\nu_{40}$ ) and ( $\nu_{42}$ ) modes for the *trans* conformer at  $366\text{ cm}^{-1}$  and  $268\text{ cm}^{-1}$ , respectively.

For the  $A''$  symmetry block of the *gauche* conformer, the peaks for the  $C_5C_2C_6$  wag ( $\nu_{24}$ ) and  $CH_2$  twist ( $\nu_{26}$ ) modes for the *gauche* conformer were assigned to the same peaks for the ( $\nu_{25}$ ) and ( $\nu_{26}$ ) modes of the *trans* conformer. The infrared spectra did not show any peaks to which we could assign the  $C_5C_2C_6$  antisymmetric stretch ( $\nu_{29}$ ) mode. However, a small shoulder was observed at  $\sim 1002\text{ cm}^{-1}$  in the Raman spectrum of the liquid. The  $C_5C_2C_6$  twist ( $\nu_{41}$ ) was assigned to the same peak in the Raman spectrum as the  $C_5C_2C_6$  deformation ( $\nu_{40}$ ) mode for the *trans* and *gauche* conformer at  $366\text{ cm}^{-1}$ .

### Conformational Stability

To determine the enthalpy difference between the two conformers of 2-methylbutane, the sample was dissolved in liquefied xenon, and the IR spectrum of the xenon solution was collected at low temperatures ranging from  $-100$  to  $-55\text{ }^\circ\text{C}$ . The band or peak intensities of the conformers were measured as a function of temperature and their ratios were determined (Fig. 6). By application of the van't Hoff equation,  $-\ln K = \Delta H/(RT) - \Delta S/R$ , the enthalpy differences were determined from a plot of  $-\ln K$  versus  $1/T$ , where  $\Delta H/R$  is the slope of the line, and  $K$  is substituted with the appropriate intensity ratios, *i.e.*  $I_{\text{conf-1}} / I_{\text{conf-2}}$ , etc. It was assumed that  $\Delta S$  is not a function of temperature in the range studied. Relatively small interactions are expected to occur between the sample and xenon, but 2-methylbutane could potentially associate with itself through van der Waals interactions. Self-association was limited by using a small concentration of sample ( $\sim 10^{-4}$  molar) and therefore only small wavenumber shifts are

anticipated for sample-noble gas interactions when passing from the gas phase into liquefied xenon. The major advantage to using xenon solutions is that vibrational bands are more well resolved compared to those in the infrared spectrum of the gas, because gas phase rotational fine structure is removed in the solution and interferences from water and CO<sub>2</sub> are reduced.

Using the vibrational assignments (Tables 1 & 2), band pairs were identified for each conformer and subsequently used to determine the energy difference between them. In a complicated vibrational spectrum, contributions of combination and overtone bands can vastly affect the results of the enthalpy determination. To minimize this effect, and for purposes of obtaining reproducible intensities, bands chosen for the energy difference determination should be in the lower wavenumber region and should be sufficiently resolved so that no other bands interfere. Therefore all bands chosen to determine the enthalpy difference were ones falling below 1300 cm<sup>-1</sup>.

In the variable temperature IR spectra of the xenon solutions, four bands at 1012, 1175, 1267 and 1297 cm<sup>-1</sup> for the *trans* conformer and two bands at 763 and 970 cm<sup>-1</sup> for the *gauche* conformer were used to determine the enthalpy difference. As previously mentioned, it is assumed that all four bands are free from impurities and have minimal mixing from other vibrational modes and were chosen because they were among the most well resolved bands in the spectra. The intensity for each band was measured in the temperature range from -100 to -55 °C, and the band pair ratios of the two conformers were determined and reported in Table 5. The enthalpy difference for each band pair was then used to determine the average enthalpy ratio. The statistical average, with a standard deviation of two sigma, was obtained by treating all the data as a single set, which yields

**Table 5.** Temperature and intensity ratios of the conformational bands of 2-methylbutane from the infrared spectra of the liquid xenon solution phase.

T(°C)	1/T ( $\times 10^3$ K <sup>-1</sup> )	I <sub>1012</sub> / I <sub>763</sub>	I <sub>1012</sub> / I <sub>970</sub>	I <sub>1175</sub> / I <sub>763</sub>	I <sub>1175</sub> / I <sub>970</sub>	I <sub>1267</sub> / I <sub>763</sub>	I <sub>1267</sub> / I <sub>970</sub>	I <sub>1297</sub> / I <sub>763</sub>	I <sub>1297</sub> / I <sub>970</sub>
-55.0	4.587	1.1156	1.1100	1.1357	1.1300	0.4975	0.4950	1.3317	1.3250
-60.0	4.692	1.1225	1.1010	1.1324	1.1106	0.4804	0.4712	1.2941	1.2692
-65.0	4.804	1.0609	1.0702	1.0478	1.0570	0.4522	0.4561	1.2348	1.2456
-70.0	4.923	1.0480	1.0565	1.0160	1.0242	0.4400	0.4435	1.1880	1.1976
-75.0	5.047	1.0036	1.0147	1.0109	1.0220	0.4203	0.4249	1.1449	1.1575
-80.0	5.177	1.0100	1.0134	0.9699	0.9732	0.4080	0.4094	1.1137	1.1174
-85.0	5.315	0.9817	0.9938	0.9421	0.9537	0.3841	0.3889	1.0549	1.0679
-90.0	4.460	0.9603	0.9686	0.9462	0.9543	0.3853	0.3886	1.0283	1.0371
-95.0	5.613	0.9553	0.9404	0.9105	0.8964	0.3737	0.3679	0.9974	0.9819
-100.0	5.775	0.9220	0.9175	0.8585	0.8544	0.3634	0.3617	0.9488	0.9442
$\Delta H^a$ (cm <sup>-1</sup> )		112 $\pm$ 9	112 $\pm$ 4	153 $\pm$ 1	153 $\pm$ 8	184 $\pm$ 13	185 $\pm$ 9	196 $\pm$ 6	196 $\pm$ 3

<sup>a</sup> Average value:  $\Delta H = 161 \pm 5$  cm<sup>-1</sup> ( $1.93 \pm 0.06$  kJ mol<sup>-1</sup>) with the *trans* conformer the more stable form and the statistical uncertainty ( $2\sigma$ ) obtained by utilizing all of the data as a single set.

a value of  $161 \pm 5 \text{ cm}^{-1}$  and indicates the *trans* conformer is the more stable form over the *gauche*. The percentage of the *gauche* conformer is estimated to be  $18 \pm 1\%$  at ambient temperature.

### Structural parameters

Many of the structural parameters for hydrocarbons, as well as many substituted ones, can be determined by adjusting the structural parameters obtained from the *ab initio* MP2(full)/6-311+G(d,p) calculations to fit the rotational constants obtained from microwave experimental data by using a computer program “A&M” (*Ab initio* and Microwave) developed in our laboratory.<sup>32</sup> In order to reduce the number of independent variables, the structural parameters are separated into sets according to their types. Bond lengths in the same set keep their relative ratio which results in a reduction of the number of independent variables. Also, the bond angles and torsional angles in the same set retain their differences in degrees. This assumption is based on the fact that errors from *ab initio* calculations are systematic. It has been shown<sup>33</sup> that *ab initio* MP2(full)/6-311+G(d,p) calculations have predicted the  $r_0$  structural parameters for more than fifty hydrocarbons, with the C-H distances predicted to better than  $0.002 \text{ \AA}$  when compared to the experimentally determined values from isolated C-H stretching frequencies. In another study, C-H bond distances determined from isolated C-H stretching frequencies were observed to be in good agreement with the same parameters determined from earlier microwave studies.<sup>34</sup> Therefore, all of the carbon-hydrogen distances can be taken from the MP2(full)/6-311+G(d,p) predicted values for the *trans* and *gauche* conformers of 2-methylbutane.

In the microwave study of 2-methylbutane,<sup>25</sup> the authors determined rotational

constants, dipole moments and centrifugal distortion constants for both the *trans* and *gauche* conformers. However, the investigators did not determine structural parameters in their study. Thus, it was found pertinent to determine the structural parameters for both *trans* and *gauche* conformers of 2-methylbutane molecule by utilizing the previously reported rotational constants.<sup>25</sup> To date, six rotational constants have been reported for 2-methyl butane - three for the *trans* conformer and three for the *gauche* conformer. By utilizing the three rotational constants for the *trans* conformer, only three structural parameters can be varied. Bond angles  $\angle C_4C_3C_2$ ,  $\angle C_5C_2C_3$ , and  $\angle C_6C_2C_3$  were allowed to vary, whereas bond distances  $r(C_2C_3)$ ,  $r(C_2C_5)$ ,  $r(C_2C_6)$ , and  $r(C_3C_4)$  are changed manually within a range of  $\pm 0.003 \text{ \AA}$  to get calculated rotational constants close to experimental values. Since the *gauche* conformer has  $C_s$  point group symmetry, calculation of the structural parameters for the *gauche* conformer are trivial in comparison to the *trans* conformer. For the *gauche* conformer, the bond distances  $r(C_2C_5)$  and  $r(C_2C_6)$  are kept in one set. Similarly, bond angles  $\angle C_5C_2C_3$  and  $\angle C_6C_2C_3$  were also kept in one set. Lastly, the bond angle  $\angle C_4C_3C_2$  was varied. Bond distances  $r(C_2C_3)$  and  $r(C_3C_4)$  were changed manually within the range of  $\pm 0.003 \text{ \AA}$  for fitting calculated rotational constants with experimental rotational constants. The final fit of the three rotational constants from the structural parameters listed in Table 6 have differences of 1.0, 0.7, and 1.1 MHz for the *trans* conformer. For the *gauche* form, differences are observed to be 0.9, 0.6, and 0.3 MHz. So we conclude that the final fit of rotational constants is reasonable for both conformers. For both *trans* and *gauche* conformers of 2-methylbutane, heavy atom bond lengths are well predicted by the B3LYP/6-311+G(d,p) basis set calculation, whereas heavy atom bond angles are well

predicted by the MP2/6-311+G(d,p) basis set calculation (Table 7).

**Table 6.** Comparison of rotational constants (MHz) obtained from *ab initio* MP2(full)/6-311+G(d,p) predictions, experimental values from microwave spectra, and from the adjusted  $r_0$  structural parameters for the *trans* and *gauche* conformers of 2-methylbutane.

	Rotational constant	MP2(full)/6-311+G(d,p)	Experimental [Ref. <sup>25</sup> ]	Adjusted $r_0$	$ \Delta $
<i>Trans</i>	A	7369.8	7303.4	7304.4	1.0
	B	3388.2	3361.3	3361.0	0.7
	C	2587.0	2568.1	2566.9	1.1
<i>Gauche</i>	A	6056.8	6029.5	6030.4	0.9
	B	3765.4	3738.8	3739.5	0.6
	C	3059.1	3038.2	3037.9	0.3

**Table 7.** Structural parameters (Å and degrees), rotational constants (MHz) and dipole moment (Debye) for 2-methylbutane.

Structural Parameters	Internal coordinates	MP2(full)/6-311+G(d,p)		B3LYP/6-311+G(d,p)		Adjusted $r_o$	
		<i>Trans</i>	<i>Gauche</i>	<i>Trans</i>	<i>Gauche</i>	<i>Trans</i>	<i>Gauche</i>
r (H <sub>1</sub> -C <sub>2</sub> )	r <sub>1</sub>	1.100	1.098	1.099	1.098	1.099 (2)	1.098 (2)
r (C <sub>2</sub> -C <sub>3</sub> )	R <sub>1</sub>	1.531	1.535	1.541	1.544	1.541 (3)	1.542 (3)
r (C <sub>3</sub> -C <sub>4</sub> )	R <sub>2</sub>	1.528	1.530	1.532	1.534	1.538 (3)	1.536 (3)
r (C <sub>2</sub> -C <sub>5</sub> )	R <sub>3</sub>	1.528	1.529	1.535	1.536	1.539 (3)	1.531 (3)
r (C <sub>2</sub> -C <sub>6</sub> )	R <sub>4</sub>	1.528	1.529	1.535	1.536	1.539 (3)	1.531 (3)
r (C <sub>3</sub> -H <sub>7</sub> )	r <sub>2</sub>	1.099	1.097	1.098	1.097	1.099 (2)	1.097 (2)
r (C <sub>3</sub> -H <sub>8</sub> )	r <sub>3</sub>	1.097	1.097	1.096	1.097	1.097 (2)	1.097 (2)
r (C <sub>4</sub> -H <sub>9</sub> )	r <sub>4</sub>	1.095	1.094	1.095	1.094	1.095 (2)	1.094 (2)
r (C <sub>4</sub> -H <sub>10</sub> )	r <sub>5</sub>	1.094	1.093	1.094	1.093	1.094 (2)	1.093 (2)
r (C <sub>4</sub> -H <sub>11</sub> )	r <sub>6</sub>	1.093	1.093	1.093	1.093	1.093 (2)	1.093 (2)
r (C <sub>5</sub> -H <sub>12</sub> )	r <sub>7</sub>	1.096	1.095	1.096	1.094	1.096 (2)	1.095 (2)
r (C <sub>5</sub> -H <sub>13</sub> )	r <sub>8</sub>	1.095	1.094	1.094	1.094	1.095 (2)	1.094 (2)
r (C <sub>5</sub> -H <sub>14</sub> )	r <sub>9</sub>	1.094	1.095	1.094	1.094	1.094 (2)	1.095 (2)
r (C <sub>6</sub> -H <sub>15</sub> )	r <sub>10</sub>	1.097	1.095	1.096	1.094	1.097 (2)	1.095 (2)
r (C <sub>6</sub> -H <sub>16</sub> )	r <sub>11</sub>	1.093	1.094	1.093	1.094	1.093 (2)	1.094 (2)
r (C <sub>6</sub> -H <sub>17</sub> )	r <sub>12</sub>	1.094	1.095	1.094	1.094	1.094 (2)	1.095 (2)
∠ H <sub>1</sub> C <sub>2</sub> C <sub>3</sub>	θ <sub>1</sub>	107.7	106.5	107.4	106.5	107.7 (5)	106.5 (5)
∠ H <sub>1</sub> C <sub>2</sub> C <sub>5</sub>	θ <sub>2</sub>	108.2	107.5	107.8	107.1	108.7 (5)	107.3 (5)
∠ H <sub>1</sub> C <sub>2</sub> C <sub>6</sub>	θ <sub>3</sub>	108.3	107.5	107.8	107.1	108.9 (5)	107.3 (5)
∠ C <sub>2</sub> C <sub>3</sub> C <sub>4</sub>	σ <sub>1</sub>	114.3	115.1	115.0	116.1	113.8 (5)	115.0 (5)
∠ C <sub>5</sub> C <sub>2</sub> C <sub>3</sub>	σ <sub>2</sub>	110.3	112.1	110.6	112.5	109.9 (5)	112.2 (5)
∠ C <sub>6</sub> C <sub>2</sub> C <sub>3</sub>	σ <sub>3</sub>	111.9	112.1	112.5	111.1	111.6 (5)	112.2 (5)
∠ C <sub>5</sub> C <sub>2</sub> C <sub>6</sub>	σ <sub>4</sub>	110.3	110.7	110.5	108.3	109.9 (5)	110.9 (5)
∠ H <sub>7</sub> C <sub>3</sub> C <sub>2</sub>	ψ <sub>1</sub>	108.5	108.4	108.7	108.3	108.5 (5)	108.4 (5)
∠ H <sub>8</sub> C <sub>3</sub> C <sub>2</sub>	ψ <sub>2</sub>	108.4	108.4	108.4	108.8	108.4 (5)	108.4 (5)
∠ H <sub>7</sub> C <sub>3</sub> C <sub>4</sub>	ψ <sub>3</sub>	109.7	109.0	109.5	108.8	110.0 (5)	109.1 (5)

**Table 7.--Continued.**

Structural Parameters	Internal coordinates	MP2(full)/6-311+G(d,p)		B3LYP/6-311+G(d,p)		Adjusted r <sub>o</sub>	
		<i>Trans</i>	<i>Gauche</i>	<i>Trans</i>	<i>Gauche</i>	<i>Trans</i>	<i>Gauche</i>
∠ H <sub>8</sub> C <sub>3</sub> C <sub>4</sub>	ψ <sub>4</sub>	109.1	109.0	108.7	108.8	109.4 (5)	109.1 (5)
∠ H <sub>7</sub> C <sub>3</sub> H <sub>8</sub>	φ <sub>1</sub>	106.4	106.4	106.0	105.9	106.4 (5)	106.4 (5)
∠ H <sub>9</sub> C <sub>4</sub> C <sub>3</sub>	λ <sub>1</sub>	110.6	110.3	111.1	110.4	110.6 (5)	110.4 (5)
∠ H <sub>10</sub> C <sub>4</sub> C <sub>3</sub>	λ <sub>2</sub>	110.9	111.6	110.9	111.9	110.9 (5)	111.6 (5)
∠ H <sub>11</sub> C <sub>4</sub> C <sub>3</sub>	λ <sub>3</sub>	111.7	111.6	112.1	111.9	111.7 (5)	111.6 (5)
∠ H <sub>9</sub> C <sub>4</sub> H <sub>10</sub>	δ <sub>1</sub>	107.9	107.5	107.5	107.3	107.9 (5)	107.5 (5)
∠ H <sub>9</sub> C <sub>4</sub> H <sub>11</sub>	δ <sub>2</sub>	107.9	107.5	107.7	107.3	108.0 (5)	107.5 (5)
∠ H <sub>10</sub> C <sub>4</sub> H <sub>11</sub>	δ <sub>3</sub>	107.6	108.5	107.3	107.8	107.6 (5)	108.1 (5)
∠ H <sub>12</sub> C <sub>5</sub> C <sub>2</sub>	β <sub>1</sub>	110.2	111.2	110.8	111.3	111.2 (5)	111.2 (5)
∠ H <sub>13</sub> C <sub>5</sub> C <sub>2</sub>	β <sub>2</sub>	111.2	111.2	111.4	111.7	111.2 (5)	111.2 (5)
∠ H <sub>14</sub> C <sub>5</sub> C <sub>2</sub>	β <sub>3</sub>	111.2	110.7	111.3	110.8	111.2 (5)	110.7 (5)
∠ H <sub>12</sub> C <sub>5</sub> H <sub>13</sub>	π <sub>1</sub>	108.0	108.1	107.7	107.8	108.0 (5)	108.1 (5)
∠ H <sub>12</sub> C <sub>5</sub> H <sub>14</sub>	π <sub>2</sub>	107.9	108.1	107.6	107.7	107.9 (5)	108.7 (5)
∠ H <sub>13</sub> C <sub>5</sub> H <sub>14</sub>	π <sub>3</sub>	108.2	107.5	107.8	107.3	108.2 (5)	107.5 (5)
∠ H <sub>15</sub> C <sub>6</sub> C <sub>2</sub>	β <sub>4</sub>	110.1	111.2	110.7	111.3	110.1 (5)	111.2 (5)
∠ H <sub>16</sub> C <sub>6</sub> C <sub>2</sub>	β <sub>5</sub>	112.1	111.2	112.2	111.7	112.1 (5)	111.2 (5)
∠ H <sub>17</sub> C <sub>6</sub> C <sub>2</sub>	β <sub>6</sub>	110.7	110.7	110.9	110.8	110.7 (5)	110.7 (5)
∠ H <sub>15</sub> C <sub>6</sub> H <sub>16</sub>	π <sub>4</sub>	108.1	108.1	107.8	107.8	108.1 (5)	108.1 (5)
∠ H <sub>15</sub> C <sub>6</sub> H <sub>17</sub>	π <sub>5</sub>	107.9	108.1	107.6	107.7	107.9 (5)	108.1 (5)
∠ H <sub>16</sub> C <sub>6</sub> H <sub>17</sub>	π <sub>6</sub>	107.7	107.5	107.4	107.3	107.7 (5)	107.5 (5)
τ H <sub>1</sub> C <sub>2</sub> C <sub>3</sub> C <sub>4</sub>	τ <sub>1</sub>	58.4	180.0	54.6	180.0	58.4 (5)	180.0
τ C <sub>5</sub> C <sub>2</sub> C <sub>3</sub> C <sub>4</sub>	τ <sub>2</sub>	176.3	62.6	172.0	63.2	176.7 (5)	62.8 (5)
τ C <sub>6</sub> C <sub>2</sub> C <sub>3</sub> C <sub>4</sub>	τ <sub>3</sub>	-60.5	-62.6	-63.9	-63.2	-61.1 (5)	-62.8 (5)
A		7369.8067	6056.8312	7267.6434	6026.0516	7304.3795 (7)	6030.4510 (7)
B		3388.2411	3765.4055	3325.2265	3684.8683	3361.0426 (6)	3739.4725 (6)
C		2587.0407	3059.1205	2542.5940	2987.0280	2566.9257 (6)	3037.8749 (6)

**Table 7.** --Continued.

Structural Parameters	Internal coordinates	MP2(full)/ 6-311+G(d,p)		B3LYP/6-311+G(d,p)		Adjusted r <sub>o</sub>	
		<i>Trans</i>	<i>Gauche</i>	<i>Trans</i>	<i>Gauche</i>	<i>Trans</i>	<i>Gauche</i>
μ <sub>a</sub>		0.035	0.012	0.038	0.014		
μ <sub>b</sub>		0.038	0.000	0.043	0.000		
μ <sub>c</sub>		0.077	0.126	0.080	0.143		
μ <sub>t</sub>		0.093	0.127	0.098	0.144		

## Discussion

When making vibrational assignments, it is important to have as close an agreement as possible between the predicted frequencies and experimental vibrational assignments. In order to quantitatively assess our vibrational assignment, the average and percent errors have been calculated between the predicted and observed frequencies for the CH<sub>2</sub> stretches of the *trans* and the *gauche* conformers of 2-methylbutane. For the *trans* conformer, the average error was 5.83 cm<sup>-1</sup>, which represents a per cent error of 0.33%. For the *gauche* conformer, the average error was 6.26 cm<sup>-1</sup>, which represents a per cent error of 0.34%. Therefore, we conclude that our predicted frequencies from *ab initio* calculations produced accurate reasonably results with respect to the vibrational assignments of the CH<sub>2</sub> stretches for both conformers.

Previous studies<sup>21,23,24</sup> of 2-methylbutane provided initial vibrational data that were used as an aid in this study; however, it is important to make some distinguishing remarks with respect to the vibrational studies performed in the present experiments. With the development of superior and more sensitive equipment, the vibrational spectra in this study, from a qualitative standpoint, are clearly more well resolved and show many more vibrational modes corresponding to the two conformers present in 2-methylbutane. Furthermore, we have provided a comprehensive vibrational study and were able to clearly distinguish and assign most of the vibrational modes to corresponding bands in the vibrational spectra. In one of the earliest vibrational studies of 2-methylbutane,<sup>23</sup> the authors assigned the bands at 1149 and 1176 cm<sup>-1</sup> to C-C stretching whereas in the present study, these bands are assigned to the CH<sub>3</sub> rocking ( $\nu_{32}$ )

and CH<sub>3</sub> wag ( $\nu_{31}$ ) modes for the *gauche* conformer, respectively. In a later study,<sup>24</sup> a shoulder band at 757 cm<sup>-1</sup> was observed apart from the band at 763 cm<sup>-1</sup> in the Raman spectrum of the gas at ambient temperatures, and that band subsequently disappeared in the spectrum of the solid phase and was attributed to the *gauche* conformer. In the current study, no prominent shoulder near the band at 762 cm<sup>-1</sup> was present in the Raman spectrum of the liquid. Therefore it is concluded that this peak only appears in gaseous phase. The result is possibly due to the fact that the barrier to internal rotation between the conformers (*i.e.* rotational isomers) is more relaxed, and thus, the substituent groups were able to rotate more freely in this state. In the liquid and solid phases of a sample, the barrier increases, thereby making the internal rotation between the two conformers somewhat more rigid.

Upon examination of the infrared spectra of the amorphous and annealed solid of 2-methylbutane (Fig. 5), the relative intensities of the bands, in particular the bands corresponding to the less stable *gauche* conformer, remained the same, and therefore little change had occurred in the spectra even after multiple attempts at annealing the solid. This same phenomenon had also been reported earlier by Szasz and Shepard<sup>23</sup> wherein they discussed the possibility of why relatively little change had occurred in the Raman spectra between cooling and solidification of the sample. In that study, the authors make two *ad hoc* assumptions to explain this peculiarity. The first assumption is that there is a large energy difference between the two rotational isomers and that a Fermi type resonance exists between some highly mixed modes, particularly at 366 and 415 cm<sup>-1</sup>. The second assumption was that there was a small energy difference between the two rotational isomers, and the presence of both isomers in the crystalline phase was made

possible by a frozen equilibrium between the two isomers, which creates a solid solution of the two conformers. In regards to the former assumption, this would be true only if the relative intensities of those mixed modes remained unchanged. However, in this study, there was relatively little change across the entire mid-infrared spectrum and therefore conclude that this assumption is highly unlikely. With respect to the determination of the energy difference between the two conformers in this study, the latter assumption is more likely due to the fact that multiple attempts to anneal the solid yielded very little change in the spectra between the amorphous and annealed solid phases of 2-methylbutane.

The enthalpy difference between the *trans* and *gauche* conformers of 2-methylbutane was determined to be  $161 \pm 5 \text{ cm}^{-1}$  ( $1.93 \pm 0.06 \text{ kJ mol}^{-1}$ ) with *trans* as the more stable form (Table 5). The average energy difference between the same conformers was determined to be  $267 \text{ cm}^{-1}$  ( $3.19 \text{ kJ mol}^{-1}$ ) and  $333 \text{ cm}^{-1}$  ( $3.98 \text{ kJ mol}^{-1}$ ) by the MP2 and B3LYP basis set calculations, respectively, with *trans* as the more stable form (Table 3). The energy difference prediction was observed to be 1.5 to 2 times higher than the average experimental enthalpy difference value. Previously, the enthalpy differences between the two conformers of 2-methylbutane were determined to be  $100 \pm 50 \text{ cal mol}^{-1}$  ( $35 \pm 17 \text{ cm}^{-1}$ ,  $0.42 \pm 0.20 \text{ kJ mol}^{-1}$ ),<sup>23</sup> and  $809 \pm 50 \text{ cal mol}^{-1}$  ( $283 \pm 17 \text{ cm}^{-1}$ ,  $9.68 \pm 0.60 \text{ kJ mol}^{-1}$ ),<sup>24</sup> by utilizing the Raman spectra of the sample in the liquid and vapor phases, respectively. In another study,<sup>35</sup> the enthalpy difference between the *trans* and *gauche* conformers was determined to be  $588 \text{ cal mol}^{-1}$  ( $205 \text{ cm}^{-1}$ ,  $2.46 \text{ kJ mol}^{-1}$ ) by utilizing infrared spectra of the sample in the gaseous state. Each time the *trans* conformer was observed to be the more stable form. We believe the enthalpy difference determined in the current study is more accurate compared to other studies because the

final enthalpy difference value is averaged from eight different band pairs. Additionally, energy differences predicted by MP2 and B3LYP basis set calculations are usually observed to be higher than the experimental enthalpy difference value.

With new insight into the conformational stability of 2-methylbutane using the data from the current study, 2-methylbutane can now be compared with other similar molecules such as 1,1-difluoropropane,<sup>36</sup> 1,1-dichloropropane,<sup>37</sup> and ethylcyclopropane.<sup>38</sup> For 1,1-difluoropropane and 1,1-dichloropropane, the enthalpy difference between the *gauche* and *trans* conformers was determined to be  $127 \pm 6 \text{ cm}^{-1}$  ( $1.52 \pm 0.07 \text{ kJ mol}^{-1}$ ) and  $216 \pm 160 \text{ cm}^{-1}$  ( $2.58 \pm 1.9 \text{ kJ mol}^{-1}$ ), respectively with *gauche* as the more stable form.<sup>36,37</sup> In case of 2-methylbutane, we followed the same nomenclature that was reported in the literature where, for the *trans* conformer, H<sub>1</sub> and H<sub>7/8</sub> are opposite to one another. However, for 1,1-difluoropropane and 1,1-dichloropropane, the authors reported the *gauche* conformation with the hydrogen of the halogen-substituted carbon and the vicinal hydrogens of the adjacent carbon to be opposite to one another.<sup>36,37</sup> As a result, when the authors reported the *gauche* conformer as the more stable form, it becomes the *trans* conformation using the same nomenclature as 2-methylbutane. Overall, the *trans* conformer is observed to be more stable form for 2-methylbutane, 1,1-difluoropropane and 1,1-dichloropropane. From our results, the enthalpy difference of 2-methylbutane falls between the enthalpy difference for 1,1-difluoropropane and 1,1-dichloropropane.

For ethylcyclopropane, in which C<sub>5</sub> and C<sub>6</sub> of 2-methylbutane are bonded to one another, the enthalpy difference between the *gauche* and *cis* conformers was determined to be  $385 \text{ cm}^{-1}$  ( $4.61 \text{ kJ mol}^{-1}$ ) with *gauche* as the most stable form.<sup>38</sup> However, similar to

1,1-difluoropropane and 1,1-dichloropropane, the nomenclature used for ethylcyclopropane is different from the nomenclature used for 2-methylbutane. Hence, *gauche* and *cis* conformers of ethylcyclopropane are equivalent to the *trans* and *gauche* conformers of 2-methylbutane, respectively.<sup>38</sup> Overall for ethylcyclopropane, the *trans* conformer is the more stable form. However, the enthalpy difference between the *trans* and *gauche* conformers of ethylcyclopropane is significantly larger compared to that of 2-methylbutane. The enthalpy difference of the ethylcyclopropane is larger probably due to the inflexibility of the cyclopropane ring when compared to isopropyl group of 2-methylbutane.

The adjusted  $r_0$  structural parameters of 2-methylbutane were compared with  $r_0$  structural parameters of 1,1-difluoropropane.<sup>39</sup> Since fluorine is the most electronegative atom in the periodic table, the C-C bond distances and bond angles should increase as fluorine atoms are substituted on carbon atoms. For the *trans* and *gauche* conformers of 2-methylbutane, the  $r(\text{C}_2\text{-C}_3)$  and  $r(\text{C}_3\text{-C}_4)$  bond distances were increased by 0.036 and 0.016 Å compared to the same bond distances of the *trans* and *gauche* conformers of 1,1-difluoropropane. Similarly,  $\angle\text{C}_2\text{C}_3\text{C}_4$  and  $\angle\text{FCF}$  were increased by 1.6 and 2.7°, respectively, for the *trans* conformer of 2-methylbutane. For the *gauche* conformer, the same angles were increased by 2.1 and 3.6°. Therefore, the change in structural parameters, when fluorine atoms of 1,1-difluoropropane are substituted on the carbon atoms, they behave as predicted.

The barriers and potential function governing the asymmetric rotor motion was predicted from the MP2(full)/6-31G(d) calculations, with the energy difference predicted to be 281  $\text{cm}^{-1}$  between the *trans* and *gauche* conformers (Table 3). The *trans* to *trans*

barrier was predicted to be 1725 cm<sup>-1</sup> and the *trans* to *gauche* barrier to be 1820 cm<sup>-1</sup> (Fig. 8). It is possible to obtain values for four terms of the potential constants of the potential function governing the internal rotation of the 2-methylbutane, which has the form:

$$V(\theta) = \frac{1}{2} \sum_{i=1}^4 V_i (1 - \cos i\theta)$$

The series coefficients,  $V_i$ , in the above equation, were determined by the non-linear least-squares fitting of the predicted energy differences and the torsional dihedral angles for the *trans* (-65.0 and 180.0°) and *gauche* (57.4°) conformers and the three transition states (123.0, 0.0 and -121.0°). The potential is essentially a three-fold internal rotation function (1988 cm<sup>-1</sup> barrier) with the following values for the first four terms of the potential function:  $V_1 = -263.36$ ,  $V_2 = -230.55$ ,  $V_3 = -1714.8$ , and  $V_4 = 134.91$  cm<sup>-1</sup>. These predicted values are expected to be reasonably near the unknown experimental ones that would be obtained from the frequencies of the asymmetric torsional modes from the two conformers.

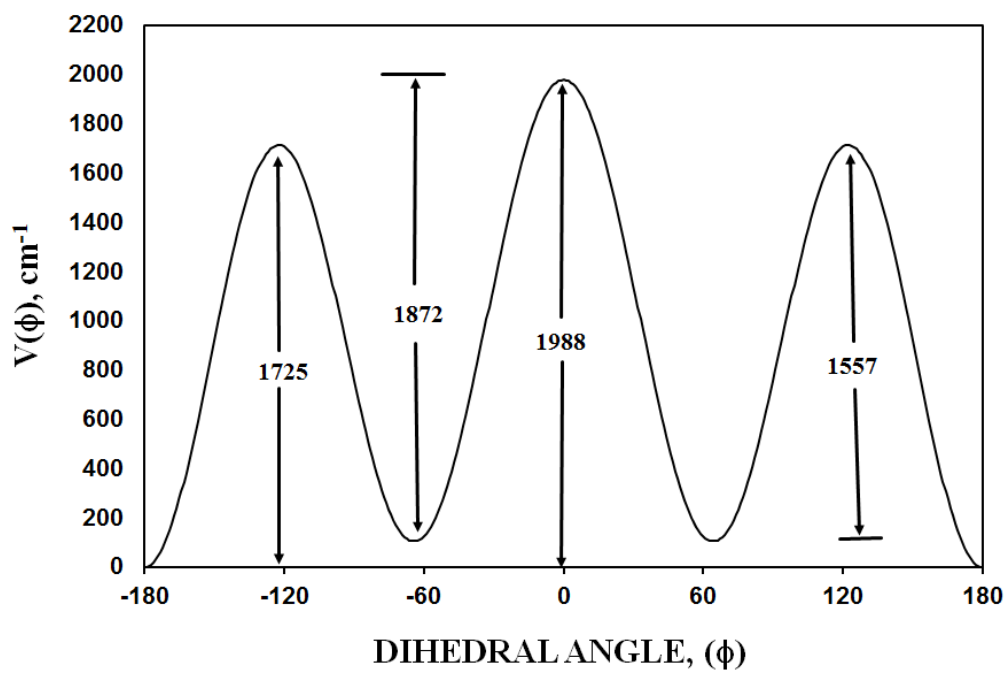


**Fig. 8** Potential energy function (MP2(full)) governing the internal rotation of the 2-methylbutane from the *gauche* ( $57.4^\circ$ ) to the *trans* ( $-65.0$  and  $180^\circ$ ) form.

To summarize this study, a complete vibrational assignment has been reported for the *trans* and *gauche* conformers of 2-methylbutane. The enthalpy difference between the *trans* and *gauche* conformers of 2-methylbutane is determined to be  $161 \pm 5 \text{ cm}^{-1}$  ( $1.93 \pm 0.06 \text{ kJ mol}^{-1}$ ) with the *trans* conformer as the more stable form. Additionally, adjusted  $r_0$  structural parameters have been reported for both conformers of 2-methylbutane.

(Manuscript of this work is in preparation.)

## CHAPTER 4

### r<sub>0</sub> STRUCTURAL PARAMETERS, CONFORMATIONAL, VIBRATIONAL STUDIES AND *AB INITIO* CALCULATIONS STUDIES OF CYANOCYCLOPENTANE

#### Introduction

Some very interesting results were observed in the spectroscopic study of monosubstituted cyclopentane derivatives like fluoro, chloro, bromo, ethynyl and isocyanocyclopentane. From earlier studies, it was concluded that fluorocyclopentane exists in the *envelope-axial* (*Ax*) form.<sup>40</sup> In further studies of chloro and bromo cyclopentane, the *Ax* conformer was found to be the most stable form of both molecules, with an enthalpy difference of  $145 \pm 15 \text{ cm}^{-1}$  ( $1.73 \pm 0.18 \text{ kJ/mol}$ ) for chlorocyclopentane<sup>41</sup> and enthalpy difference of  $233 \pm 23 \text{ cm}^{-1}$  ( $2.79 \pm 0.28 \text{ kJ/mol}$ ) for bromocyclopentane.<sup>42</sup> At ambient temperature, chlorocyclopentane exhibits  $67 \pm 2\%$  of the *Ax* conformer and for bromocyclopentane  $75 \pm 2\%$  of the molecules are estimated to be in the *Ax* form.<sup>41,42</sup> Later, in a detailed spectroscopic study of fluorocyclopentane, the *twist* conformer was observed to be the most stable conformer.<sup>43</sup> From a comparison of conformational stability data obtained for fluoro and chlorocyclopentane, as the atomic size of substituents on the cyclopentane ring increases the conformational stability of the molecules changed from the *twist* to the *Ax* form. Similarly for chloro and bromocyclopentane as the atomic size increases the enthalpy difference between the two conformers also increases.

In a recent study of ethynylcyclopentane, the *Eq* conformer was observed to be the most stable form with an enthalpy difference of  $94 \pm 9 \text{ cm}^{-1}$  ( $1.12 \pm 0.11 \text{ kJ/mol}$ ) and at ambient temperature  $62 \pm 1\%$  of the conformer is present in the *Eq* form.<sup>44</sup> However, for isocyanocyclopentane, the *Ax* conformer was observed to be the most stable form

with the enthalpy difference of  $102 \pm 10 \text{ cm}^{-1}$  ( $1.21 \pm 0.11 \text{ kJ/mol}$ ), and at ambient temperature  $62 \pm 1\%$  is estimated as the abundance of the *Ax* form.<sup>45</sup> Thus in the study of ethynylcyclopentane and isocyanocyclopentane, two different conformers were observed to be the most stable form.

In the microwave study of normal and 1-D isotopic species of cyanocyclopentane, the *Ax* and *Eq* conformers were observed and rotational constants were reported for both conformers.<sup>46</sup> By utilizing rotational constants obtained from the microwave study, the authors also determined structural parameters for both *Ax* and *Eq* conformers of cyanocyclopentane. Based on relative intensity measurements, the ground state energy difference between the *Ax* and *Eq* conformers was reported to be  $0 \pm 200 \text{ cal/mol}$  ( $0 \pm 70 \text{ cm}^{-1}$ ).<sup>46</sup> The reported enthalpy difference between the two conformers of cyanocyclopentane is very low compared to the enthalpy differences obtained for other similar molecules like fluoro, chloro, bromo, ethynyl and isocyanocyclopentane. Additionally, the authors were not able to determine the most stable conformer, but they proposed that *Eq* conformer may be the most stable form.<sup>46</sup> In another infrared study of cyanocyclopentane carried out at variable temperatures, the authors reported the *Ax* conformer to be most stable form with an enthalpy difference of  $109 \pm 37 \text{ cm}^{-1}$  ( $312 \pm 106 \text{ cal/mol}$ ), and at ambient temperature, the *Ax* conformer was estimated to be  $59 \pm 7\%$  abundant.<sup>47</sup> However, in this infrared study the vibrational assignments were made for both *Ax* and *Eq* conformers, but the assignments were incomplete. Also, in determination of the enthalpy difference between the two conformers of cyanocyclopentane, the authors used only one band pair from the infrared spectrum of the sample dissolved in liquid Xe solution.<sup>47</sup> Hence, the results obtained from this infrared study of cyanocyclopentane are

somewhat suspect, and therefore, we have reinvestigated the conformational stability and enthalpy difference between the *Eq* and *Ax* conformers (Fig. 9) of cyanocyclopentane. Results obtained from this investigation will be useful for understanding the effect of the  $C\equiv N$  group on conformational stability and enthalpy difference between different conformers of cyanocyclobutane, cyanocyclopentane, and cyanocyclohexane. Additionally, this study will be also helpful for understanding the effect of different substituents on the cyclopentane ring.

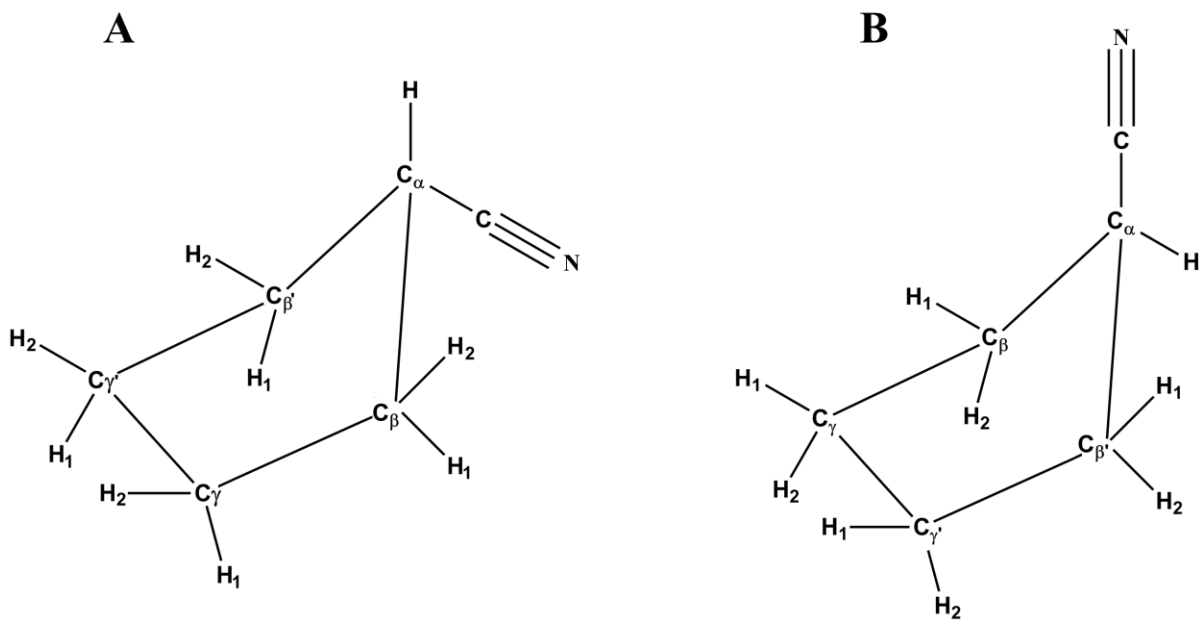


**Fig. 9** Conformers of cyanocyclopentane (A) *Eq*; (B) *Ax*.

For identifying fundamental vibrational modes of cyanocyclopentane, the Raman spectrum of the liquid and infrared spectra of the gas, amorphous and annealed spectra of solid were also investigated. For the determination of the enthalpy difference between the two possible conformers, the infrared spectra of the sample at varying temperatures in xenon solution was also investigated. To support the vibrational study, *ab initio* calculations with basis sets up to aug-cc-pVTZ as well as those with diffuse functions, *i.e.*, 6-311+G(2df,2pd), have been carried out. Density functional theory (DFT) calculations by the B3LYP method with the same basis sets have also been performed. Optimized geometries, conformational stabilities, harmonic force fields, infrared intensities, Raman activities, and depolarization ratios are also calculated. The results of these spectroscopic, structural, and theoretical studies of cyanocyclopentane are reported herein.

## Methods

The sample of cyanocyclopentane was purchased from Alfa Aesar, with a stated purity of  $\geq 98\%$ . The sample was further purified by using a low-temperature, low-pressure fractionation column. The purity of the sample was checked and verified by the infrared spectra obtained.

The mid-infrared spectrum of cyanocyclopentane in the gas and solid phase (Fig. 10 and 11) were obtained from 3100 to 400  $\text{cm}^{-1}$  on a Perkin-Elmer model 2000 Fourier transform spectrometer. The mid-infrared spectra (3100 to 400  $\text{cm}^{-1}$ ) of the sample dissolved in liquefied xenon (Fig. 10B) at ten different temperatures (-60 to -100 °C) were recorded on a Bruker model IFS-66 Fourier transform spectrometer. The Raman spectra (Fig. 12) of cyanocyclopentane in the liquid state were recorded on a

Spex model 1403 spectrophotometer equipped with a Spectra-Physics model 2017 laser. All of the observed bands in the Raman spectra of the liquid along with their proposed assignments and depolarization values are listed in Tables 8 and 9. The predicted conformational energy differences calculated from *ab initio* calculations by using the Møller-Plesset perturbation method to the second order (MP2) with full electron correlation, as well as with density functional theory by the B3LYP method with different basis sets are listed in Table 10. The experimental methods of recording infrared and Raman spectra are provided in detail in Chapter 2.

In order to obtain descriptions of the molecular motions involved in the fundamental modes of cyanocyclopentane, a normal coordinate analysis was carried out. The force field in Cartesian coordinates was obtained with the Gaussian 03 program at the MP2(full) level with the 6-31G(d) basis set (see Chapter 2). The internal coordinates used to calculate the B and G matrices are given for the *Eq* and *Ax* conformers in Table 11. By using the B matrix<sup>48</sup>, the force field in Cartesian coordinates was converted to force constants in internal coordinates. Subsequently, a scaling factor of 0.88 was used for the CH stretches and deformations, and scaling factor of 0.90 was used for all other modes except for the heavy atom bends and  $\text{-C}\equiv\text{N}$  stretch to obtain the fixed scaled force constants and resultant wavenumbers. A set of symmetry coordinates was used (Table 11) to determine the corresponding potential energy distributions (P.E.D.s). A comparison between the observed and calculated wavenumbers, along with the calculated infrared intensities, Raman activities, depolarization ratios, and potential energy distributions for the *Eq* and *Ax* conformers of cyanocyclopentane are given in Tables 8 and 9, respectively.

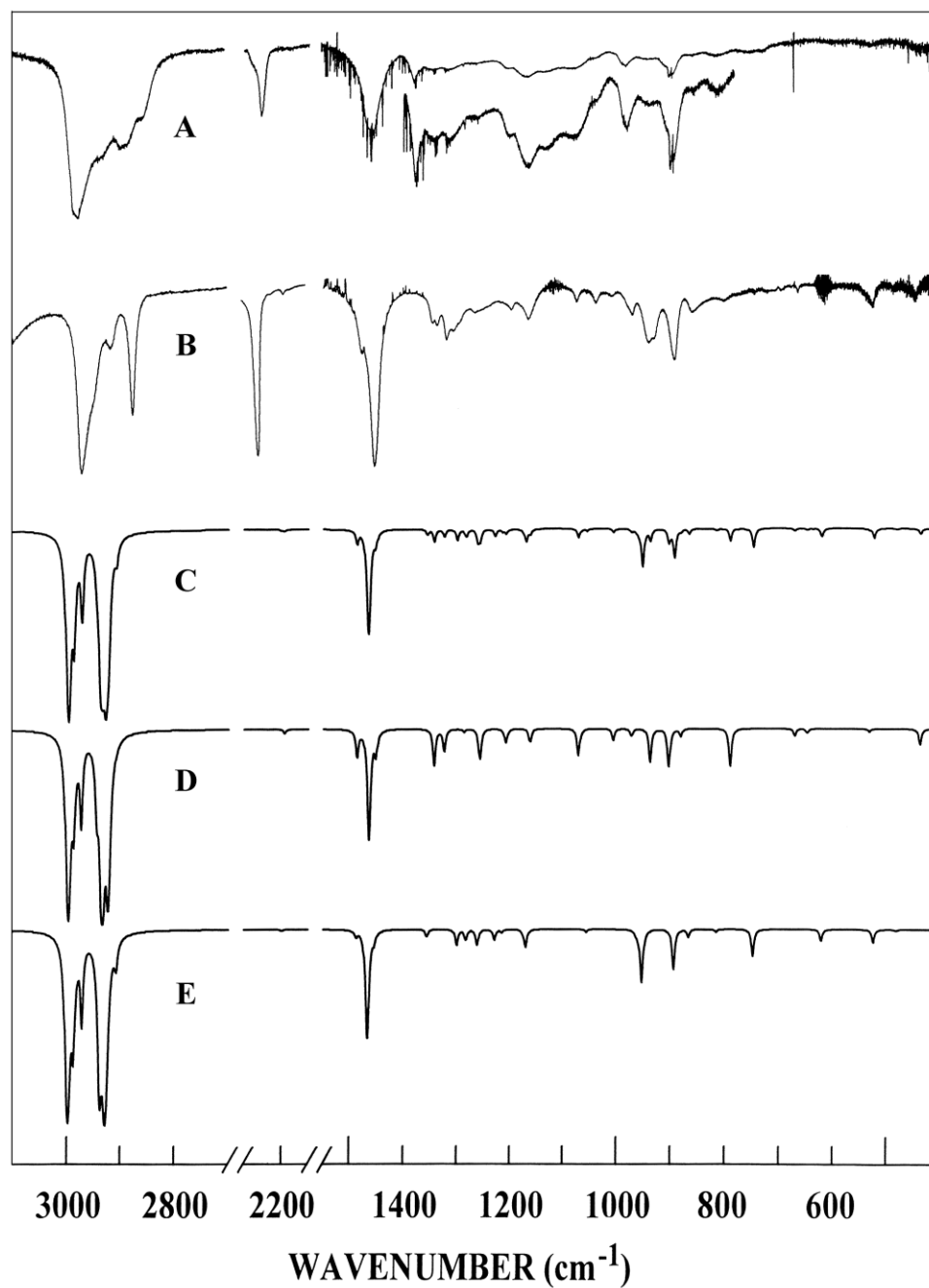


**Fig. 10** Comparison of experimental and calculated infrared spectra of cyanocyclopentane: (A) observed spectrum of the gas; (B) observed spectrum of the Xe solution at  $-70\text{ }^{\circ}\text{C}$ ; (C) simulated spectrum of a mixture of *Eq* and *Ax* conformers ( $\Delta H = 55\text{ cm}^{-1}$ ) at  $25\text{ }^{\circ}\text{C}$ ; (D) simulated spectrum of the *Ax* conformer; (E) simulated spectrum of the *Eq* conformer.

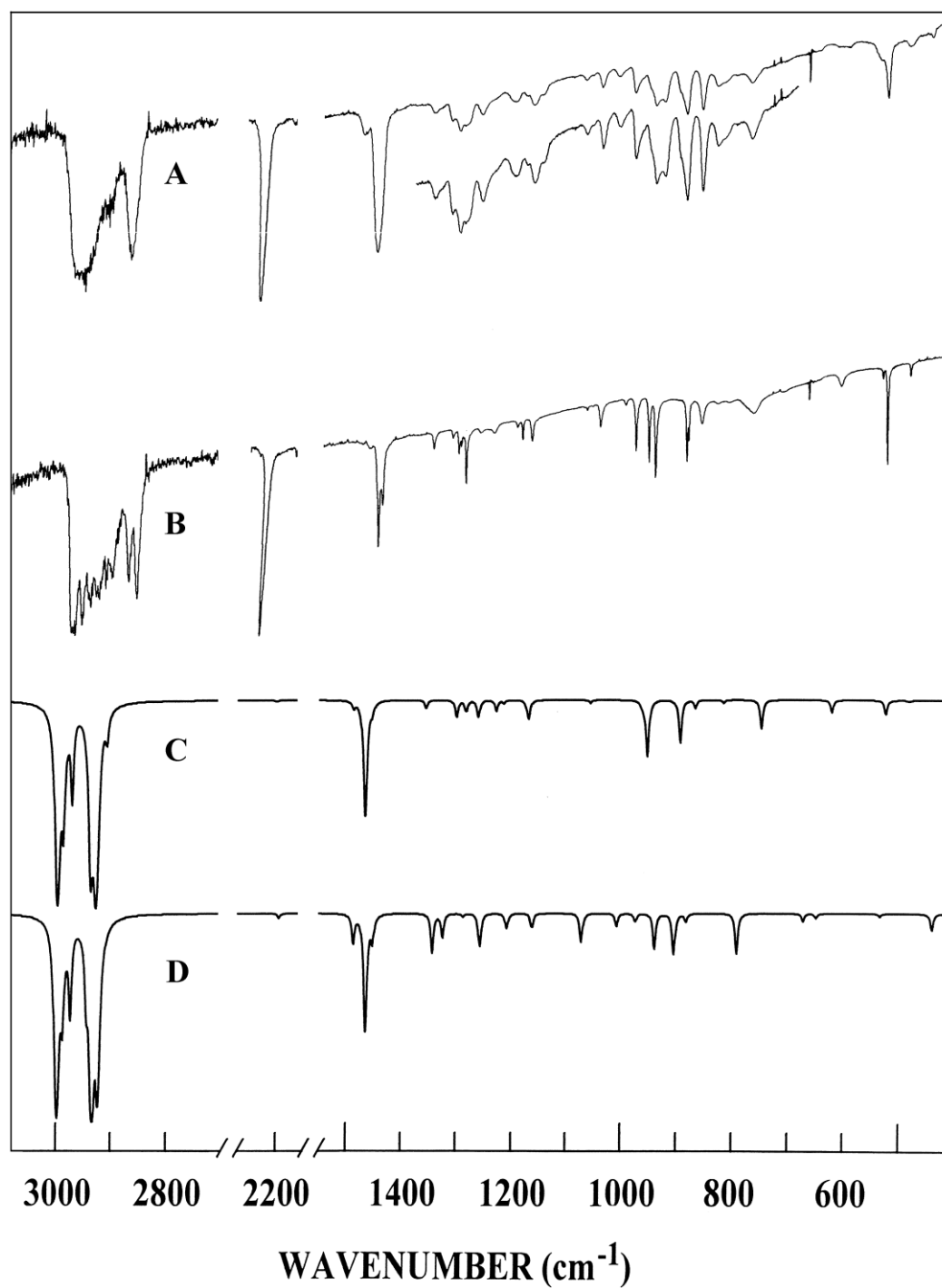


**Fig. 11** Comparison of experimental and calculated infrared spectra of cyanocyclopentane: (A) observed spectrum of the amorphous solid; (B) observed spectrum of the annealed solid; (C) simulated spectrum of the *Eq* conformer; (D) simulated spectrum of the *Ax* conformer.

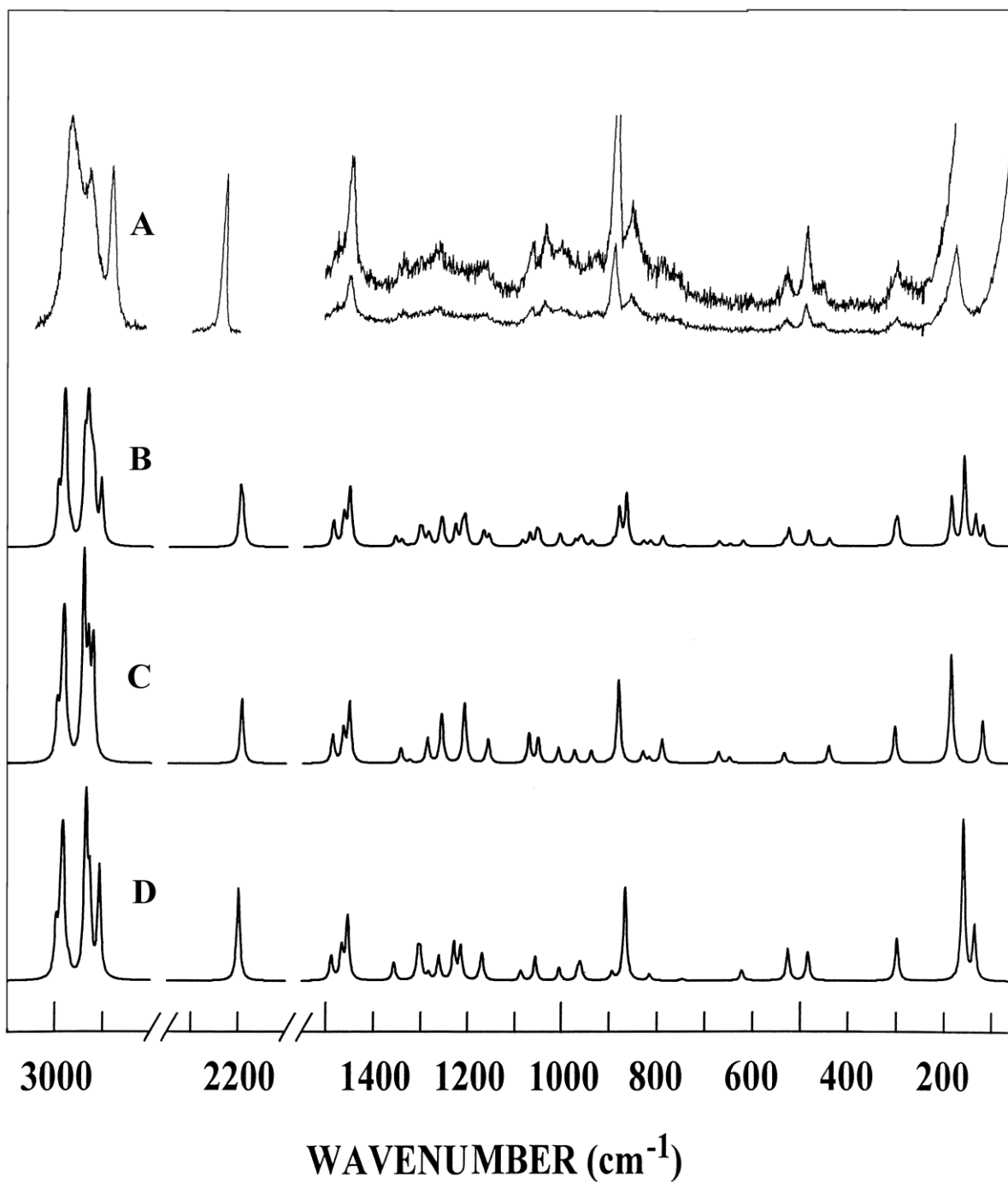


**Fig. 12** Comparison of experimental and calculated Raman spectra of cyanocyclopentane: (A) observed spectrum of the liquid; (B) simulated spectrum of a mixture of *Eq* and *Ax* conformers ( $\Delta H = 55 \text{ cm}^{-1}$ ) at  $25 \text{ }^\circ\text{C}$ ; (C) simulated spectrum of the *Ax* conformer; (D) simulated spectrum of the *Eq* conformer.

**Table 8.** Observed and calculated<sup>a</sup> frequencies (cm<sup>-1</sup>) and potential energy distributions (P.E.D.s) for the *Eq* (C<sub>s</sub>) conformer of cyanocyclopentane.

Vib. No.	Approx. description	<i>ab initio</i>	Fixed scaled <sup>b</sup>	IR int.	Raman act.	dp ratio	Infrared				Raman liquid	P.E.D. <sup>c</sup>	Band Contour		
							gas	Xe soln.	Solid amph	Solid annealed			A	B	C
A' v <sub>1</sub>	γ-CH <sub>2</sub> antisymmetric stretch	3194	2998	43.5	50.6	0.73	2973	2973	2968	2972	2971	61S <sub>1</sub> ,37S <sub>2</sub>	1	-	99
v <sub>2</sub>	β-CH <sub>2</sub> antisymmetric stretch	3180	2984	1.2	117.8	0.45	2973	2973	2968	2972	2971	56S <sub>2</sub> ,36S <sub>1</sub>	95	-	5
v <sub>3</sub>	γ-CH <sub>2</sub> symmetric stretch	3131	2937	24.8	172.1	0.04	2941	2947	2939	2940	2945	91S <sub>3</sub>	99	-	1
v <sub>4</sub>	β-CH <sub>2</sub> symmetric stretch	3123	2929	20.9	53.5	0.24	2930	2947	2928	2928	2928	86S <sub>4</sub>	49	-	51
v <sub>5</sub>	α-CH stretch	3100	2908	1.8	106.9	0.24	2886	2876	2873	2873	2873	84S <sub>5</sub>	0	-	100
v <sub>6</sub>	C≡N stretch	2214	2200	0.1	57.7	0.29	2237	2243	2238	2239	2238	89S <sub>6</sub> ,11S <sub>15</sub>	87	-	13
v <sub>7</sub>	γ-CH <sub>2</sub> deformation	1583	1488	0.4	8.5	0.68	1477	1477	1477	1479	1477	71S <sub>7</sub> ,28S <sub>8</sub>	54	-	46
v <sub>8</sub>	β-CH <sub>2</sub> deformation	1560	1467	8.1	7.3	0.74	1467	1463	1466	1466	1467	71S <sub>8</sub> ,29S <sub>7</sub>	34	-	66
v <sub>9</sub>	β-CH <sub>2</sub> rock	1425	1356	0.5	5.7	0.57	1349	1347	1347	1349	1348	41S <sub>9</sub> ,36S <sub>11</sub>	96	-	4
v <sub>10</sub>	γ-CH <sub>2</sub> rock	1374	1305	0.0	8.0	0.75	-	-	-	-	1301	58S <sub>10</sub> ,24S <sub>12</sub>	51	-	49
v <sub>11</sub>	α-CH bend (in-plane)	1350	1283	0.7	2.0	0.72	1286	1286	1284	1282	1282	31S <sub>11</sub> ,25S <sub>9</sub> ,24S <sub>13</sub>	29	-	71
v <sub>12</sub>	β-CH <sub>2</sub> twist	1275	1215	0.2	9.1	0.73	1214	1214	1211	1212	1214	47S <sub>12</sub> ,19S <sub>10</sub> ,11S <sub>17</sub>	74	-	26
v <sub>13</sub>	γ-CH <sub>2</sub> twist	1230	1170	1.2	6.7	0.49	1165	1169	1168	1171	1169	41S <sub>13</sub> ,15S <sub>9</sub> ,13S <sub>11</sub>	86	-	14
v <sub>14</sub>	Ring deformation	1109	1057	0.2	5.6	0.72	1047	1039	1047	1046	1047	25S <sub>14</sub> ,20S <sub>17</sub> ,12S <sub>10</sub>	99	-	1
v <sub>15</sub>	C-C stretch	1053	1005	0.0	2.9	0.24	-	-	-	-	999	36S <sub>15</sub> ,28S <sub>14</sub> ,15S <sub>18</sub>	94	-	6
v <sub>16</sub>	β-CH <sub>2</sub> wag	1008	960	0.4	3.1	0.26	957	941	957	958	957	33S <sub>16</sub> ,28S <sub>23</sub>	0	-	100
v <sub>17</sub>	Ring deformation	930	894	3.0	1.5	0.05	888	891	889	889	893	48S <sub>17</sub> ,19S <sub>14</sub>	96	-	4
v <sub>18</sub>	Ring breathing	903	867	0.5	16.7	0.09	-	860	861	861	859	53S <sub>18</sub> ,12S <sub>16</sub> ,11S <sub>21</sub>	97	-	3
v <sub>19</sub>	γ-CH <sub>2</sub> wag	787	748	1.9	0.3	0.15	747	-	-	-	747	81S <sub>19</sub>	2	-	98
v <sub>20</sub>	Ring-CN bend (in-plane)	537	526	0.9	2.1	0.35	526	524	528	528	525	35S <sub>20</sub> ,28S <sub>23</sub> ,11S <sub>16</sub> ,10S <sub>21</sub>	65	-	35
v <sub>21</sub>	Ring deformation	495	484	0.1	2.4	0.23	488	486	487	487	488	51S <sub>21</sub> ,22S <sub>15</sub>	83	-	17
v <sub>22</sub>	Ring puckering	301	299	1.1	1.8	0.71	-	-	-	-	297	50S <sub>22</sub> , 36S <sub>20</sub>	31	-	69
v <sub>23</sub>	C-C≡N bend(in-plane)	137	136	3.9	1.2	0.70	-	-	-	-	-	40S <sub>23</sub> ,35S <sub>22</sub> ,22S <sub>20</sub>	8	-	92
A'' v <sub>24</sub>	β-CH <sub>2</sub> antisymmetric stretch	3186	2988	10.8	70.8	0.75	2973	2973	2968	2972	2971	80S <sub>24</sub> ,16S <sub>25</sub>	-	100	-
v <sub>25</sub>	γ-CH <sub>2</sub> antisymmetric stretch	3168	2972	7.6	12.1	0.75	2973	2973	2968	2972	2971	79S <sub>25</sub> ,13S <sub>24</sub>	-	100	-
v <sub>26</sub>	γ-CH <sub>2</sub> symmetric stretch	3121	2928	22.3	23.8	0.75	2930	2947	2928	2928	2928	91S <sub>26</sub>	-	100	-
v <sub>27</sub>	β-CH <sub>2</sub> symmetric stretch	3119	2926	8.0	11.8	0.75	2930	2947	2928	2928	2928	90S <sub>27</sub>	-	100	-

Table 8.--Continued

Vib. No.	Approx. description	<i>ab initio</i>	Fixed scaled <sup>b</sup>	IR int.	Raman act.	dp ratio	Infrared				Raman liquid	P.E.D. <sup>c</sup>	Band Contour		
							gas	Xe soln.	Solid amph	Solid annealed			A	B	C
v <sub>29</sub>	β-CH <sub>2</sub> deformation	1546	1454	0.6	21.8	0.75	1453	1453	1454	1453	1454	68S <sub>29</sub> ,33S <sub>28</sub>	-	100	-
v <sub>30</sub>	γ-CH <sub>2</sub> rock	1383	1313	0.0	0.0	0.75	-	-	-	-	1312	49S <sub>30</sub> ,20S <sub>32</sub> ,10S <sub>34</sub>	-	100	-
v <sub>31</sub>	α-CH bend (out-of-plane)	1369	1300	1.1	7.1	0.75	1302	1304	1301	1303	1301	44S <sub>31</sub> ,24S <sub>30</sub> ,12S <sub>34</sub> ,10S <sub>32</sub>	-	100	-
v <sub>32</sub>	β-CH <sub>2</sub> rock	1329	1261	1.1	7.0	0.75	1263	1264	1261	1263	1261	30S <sub>32</sub> ,29S <sub>33</sub> ,20S <sub>31</sub> ,16S <sub>30</sub>	-	100	-
v <sub>33</sub>	γ-CH <sub>2</sub> twist	1293	1229	0.7	10.3	0.75	1228	-	1227	-	1228	52S <sub>33</sub> ,28S <sub>32</sub>	-	100	-
v <sub>34</sub>	β-CH <sub>2</sub> twist	1235	1175	0.2	1.1	0.75	1171	1169	1173	1173	1171	40S <sub>34</sub> ,26S <sub>37</sub> ,11S <sub>38</sub>	-	100	-
v <sub>35</sub>	Ring deformation	1135	1088	0.0	2.5	0.75	-	-	-	-	1088	46S <sub>35</sub> ,16S <sub>39</sub> ,16S <sub>36</sub> ,10S <sub>37</sub>	-	100	-
v <sub>36</sub>	Ring deformation	1010	965	0.2	2.0	0.75	957	941	958	958	962	29S <sub>36</sub> ,24S <sub>35</sub> ,18S <sub>34</sub>	-	100	-
v <sub>37</sub>	γ-CH <sub>2</sub> wag	995	953	4.0	0.2	0.75	949	941	946	946	948	22S <sub>37</sub> ,22S <sub>36</sub> ,19S <sub>38</sub> ,15S <sub>31</sub>	-	100	-
v <sub>38</sub>	β-CH <sub>2</sub> wag	854	816	0.2	1.0	0.75	817	-	816	811	817	44S <sub>38</sub> ,19S <sub>37</sub> ,16S <sub>39</sub> ,11S <sub>35</sub>	-	100	-
v <sub>39</sub>	Ring deformation	636	622	0.8	1.2	0.75	611	-	610	610	611	58S <sub>39</sub> ,17S <sub>38</sub>	-	100	-
v <sub>40</sub>	C≡N bend(out-of-plane)	528	526	0.0	0.9	0.75	-	-	-	-	525	49S <sub>40</sub> ,33S <sub>41</sub> ,10S <sub>30</sub>	-	100	-
v <sub>41</sub>	Ring-CN bend (out-of-plane)	160	160	5.0	2.5	0.75	-	-	-	-	161	51S <sub>41</sub> ,47S <sub>40</sub>	-	100	-
v <sub>42</sub>	Ring twisting	36	36	0.1	0.0	0.75	-	-	-	-	-	94S <sub>42</sub>	-	100	-

<sup>a</sup>MP2(full)/6-31G(d) *ab initio* calculations, scaled frequencies, infrared intensities (km/mol), Raman activities (Å<sup>4</sup>/u) and potential energy distributions (P.E.D.s)

<sup>b</sup>Scaled *ab initio* calculations with factors of 0.88 for CH<sub>2</sub> stretches and CH<sub>2</sub> deformations, 0.90 for all other modes except torsions, heavy atom bends and C≡N stretch.

<sup>c</sup>Symmetry coordinates with P.E.D. contributions less than 10% are omitted.

**Table 9.** Observed and calculated<sup>a</sup> frequencies (cm<sup>-1</sup>) and potential energy distributions (P.E.D.s) for the *A<sub>x</sub>* (C<sub>s</sub>) conformer of cyanocyclopentane.

Vib. No.	Approx. description	<i>ab initio</i>	Fixed scaled <sup>b</sup>	IR int.	Raman act.	dp ratio	Infrared				Raman liquid	P.E.D. <sup>c</sup>	Band Contour		
							gas	Xe soln.	Solid amorphous	Solid annealed			A	B	C
A' v <sub>1</sub>	γ-CH <sub>2</sub> antisymmetric stretch	3196	2998	41.4	50.0	0.74	2973	2973	2968	2972	2971	74S <sub>1</sub> ,26S <sub>2</sub>	83	-	17
v <sub>2</sub>	β-CH <sub>2</sub> antisymmetric stretch	3181	2984	0.6	119.3	0.54	2973	2973	2968	2972	2971	67S <sub>2</sub> ,25S <sub>1</sub>	0	-	100
v <sub>5</sub>	α-CH stretch	3139	2944	5.2	196.7	0.08	2941	2947	2939	2940	2945	93S <sub>5</sub> ,11S <sub>3</sub>	6	-	94
v <sub>3</sub>	γ-CH <sub>2</sub> symmetric stretch	3134	2934	31.2	71.9	0.10	2930	2917	2928	2928	2928	88S <sub>3</sub> ,11S <sub>5</sub>	27	-	73
v <sub>4</sub>	β-CH <sub>2</sub> symmetric stretch	3117	2924	19.5	101.8	0.25	2930	2917	2928	2928	2928	84S <sub>4</sub>	17	-	83
v <sub>6</sub>	C≡N stretch	2209	2195	0.3	40.4	0.27	2237	2243	2238	2239	2238	90S <sub>6</sub> ,10S <sub>15</sub>	2	-	98
v <sub>7</sub>	γ-CH <sub>2</sub> deformation	1582	1487	1.9	10.0	0.67	1477	1477	1477	1479	1479	80S <sub>7</sub> ,20S <sub>8</sub>	40	-	6
v <sub>8</sub>	β-CH <sub>2</sub> deformation	1558	1465	6.9	5.9	0.74	1463	1463	1463	1463	1463	80S <sub>8</sub> ,20S <sub>7</sub>	7	-	93
v <sub>11</sub>	α-CH bend (in-plane)	1412	1343	2.7	4.7	0.65	1341	1336	1341	1343	1341	44S <sub>11</sub> ,27S <sub>12</sub>	100	-	0
v <sub>9</sub>	β-CH <sub>2</sub> rock	1392	1324	1.1	0.7	0.41	1314	1317	1316	1314	1314	56S <sub>9</sub> ,28S <sub>10</sub>	7	-	93
v <sub>10</sub>	γ-CH <sub>2</sub> rock	1354	1287	0.2	7.5	0.63	1291	1292	1292	1290	1291	29S <sub>10</sub> ,24S <sub>13</sub> ,14S <sub>11</sub> ,11S <sub>19</sub>	4	-	96
v <sub>12</sub>	β-CH <sub>2</sub> twist	1270	1209	0.9	15.7	0.73	1201	1197	1190	1203	1198	31S <sub>12</sub> ,23S <sub>10</sub> ,12S <sub>13</sub>	86	-	14
v <sub>13</sub>	γ-CH <sub>2</sub> twist	1220	1163	0.9	0.4	0.19	1164	1164	1163	1162	1164	32S <sub>13</sub> ,28S <sub>11</sub> ,11S <sub>12</sub>	22	-	78
v <sub>14</sub>	Ring deformation	1105	1052	0.0	5.8	0.72	-	-	-	-	1041	34S <sub>14</sub> ,23S <sub>17</sub> ,12S <sub>10</sub>	66	-	34
v <sub>15</sub>	C-C stretch	1022	974	0.5	2.7	0.44	972	970	970	-	972	17S <sub>15</sub> ,23S <sub>13</sub> ,12S <sub>14</sub> ,12S <sub>12</sub> ,11S <sub>9</sub>	16	-	84
v <sub>17</sub>	Ring deformation	982	939	2.4	2.5	0.24	930	930	929	-	927	34S <sub>17</sub> ,23S <sub>19</sub> ,10S <sub>14</sub>	92	-	8
v <sub>21</sub>	Ring breathing	925	882	0.5	15.2	0.07	888	891	879	881	881	63S <sub>21</sub> ,12S <sub>14</sub> ,11S <sub>17</sub>	53	-	47
v <sub>18</sub>	Ring deformation	859	831	0.0	1.9	0.29	-	-	-	-	829	31S <sub>18</sub> ,19S <sub>14</sub> ,13S <sub>23</sub> ,12S <sub>19</sub> ,10S <sub>15</sub>	99	-	1
v <sub>16</sub>	γ-CH <sub>2</sub> wag	830	791	2.8	3.8	0.05	788	787	788	-	789	52S <sub>16</sub> ,21S <sub>17</sub> ,11S <sub>21</sub>	93	-	7
v <sub>19</sub>	β-CH <sub>2</sub> wag	699	672	0.5	1.5	0.07	666	-	668	668	666	11S <sub>19</sub> ,30S <sub>16</sub> ,21S <sub>18</sub> ,17S <sub>15</sub>	81	-	19
v <sub>20</sub>	Ring-CN bend (in-plane)	446	441	1.1	1.3	0.62	448	449	448	-	448	33S <sub>20</sub> ,25S <sub>18</sub> ,24S <sub>23</sub>	1	-	99
v <sub>22</sub>	Ring puckering	305	304	0.8	1.6	0.61	-	-	-	-	303	55S <sub>22</sub> , 32S <sub>20</sub>	56	-	44
v <sub>23</sub>	C-C≡N bend(in-plane)	121	120	3.5	1.6	0.70	-	-	-	-	118	40S <sub>23</sub> ,35S <sub>22</sub> ,24S <sub>20</sub>	60	-	40
A'' v <sub>24</sub>	β-CH <sub>2</sub> antisymmetric stretch	3186	2988	7.8	66.6	0.75	2973	2973	2968	2972	2971	73S <sub>24</sub> ,22S <sub>25</sub>	-	100	-
v <sub>25</sub>	γ-CH <sub>2</sub> antisymmetric stretch	3170	2974	7.8	9.9	0.75	2973	2973	2968	2972	2971	77S <sub>25</sub> ,18S <sub>24</sub>	-	100	-
v <sub>26</sub>	γ-CH <sub>2</sub> symmetric stretch	3126	2933	17.0	25.1	0.75	2930	2947	2928	2928	2928	98S <sub>26</sub>	-	100	-

Table 9. --Continued

Vib. No.	Approx. description	<i>ab initio</i>	Fixed scaled <sup>b</sup>	IR int.	Raman act.	dp ratio	Infrared				Raman	P.E.D. <sup>c</sup>	Band Contour		
							gas	Xe soln.	Solid amorphous	Solid annealed					
v <sub>27</sub>	β-CH <sub>2</sub> symmetric stretch	3115	2922	11.2	9.5	0.75	2930	2928	2928	2928	2928	91S <sub>27</sub>	-	100	-
v <sub>28</sub>	γ-CH <sub>2</sub> deformation	1557	1464	4.2	5.5	0.75	1463	1463	1463	1463	1463	82S <sub>28</sub> ,18S <sub>29</sub>	-	100	-
v <sub>29</sub>	β-CH <sub>2</sub> deformation	1544	1452	1.6	20.5	0.75	1453	1453	1452	1450	1450	82S <sub>29</sub> ,18S <sub>28</sub>	-	100	-
v <sub>30</sub>	γ-CH <sub>2</sub> rock	1394	1325	0.5	0.2	0.75	1314	1317	1316	1314	1314	49S <sub>30</sub> ,21S <sub>32</sub> ,11S <sub>31</sub>	-	100	-
v <sub>32</sub>	β-CH <sub>2</sub> rock	1345	1276	0.0	0.0	0.75	-	-	-	-	-	52S <sub>32</sub> ,37S <sub>30</sub>	-	100	-
v <sub>33</sub>	γ-CH <sub>2</sub> twist	1323	1257	2.2	14.0	0.75	1256	1254	1255	1257	1254	57S <sub>33</sub> ,21S <sub>31</sub> ,11S <sub>34</sub>	-	100	-
v <sub>34</sub>	β-CH <sub>2</sub> twist	1267	1205	0.1	1.3	0.75	1201	1196	1198	1203	1198	31S <sub>34</sub> ,27S <sub>33</sub> ,22S <sub>37</sub>	-	100	-
v <sub>31</sub>	α-CH bend (out-of-plane)	1214	1159	0.0	6.0	0.75	1155	-	-	-	1155	20S <sub>31</sub> ,25S <sub>34</sub> ,22S <sub>35</sub> ,11S <sub>39</sub>	-	100	-
v <sub>37</sub>	γ-CH <sub>2</sub> wag	1125	1072	1.9	6.9	0.75	1071	1074	1073	1074	1070	17S <sub>37</sub> ,22S <sub>38</sub> ,21S <sub>34</sub> ,14S <sub>35</sub> ,10S <sub>31</sub>	-	100	-
v <sub>35</sub>	Ring deformation	1059	1008	0.8	3.4	0.75	1000	1009	1000	1000	1005	36S <sub>35</sub> ,22S <sub>37</sub> ,14S <sub>32</sub>	-	100	-
v <sub>36</sub>	Ring deformation	940	904	2.8	0.2	0.75	902	902	902	-	903	71S <sub>36</sub> ,13S <sub>33</sub>	-	100	-
v <sub>38</sub>	β-CH <sub>2</sub> wag	856	818	0.0	0.8	0.75	-	-	-	-	817	42S <sub>38</sub> ,18S <sub>37</sub> ,16S <sub>39</sub> ,13S <sub>35</sub>	-	100	-
v <sub>39</sub>	Ring deformation	659	649	0.3	0.7	0.75	649	-	648	-	649	49S <sub>39</sub> ,16S <sub>40</sub> ,10S <sub>37</sub>	-	100	-
v <sub>41</sub>	Ring-CN bend (out-of-plane)	541	535	0.2	1.0	0.75	535	-	536	536	535	28S <sub>41</sub> ,35S <sub>40</sub> ,15S <sub>39</sub>	-	100	-
v <sub>40</sub>	C-C≡N bend(out-of-plane)	187	187	3.5	2.2	0.75	-	-	-	-	177	52S <sub>40</sub> ,43S <sub>41</sub>	-	100	-
v <sub>42</sub>	Ring twisting	63	63	0.5	0.2	0.75	-	-	-	-	-	91S <sub>42</sub>	-	100	-

<sup>a</sup>MP2(full)/6-31G(d) *ab initio* calculations, scaled frequencies, infrared intensities (km/mol), Raman activities (Å<sup>4</sup>/u) and potential energy distributions (P.E.D.s)

<sup>b</sup>Scaled *ab initio* calculations with factors of 0.88 for CH<sub>2</sub> stretches and CH<sub>2</sub> deformations, 0.90 for all other modes except torsions, heavy atom bends and C≡N stretch.

<sup>c</sup>Symmetry coordinates with P.E.D. contributions less than 10% are omitted.

**Table 10.** Calculated electronic energies (Hartrees, H) for the *Ax* ( $C_s$ ) and energy differences ( $\text{cm}^{-1}$ ) for *Eq* ( $C_s$ ), *Twist* ( $C_1$ ), and *Planar* ( $C_s$ ) forms of cyanocyclopentane.

Method/Basis Set	# of Basis Sets	<i>Ax</i> ( $C_s$ ) <sup>a</sup>	<i>Eq</i> ( $C_s$ ) <sup>b</sup>	<i>Twist</i> ( $C_1$ ) <sup>b, c</sup>	<i>Planar</i> ( $C_s$ ) <sup>b</sup>
MP2(full)/6-31G(d)	123	0.8627790	186	182	2406
MP2(full)/6-31+G(d)	151	0.8773395	131	206	2406
MP2(full)/6-311G(d,p)	180	1.1305983	206	198	2432
MP2(full)/6-311+G(d,p)	208	1.1373468	188	200	2397
MP2(full)/6-311G(2d,2p)	242	1.2083846	189	201	2558
MP2(full)/6-311+G(2d,2p)	270	1.2137348	143	184	2496
MP2(full)/6-311G(2df,2pd)	336	1.3177753	187	-	2593
MP2(full)/6-311+G(2df,2pd)	364	1.3222165	138	191	2539
MP2(full)/aug-cc-pVTZ	529	1.9036352	86	141	2277
B3LYP/6-31G(d)	123	1.7970749	-186	67	1597
B3LYP/6-31+G(d)	151	1.8072032	-175	81	1553
B3LYP/6-311G(d,p)	180	1.8737192	-149	73	1556
B3LYP/6-311+G(d,p)	208	1.8770573	-165	74	1526
B3LYP/6-311G(2d,2p)	242	1.8838247	-160	63	1488
B3LYP/6-311+G(2d,2p)	270	1.8872184	-181	71	1468
B3LYP/6-311G(2df,2pd)	336	1.8919200	-170	63	1505
B3LYP/6-311+G(2df,2pd)	364	1.8950024	-187	68	1480
B3LYP/aug-cc-pVTZ	529	1.9036352	-193	72	1482

<sup>a</sup> Energy of conformer is given as  $-(E+287)$  H.

<sup>b</sup> Difference is relative to *Ax* form and given in  $\text{cm}^{-1}$ .

<sup>c</sup> Ring parameters fixed due to optimization ending in an *Ax* conformer minima

**Table 11.** Symmetry coordinates for cyanocyclopentane.

Description		Symmetry Coordinate <sup>a</sup>	
A'	$\gamma$ -CH <sub>2</sub> antisymmetric stretch	S <sub>1</sub>	= $r_4 - r_5 + r_4' - r_5'$
	$\beta$ -CH <sub>2</sub> antisymmetric stretch	S <sub>2</sub>	= $r_2 - r_3 + r_2' - r_3'$
	$\gamma$ -CH <sub>2</sub> symmetric stretch	S <sub>3</sub>	= $r_4 + r_5 + r_4' + r_5'$
	$\beta$ -CH <sub>2</sub> symmetric stretch	S <sub>4</sub>	= $r_2 + r_3 + r_2' + r_3'$
	$\alpha$ -CH stretch	S <sub>5</sub>	= $r_1$
	C $\equiv$ N stretch	S <sub>6</sub>	= $R_1$
	$\gamma$ -CH <sub>2</sub> deformation	S <sub>7</sub>	= $\pi_5 + \pi_5'$
	$\beta$ -CH <sub>2</sub> deformation	S <sub>8</sub>	= $\lambda_5 + \lambda_5'$
	$\beta$ -CH <sub>2</sub> rock	S <sub>9</sub>	= $\lambda_1 - \lambda_2 + \lambda_3 - \lambda_4 + \lambda_1' - \lambda_2' + \lambda_3' - \lambda_4'$
	$\gamma$ -CH <sub>2</sub> rock	S <sub>10</sub>	= $\pi_1 - \pi_2 + \pi_3 - \pi_4 + \pi_1' - \pi_2' + \pi_3' - \pi_4'$
	$\alpha$ -CH bend (in-plane)	S <sub>11</sub>	= $\delta + \delta' + 2\psi$
	$\beta$ -CH <sub>2</sub> twist	S <sub>12</sub>	= $\lambda_1 - \lambda_2 - \lambda_3 + \lambda_4 + \lambda_1' - \lambda_2' - \lambda_3' + \lambda_4'$
	$\gamma$ -CH <sub>2</sub> twist	S <sub>13</sub>	= $\pi_1 - \pi_2 - \pi_3 + \pi_4 + \pi_1' - \pi_2' - \pi_3' + \pi_4'$
	Ring deformation	S <sub>14</sub>	= $R_3 + R_4 + R_3' + R_4' - 4R_5$
	C-C stretch	S <sub>15</sub>	= $R_2$
	$\beta$ -CH <sub>2</sub> wag	S <sub>16</sub>	= $\lambda_1 + \lambda_2 - \lambda_3 - \lambda_4 + \lambda_1' + \lambda_2' - \lambda_3' - \lambda_4'$
	Ring deformation	S <sub>17</sub>	= $R_3 - R_4 + R_3' - R_4'$
	Ring breathing	S <sub>18</sub>	= $R_3 + R_4 + R_3' + R_4' + R_5$
	$\gamma$ -CH <sub>2</sub> wag	S <sub>19</sub>	= $\pi_1 + \pi_2 - \pi_3 - \pi_4 + \pi_1' + \pi_2' - \pi_3' - \pi_4'$
	Ring-CN bend (in-plane)	S <sub>20</sub>	= $\phi_2 + \phi_2'$
	Ring deformation	S <sub>21</sub>	= $3\theta_1 - 2\theta_2 - 2\theta_3 + \theta_2' + \theta_3'$
	Ring puckering	S <sub>22</sub>	= $\tau_1 + \tau_1'$
	C-C $\equiv$ N linear bend (in-plane)	S <sub>23</sub>	= $\phi_1$
A''	$\beta$ -CH <sub>2</sub> antisymmetric stretch	S <sub>24</sub>	= $r_2 - r_3 - r_2' + r_3'$
	$\gamma$ -CH <sub>2</sub> antisymmetric stretch	S <sub>25</sub>	= $r_4 - r_5 - r_4' + r_5'$
	$\gamma$ -CH <sub>2</sub> symmetric stretch	S <sub>26</sub>	= $r_4 + r_5 - r_4' - r_5'$
	$\beta$ -CH <sub>2</sub> symmetric stretch	S <sub>27</sub>	= $r_2 + r_3 - r_2' - r_3'$
	$\gamma$ -CH <sub>2</sub> deformation	S <sub>28</sub>	= $\pi_5 - \pi_5'$
	$\beta$ -CH <sub>2</sub> deformation	S <sub>29</sub>	= $\lambda_5 - \lambda_5'$
	$\gamma$ -CH <sub>2</sub> rock	S <sub>30</sub>	= $\pi_1 - \pi_2 + \pi_3 - \pi_4 - \pi_1' + \pi_2' - \pi_3' + \pi_4'$
	$\alpha$ -CH bend (out-of-plane)	S <sub>31</sub>	= $\delta - \delta'$
	$\beta$ -CH <sub>2</sub> rock	S <sub>32</sub>	= $\lambda_1 - \lambda_2 + \lambda_3 - \lambda_4 - \lambda_1' + \lambda_2' - \lambda_3' + \lambda_4'$
	$\gamma$ -CH <sub>2</sub> twist	S <sub>33</sub>	= $\pi_1 - \pi_2 - \pi_3 + \pi_4 - \pi_1' + \pi_2' + \pi_3' - \pi_4'$
	$\beta$ -CH <sub>2</sub> twist	S <sub>34</sub>	= $\lambda_1 - \lambda_2 - \lambda_3 + \lambda_4 - \lambda_1' + \lambda_2' + \lambda_3' - \lambda_4'$
	Ring deformation	S <sub>35</sub>	= $R_3 - R_4 - R_3' + R_4'$
	Ring deformation	S <sub>36</sub>	= $R_3 + R_4 - R_3' - R_4'$
	$\gamma$ -CH <sub>2</sub> wag	S <sub>37</sub>	= $\pi_1 + \pi_2 - \pi_3 - \pi_4 - \pi_1' - \pi_2' + \pi_3' + \pi_4'$
	$\beta$ -CH <sub>2</sub> wag	S <sub>38</sub>	= $\lambda_1 + \lambda_2 - \lambda_3 - \lambda_4 - \lambda_1' - \lambda_2' + \lambda_3' + \lambda_4'$
	Ring deformation	S <sub>39</sub>	= $\theta_2 - \theta_3 - \theta_2' + \theta_3'$

**Table 11.** --Continued.

Description	Symmetry Coordinate <sup>a</sup>		
C-C≡N (out-of-plane)	$S_{40}$	=	$\tau_4$
Ring-CN bend (out-of-plane)	$S_{41}$	=	$\phi_2 - \phi_2'$
Ring twisting	$S_{42}$	=	$\tau_1 - \tau_1'$

<sup>a</sup> Not normalized.

A comparison of experimental and simulated infrared spectra of *c*-C<sub>5</sub>H<sub>9</sub>CN are shown in Fig. 10 and 11. The infrared spectrum of the gas and the predicted infrared spectra of the individual *Eq* and *Ax* conformers, along with the mixture of the two conformers with relative concentrations calculated for the equilibrium mixture at 25 °C by using the experimentally determined enthalpy difference are shown in Fig. 10 (A-E). The predicted spectra of the isolated molecule should be comparable to the spectrum of the vapor phase. The predicted spectrum of the mixture of conformer is in good agreement with the experimental spectrum which shows the utility of the scaled predicted frequencies for supporting the vibrational assignment.

The Raman spectra of the liquid and the predicted Raman spectra for the pure *Eq* and *Ax* conformers and the mixture of the two conformers with their relative concentrations obtained by using the experimentally determined enthalpy difference (55 cm<sup>-1</sup>) are shown in Fig. 12(A-D). The predicted spectra should be comparable to that of the liquid as the frequency shift due to the intermolecular interactions of the liquid are relatively small with an average value of 3 cm<sup>-1</sup>. The spectrum of the mixture should be compared to that of the Raman spectrum of the liquid at room temperature. The predicted

spectrum is indeed in reasonable agreement with the experimental spectrum, which shows the utility of the predicted Raman spectra for supporting the vibrational assignments discussed later.

### **Vibrational Assignment**

In order to determine the enthalpy difference between the stable conformers, it is essential to have a confident assignment for all of the fundamental modes of the stable forms and identify vibrations which are specifically assigned for each stable conformer of cyanocyclopentane. The vibrations of the CH<sub>2</sub> group are expected to be very similar to those found in the usual five membered rings with just carbon atoms so a discussion of their assignments is not necessary. Therefore, the assignments of the nine fundamentals of the ring and the vibrational assignments involving the C-C≡N modes will be provided in detail. For this purpose, significant assistance was obtained from the *ab initio* MP2(full)/6-31G(d) calculations with two scaling factors used to obtain the force constants. From these data, the frequencies, infrared intensities, Raman activities, band contours, and depolarization ratios were predicted. The “fingerprint” region of the spectra for this study, which is below 1100 cm<sup>-1</sup>, is mainly used for providing suitable fundamentals for the ΔH determination. Previous authors used the infrared spectrum of the gas, infrared spectrum of the sample dissolved in liquid xenon solution, and the Raman spectrum of the liquid for making vibrational assignments for the *Eq* and the *Ax* conformers of cyanocyclopentane. However, the vibrational assignments made for both conformers of cyanocyclopentane were incomplete and it is worthwhile to make a complete vibrational assignment. Along with the infrared spectrum of the gas, infrared spectrum of the sample dissolved in liquid xenon and the Raman spectrum of the liquid,

infrared spectra of the amorphous and annealed solid are also utilized for making a confident vibrational assignment for the cyanocyclopentane conformers. Both the *Eq* and *Ax* conformers of cyanocyclopentane have  $C_s$  symmetry and the vibrational modes are divided into two ( $A'$  and  $A''$ ) (Table 8 and 9). For both conformers, three ring deformations, C-C stretch, ring breathing, ring-CN bend (in-plane), ring puckering, and C-CN bend (in-plane) fundamental modes are in the  $A'$  block, whereas three ring deformations, C-C $\equiv$ N bend (out-of-plane), ring-CN bend (out-of-plane) and the ring twisting fundamental modes are in the  $A''$  block (Table 8 and 9). The CN stretching fundamental mode was predicted at approximately  $2200\text{ cm}^{-1}$  with very low infrared intensity and medium Raman activity for both the *Eq* and the *Ax* conformers of cyanocyclopentane. A low intensity band observed at  $2237\text{ cm}^{-1}$  in the infrared spectrum of the gas, and a strong intensity band observed at  $2238\text{ cm}^{-1}$  in the Raman spectrum of the liquid are assigned for the CN stretching fundamental mode.

In the  $A'$  block of the *Eq* conformer of cyanocyclopentane, the ring deformations ( $\nu_{14}$ ,  $\nu_{17}$  and  $\nu_{21}$ ) are assigned for the peaks observed at  $1047$ ,  $889$  and  $487\text{ cm}^{-1}$  in the infrared spectra of the amorphous and annealed solid. The C-C stretch ( $\nu_{15}$ ) fundamental mode is predicted at  $1005\text{ cm}^{-1}$  with  $0.0\text{ km/mol}$  infrared intensity and  $2.9\text{ \AA}^4/\text{u}$  Raman activity. A very small peak observed at  $1005\text{ cm}^{-1}$  in the Raman spectrum of the liquid is assigned for this C-C stretching mode. The ring breathing ( $\nu_{18}$ ) fundamental mode is predicted at  $867\text{ cm}^{-1}$  with very low infrared intensity and medium Raman activity. The medium intense peak observed at  $860\text{ cm}^{-1}$  in the infrared spectrum of the sample dissolved in xenon solution, and a strong intensity peak observed at  $860\text{ cm}^{-1}$  in the infrared spectrum of the amorphous and annealed solid, and a medium intensity peak

observed at  $859\text{ cm}^{-1}$  in the Raman spectrum of the liquid, are assigned to the ring breathing fundamental mode. The ring-CN (in-plane) bend ( $\nu_{20}$ ) fundamental mode is predicted at  $526\text{ cm}^{-1}$  with low infrared intensity and low Raman activity. In the infrared spectra of the amorphous and annealed solid, a strong peak observed at  $528\text{ cm}^{-1}$  and a medium intensity peak observed at  $525\text{ cm}^{-1}$  in the Raman spectrum of the liquid is assigned to this fundamental mode. The ring puckering ( $\nu_{21}$ ) fundamental mode, which is predicted at  $299\text{ cm}^{-1}$  with low Raman intensity is assigned to a small peak observed at  $297\text{ cm}^{-1}$ . In the  $A''$  block of cyanocyclopentane one ring deformation fundamental mode is assigned to a peak observed at  $1088\text{ cm}^{-1}$  in the Raman spectrum of the liquid ( $\nu_{35}$ ) and the remaining two ring deformation modes ( $\nu_{36}$  and  $\nu_{39}$ ) are assigned to the weak peaks observed at  $958$  and  $610\text{ cm}^{-1}$  in the infrared spectra of the amorphous and annealed solid. The C-C $\equiv$ N bend (out-of-plane) mode ( $\nu_{40}$ ) is predicted at  $526\text{ cm}^{-1}$  with low Raman activity and  $0.0\text{ km/mol}$  infrared intensity. In the Raman spectrum of the liquid a low intensity peak observed at  $525\text{ cm}^{-1}$  is assigned to this C-C $\equiv$ N bending mode and a shoulder peak observed at  $161\text{ cm}^{-1}$  is assigned to the ring-CN bend (out-of-plane) fundamental mode ( $\nu_{41}$ ).

In the  $A'$  block of the  $A_x$  conformer of cyanocyclopentane small peaks observed at  $1041$  and  $829\text{ cm}^{-1}$  in the Raman spectrum of the liquid are assigned as the ring deformation ( $\nu_{14}$  and  $\nu_{18}$ ) fundamental modes. The third ring deformation ( $\nu_{17}$ ) is assigned to a strong peak observed at  $929\text{ cm}^{-1}$  in the infrared spectrum of the amorphous solid. The C-C stretch ( $\nu_{15}$ ) fundamental mode is predicted at  $972\text{ cm}^{-1}$  with low infrared intensity and low Raman activity. A medium, sharp peak observed at  $970\text{ cm}^{-1}$  in the infrared spectrum of the gas, a shoulder peak observed at  $970\text{ cm}^{-1}$  in the infrared spectra

of the amorphous and annealed solid and a small peak observed at  $972\text{ cm}^{-1}$  in the Raman spectra of the liquid are assigned as this C-C stretching motion. A medium intensity peak observed at  $891\text{ cm}^{-1}$  is assigned to the ring breathing ( $\nu_{21}$ ) fundamental mode. The ring-CN bend (in-plane) ( $\nu_{20}$ ) is assigned to the small peak observed at  $448\text{ cm}^{-1}$  in the infrared spectrum of the amorphous solid. The ring puckering ( $\nu_{22}$ ) and the C-C $\equiv$ N bend (in-plane) ( $\nu_{23}$ ) fundamental modes are assigned to the peaks observed at  $303$  and  $118\text{ cm}^{-1}$  in the Raman spectrum of the liquid, respectively. In the  $A''$  block of the  $A_x$  conformer of cyanocyclopentane, peaks observed at  $1000$ ,  $902$ , and  $648\text{ cm}^{-1}$  are assigned to the ring deformation ( $\nu_{35}$ ,  $\nu_{36}$  and  $\nu_{39}$ ) fundamental modes. The ring-CN bend (out-of-plane) ( $\nu_{41}$ ) fundamental mode is assigned as the shoulder peak observed at  $536\text{ cm}^{-1}$  in the infrared spectrum of the amorphous solid. The C-C $\equiv$ N bend (out-of-plane) ( $\nu_{40}$ ) fundamental mode is assigned to the peak observed at  $177\text{ cm}^{-1}$  in the Raman spectra of the liquid.

Mixing of the vibrations is indicated by the potential energy distributions, and practically all of the modes have major contributions from two or more symmetry coordinates. Their approximate descriptions are given in Tables 8 and 9. In general, for the  $E_q$  conformer (Table 8) the mixing was extensive for the fundamentals starting at  $1312\text{ cm}^{-1}$  and proceeding to lower frequencies. Most of the fundamentals have extensive contributions from four or more modes. The  $A_x$  conformer (Table 9) is similar with extensive mixing also from  $1312\text{ cm}^{-1}$  and below. In the  $E_q$  conformer, the descriptions of the  $\nu_{14}$  and  $\nu_{37}$  fundamental modes are largely for “bookkeeping” purposes and the mixing is extensive for the  $\nu_{20}$ ,  $\nu_{31}$ ,  $\nu_{32}$ ,  $\nu_{35}$ , and  $\nu_{37}$  fundamentals with contributions of more than 10% from 4 different modes. In the  $A_x$  form, the descriptions of the  $\nu_{15}$ ,  $\nu_{31}$ ,

and  $\nu_{37}$  fundamental modes were also primarily for “bookkeeping” purposes. The *Ax* conformer has extensive mixing for the  $\nu_{17}$ ,  $\nu_{18}$ , and  $\nu_{37}$  fundamental modes with contributions of more than 10% from five different modes. For the *Eq* form, the  $\nu_{14}$  fundamental mode has been assigned as  $S_{14}$  (ring deformation), with a 25% contribution from  $S_{14}$ , and the  $\nu_{37}$  fundamental has been assigned as  $S_{37}$  ( $\gamma$ -CH<sub>2</sub> wag) with a 22% contribution from  $S_{37}$  (Table 8). For the *Ax* form, the  $\nu_{15}$  fundamental has been assigned to  $S_{15}$  (C-C stretch) with a 17% contribution from  $S_{15}$ , whereas the  $\nu_{31}$  fundamental has been assigned as  $S_{31}$  ( $\alpha$ -CH bend (out-of-plane)) with a 20% contribution by  $S_{31}$ . While the  $\nu_{37}$  fundamental has been assigned as  $S_{37}$  ( $\gamma$ -CH<sub>2</sub> wag), there is 17% contribution from  $S_{37}$  (Table 8). Overall, for both *Ax* and *Eq* forms, CH<sub>2</sub> bends and ring deformations are prominently mixed with each other, which causes shifts in some predicted frequencies to lower wavenumbers. Hence, observed frequencies of some CH<sub>2</sub> bends and ring deformations are higher than their predicted frequencies. With these assignments, the remaining vibrational modes are easily assigned, so the vibrational descriptions of the fundamentals for the *Eq* and *Ax* conformers of cyanocyclopentane have been confidently and more completely attributed.

### Conformational stability

For cyanocyclopentane, the *Eq*, *Ax*, *twist (Tw)*, and *planar (Pl)* forms are possible conformers. For predictions of the most stable conformer, the MP2(full) and B3LYP calculations utilizing 18 basis sets from 6-31G(d) to aug-cc-p-VTZ were undertaken. From MP2(full)/6-31G(d) frequency calculations, the *Ax* and *Eq* conformers are predicted to have only positive frequencies, whereas the *Tw* and *Pl* forms are predicted to have at least one negative frequency. From these calculations, it was predicted that the *Eq*

and *Ax* forms are stable conformers, whereas the *Tw* and *Pl* forms are not stable conformers and may represent transition states. This prediction was confirmed by the lack of unassigned bands that should be present if a *Tw* or *Pl* form was present in the sample.

In order to determine the more stable conformer between the *Ax* and *Eq* forms, the electronic energies were calculated (Table 10). From the MP2(full) basis set calculations, it is predicted that the *Ax* form is the more stable conformer, whereas in calculations from the DFT method the *Eq* form is predicted as the more stable conformer. Thus, from energy calculations alone, the prediction of the more stable form between the *Eq* and *Ax* conformational isomers of cyanocyclopentane is difficult.

To determine the more stable conformer, and the enthalpy difference between the *Eq* and *Ax* forms of cyanocyclopentane, the sample was dissolved in liquefied xenon and mid-infrared spectra were recorded as a function of temperature from -60 to -100 °C. Very small interactions are expected to occur between xenon and the sample though the sample can associate with itself forming a dimer, trimer, or higher order complexes. However, due to the very small concentration of the sample ( $\sim 10^{-4}$  molar) self-association is greatly reduced. Therefore, only small frequency shifts are anticipated from xenon interactions when passing from the gas phase infrared spectrum to that obtained in the liquefied xenon solution, which is confirmed by an average frequency shift of one  $\text{cm}^{-1}$ . A significant advantage of this study is that the conformer bands are better resolved in the xenon solution in comparison to those observed in the infrared spectrum of the gas (Fig. 13). From *ab initio* calculations, the dipole moments of the two conformers are predicted to have similar values, and the molecular sizes of the two conformers are nearly the same,

so the  $\Delta H$  value obtained from the temperature dependent FT-IR study from the xenon solution is expected to be near to that for the gas (Fig. 13).<sup>27,29,30,31,49</sup>

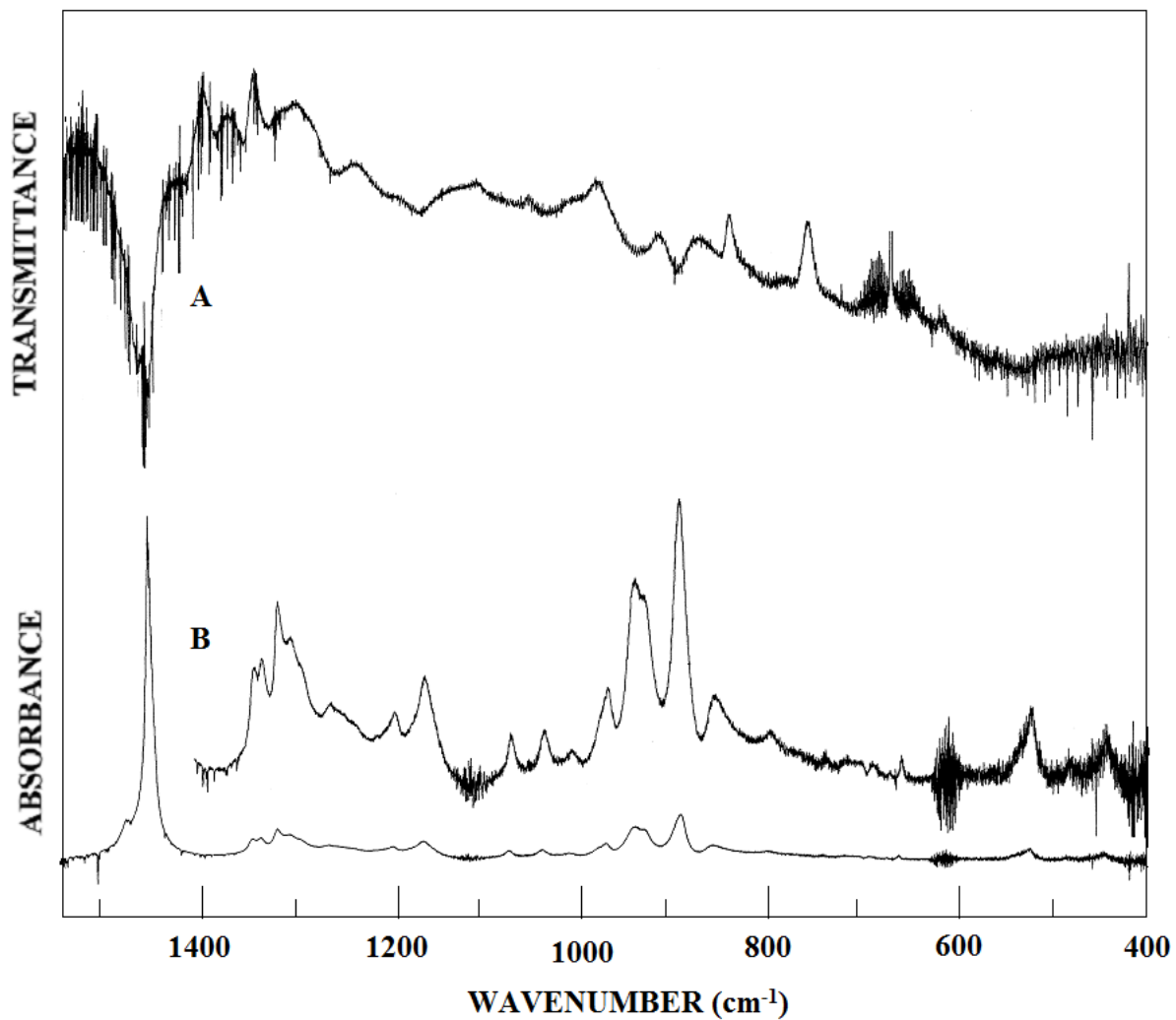


**Fig. 13** Infrared spectra of cyanocyclopentane (A) gas; (B) Xe solution at -70 °C.

Once confident assignments have been made for the fundamentals of the two observed conformers, the task was then to find pairs of bands from which the enthalpy difference could be obtained. The bands should be sufficiently resolved for determining their relative intensities more accurately. These bands should come from the region from 1200 to 400  $\text{cm}^{-1}$ , where there are a limited number of overtone and combination bands possible. The bands at 526 and 860  $\text{cm}^{-1}$  were confidently assigned to the *Eq* conformer, and 972 and 1076  $\text{cm}^{-1}$  were definitely assigned to the *Ax* form (Fig. 10 and 11). These bands are well resolved and believed to be relatively free from combination and overtone bands, thus they were used for the enthalpy difference determinations. In order to avoid the interference of other bands, a curve fitting method was used for the peaks observed at 526, 860, and 972  $\text{cm}^{-1}$ . The intensities of these individual bands were measured as a function of temperature (Fig. 14), and their ratios were determined (Table 12). By application of the van't Hoff equation  $-\ln K = \Delta H/(RT) - \Delta S/R$ , the enthalpy difference was determined from a plot of  $-\ln K$  versus  $1/T$ , where  $\Delta H/R$  is the slope of the line and  $K$  is substituted with the appropriate intensity ratios, *i.e.*  $I_{conf-1} / I_{conf-2}$ , etc. It was assumed that  $\Delta S$  and van't Hoff factor  $\alpha$  are not functions of temperature in this relatively small temperature range utilized.

These four bands, with two from the *Eq* form and two from the *Ax* conformer, were utilized for the determination of the enthalpy difference by combining them to form 4 band pairs. By using these band pairs for the *Eq* and *Ax* conformers, the individually determined enthalpy differences ranged from the low value of  $28 \pm 22 \text{ cm}^{-1}$  to the highest value of  $82 \pm 20 \text{ cm}^{-1}$  (Table 12). However, an average value was obtained by taking the data from all four band pairs as a single data set. By this method, the average value of

$55 \pm 12 \text{ cm}^{-1}$  was obtained. The error limit was derived from the statistical standard deviation of two sigma. These error limits do not take into account small associations with the liquid xenon or the interference of overtones and combination bands in near coincidence with the measured fundamentals. The variations in the individual values are undoubtedly due to these types of interferences, but by taking several band pairs for the determination, the effect of such interferences should cancel. However, this statistical uncertainty is probably better than can be expected from this technique and, therefore, an uncertainty of about  $12 \text{ cm}^{-1}$  in the enthalpy difference is probably a more realistic, *i.e.*,  $55 \pm 12 \text{ cm}^{-1}$ . From these enthalpy differences, the abundance of the *Eq* conformer at ambient temperature is estimated to be 55% and  $45 \pm 1\%$  for *Ax* form.

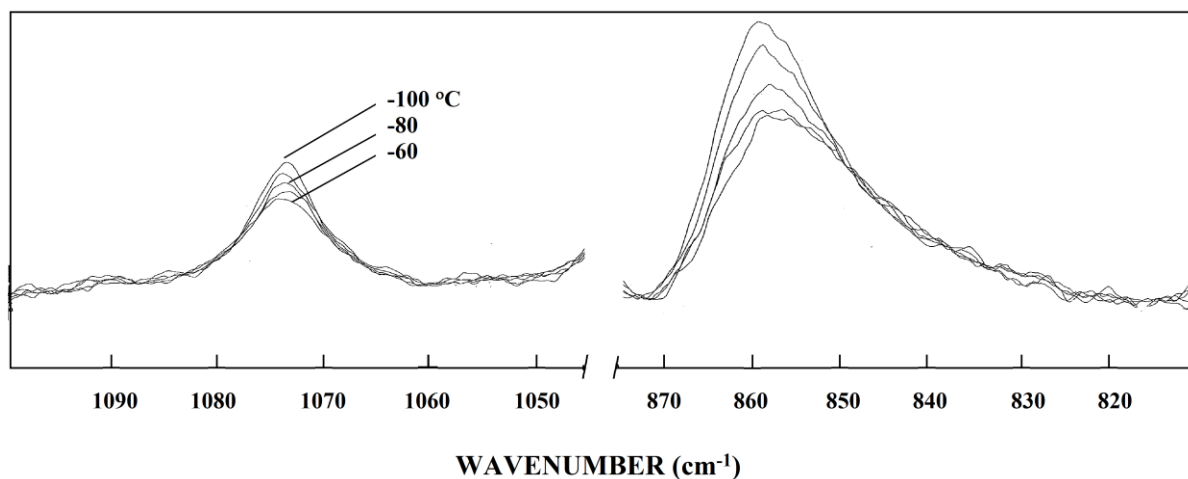


**Fig. 14** Temperature (-70 to -100 °C) dependent infrared spectrum of cyanocyclopentane dissolved in liquid xenon solution.

**Table 12.** Temperature and intensity ratios of the *Eq* and *Ax* bands of cyanocyclopentane.

T(°C)	1/T ( $\times 10^3$ K <sup>-1</sup> )	I <sub>524</sub> / I <sub>970</sub>	I <sub>524</sub> / I <sub>1074</sub>	I <sub>860</sub> / I <sub>970</sub>	I <sub>860</sub> / I <sub>1074</sub>
-60.0	4.692	0.6166	1754.6	1.1085	3154.4
-65.0	4.804	0.6417	1707.2	1.1284	3002.0
-70.0	4.923	0.6648	1753.2	1.1590	3056.4
-75.0	5.047	0.6632	1755.4	1.1181	2959.2
-80.0	5.177	0.6453	1654.9	1.1543	2960.0
-85.0	5.315	0.6611	1668.2	1.1631	2934.7
-90.0	4.460	0.6369	1693.2	1.1279	2998.7
-95.0	5.613	0.6170	1657.0	0.9900	2658.4
-100.0	5.775	0.6037	1671.5	0.9939	2751.7

---

$\Delta H^a$ (cm <sup>-1</sup> )	28 ± 22	34 ± 12	76 ± 33	82 ± 20
----------------------------------	---------	---------	---------	---------

<sup>a</sup> Average value:  $\Delta H = 55 \pm 12$  cm<sup>-1</sup> ( $0.66 \pm 0.14$  kJ mol<sup>-1</sup>) with the *Eq* conformer the more stable form, and the statistical uncertainty ( $2\sigma$ ) is obtained by utilizing all of the data as a single set.

### Structural Parameters

Initially, structural parameters for both the *Eq* and *Ax* conformers of cyanocyclopentane were determined from the data obtained in the microwave study of the molecule.<sup>46</sup> However, in this microwave study, the authors assumed that all ring CC bond distances are equal, and CN, C-(CN), CH bond distances and  $\angle$ HCH bond angle values were transferred from other analogous molecules. In the electron diffraction study, authors determined structural parameters of cyanocyclopentane, but were not able to determine structural parameters individually for the *Eq* and the *Ax* conformers of cyanocyclopentane. Also, these authors determined only an average CC bond distance for cyclopentane ring.<sup>50</sup> Recently, structural parameters for both the *Eq* and *Ax* conformers of cyanocyclopentane were determined by utilizing rotational constants obtained from the

microwave study,<sup>47</sup> and structural parameters predicted from the *ab initio* MP2(full) 6-311+G(d,p) calculation. However, the results obtained were not satisfactory, hence we decided to redetermine the structural parameters of cyanocyclopentane.

It has been shown in this laboratory that *ab initio* MP2(full)/6-311+G(d,p) calculations predict the carbon-hydrogen  $r_0$  structural parameters for more than fifty hydrocarbons to at least 0.002 Å compared with the experimentally determined values from isolated CH stretching frequencies which agree to previously determined values from earlier microwave studies.<sup>32,34</sup> Therefore, all of the carbon-hydrogen parameters can be taken from the MP2(full)/6-311+G(d,p) predicted values for the *Eq* and *Ax* conformers of cyanocyclopentane.

Previous results in this lab have showed that good structural parameters for hydrocarbons, and many substituted ones can be determined by adjusting the structural parameters obtained from the *ab initio* MP2(full)/6-311+G(d,p) calculations to fit the rotational constants obtained from microwave experimental data by using a computer program “A&M” (*Ab initio* and Microwave) developed<sup>51</sup> in our laboratory. In order to reduce the number of independent variables, the structural parameters are separated into sets according to their types, where bond distances in the same set keep their relative ratio, and the bond angles and torsional angles in the same set retain their difference in degrees. This assumption is based on the fact that errors from *ab initio* calculations are systematic. Additionally, we have also shown that the differences in predicted distances and angles from the *ab initio* calculations for different conformers of the same molecule can usually be used as one parameter with the *ab initio* predicted differences except for some dihedral angles. Also, the C≡N distance is nearly constant irrespective of its

substitutions.<sup>31</sup> Therefore, it should be possible to obtain “adjusted  $r_0$ ” structural parameters for the six values for the of the five heavy atoms in the ring by utilizing the previously reported six rotational constants from the earlier microwave study.<sup>46</sup> We have obtained the complete structural parameters for the *Eq* and *Ax* forms of cyanocyclopentane.

The resulting adjusted  $r_0$  parameters are listed in Table 13, where it is believed that the CN and C-C distances should be accurate to  $\pm 0.003$  Å, the C-H distances accurate to  $\pm 0.002$  Å, and the angles should be within  $\pm 0.5^\circ$ . The fit of the six determined rotational constants by the adjusted  $r_0$  structural parameters for both conformers is good with the differences being less than 0.9 MHz. Therefore, it is believed that the suggested uncertainties are realistic values, and the determined structural parameters are probably as accurate as can be obtained for the molecule in the gas phase by either electron diffraction or microwave substitution methods.

The C $\equiv$ N bond distance for the *Eq* and the *Ax* conformers of cyanocyclopentane was predicted to be 1.175 Å by the MP2(full)/6-311+G(d,p) basis set calculation and 1.154 Å by the B3LYP/6-311+G(d,p) basis set calculation. As explained previously for the C $\equiv$ N bond distance was kept constant at 1.160 Å (Table 13). When the predicted rotational constants were adjusted to fit the experimental rotational constants, major changes were observed in the  $\angle C_\beta C_\alpha C_{\beta'}$ ,  $\angle C_\alpha C_\beta C_\gamma$ , angles and  $\tau C_\beta C_\alpha C_{\beta'} C_\gamma$ , the dihedral angle (Table 13, Fig. 9). For the *Eq* conformer of cyanocyclopentane, the  $\angle C_\beta C_\alpha C_{\beta'}$  angle was increased by  $0.7^\circ$  over the value predicted by the MP2(full)/6-311+G(d,p) calculation, whereas for the *Ax* conformer the  $\angle C_\beta C_\alpha C_{\beta'}$  angle was well predicted by the

MP2(full)/6-311+G(d,p) calculation. Similarly, for the *Eq* and the *Ax* conformer of cyanocyclopentane, the  $\angle C_\alpha C_\beta C_\gamma$  angle was increased by 0.9 and 1.0°, respectively, over their values predicted by the MP2(full)/6-311+G(d,p) calculation. However, the same angle ( $\angle C_\alpha C_\beta C_\gamma$ ) of the *Eq* and the *Ax* conformers of cyanocyclopentane was well predicted by the B3LYP/6-311+G(d,p) calculation. The  $\angle H_1 C_\beta C_\gamma$  angle was decreased by 4.3° for the *Eq* conformer whereas for the *Ax* conformer that angle was increased by 1.6° over the values predicted by both MP2(full)/6-311+G(d,p) and B3LYP/6-311+G(d,p) calculations. For the *Eq* conformer the  $\angle H_2 C_\beta C_\gamma$  angle was increased by 3.1°, and for the *Ax* conformer, the  $\angle H_2 C_\beta C_\gamma$  angle was decreased by 2.7° compared to the predicted value by both MP2(full)/6-311+G(d,p) and B3LYP/6-311+G(d,p) calculations. For the *Eq* conformer the  $\tau C_\beta C_\alpha C_\beta C_\gamma$  dihedral angle was decreased by 3.8° and 1.2° as compared to the value predicted by MP2(full)/6-311+G(d,p) and B3LYP/6-311+G(d,p) calculations, respectively. In the case of the *Ax* conformer, the same dihedral angle was decreased by 2.9° and increased by 0.7° compared to the value predicted by MP2(full)/6-311+G(d,p) and B3LYP/6-311+G(d,p) calculations, respectively. With these changes, the remaining structural parameters were well predicted by the MP2(full)/6-311+G(d,p) basis set calculation for both *Eq* and *Ax* conformers of cyanocyclopentane.

**Table 13.** Structural parameters (Å and degrees), rotational constants (MHz) and dipole moment (Debye) for *Eq* and *Ax* ( $C_s$ ) forms of cyanocyclopentane.

Structural Parameters	Internal coordinate	MP2(full)/6-311+G(d,p)		B3LYP/6-311+G(d,p)		MW <sup>46</sup>		Adjusted $r_0$	
		<i>Eq</i>	<i>Ax</i>	<i>Eq</i>	<i>Ax</i>	<i>Eq</i>	<i>Ax</i>	<i>Eq</i>	<i>Ax</i>
r C≡N	R <sub>1</sub>	1.175	1.175	1.154	1.154	1.157 *	1.157 *	1.160 (3)	1.160 (3)
r C <sub>α</sub> -C	R <sub>2</sub>	1.459	1.465	1.459	1.465	1.470 *	1.470 *	1.463 (3)	1.469 (3)
r C <sub>α</sub> -C <sub>β</sub> , C <sub>β</sub> '	R <sub>3</sub>	1.537	1.539	1.547	1.550	1.541	1.546	1.543 (3)	1.545 (3)
r C <sub>β</sub> -C <sub>γ</sub> , rC <sub>β</sub> '-C <sub>γ</sub> '	R <sub>4</sub>	1.539	1.540	1.544	1.545	1.541	1.546	1.540 (3)	1.541 (3)
r C <sub>γ</sub> -C <sub>γ</sub> '	R <sub>5</sub>	1.554	1.553	1.559	1.557	1.541	1.546	1.552 (3)	1.553 (3)
r C <sub>α</sub> -H	r <sub>1</sub>	1.098	1.094	1.097	1.093	1.100 *	1.100 *	1.098 (2)	1.094 (2)
r C <sub>β</sub> -H <sub>1</sub> , C <sub>β</sub> '-H <sub>1</sub>	r <sub>2</sub>	1.095	1.093	1.094	1.090	1.100 *	1.100 *	1.095 (2)	1.093 (2)
r C <sub>β</sub> -H <sub>2</sub> , C <sub>β</sub> '-H <sub>2</sub>	r <sub>3</sub>	1.093	1.095	1.091	1.094	1.100 *	1.100 *	1.093 (2)	1.095 (2)
r C <sub>γ</sub> -H <sub>1</sub> , C <sub>γ</sub> '-H <sub>1</sub>	r <sub>4</sub>	1.092	1.093	1.092	1.092	1.100 *	1.100 *	1.092 (2)	1.093 (2)
r C <sub>γ</sub> -H <sub>2</sub> , C <sub>γ</sub> '-H <sub>2</sub>	r <sub>5</sub>	1.094	1.093	1.093	1.092	1.100 *	1.100 *	1.094 (2)	1.093 (2)
∠C <sub>α</sub> -C≡N	φ <sub>1</sub>	179.0	178.9	179.3	179.6			179.0 (5)	178.9 (5)
∠C <sub>β</sub> C <sub>α</sub> -C	φ <sub>2</sub>	113.8	110.4	114.1	111.6			113.1 (5)	110.1 (5)
∠C <sub>β</sub> C <sub>α</sub> C <sub>β</sub> '	θ <sub>1</sub>	102.3	101.8	102.9	102.4			103.0 (5)	102.1 (5)
∠C <sub>α</sub> C <sub>β</sub> C <sub>γ</sub>	θ <sub>2</sub>	103.2	103.8	103.8	104.8			104.1 (5)	104.8 (5)
∠C <sub>β</sub> C <sub>γ</sub> C <sub>γ</sub> '	θ <sub>3</sub>	105.8	105.7	106.2	106.1			106.3 (5)	106.0 (5)
∠HC <sub>α</sub> -C	ψ	108.2	108.5	107.5	107.4	113.9	106.5	108.2 (5)	108.5 (5)
∠HC <sub>α</sub> C <sub>β</sub>	δ	109.3	112.8	109.0	111.9			109.7 (5)	113.0 (5)
∠H <sub>1</sub> C <sub>β</sub> C <sub>α</sub>	λ <sub>1</sub>	108.4	113.1	108.9	112.8			108.4 (5)	113.1 (5)
∠H <sub>1</sub> C <sub>β</sub> C <sub>γ</sub>	λ <sub>2</sub>	110.7	113.3	110.8	113.3			106.4 (5)	114.9 (5)
∠H <sub>2</sub> C <sub>β</sub> C <sub>α</sub>	λ <sub>3</sub>	112.9	107.6	112.5	107.5			112.9 (5)	107.6 (5)
∠H <sub>2</sub> C <sub>β</sub> C <sub>γ</sub>	λ <sub>4</sub>	113.5	110.6	113.4	110.7			116.6 (5)	107.9 (5)
∠H <sub>1</sub> C <sub>β</sub> H <sub>2</sub>	λ <sub>5</sub>	108.0	108.2	107.5	107.6	109.5 *	109.5 *	108.0 (5)	108.2 (5)
∠H <sub>1</sub> C <sub>γ</sub> C <sub>β</sub>	π <sub>1</sub>	111.3	110.0	111.1	110.2			111.2 (5)	110.0 (5)
∠H <sub>1</sub> C <sub>γ</sub> C <sub>γ</sub> '	π <sub>2</sub>	112.2	110.2	112.2	110.3			113.8 (5)	108.7 (5)
∠H <sub>2</sub> C <sub>γ</sub> C <sub>β</sub>	π <sub>3</sub>	110.0	111.3	110.3	111.1			110.0 (5)	111.3 (5)
∠H <sub>2</sub> C <sub>γ</sub> C <sub>γ</sub> '	π <sub>4</sub>	110.3	112.3	110.3	112.3			108.2 (5)	113.5 (5)
∠H <sub>1</sub> C <sub>γ</sub> H <sub>2</sub>	π <sub>5</sub>	107.2	107.3	106.7	106.9	109.5 *	109.5 *	107.2 (5)	107.3 (5)

**Table 13.** --Continued.

Structural Parameters	Internal coordinate	MP2(full)/ 6-311+G(d,p)		B3LYP/ 6-311+G(d,p)		MW <sup>46</sup>		Adjusted $r_0$	
		<i>Eq</i>	<i>Ax</i>	<i>Eq</i>	<i>Ax</i>	<i>Eq</i>	<i>Ax</i>	<i>Eq</i>	<i>Ax</i>
$\tau_{C_\beta C_\alpha C_{\beta'} C_{\gamma'}}$	$\tau_1$	42.5	-41.8	39.9	-38.2			38.7 (5)	-38.9 (5)
$\tau_{C_\beta C_\gamma C_{\gamma'} C_{\beta'}}$	$\tau_2$	0.0	0.0	0.0	0.0			0.0 (5)	0.0 (5)
A(MHz)		6398.6	4256.8	6320.7	4359.5	6324.905 (170)	4297.196 (12)	6325.5	4297.0
B(MHz)		1782.6	2233.7	1781.3	2157.0	1790.937 (14)	2210.245 (9)	1791.6	2209.8
C(MHz)		1492.6	2095.8	1486.0	1986.9	2057.205 (10)	1497.792 (3)	1497.3	2057.4
$ \mu_a $		4.715	3.901	4.459	3.372				
$ \mu_b $		0.000	0.000	0.000	0.000				
$ \mu_c $		0.739	2.168	0.726	2.608				
$ \mu_t $		4.773	4.463	4.518	4.263				

\* Values are assumed parameters.

## Discussion

Average and percent errors have been calculated between predicted and observed frequencies for the *Eq* and the *Ax* conformers of cyanocyclopentane. For the *Eq* conformer, A' and A'' modes have an average error of 6.19 and 4.41  $\text{cm}^{-1}$ , respectively, which represents percent errors of 0.40 and 0.25%, respectively, whereas for the *Ax* conformer A' and A'' modes have an average error of 8.47 and 4.00  $\text{cm}^{-1}$ , respectively, which represents percent error of 0.52 and 0.25%, respectively. Both the average and percent errors are reasonable and show that predicted frequencies are meaningful with respect to the vibrational assignments.

Similar to isocyanocyclopentane (see Chapter 5) we did not observe any A, B, and C type band contours in the IR spectra of gas of cyanocyclopentane (Fig. 10). However theoretical calculations show that there should be A, B, and C type band contours. Predicted A, B, and C type band contours for both the *Ax* and *Eq* conformers are shown in Fig. 15. Exact reasons for this unusual behavior should be investigated. This has little, however, effect on the experimental results in this study as the bands are well resolved in the infrared spectra of the xenon solutions.

In the infrared spectrum of the annealed solid peak intensities of fundamentals assigned for the *Eq* conformer of cyanocyclopentane observed at 1173, 1047, 861, and 528  $\text{cm}^{-1}$ , increase compared to the peak intensities of the same fundamentals observed in the infrared spectrum of the amorphous solid. On the other hand, peak intensities of the fundamentals assigned for the *Ax* conformer at 1073, 970, 902, and 788  $\text{cm}^{-1}$  in the infrared spectrum of the cyanocyclopentane in its annealed solid form

decrease compared to the peak intensities of the same fundamentals observed in the infrared spectrum of the amorphous solid. Hence, for cyanocyclopentane, the *Eq* conformer can be concluded to be the more stable form compared to the *Ax* form.

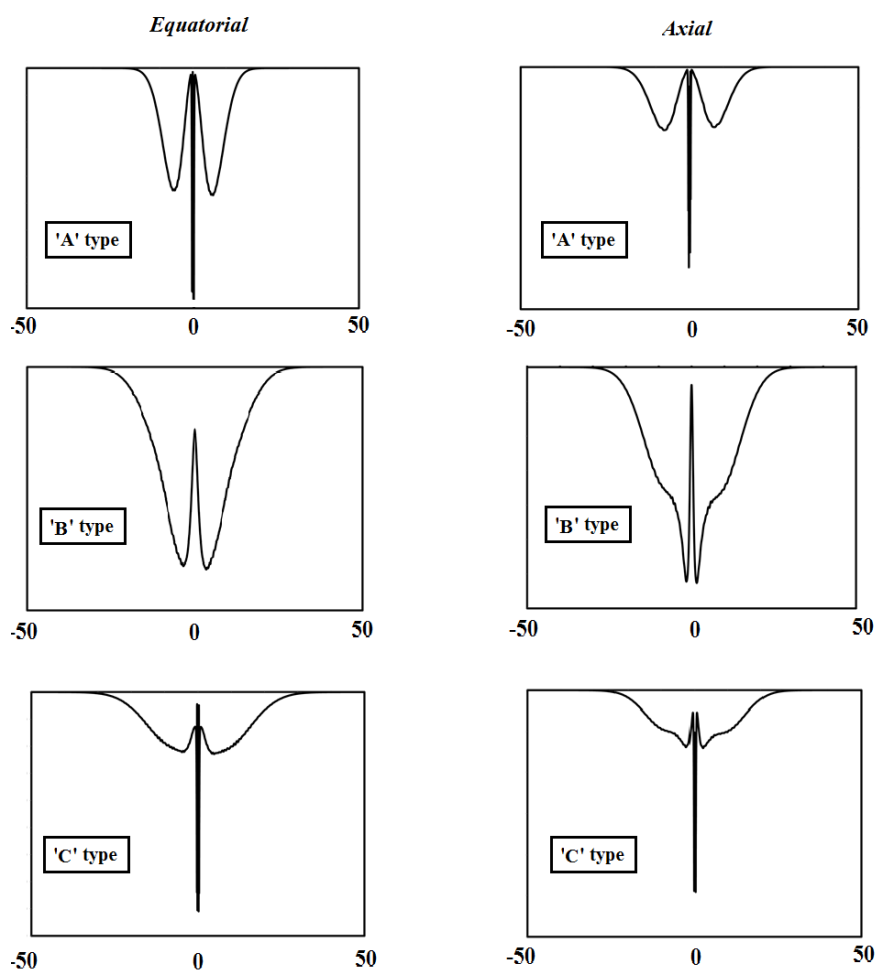


**Fig. 15** Band contour predictions for the *Eq* and *Ax* conformers of cyanocyclopentane.

From the MP2(full) calculations the *Ax* conformer was predicted as the more stable form with an average energy difference of  $161\text{ cm}^{-1}$  ( $1.93\text{ kJ/mol}$ ), whereas from the B3LYP calculations the *Eq* conformer was observed to be the more stable form compared to the *Ax* form, with an average energy difference of  $174\text{ cm}^{-1}$ . In determination of the enthalpy difference between the two conformers the variable temperature ( $-60$  to  $-100\text{ }^{\circ}\text{C}$ ) studies of the infrared spectra of the sample dissolved in the liquid xenon were carried out. From this method, the enthalpy difference between the *Eq* and the *Ax* conformers of cyanocyclopentane was determined to be  $55 \pm 12\text{ cm}^{-1}$  ( $0.66 \pm 0.14\text{ kJ/mol}$ ), with the *Eq* conformer the more stable form. B3LYP calculations predicted the conformational stability more accurately for this molecule as compared to the MP2(full) calculations. However, the experimentally determined enthalpy difference value was approximately one third the average energy difference value predicted by both B3LYP and MP2(full) calculations. Since the enthalpy difference between the two conformers of cyanocyclopentane was determined to be very small, some interconversion of the *Eq* and the *Ax* forms of cyanocyclopentane may be occur at ambient temperature. Previously, authors reported the *Ax* conformer to be the more stable form with a enthalpy difference of  $109 \pm 37\text{ cm}^{-1}$  ( $1.30 \pm 0.44\text{ kJ/mol}$ ).<sup>47</sup> In this case, the authors obtained incorrect results because they used only one band pair for determining the enthalpy difference between the two conformers, and the band pair they selected was not well resolved. From the microwave study, the authors estimated that the *Eq* conformer should be the more stable form with a possible energy difference of  $0 \pm 200\text{ cal/mol}$  ( $0 \pm 0.70\text{ cm}^{-1}$ ,  $0 \pm 0.84\text{ kJ/mol}$ )<sup>46</sup>. In another attempt, the enthalpy difference between the *Eq* and *Ax* forms of cyanocyclopentane was obtained by using the gas phase electron diffraction

method, from which it was determined to be 180 (330) cal/mol ( $63 \pm 115 \text{ cm}^{-1}$ ,  $0.75 \pm 1.38 \text{ kJ/mol}$ ) with the *Eq* form preferred over the *Ax* conformer.<sup>50</sup> However, the enthalpy difference obtained by this electron diffraction method has a high error range, and consequently it was difficult to determine the most stable conformer of cyanocyclopentane. The enthalpy difference determined by our method provides a reasonable value with minimum error and the *Eq* conformer as the most stable form.

The conformational stability and the enthalpy difference values obtained for cyanocyclopentane can be compared with other, similar molecules. For ethynylcyclopentane, the *Eq* conformer was preferred over the *Ax* form with an enthalpy difference of  $94 \pm 9 \text{ cm}^{-1}$  ( $1.12 \pm 0.11 \text{ kJ/mol}$ )<sup>44</sup> whereas for isocyanocyclopentane the *Ax* conformer was determined to be the most stable form with an enthalpy difference of  $102 \pm 10 \text{ cm}^{-1}$  ( $1.21 \pm 0.11 \text{ kJ/mol}$ ).<sup>45</sup> It is noted that the conformational stability of cyclopentane derivatives changed from the *Eq* to the *Ax* form as attached functional groups changed from ethynyl or cyano functional groups to the isocyano functional group. For cyanocyclobutane, the enthalpy difference was determined to be  $254 \pm 12 \text{ cm}^{-1}$  ( $3.03 \pm 0.15 \text{ kJ/mol}$ ) with the *equatorial* conformer as the more stable form,<sup>52</sup> whereas for cyanocyclohexane, which has *chair-equatorial* and *chair-axial* conformers, the *chair-axial* conformer was observed to be more the stable form with a enthalpy difference of  $63 \pm 9 \text{ cm}^{-1}$  ( $0.75 \pm 0.11 \text{ kJ/mol}$ ).<sup>53</sup> For cyano substitution on cyclobutane and cyclopentane rings, the *equatorial* and the *Eq* conformers were determined to be the more stable form but the enthalpy difference between the two conformers decreases as ring size increases. However, a further increase in ring size (from cyclopentane to cyclohexane) results in a change in conformational stability from the *Eq* to the

*chair-axial* form. The effect of the cyano, ethynyl, and isocyano moieties on the cyclopentane ring was studied by comparing structural parameters obtained for cyanocyclopentane and structural parameters previously reported for ethynyl and isocyanocyclopentane.<sup>44,45</sup> The structural parameters of the cyclopentane ring was unchanged, irrespective of their functional group except for the  $\angle C_{\beta}C_{\alpha}C_{\beta'}$  angle. For the *Eq* and the *Ax* conformers of cyano and ethynyl cyclopentane, the  $\angle C_{\beta}C_{\alpha}C_{\beta'}$  angle almost remained the same. These results are somewhat expected because the carbon atom of the functional group attached to the  $C_{\alpha}$  carbon atom of the cyclopentane ring remained the same even through the functional group on the cyclopentane ring was changed. However, when the functional group on the cyclopentane ring was changed from cyano to an isocyano group, for the *Eq* conformer of cyano and isocyanocyclopentane the  $\angle C_{\beta}C_{\alpha}C_{\beta'}$  angle was increased by  $11.2^{\circ}$ , whereas for the *Ax* conformer no significant change in the  $\angle C_{\beta}C_{\alpha}C_{\beta'}$  angle was observed. Available data is not good enough for making any firm conclusion hence here, future studies of other similar molecules would be necessary.

A comparison of the  $r_0$  structural parameters of cyanocyclobutane, cyanocyclopentane and cyanocyclohexane helped enable a study of the effect of the cyano group on different cyclic rings.<sup>52,53</sup> Since cyclobutane, cyclopentane, and cyclohexane rings have different structural parameters, the study was mainly limited to the  $C_{\alpha}$ -CN bond distance and the  $\angle C_{\beta}C_{\alpha}(\text{CN})$  bond angle. Even through the  $C_{\alpha}$ -CN bond distance was different for the *Eq* and the *Ax* conformers of cyanocyclobutane, cyanocyclopentane, and cyanocyclohexane molecules. Within each conformer of these different molecules, the  $C_{\alpha}$ -CN bond distance remained essentially same

irrespective of its cyclic ring. However, the  $\angle C_{\beta}C_{\alpha}(CN)$  bond angle was determined to be  $118.0 (5)^{\circ}$  for the *equatorial* conformer of cyanocyclobutane,  $131.1 (5)^{\circ}$  for the *Eq* form of cyanocyclopentane, and  $110.8 (5)^{\circ}$  for the *chair-equatorial* form of cyanocyclohexane. A similar trend was observed for the *Ax* conformer of cyanocyclopentane and *axial* conformer of cyanocyclobutane. Overall, as the ring size increases, the  $C_{\alpha}$ -CN bond distance remains same and the  $\angle C_{\beta}C_{\alpha}(CN)$  bond angle decreases.

A natural population analysis (NPA) was carried out for the *Eq* and *Ax* conformers of cyanocyclopentane using the MP2(full) method at the 6-311+G(d,p) basis set level for the calculation. Charge distributions for the *Eq* [*Ax*] conformers of cyanocyclopentane were determined as  $C_{\alpha} = -0.32 [-0.31]$ ,  $C_{\beta} = -0.31 [-0.32]$ ,  $C_{\gamma} = -0.34 [-0.35]$ ,  $-C^{*}\equiv N = 0.35 [0.34]$ , and  $N = -0.39 [-0.39]$ . Charge distribution of isocyano- and cyanocyclopentane did not show any major change at the  $C_{\beta}$  and  $C_{\gamma}$  carbon atom positions. However, the charge distribution on the  $C_{\alpha}$  carbon atom changed from  $-0.32[-0.31]$  to  $0.00[0.01]$  as the cyano group of cyanocyclopentane was replaced by the isocyano group.<sup>45</sup> This change may be due to the presence of positive charge on the carbon atom of the cyano group of cyanocyclopentane and the presence of negative charge on the nitrogen atom of the isocyano group of isocyanocyclopentane.

In summary, we found that for cyanocyclopentane the enthalpy difference between the *Eq* and the *Ax* conformer was  $55 \pm 12 \text{ cm}^{-1}$  ( $0.66 \pm 0.14 \text{ kJ/mol}$ ) with the *Eq* conformer the more stable form. The enthalpy difference between two conformers of cyanocyclobutane and cyanocyclopentane decreases as the ring size increases. In the case of cyanocyclopentane and cyanocyclohexane, the conformational stability changes from the *Eq* form to the *chair-axial* form as ring size increases. The conformational stability

and enthalpy difference data of cyanocyclopentane was observed to be similar with that for ethynylcyclopentane meso so than for isocyanocyclopentane. The  $\angle C_{\beta}C_{\alpha}(CN)$  bond angle has been observed to be a maximum for cyanocyclopentane compared to the  $\angle C_{\beta}C_{\alpha}(CN)$  bond angle observed in cyanocyclobutane and cyanocyclohexane. In the future, it would be interesting to study molecules like Cp-Si $\equiv$ C-H, Cp-Ge $\equiv$ C-H (where Cp is cyclopentane), which would help in understanding the effect of the atomic size of the substituent on the conformational stability and the structural parameters of the cyclopentane ring. Also, a microwave study of cyanocyclopentane and its isotopologues will provide more rotational constants from which even more accurate structural parameters of cyanocyclopentane could be determined.

(This work has been published in *Spectrochimica Acta A*<sup>54</sup>.)

## CHAPTER 5

### r<sub>0</sub> STRUCTURAL PARAMETERS, CONFORMATIONAL, VIBRATIONAL STUDIES AND *AB INITIO* CALCULATIONS OF ISOCYANOCYCLOPENTANE

#### Introduction

Monosubstituted cyclopentanes have been of interest for many decades since the cyclopentane ring vibration was proposed to have a motion described as pseudorotation.<sup>55</sup> After the initial prediction of the pseudorotational motion in saturated five-membered rings, twelve years later Pitzer and Donath<sup>56</sup> proposed that several mono-substituted cyclopentanes should have the bent conformation (*envelope*) as the preferred form. Relatively, complete vibrational<sup>57,58</sup> studies of the cyclopentyl halides (F, Cl, and Br) were carried out utilizing infrared and Raman spectra, and it was concluded that the F, Cl, and Br compounds all had doublets for the carbon-halogen stretches arising from *envelope-equatorial* (*Eq*) and *envelope-axial* (*Ax*) conformers for the *envelope* form of these halo substituted cyclopentanes. A recent study determined<sup>41,42</sup> the enthalpy differences between the two stable forms of the chloride and bromide by variable temperature studies of the infrared spectra of rare gas solutions. The *axial* conformer the more stable form for both molecules. Also, from the initial study<sup>57,58</sup> of fluorocyclopentane, it was also concluded that both the *Ax* and *Eq* forms were present in the fluid phases, but from a later Raman study,<sup>59</sup> it was determined there was only a single conformer present in the fluid states but its conformation was not determined. However, from CNDO/2 calculations,<sup>60</sup> the predicted result was that only one conformer exists, and it was the *Eq* form. As a continuation of previous studies of the conformational stabilities of mono-substituted cyclopentanes, the infrared and Raman

spectra of fluorocyclopentane<sup>43</sup> were reinvestigated. Again a single stable conformer was found in the fluid phases but it is neither the *Ax* nor *Eq* form, but the twisted form. Based on these results, it was expected that there may be several other monosubstituted cyclopentane molecules where the previously determined conformer stability is in error. Thus, the studies of cyclopentane molecules, which might be expected to have more than one conformer present at ambient temperature were initiated. Cyanocyclopentane<sup>47</sup> was the first of these molecules to be investigated, and from the variable temperature studies of the infrared spectra of rare gas solutions, two conformers were identified. It was determined that the conformers were the *axial* and *equatorial* forms, and the *axial* conformer was determined to be the more stable form. A similar variable temperature study was carried out on the ethynylcyclopentane molecule,<sup>44</sup> and it was found that the *equatorial* conformer was the stable form in contrast to the *axial* conformer, which was the more stable form for cyanocyclopentane. Currently, it is not clear what factors are important to determine the conformer that is the more stable form for these monosubstituted cyclopentane molecules. Therefore, as a continuation of these studies of the monosubstituted cyclopentane molecules, isocyanocyclopentane, *c*-C<sub>5</sub>H<sub>9</sub>NC, was selected as the next molecule to be investigated for determining its conformational stabilities and structural parameters.

There has not been a previous report of the conformational stability of isocyanocyclopentane, and there is, in general, limited conformational and structural data of organoisocyanides in the vapor state. Therefore, it was considered desirable to obtain an accurate enthalpy difference between the expected two conformers (Fig. 16) and obtain structural parameters, if possible, as well as to obtain the identity of the more

stable conformer. Therefore, vibrational spectra of isocyanocyclopentane were recorded, in the infrared spectra of the gas, xenon solutions, and solid. Additionally the Raman spectra of the liquid was obtained as well as infrared spectra at variable temperatures in xenon solutions. To support the vibrational study, we have carried out *ab initio* calculations with basis sets up to aug-cc-pVTZ as well as those with diffuse functions, *i.e.*, 6-311+G(2df,2pd). Density functional theory (DFT) calculations by the B3LYP method with the same basis sets were also carried out, and optimized geometries, conformational stabilities, harmonic force fields, infrared intensities, Raman activities, and depolarization ratios were calculated. The results of these spectroscopic, structural, and theoretical studies are reported herein.

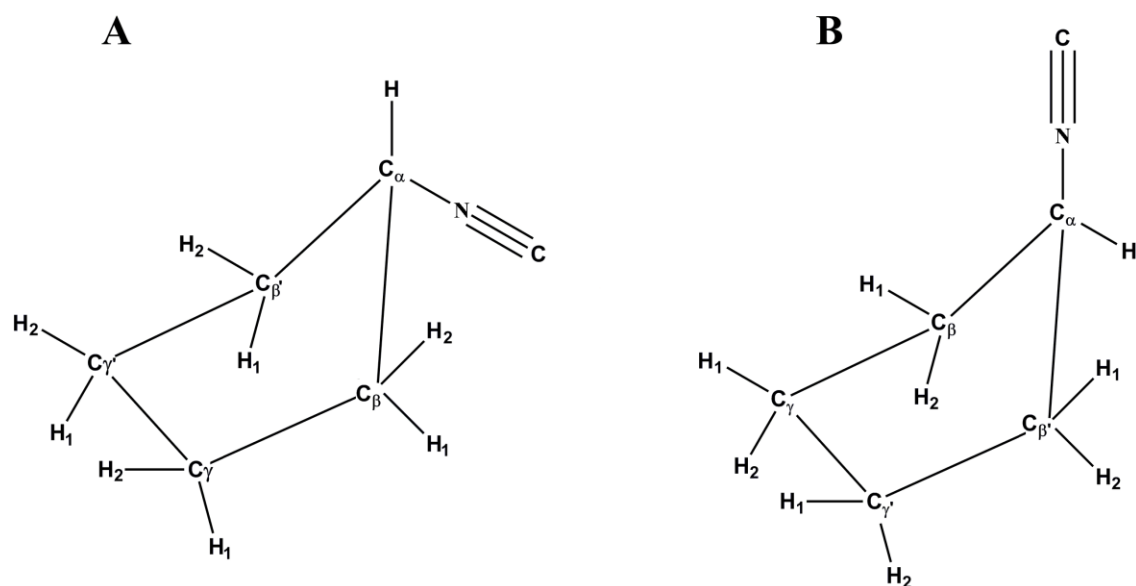


**Fig. 16** Conformers of isocyanocyclopentane (A) *Eq*; (B) *Ax*.

## Methods

The sample of isocyanocyclopentane was purchased from Acros Organics with stated purity of  $\geq 96\%$ . The sample was further purified by low-temperature, low-pressure fractionation column. The purity of the sample was checked and verified by the infrared spectra.

Microwave spectra of isocyanocyclopentane were recorded on a “mini-cavity” Fourier-transform microwave spectrometer<sup>61,62</sup> at Kent State University. The Fabry-Perot resonant cavity is established by two 7.5-inch diameter diamond-tip finished aluminum mirrors with a 30.5-cm spherical radius. The Fabry-Perot cavity resides inside a vacuum chamber formed by a 6-way cross and a 15-inch long, 8-inch diameter extension tube. One of the cavity mirrors is formed on an 8-inch diameter vacuum flange and mounted on the 6-way cross. The second mirror is mounted on 0.75-inch diameter steel rails that pass through ball bearing brackets mounted inside the extension arm. A motorized micrometer is used to position the movable mirror over a two-inch travel range. The two cavity mirrors are nominally separated by 30 cm. The vacuum chamber is pumped by a Varian VHS-6 diffusion pump ( $2400 \text{ L s}^{-1}$ ) backed by a two-stage Edwards E2M30 rotary pump.

The isocyanocyclopentane sample was entrained in 70:30 Ne-He carrier gas mixtures at 2 atm and expanded into the cavity with a reservoir nozzle<sup>62</sup> made from a modified Series-9 General Valve. The reservoir nozzle is mounted in a recessed region of the mirror flange, which is external to the vacuum chamber, and the expansion passes through a 0.182-inch diameter hole into the resonant cavity. The center of the expansion is offset from the center of the mirror by 1 inch.

The sample was irradiated by microwave radiation generated by an Agilent Technologies E8247C PSG CW synthesizer, and the details of the irradiation and heterodyne detection circuitry can be found in Reference.<sup>63</sup> Labview software controls the timing of the gas and irradiation pulses, as well as the detection of any free induction decay signal. The software performs signal averaging and can scan the spectrometer by stepping both the frequency source and the cavity. Microwave circuit elements allow for a spectral range from 10.5 to 26 GHz. The digital frequency resolution is 2.5 kHz and governed by the sampling rate and by the length of the free induction decay record. Rotational transitions are split into Doppler doublets by typically 13 kHz centered at the transition frequency due to the coaxial orientation of the gas expansion to the cavity axis and the FWHM of each Doppler component. The assigned microwave lines are listed in Table 14, and the rotational and centrifugal distortion constants are listed in Table 15.

**Table 14.** Rotational transition frequencies (MHz) of the ground vibrational state of the *Ax* form of isocyanocyclopentane

Transitions	<i>c</i> -C <sub>5</sub> H <sub>9</sub> NC	
	$\nu_{\text{obs}}$	$\Delta\nu^{\text{a}}$
4 <sub>14</sub> ← 3 <sub>22</sub>	11050.297	14
3 <sub>03</sub> ← 2 <sub>11</sub>	11206.204	-6
2 <sub>11</sub> ← 1 <sub>01</sub>	11356.812	0
5 <sub>24</sub> ← 4 <sub>32</sub>	12301.678	-2
4 <sub>13</sub> ← 3 <sub>21</sub>	12719.040	-6
3 <sub>13</sub> ← 2 <sub>12</sub>	13304.770	-3
3 <sub>03</sub> ← 2 <sub>02</sub>	13527.017	-4
3 <sub>22</sub> ← 2 <sub>21</sub>	13570.266	7
3 <sub>21</sub> ← 2 <sub>20</sub>	13613.488	4
3 <sub>12</sub> ← 2 <sub>11</sub>	13822.098	-1
5 <sub>15</sub> ← 4 <sub>23</sub>	15107.086	0
2 <sub>20</sub> ← 1 <sub>10</sub>	15124.653	4
2 <sub>21</sub> ← 1 <sub>11</sub>	15286.347	0
4 <sub>04</sub> ← 3 <sub>12</sub>	15371.362	-4
3 <sub>12</sub> ← 2 <sub>02</sub>	16142.913	3
5 <sub>14</sub> ← 4 <sub>22</sub>	17523.678	6
4 <sub>14</sub> ← 3 <sub>13</sub>	17727.813	-2
4 <sub>04</sub> ← 3 <sub>03</sub>	17987.253	-2
4 <sub>23</sub> ← 3 <sub>22</sub>	18085.072	-1
4 <sub>22</sub> ← 3 <sub>21</sub>	18191.327	-2
4 <sub>04</sub> ← 3 <sub>12</sub>	18415.617	-4
5 <sub>05</sub> ← 4 <sub>13</sub>	19366.800	-1
4 <sub>13</sub> ← 3 <sub>03</sub>	21031.511	1

<sup>a</sup>  $\Delta\nu = \nu_{\text{obs}} - \nu_{\text{calc}}$  in kHz.

**Table 15.** Experimental rotational and centrifugal distortion constants of the  $A_x$  form of isocyanocyclopentane

	MP2(full)/ 6-31G(d)	MP2(full)/ 6-311+G(d,p)	B3LYP/ 6-311+G(d,p)	Experimental
$A$ (MHz)	4280.6003	4255.6016	4378.9869	4312.7954(7)
$B$ (MHz)	2380.3796	2391.5263	2284.8714	2348.0136(2)
$C$ (MHz)	2220.4767	2236.0916	2094.9175	2175.4439(2)
$\Delta_J$ (kHz)	1.034	1.097	0.924	1.197(7)
$\Delta_{JK}$ (kHz)	-0.36	-0.55	5.02	-0.59(8)
$\Delta_K$ (kHz)	1.3	1.4	-3.5	2.0(1)
$\delta_J$ (kHz)	-0.109	-0.117	-0.091	-0.162(9)
$\delta_K$ (kHz)	-0.4	-0.4	3.5	-1.0(2)
$N^a$				23
$\sigma_{\text{fit}}$ (kHz) <sup>c</sup>				3

<sup>a</sup> Number of frequencies fitted.

The mid-infrared spectra of isocyanocyclopentane in the gas and solid states (Fig. 17) were obtained from 4000 to 220  $\text{cm}^{-1}$  on a Perkin-Elmer model 2000 Fourier transform spectrometer. The mid-infrared spectra (3600 to 400  $\text{cm}^{-1}$ ) of the sample dissolved in liquefied xenon (Fig. 17B) at ten different temperatures (-65 to -100°C) were recorded on a Bruker model IFS-66 Fourier transform spectrometer. The Raman spectrum (Fig. 18) as recorded on a Spex model 1403 spectrophotometer equipped with a Spectra-Physics model 2017. All of the observed bands in the Raman spectrum of the liquid along with their proposed assignments and depolarization values are listed in Tables 16 and 17. The predicted conformational energy differences calculated from *ab initio* calculations by

using the Møller-Plesset perturbation method to the second order (MP2), with full electron correlation, as well as with density functional theory by the B3LYP method with different basis sets are listed in Table 18. The experimental methods of recording infrared and Raman spectra are provided in detail in Chapter 2.

In order to obtain descriptions of the molecular motions involved in the fundamental modes of isocyanocyclopentane, a normal coordinate analysis was carried out. The force field in Cartesian coordinates was obtained with the Gaussian 03 program at the MP2(full) level with the 6-31G(d) basis set (Chapter 2). The internal coordinates used to calculate the B and G matrices are given for the *Ax* and *Eq* conformers in Table 19. By using the B matrix,<sup>48</sup> the force field in Cartesian coordinates was converted to force constants in internal coordinates. Subsequently, 0.88 was used as the scaling factor for the CH stretches and deformations, and 0.90 was used for all other modes excluding the heavy atom bends and  $\text{C}\equiv\text{N}$  stretch, to obtain the fixed scaled force constants and resultant wavenumbers. A set of symmetry coordinates was used (Table 20) to determine the corresponding potential energy distributions (P.E.D.s). A comparison between the observed and calculated wavenumbers, along with the calculated infrared intensities, Raman activities, depolarization ratios and potential energy distributions for the *Ax* and *Eq* conformers of isocyanocyclopentane are given in Tables 16 and 17, respectively.

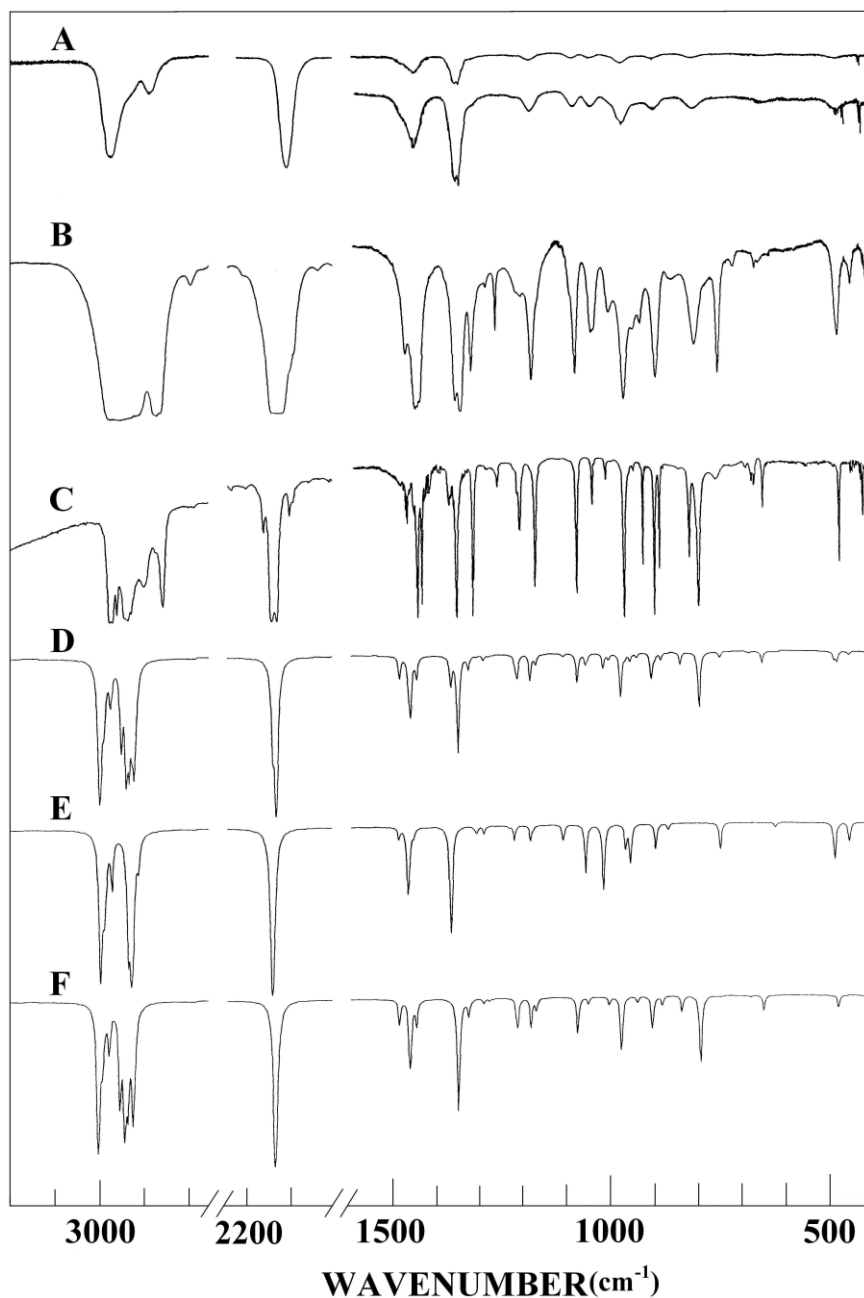


**Fig. 17** Comparison of experimental and calculated infrared spectra of isocyanocyclopentane: (A) observed spectrum of the gas; (B) observed spectrum of the Xe solution at  $-70\text{ }^{\circ}\text{C}$ ; (C) observed spectrum of the solid; (D) simulated spectrum of a mixture of *Ax* and *Eq* conformers ( $\Delta H = 102\text{ cm}^{-1}$ ) at  $25\text{ }^{\circ}\text{C}$ ; (E) simulated spectrum of the *Eq* conformer; (F) simulated spectrum of the *Ax* conformer.

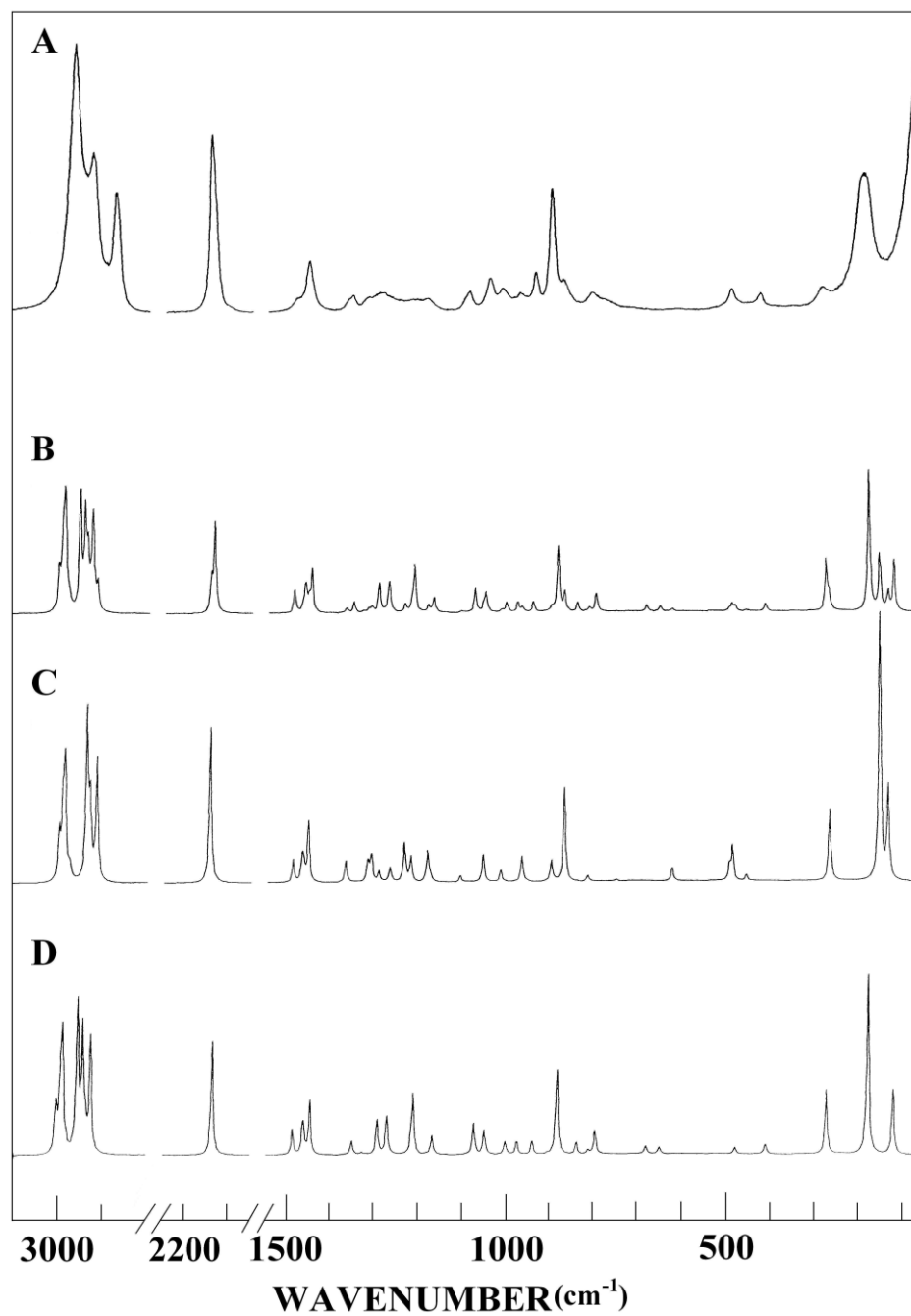


**Fig. 18** Comparison of experimental and calculated Raman spectra of isocyanocyclopentane: (A) observed spectrum of the liquid; (B) simulated spectrum of a mixture of *Ax* and *Eq* conformers ( $\Delta H = 102 \text{ cm}^{-1}$ ) at 25 °C; (C) simulated spectrum of the *Eq* conformer; (D) simulated spectrum of the *Ax* conformer.

**Table 16.** Observed and calculated<sup>a</sup> frequencies (cm<sup>-1</sup>) and potential energy distributions (P.E.D.s) for the Ax (C<sub>s</sub>) conformer of isocyanocyclopentane.

Vib. No.	Approx. description	<i>ab initio</i>	Fixed scaled <sup>b</sup>	IR int.	Raman act.	dp ratio	Infrared			Raman liquid	P.E.D. <sup>c</sup>	Band Contour			
							gas	Xe soln.	solid			A	B	C	
A'	v <sub>1</sub>	γ-CH <sub>2</sub> antisymmetric stretch	3201	3003	39.7	46.1	0.75	2980	2978	2976	2973	74S <sub>1</sub> ,26S <sub>2</sub>	79	-	21
	v <sub>2</sub>	β-CH <sub>2</sub> antisymmetric stretch	3186	2989	0.3	114.7	0.56	2980	2978	2976	2973	67S <sub>2</sub> ,26S <sub>1</sub>	3	-	97
	v <sub>3</sub>	α-CH stretch	3150	2956	15.9	148.4	0.13	2961	2960	2966	2959	93S <sub>3</sub>	0	-	100
	v <sub>4</sub>	γ-CH <sub>2</sub> symmetric stretch	3138	2945	27.5	119.5	0.06	2961	2960	2966	2959	97S <sub>4</sub>	41	-	59
	v <sub>5</sub>	β-CH <sub>2</sub> symmetric stretch	3121	2927	17.9	109.0	0.22	2931	2930	2934	2930	87S <sub>5</sub>	9	-	91
	v <sub>6</sub>	N≡C stretch	2148	2136	62.4	68.6	0.27	2138	2137	2151/2138	2143	90S <sub>6</sub> ,10S <sub>15</sub>	67	-	33
	v <sub>7</sub>	γ-CH <sub>2</sub> deformation	1581	1487	3.0	9.4	0.67	1482	1482	1481	1480	86S <sub>7</sub> ,14S <sub>8</sub>	52	-	48
	v <sub>8</sub>	β-CH <sub>2</sub> deformation	1553	1461	6.6	5.8	0.73	1457	1457	1457	1452	85S <sub>8</sub> ,15S <sub>7</sub>	11	-	89
	v <sub>9</sub>	α-CH bend (in-plane)	1421	1350	19.7	4.5	0.37	1349	1346	1355	1350	64S <sub>9</sub> ,18S <sub>12</sub>	98	-	2
	v <sub>10</sub>	β-CH <sub>2</sub> wag	1395	1326	1.6	0.2	0.26	1322	1321	1318	1318	63S <sub>10</sub> ,20S <sub>11</sub>	2	-	98
	v <sub>11</sub>	γ-CH <sub>2</sub> wag	1360	1291	0.6	10.4	0.65	1287	1287	1284	1287	35S <sub>11</sub> ,20S <sub>13</sub> ,13S <sub>12</sub> ,11S <sub>9</sub> ,10S <sub>10</sub>	85	-	15
	v <sub>12</sub>	β-CH <sub>2</sub> twist	1272	1211	3.2	15.5	0.74	1205	1205	1208	1205	36S <sub>12</sub> ,25S <sub>11</sub>	77	-	23
	v <sub>13</sub>	γ-CH <sub>2</sub> twist	1238	1180	3.6	0.2	0.19	1181	1178	1170	1178	38S <sub>13</sub> ,13S <sub>9</sub> ,12S <sub>20</sub>	7	-	93
	v <sub>14</sub>	Ring deformation	1103	1050	0.8	5.7	0.73	1040	1038	1041	1038	35S <sub>14</sub> ,23S <sub>16</sub> ,12S <sub>11</sub> ,10S <sub>18</sub>	97	-	3
	v <sub>15</sub>	C-N stretch	1024	976	7.0	2.7	0.49	973	970	968	967	18S <sub>15</sub> ,25S <sub>13</sub> ,13S <sub>20</sub> ,12S <sub>12</sub>	52	-	48
	v <sub>16</sub>	Ring deformation	981	939	0.7	2.7	0.21	-	929	924	931	32S <sub>16</sub> ,20S <sub>20</sub> ,12S <sub>14</sub> ,10S <sub>17</sub>	23	-	77
	v <sub>17</sub>	Ring breathing	926	883	1.0	15.6	0.07	889	887	885	892	64S <sub>17</sub> ,13S <sub>16</sub> ,11S <sub>14</sub>	73	-	27
	v <sub>18</sub>	Ring deformation	868	837	1.8	2.1	0.32	-	-	839	-	30S <sub>18</sub> ,22S <sub>14</sub> ,14S <sub>15</sub> ,13S <sub>20</sub> ,12S <sub>21</sub>	6	-	44
	v <sub>19</sub>	γ-CH <sub>2</sub> rock	833	794	9.2	3.8	0.07	804	803	794	799	50S <sub>19</sub> ,21S <sub>15</sub> ,10S <sub>17</sub>	87	-	13
	v <sub>20</sub>	β-CH <sub>2</sub> rock	709	680	0.2	1.1	0.10	-	711/661	683	~711	11S <sub>20</sub> ,34S <sub>19</sub> ,19S <sub>18</sub> ,16S <sub>15</sub>	52	-	48
	v <sub>21</sub>	Ring-NC bend (in-plane)	416	411	1.0	0.7	0.49	-	407	409	415	38S <sub>21</sub> ,23S <sub>18</sub> ,12S <sub>20</sub> ,11S <sub>23</sub> ,10S <sub>22</sub>	95	-	5
	v <sub>22</sub>	Ring puckering	273	273	0.0	2.4	0.66	-	-	-	271	51S <sub>22</sub> ,47S <sub>23</sub>	1	-	99
	v <sub>23</sub>	C-N≡C bend (in-plane)	122	122	3.7	2.3	0.69	-	-	-	-	39S <sub>23</sub> ,32S <sub>22</sub> ,30S <sub>21</sub>	61	-	39
A''	v <sub>24</sub>	β-CH <sub>2</sub> antisymmetric stretch	3191	2994	7.0	66.0	0.75	2980	2978	2976	2973	73S <sub>24</sub> ,22S <sub>25</sub>	-	100	-

**Table 16.** - - Continued.

Vib. No.	Approx. description	<i>ab initio</i>	Fixed scaled <sup>b</sup>	IR int.	Raman act.	dp ratio	Infrared			Raman		P.E.D. <sup>c</sup>	Band Contour		
							gas	Xe soln	solid	liquid			A	B	C
v <sub>25</sub>	$\gamma$ -CH <sub>2</sub> antisymmetric stretch	3176	2980	5.6	9.3	0.75	2980	2978	2976	2973	77S <sub>25</sub> ,18S <sub>24</sub>	-	100	-	
v <sub>26</sub>	$\gamma$ -CH <sub>2</sub> symmetric stretch	3131	2938	17.2	25.1	0.75	2931	2930	2934	2931	99S <sub>26</sub>	-	100	-	
v <sub>27</sub>	$\beta$ -CH <sub>2</sub> symmetric stretch	3118	2924	8.7	9.6	0.75	2931	2930	2934	2931	90S <sub>27</sub>	-	100	-	
v <sub>28</sub>	$\gamma$ -CH <sub>2</sub> deformation	1556	1463	4.1	6.9	0.75	1459	1457	1457	1457	90S <sub>28</sub> ,10S <sub>29</sub>	-	100	-	
v <sub>29</sub>	$\beta$ -CH <sub>2</sub> deformation	1538	1447	3.1	18.8	0.75	1448	1448	1447	1449	90S <sub>29</sub> ,10S <sub>28</sub>	-	100	-	
v <sub>30</sub>	$\gamma$ -CH <sub>2</sub> wag	1396	1327	0.4	0.5	0.75	1322	1321	1315	1320	46S <sub>30</sub> ,20S <sub>31</sub> ,17S <sub>32</sub>	-	100	-	
v <sub>31</sub>	$\beta$ -CH <sub>2</sub> wag	1347	1278	0.3	0.3	0.75	1282	1280	1280	1281	51S <sub>31</sub> ,36S <sub>30</sub>	-	100	-	
v <sub>32</sub>	$\alpha$ -CH bend (out-of-plane)	1335	1269	0.1	11.1	0.75	1266	1264	1260	1260	28S <sub>32</sub> ,39S <sub>33</sub> ,15S <sub>34</sub>	-	100	-	
v <sub>33</sub>	$\gamma$ -CH <sub>2</sub> twist	1278	1215	1.2	3.2	0.75	-	1214	1213	1212	47S <sub>33</sub> ,15S <sub>35</sub> ,14S <sub>34</sub>	-	100	-	
v <sub>34</sub>	$\beta$ -CH <sub>2</sub> twist	1224	1167	1.4	4.9	0.75	1165	1163	1167	1167	38S <sub>34</sub> ,19S <sub>36</sub> ,10S <sub>38</sub> ,10S <sub>32</sub>	-	100	-	
v <sub>35</sub>	$\gamma$ -CH <sub>2</sub> rock	1127	1074	4.4	7.4	0.75	1082	1080	1077	1084	17S <sub>35</sub> ,20S <sub>34</sub> ,18S <sub>38</sub> ,16S <sub>32</sub> ,12S <sub>36</sub>	-	100	-	
v <sub>36</sub>	Ring deformation	1054	1003	0.9	2.9	0.75	1003	1003	999	1004	35S <sub>36</sub> ,23S <sub>35</sub> ,15S <sub>31</sub>	-	100	-	
v <sub>37</sub>	Ring deformation	941	905	3.9	0.2	0.75	897	897	898	902	71S <sub>37</sub> ,13S <sub>32</sub>	-	100	-	
v <sub>38</sub>	$\beta$ -CH <sub>2</sub> rock	848	810	0.0	0.7	0.75	-	-	-	810	44S <sub>38</sub> ,17S <sub>35</sub> ,16S <sub>39</sub> ,13S <sub>36</sub>	-	100	-	
v <sub>39</sub>	Ring deformation	662	650	1.8	0.9	0.75	650	650	645	655	57S <sub>39</sub> ,13S <sub>40</sub> ,11S <sub>35</sub>	-	100	-	
v <sub>40</sub>	Ring-NC bend (out-of-plane)	485	480	1.4	0.6	0.75	476	474	472	475	51S <sub>40</sub> ,22S <sub>41</sub> ,10S <sub>38</sub>	-	100	-	
v <sub>41</sub>	C-N≡C bend(out-of-plane)	179	179	2.6	3.4	0.75	-	-	-	182	73S <sub>41</sub> ,23S <sub>40</sub>	-	100	-	
v <sub>42</sub>	Ring twisting	64	64	0.6	0.2	0.75	-	-	-	-	92S <sub>42</sub>	-	100	-	

<sup>a</sup>MP2(full)/6-31G(d) *ab initio* calculations, scaled frequencies, infrared intensities (km/mol), Raman activities ( $\text{\AA}^4/\text{u}$ ) and potential energy distributions (P.E.D.s)

<sup>b</sup>Scaled *ab initio* calculations with factors of 0.88 for CH<sub>2</sub> stretches and CH<sub>2</sub> deformations, 0.90 for all other modes except torsions, heavy atom bends and N≡C stretch.

<sup>c</sup>Symmetry coordinates with P.E.D. contributions less than 10% are omitted.

**Table 17.** Observed and calculated<sup>a</sup> frequencies (cm<sup>-1</sup>) and potential energy distributions (P.E.D.s) for the *Eq* (C<sub>s</sub>) conformer of isocyanocyclopentane.

Vib. No.	Approx. description	<i>ab initio</i>	Fixed scaled <sup>b</sup>	IR int.	Raman act.	dp ratio	Infrared			Raman liquid	P.E.D. <sup>c</sup>	Band Contour			
							gas	Xe soln.	solid			A	B	C	
A'	v <sub>1</sub>	γ-CH <sub>2</sub> antisymmetric stretch	3198	3000	41.3	49.0	0.73	2980	2976	2976	2973	58S <sub>1</sub> ,40S <sub>2</sub>	1	-	99
	v <sub>2</sub>	β-CH <sub>2</sub> antisymmetric stretch	3184	2987	1.3	117.7	0.44	2980	2976	2976	2973	53S <sub>2</sub> ,39S <sub>1</sub>	90	-	10
	v <sub>4</sub>	γ-CH <sub>2</sub> symmetric stretch	3133	2939	24.8	166.7	0.04	2931	2930	2934	2931	93S <sub>4</sub>	98	-	2
	v <sub>5</sub>	β-CH <sub>2</sub> symmetric stretch	3126	2932	23.4	46.8	0.25	2931	2930	2934	2931	83S <sub>5</sub> ,11S <sub>3</sub>	51	-	49
	v <sub>3</sub>	α-CH stretch	3109	2916	3.3	120.1	0.22	2918	2917	2920	2916	87S <sub>3</sub> ,10S <sub>5</sub>	1	-	99
	v <sub>6</sub>	N≡C stretch	2156	2144	69.6	95.2	0.28	2138	2136	2151/2138	2143	90S <sub>6</sub> ,10S <sub>15</sub>	97	-	3
	v <sub>7</sub>	γ-CH <sub>2</sub> deformation	1583	1489	1.3	8.5	0.68	1485	1482	1484	1482	71S <sub>7</sub> ,28S <sub>8</sub>	72	-	28
	v <sub>8</sub>	β-CH <sub>2</sub> deformation	1560	1468	7.5	7.3	0.72	1463	1463	1465	1460	71S <sub>8</sub> ,29S <sub>7</sub>	22	-	78
	v <sub>9</sub>	α-CH bend (in-plane)	1437	1367	18.2	7.2	0.44	1358	1358	1356	1359	54S <sub>9</sub> ,29S <sub>20</sub>	100	-	-
	v <sub>19</sub>	γ-CH <sub>2</sub> rock	1375	1307	0.5	6.7	0.72	1313	1310	1310	1311	56S <sub>19</sub> ,17S <sub>12</sub> ,11S <sub>9</sub>	90	-	10
	v <sub>20</sub>	β-CH <sub>2</sub> rock	1360	1290	0.9	3.2	0.73	1287	1287	1284	1287	34S <sub>20</sub> ,23S <sub>13</sub> ,20S <sub>9</sub> ,15S <sub>12</sub>	84	-	16
	v <sub>12</sub>	β-CH <sub>2</sub> twist	1279	1219	1.8	7.0	0.70	1218	1217	1221	1212	45S <sub>12</sub> ,16S <sub>19</sub> ,14S <sub>10</sub> ,10S <sub>16</sub>	77	-	23
	v <sub>13</sub>	γ-CH <sub>2</sub> twist	1240	1180	1.8	8.4	0.60	1180	~1180	1170	1184	41S <sub>13</sub> ,14S <sub>20</sub>	96	-	4
	v <sub>14</sub>	Ring deformation	1106	1055	6.2	6.4	0.70	1044	1042	1036	1037	23S <sub>14</sub> ,20S <sub>16</sub> ,13S <sub>15</sub> ,11S <sub>19</sub> ,10S <sub>18</sub>	97	-	3
	v <sub>15</sub>	C-N stretch	1064	1015	9.0	2.7	0.16	1003	1003	999	1003	40S <sub>15</sub> ,28S <sub>14</sub> ,25S <sub>17</sub>	96	-	4
	v <sub>10</sub>	β-CH <sub>2</sub> wag	1014	965	1.5	3.0	0.25	970	968	961	965	31S <sub>10</sub> ,30S <sub>13</sub>	1	-	99
	v <sub>16</sub>	Ring deformation	931	897	3.0	4.0	0.15	896	894	898	893	53S <sub>16</sub> ,16S <sub>14</sub>	100	-	0
	v <sub>17</sub>	Ring breathing	909	868	0.7	17.1	0.08	869	867	877	866	58S <sub>17</sub> ,12S <sub>14</sub> ,11S <sub>10</sub>	72	-	28
	v <sub>11</sub>	γ-CH <sub>2</sub> wag	788	748	3.1	0.3	0.18	749	749	755	746	82S <sub>11</sub>	0	-	100
	v <sub>18</sub>	Ring deformation	505	494	0.1	1.3	0.48	480	477	484	481	61S <sub>18</sub> ,18S <sub>10</sub>	29	-	71
	v <sub>21</sub>	Ring-NC bend (in-plane)	500	487	4.4	3.0	0.19	474	474	476	475	44S <sub>21</sub> ,19S <sub>15</sub> ,12S <sub>23</sub> ,10S <sub>17</sub>	85	-	15
	v <sub>22</sub>	Ring puckering	267	266	0.1	2.6	0.74	-	-	-	271	48S <sub>22</sub> ,48S <sub>23</sub>	85	-	15
	v <sub>23</sub>	C-N≡C bend(in-plane)	137	136	3.8	2.1	0.70	-	-	-	-	36S <sub>23</sub> ,32S <sub>22</sub> ,29S <sub>21</sub>	8	-	92
A''	v <sub>25</sub>	γ-CH <sub>2</sub> antisymmetric stretch	3189	2992	10.6	68.0	0.75	2980	2976	2976	2973	82S <sub>25</sub> ,15S <sub>24</sub>	-	100	-
	v <sub>24</sub>	β-CH <sub>2</sub> antisymmetric stretch	3172	2976	7.1	13.3	0.75	2980	2976	2976	2973	80S <sub>24</sub> ,12S <sub>25</sub>	-	100	-
	v <sub>26</sub>	γ-CH <sub>2</sub> symmetric stretch	3124	2931	19.3	25.8	0.75	2931	2930	2934	2931	93S <sub>26</sub>	-	100	-
	v <sub>27</sub>	β-CH <sub>2</sub> symmetric stretch	3121	2928	8.0	9.3	0.75	2931	2930	2934	2931	92S <sub>27</sub>	-	100	-

**Table 17. - - Continued.**

Vib. No.	Approx. description	<i>ab initio</i>	Fixed scaled <sup>b</sup>	IR int.	Raman act.	dp ratio	Infrared		Raman		P.E.D. <sup>c</sup>	Band Contour		
							gas	Xe soln.	solid	liquid		A	B	C
V <sub>28</sub>	γ-CH <sub>2</sub> deformation	1557	1465	3.8	4.9	0.75	1463	1463	1464	1460	72S <sub>28</sub> ,28S <sub>29</sub>	-	100	-
V <sub>29</sub>	β-CH <sub>2</sub> deformation	1545	1454	0.9	21.4	0.75	1455	1453	1452	1452	72S <sub>29</sub> ,28S <sub>28</sub>	-	100	-
V <sub>35</sub>	γ-CH <sub>2</sub> rock	1383	1315	0.2	6.1	0.75	1313	1310	1310	1315	50S <sub>35</sub> ,28S <sub>32</sub>	-	100	-
V <sub>32</sub>	α-CH bend (out-of-plane)	1378	1309	0.4	1.9	0.75	1310	1310	1310	1311	31S <sub>32</sub> ,20S <sub>38</sub> ,19S <sub>34</sub> ,17S <sub>35</sub>	-	100	-
V <sub>38</sub>	β-CH <sub>2</sub> rock	1333	1265	0.1	4.3	0.75	1266	1264	1260	1267	41S <sub>38</sub> ,23S <sub>33</sub> ,21S <sub>35</sub> ,11S <sub>32</sub>	-	100	-
V <sub>33</sub>	γ-CH <sub>2</sub> twist	1297	1233	0.2	11.0	0.75	1233	1230	1221	1230	56S <sub>33</sub> ,26S <sub>38</sub>	-	100	-
V <sub>34</sub>	β-CH <sub>2</sub> twist	1233	1173	0.3	1.3	0.75	1179	1178	1170	1178	42S <sub>34</sub> ,27S <sub>30</sub> ,10S <sub>31</sub>	-	100	-
V <sub>36</sub>	Ring deformation	1155	1107	1.8	1.6	0.75	1096	1096	-	1097	42S <sub>36</sub> ,16S <sub>39</sub> ,16S <sub>37</sub>	-	100	-
V <sub>37</sub>	Ring deformation	1010	966	1.3	2.7	0.75	970	968	961	967	33S <sub>37</sub> ,26S <sub>36</sub> ,16S <sub>34</sub>	-	100	-
V <sub>30</sub>	γ-CH <sub>2</sub> wag	998	954	4.7	0.2	0.75	949	947	946	947	15S <sub>30</sub> ,22S <sub>38</sub> ,16S <sub>32</sub> ,15S <sub>37</sub> ,13S <sub>34</sub>	-	100	-
V <sub>31</sub>	β-CH <sub>2</sub> wag	852	813	0.0	0.9	0.75	-	-	-	799	44S <sub>31</sub> ,21S <sub>30</sub> ,15S <sub>39</sub> ,11S <sub>36</sub>	-	100	-
V <sub>39</sub>	Ring deformation	636	622	0.5	1.6	0.75	-	629	625	-	58S <sub>39</sub> ,16S <sub>31</sub>	-	100	-
V <sub>40</sub>	Ring-NC bend (out-of-plane)	457	454	2.2	0.5	0.75	444	444	442	443	51S <sub>40</sub> ,32S <sub>41</sub> ,11S <sub>37</sub>	-	100	-
V <sub>41</sub>	C-N≡C bend(out-of-plane)	155	155	4.2	4.0	0.75	-	-	-	-	67S <sub>41</sub> ,31S <sub>40</sub>	-	100	-
V <sub>42</sub>	Ring twisting	43	43	0.1	0.0	0.75	-	-	-	-	93S <sub>42</sub>	-	100	-

<sup>a</sup>MP2(full)/6-31G(d) *ab initio* calculations, scaled frequencies, infrared intensities (km/mol), Raman activities (Å<sup>4</sup>/u) and potential energy distributions (P.E.D.s)

<sup>b</sup>Scaled *ab initio* calculations with factors of 0.88 for CH<sub>2</sub> stretches and CH<sub>2</sub> deformations, 0.90 for all other modes except torsions, heavy atom bends and N≡C stretch.

<sup>c</sup>Symmetry coordinates with P.E.D. contributions less than 10% are omitted.

**Table 18.** Calculated electronic energies (Hartrees, H) for the *Ax* ( $C_s$ ) and energy differences ( $\text{cm}^{-1}$ ) for *Eq* ( $C_s$ ), *Twist* ( $C_1$ ) and *Planar* ( $C_s$ ) forms of isocyanocyclopentane.

Method/Basis Set	# of Basis Sets	<i>Ax</i> ( $C_s$ )	<i>Eq</i> ( $C_s$ )	<i>Twist</i> ( $C_1$ ) <sup>c</sup>	<i>Planar</i> ( $C_s$ )
MP2(full)/6-31G(d)	123	0.823376	472	194	2632
MP2(full)/6-31+G(d)	151	0.841373	405	207	2579
MP2(full)/6-311G(d,p)	180	1.092543	496	189	2657
MP2(full)/6-311+G(d,p)	208	1.099296	460	194	2612
MP2(full)/6-311G(2d,2p)	242	1.171390	421	223	2788
MP2(full)/6-311+G(2d,2p)	270	1.176539	430	223	2763
MP2(full)/6-311G(2df,2pd)	336	1.279727	398	229	2806
MP2(full)/6-311+G(2df,2pd)	364	1.284195	413	234	2784
MP2(full)/aug-cc-pVTZ	529	1.297561	372	186	2512
B3LYP/6-31G(d)	123	1.763988	-18	80	1760
B3LYP/6-31+G(d)	151	1.776886	-35	88	1678
B3LYP/6-311G(d,p)	180	1.840708	55	83	1748
B3LYP/6-311+G(d,p)	208	1.843920	17	90	1695
B3LYP/6-311G(2d,2p)	242	1.851564	16	81	1668
B3LYP/6-311+G(2d,2p)	270	1.854423	1	95	1646
B3LYP/6-311G(2df,2pd)	336	1.860152	1	81	1686
B3LYP/6-311+G(2df,2pd)	364	1.862786	-11	93	1654
B3LYP/aug-cc-pVTZ	529	1.871245	-15	95	1652

<sup>a</sup> Energy of conformer is given as  $-(E+287)$  H.

<sup>b</sup> Difference is relative to *Ax* form and given in  $\text{cm}^{-1}$ .

<sup>c</sup> Ring parameters fixed due to optimization ending in an *Ax* conformer minima

**Table 19.** Structural parameters (Å and degrees), rotational constants (MHz) and dipole moment (Debye) for isocyanocyclopentane *Ax* and *Eq* (*C<sub>s</sub>*) forms.

Structural Parameters	Int. coord.	MP2(full)/6-311+G(d,p)		B3LYP/6-311+G(d,p)		Adjusted $r_0$	Predicted
		<i>Ax</i>	<i>Eq</i>	<i>Ax</i>	<i>Eq</i>		
r N≡C	R <sub>1</sub>	1.186	1.186	1.170	1.170	1.176 (3)	1.176
r C <sub>α</sub> -N	R <sub>2</sub>	1.431	1.422	1.436	1.427	1.432 (3)	1.423
r C <sub>α</sub> -C <sub>β</sub> , C <sub>β</sub> '	R <sub>3</sub>	1.531	1.530	1.540	1.540	1.534 (3)	1.533
r C <sub>β</sub> -C <sub>γ</sub> , rC <sub>β</sub> '-C <sub>γ</sub> '	R <sub>4</sub>	1.541	1.538	1.546	1.544	1.542 (3)	1.539
r C <sub>γ</sub> -C <sub>γ</sub> '	R <sub>5</sub>	1.554	1.556	1.558	1.561	1.554 (3)	1.556
r C <sub>α</sub> -H	r <sub>1</sub>	1.093	1.096	1.092	1.095	1.092 (2)	1.095
r C <sub>β</sub> -H <sub>1</sub> , C <sub>β</sub> '-H <sub>1</sub>	r <sub>2</sub>	1.092	1.095	1.091	1.094	1.092 (2)	1.095
r C <sub>β</sub> -H <sub>2</sub> , C <sub>β</sub> '-H <sub>2</sub>	r <sub>3</sub>	1.095	1.092	1.094	1.091	1.095 (2)	1.092
r C <sub>γ</sub> -H <sub>1</sub> , C <sub>γ</sub> '-H <sub>1</sub>	r <sub>4</sub>	1.093	1.092	1.092	1.091	1.093 (2)	1.092
r C <sub>γ</sub> -H <sub>2</sub> , C <sub>γ</sub> '-H <sub>2</sub>	r <sub>5</sub>	1.092	1.094	1.092	1.093	1.092 (2)	1.094
∠C <sub>α</sub> -N≡C	φ <sub>1</sub>	177.3	179.0	179.4	179.7	177.8 (5)	179.5
∠C <sub>β</sub> C <sub>α</sub> -N	φ <sub>2</sub>	109.4	113.0	110.8	113.5	110.4 (5)	114.0
∠C <sub>β</sub> C <sub>α</sub> C <sub>β</sub> '	θ <sub>1</sub>	102.4	102.8	102.9	103.3	102.9 (5)	113.3
∠C <sub>α</sub> C <sub>β</sub> C <sub>γ</sub>	θ <sub>2</sub>	103.7	103.0	104.8	103.6	103.6 (5)	102.9
∠C <sub>β</sub> C <sub>γ</sub> C <sub>γ</sub> '	θ <sub>3</sub>	105.7	105.7	106.0	106.1	105.9 (5)	105.9
∠HC <sub>α</sub> -N	ψ	108.0	107.7	107.1	107.1	108.0 (5)	107.7
∠HC <sub>α</sub> C <sub>β</sub>	δ	113.7	110.1	112.7	109.7	112.5 (5)	108.9
∠H <sub>1</sub> C <sub>β</sub> C <sub>α</sub>	λ <sub>1</sub>	112.6	107.9	112.3	108.3	112.6 (5)	107.9
∠H <sub>1</sub> C <sub>β</sub> C <sub>γ</sub>	λ <sub>2</sub>	113.6	111.0	113.6	111.1	115.9 (5)	113.3
∠H <sub>2</sub> C <sub>β</sub> C <sub>α</sub>	λ <sub>3</sub>	107.6	112.8	107.5	112.5	107.5 (5)	112.7
∠H <sub>2</sub> C <sub>β</sub> C <sub>γ</sub>	λ <sub>4</sub>	110.9	113.8	110.7	113.4	108.4 (5)	111.3
∠H <sub>1</sub> C <sub>β</sub> H <sub>2</sub>	λ <sub>5</sub>	108.5	108.2	107.8	107.7	108.4 (5)	108.1
∠H <sub>1</sub> C <sub>γ</sub> C <sub>β</sub>	π <sub>1</sub>	110.0	111.3	110.3	111.2	110.0 (5)	111.3
∠H <sub>1</sub> C <sub>γ</sub> C <sub>γ</sub> '	π <sub>2</sub>	110.2	112.2	110.3	112.1	109.6 (5)	111.6
∠H <sub>2</sub> C <sub>γ</sub> C <sub>β</sub>	π <sub>3</sub>	111.3	110.2	111.2	110.5	111.3 (5)	110.2
∠H <sub>2</sub> C <sub>γ</sub> C <sub>γ</sub> '	π <sub>4</sub>	112.4	110.3	112.2	110.3	112.6 (5)	110.5
∠H <sub>1</sub> C <sub>γ</sub> H <sub>2</sub>	π <sub>5</sub>	107.4	107.1	106.9	106.7	107.4 (5)	107.1
τC <sub>β</sub> C <sub>α</sub> C <sub>β</sub> 'C <sub>γ</sub> '	τ <sub>1</sub>	41.7	42.8	38.0	40.0	40.7 (5)	41.8
τC <sub>β</sub> C <sub>γ</sub> C <sub>γ</sub> 'C <sub>β</sub> '	τ <sub>2</sub>	0.0	0.0	0.0	0.0	0.0	0.0
A(MHz)		4255.6	6401.8	4379.0	6334.9	4312.7954(7)	6426.9
B(MHz)		2391.5	1893.1	2284.9	1879.8	2348.0136(2)	1884.1
C(MHz)		2236.1	1570.1	2094.9	1554.6	2175.4439(2)	1562.0
μ <sub>a</sub>		3.115	3.884	3.537	4.299		
μ <sub>b</sub>		0.000	0.000	0.000	0.000		
μ <sub>c</sub>		1.949	0.640	2.119	0.733		
μ <sub>t</sub>		3.674	3.936	4.123	4.361		

**Table 20.** Symmetry coordinates for Isocyanocyclopentane.

Description		Symmetry Coordinate <sup>a</sup>	
A'	$\gamma$ -CH <sub>2</sub> antisymmetric stretch	S <sub>1</sub>	= $r_4 - r_5 + r_4' - r_5'$
	$\beta$ -CH <sub>2</sub> antisymmetric stretch	S <sub>2</sub>	= $r_2 - r_3 + r_2' - r_3'$
	$\alpha$ -CH stretch	S <sub>3</sub>	= $r_1$
	$\gamma$ -CH <sub>2</sub> symmetric stretch	S <sub>4</sub>	= $r_4 + r_5 + r_4' + r_5'$
	$\beta$ -CH <sub>2</sub> symmetric stretch	S <sub>5</sub>	= $r_2 + r_3 + r_2' + r_3'$
	N $\equiv$ C stretch	S <sub>6</sub>	= $R_1$
	$\gamma$ -CH <sub>2</sub> deformation	S <sub>7</sub>	= $\pi_5 + \pi_5'$
	$\beta$ -CH <sub>2</sub> deformation	S <sub>8</sub>	= $\lambda_5 + \lambda_5'$
	$\alpha$ -CH bend (in-plane)	S <sub>9</sub>	= $\delta + \delta' + 2 \psi$
	$\beta$ -CH <sub>2</sub> wag	S <sub>10</sub>	= $\lambda_1 + \lambda_2 - \lambda_3 - \lambda_4 + \lambda_1' + \lambda_2' - \lambda_3' - \lambda_4'$
	$\gamma$ -CH <sub>2</sub> wag	S <sub>11</sub>	= $\pi_1 + \pi_2 - \pi_3 - \pi_4 + \pi_1' + \pi_2' - \pi_3' - \pi_4'$
	$\beta$ -CH <sub>2</sub> twist	S <sub>12</sub>	= $\lambda_1 - \lambda_2 - \lambda_3 + \lambda_4 + \lambda_1' - \lambda_2' - \lambda_3' + \lambda_4'$
	$\gamma$ -CH <sub>2</sub> twist	S <sub>13</sub>	= $\pi_1 - \pi_2 - \pi_3 + \pi_4 + \pi_1' - \pi_2' - \pi_3' + \pi_4'$
	Ring deformation	S <sub>14</sub>	= $R_3 + R_4 + R_3' + R_4' - 4R_5$
	C-N stretch	S <sub>15</sub>	= $R_2$
	Ring deformation	S <sub>16</sub>	= $R_3 - R_4 + R_3' - R_4'$
	Ring breathing	S <sub>17</sub>	= $R_3 + R_4 + R_3' + R_4' + R_5$
	Ring deformation	S <sub>18</sub>	= $3\theta_1 - 2\theta_2 - 2\theta_3 + \theta_2' + \theta_3'$
	$\gamma$ -CH <sub>2</sub> rock	S <sub>19</sub>	= $\pi_1 - \pi_2 + \pi_3 - \pi_4 + \pi_1' - \pi_2' + \pi_3' - \pi_4'$
	$\beta$ -CH <sub>2</sub> rock	S <sub>20</sub>	= $\lambda_1 - \lambda_2 + \lambda_3 - \lambda_4 + \lambda_1' - \lambda_2' + \lambda_3' - \lambda_4'$
	Ring-NC bend (in-plane)	S <sub>21</sub>	= $\phi_2 + \phi_2'$
	Ring puckering	S <sub>22</sub>	= $\tau_1 + \tau_1'$
	C-N $\equiv$ C linear bend (in-plane)	S <sub>23</sub>	= $\phi_1$
A''	$\beta$ -CH <sub>2</sub> antisymmetric stretch	S <sub>24</sub>	= $r_2 - r_3 - r_2' + r_3'$
	$\gamma$ -CH <sub>2</sub> antisymmetric stretch	S <sub>25</sub>	= $r_4 - r_5 - r_4' + r_5'$
	$\gamma$ -CH <sub>2</sub> symmetric stretch	S <sub>26</sub>	= $r_4 + r_5 - r_4' - r_5'$
	$\beta$ -CH <sub>2</sub> symmetric stretch	S <sub>27</sub>	= $r_2 + r_3 - r_2' - r_3'$
	$\gamma$ -CH <sub>2</sub> deformation	S <sub>28</sub>	= $\pi_5 - \pi_5'$
	$\beta$ -CH <sub>2</sub> deformation	S <sub>29</sub>	= $\lambda_5 - \lambda_5'$
	$\gamma$ -CH <sub>2</sub> wag	S <sub>30</sub>	= $\pi_1 + \pi_2 - \pi_3 - \pi_4 - \pi_1' - \pi_2' + \pi_3' + \pi_4'$
	$\beta$ -CH <sub>2</sub> wag	S <sub>31</sub>	= $\lambda_1 + \lambda_2 - \lambda_3 - \lambda_4 - \lambda_1' - \lambda_2' + \lambda_3' + \lambda_4'$
	$\alpha$ -CH bend (out-of-plane)	S <sub>32</sub>	= $\delta - \delta'$
	$\gamma$ -CH <sub>2</sub> twist	S <sub>33</sub>	= $\pi_1 - \pi_2 - \pi_3 + \pi_4 - \pi_1' + \pi_2' + \pi_3' - \pi_4'$
	$\beta$ -CH <sub>2</sub> twist	S <sub>34</sub>	= $\lambda_1 - \lambda_2 - \lambda_3 + \lambda_4 - \lambda_1' + \lambda_2' + \lambda_3' - \lambda_4'$
	$\gamma$ -CH <sub>2</sub> rock	S <sub>35</sub>	= $\pi_1 - \pi_2 + \pi_3 - \pi_4 - \pi_1' + \pi_2' - \pi_3' + \pi_4'$
	Ring deformation	S <sub>36</sub>	= $R_3 - R_4 - R_3' + R_4'$
	Ring deformation	S <sub>37</sub>	= $R_3 + R_4 - R_3' - R_4'$
	$\beta$ -CH <sub>2</sub> rock	S <sub>38</sub>	= $\lambda_1 - \lambda_2 + \lambda_3 - \lambda_4 - \lambda_1' + \lambda_2' - \lambda_3' + \lambda_4'$

**Table 20.** - - Continued.

Description	Symmetry Coordinate <sup>a</sup>		
Ring deformation	S <sub>39</sub>	=	$\theta_2 - \theta_3 - \theta_2' + \theta_3'$
Ring-NC bend (out-of-plane)	S <sub>40</sub>	=	$\phi_2 - \phi_2'$
C-N≡C (out-of-plane)	S <sub>41</sub>	=	$\tau_4$
Ring twisting	S <sub>42</sub>	=	$\tau_1 - \tau_1'$

<sup>a</sup> Not normalized.

A comparison of experimental and simulated infrared spectra of *c*-C<sub>5</sub>H<sub>9</sub>NC is shown in Fig. 17. The infrared spectrum of the gas, the predicted infrared spectra of the pure *Ax* and *Eq* conformers, and the mixture of the two conformers with relative concentrations calculated for the equilibrium mixture at 25 °C by using the experimentally determined enthalpy difference are shown in Fig. 17 (A-D). The predicted spectra are those for isolated molecules and should be comparable to the spectrum of the vapor phase. The predicted spectrum is in good agreement with the experimental spectrum, which shows the utility of the scaled predicted frequencies and predicted intensities for supporting the vibrational assignment.

The Raman spectrum of the liquid, the predicted Raman spectra for the pure *Ax* and *Eq* conformers and the mixture of the two conformers with their relative concentrations are obtained by using the experimentally determined enthalpy difference (102 cm<sup>-1</sup>) and are shown in Fig. 18(A-D). The predicted spectra should be comparable to that of the liquid as the frequency shift due to the intermolecular interactions of the liquid are relatively small with an average value of 3 cm<sup>-1</sup>. The spectrum of the mixture should be compared to that of the Raman spectrum of the liquid at room temperature. The

predicted spectrum is in reasonable agreement with the experimental spectrum, which shows the utility of the predicted Raman spectra for the supporting vibrational assignments.

### **Microwave Results**

The the rotational spectra were fitted to obtain the microwave constants. An overview of the fit rotational parameters for isocyanocyclopentane and the comparison to *ab initio* results can be found in Table 15. The spectrum was satisfactorily fit (Table 14) using a standard Watson semi-rigid rotor Hamiltonian of the A-reduction type in the F representation<sup>64</sup> with 3 kHz RMS error, which is better than the experimental uncertainty of approximately 25 kHz (line centers determined to  $\pm 12.5$  kHz). A summary of the fit can be found in Table 15.

The largest value of J is  $J = 5$ , and the largest value of  $K_a$  is  $K_a = 2$ . This leads to a lack of information with which to determine the centrifugal distortion constants (CDCs) as the magnitude of the effects are dependent on the energy level. To obtain the CDCs the transitions were fit while keeping the determined rotational constants fixed. The final fit was then obtained with the CDCs kept constant at the determined values. These CDCs are well fit except for the K constants which have higher uncertainty as all of the transitions assigned are  $K_a \leq 2$ .

### **Vibrational Assignment**

In order to determine the enthalpy difference between the stable conformers, it is essential to have a confident assignment for all of the fundamentals of the stable forms and identify vibrations, which cannot be assigned to these conformers. The vibrations of the CH<sub>2</sub> group are expected to be very similar to those found in the usual five membered

rings with just carbon atoms so a discussion of their assignments is not necessary. Therefore, the assignments of the nine fundamentals of the ring will be provided first, and this will be followed by the vibrational assignments involving the C-N≡C modes.

The assignments of the ring fundamentals for the mono substituted five membered rings are greatly simplified by their pattern in the vibrational spectra, which can be clearly demonstrated from the data in Table 21. The first two ring deformations are ~1050 to 1000  $\text{cm}^{-1}$  and are the first ring deformations in the A' and A'' blocks. The next set of two ring deformations are at ~900  $\text{cm}^{-1}$ , one in each the A' and A'' blocks. The A' block ring deformation in this case is relatively variable in its position changing with substituent and conformation. This is near the ring breathing mode in the A' block, which always appears at ~880  $\text{cm}^{-1}$  and changes very little with different substituents. The next ring deformation is in the A' block and is lower in frequency than the ring breathing and this ring deformation appears between 850 to 650  $\text{cm}^{-1}$ . This is the deformation most affected by substituent identity and conformer changes. It also has a great deal of mixing with other modes, which change considerably with changes in conformation and substituent, and so its motion is often split between a number of fundamentals in this region. The remaining ring deformation is located lower in frequency, between 650-600  $\text{cm}^{-1}$ , and is also relatively variable in frequency with significant changes from conformational or substituent change. The final ring fundamentals are the ring puckering and ring twisting modes, which are assigned near 300  $\text{cm}^{-1}$  and 100  $\text{cm}^{-1}$ , respectively. These modes are also well known to change considerably with substituent and conformational changes. This well understood pattern of the ring fundamentals aids considerably in their assignments, and therefore, they are excellent for use in the enthalpy

**Table 21.** Comparison of frequencies ( $\text{cm}^{-1}$ ) of ring fundamentals for the  $A_x$  conformer of molecules of the form  $c\text{-C}_5\text{H}_9\text{-X}$ .

		Isocyanocyclopentane		Cyanocyclopentane		Ethyneyl cyclopentane		Bromocyclopentane		Chlorocyclopentane	
		Predicted	This Study	Predicted	Ref <sup>47</sup>	Predicted	Ref <sup>44</sup>	Predicted	Ref <sup>42</sup>	Predicted	Ref <sup>41</sup>
A'	Ring deformation	1050	1040	1049	1038	1052	1041	1042	1038	1044	1030
	Ring deformation	939	929	815	812	941	937	910	910	918	914
	Ring breathing	883	889	878	884	883	893	877	884	877	889
	Ring deformation	837	839	664	-	834	803	689	690	791	805
	Ring puckering	273	271	290	298	294	282	323	310	161	185
A''	Ring deformation	1003	1003	1005	1004	1006	1002	1058	1069	1064	1067
	Ring deformation	905	897	892	893	904	895	891	890	892	903
	Ring deformation	650	650	626	633	645	629	610	613	611	617
	Ring twisting	64	-	60	-	74	-	96	115	86	87

determination from the vibrational spectra of the variable temperature xenon solutions.

The heavy atom modes of the five membered ring isocyanocyclopentane also produce a total of nine fundamentals, with five of them in the  $A'$  block and the remaining four in the  $A''$  block, for both  $Ax$  and  $Eq$  conformers. For the cyclopentane ring in the  $A'$  block, there are three ring deformations, a ring breathing mode, and a ring puckering vibration. The deformations for the  $Ax$  form are assigned at 1040, 929, and 839  $\text{cm}^{-1}$  and the ring breathing fundamental, assigned at 889  $\text{cm}^{-1}$  with the fifth fundamental for the  $A'$  block, which is a ring puckering fundamental, assigned at 271  $\text{cm}^{-1}$ . Three ring deformations and a ring twisting fundamental are possible in the  $A''$  block. The three ring deformations were observed at 1003, 897, and 650  $\text{cm}^{-1}$ , but the ring twist fundamental was not observed, even though it was predicted at 64  $\text{cm}^{-1}$  with IR intensity of 0.6  $\text{km/mol}$ .

There are an additional two heavy atoms for the isocyanocyclopentane molecule which generate six fundamentals with four of them in the  $A'$  block and the other two in the  $A''$  block. The  $\text{N}\equiv\text{C}$  stretch for the  $Ax$  conformer was observed at 2138  $\text{cm}^{-1}$  in the  $A'$  block. The C-N stretch and ring-NC bend were assigned at 973  $\text{cm}^{-1}$  and 407  $\text{cm}^{-1}$ , respectively. The C-N $\equiv$ C in-plane bend was not observed but it was predicted at 122  $\text{cm}^{-1}$  with IR intensity of 3.7  $\text{km/mol}$  and Raman activity of 2.3  $\text{\AA}^4/\text{u}$ . In the  $A''$  block of the  $Ax$  conformer, the ring-NC out-of-plane bend has been observed at 476  $\text{cm}^{-1}$ . From the Raman spectrum of the liquid, the C-N $\equiv$ C out-of-plane bend has been assigned at 182  $\text{cm}^{-1}$ .

Similar to the  $Ax$  conformer, the  $Eq$  conformer also has three ring deformations, a ring breathing, and a ring puckering fundamentals in the  $A'$  block. Ring deformations are

assigned at 1044, 896, and 480  $\text{cm}^{-1}$ . The ring breathing is observed at 869  $\text{cm}^{-1}$ , and the band at 271  $\text{cm}^{-1}$  has been assigned to the ring puckering fundamental. For the *Eq* conformer, three ring deformations and a ring twisting mode occur in the  $A''$  block. The ring deformations are assigned at 1096, 970, and 629  $\text{cm}^{-1}$ .

The band at 2138  $\text{cm}^{-1}$ , which was assigned to the  $\text{N}\equiv\text{C}$  stretch of the *Ax* form, was also assigned for the similar stretch of the *Eq* conformer. In the  $A'$  block of the *Eq* form, the ring-NC in-plane bend was assigned to the band at 474  $\text{cm}^{-1}$ , and the ring-NC out-of-plane bend mode of the  $A''$  block was observed at 444  $\text{cm}^{-1}$ . The C-NC in-plane bend, ring twisting, and the  $\text{C-N}\equiv\text{C}$  out-of-plane bend of the *Eq* form were not assigned because these vibrations were not observed in the spectra.

The mixing of the vibrations is indicated by the potential energy distributions, and practically all of the modes have major contributions from two or more symmetry coordinates. Their approximate descriptions are given in Tables 16 and 17. In general, for the *Ax* conformer (Table 16) the mixing was extensive for the fundamentals starting at 1287  $\text{cm}^{-1}$  and proceeding to lower frequencies. Most of the fundamentals have extensive contributions from four or more modes. The *Eq* conformer (Table 17) is similar and has extensive mixing starting from the vibration at 1310  $\text{cm}^{-1}$  and below. However, the *Eq* form shows a significant reduction in mixing with most of the modes with contributions of 10% or more from three modes. In the *Ax* conformer, the descriptions of the  $\nu_{15}$ ,  $\nu_{20}$  and  $\nu_{35}$  fundamentals are largely for bookkeeping purposes, and the mixing is extensive for the  $\nu_{11}$ ,  $\nu_{18}$ ,  $\nu_{21}$ , and  $\nu_{35}$  fundamentals with contributions of more than 10% from 5 different modes. In the *Eq* form, the description of the  $\nu_{30'}$  fundamental was primarily for bookkeeping purposes. The *Eq* conformer has extensive mixing for the  $\nu_{14'}$  and  $\nu_{30'}$

fundamentals with contributions of more than 10% from 5 different modes. For the *Ax* form, the  $\nu_{15}$  fundamental has been assigned as  $S_{15}$  (C-N stretch) with 18% contribution by from this symmetry coordinate  $S_{15}$ , whereas  $\nu_{20}$  fundamental has been assigned as  $S_{20}$  ( $\gamma$ -CH<sub>2</sub> wag) with 11% contribution by  $S_{20}$ . The  $\nu_{35}$  fundamental has been assigned as  $S_{35}$  ( $\gamma$ -CH<sub>2</sub> wag) with 17% contribution by  $S_{35}$ . For the *Eq* form, the  $\nu_{14'}$  fundamental has been assigned as  $S_{14}$  (ring deformation) with 23% contribution from  $S_{14}$ , and  $\nu_{30'}$  fundamental has been assigned as  $S_{30}$  ( $\gamma$ -CH<sub>2</sub> wag), with 15% contribution from  $S_{30}$ . Overall, for both *Ax* and *Eq* forms, CH<sub>2</sub> bends and ring deformations are prominently mixed with each other, which causes shifts in some predicted frequencies to lower wavenumbers. Hence observed frequencies of some CH<sub>2</sub> bends and ring deformations are higher than their predicted frequencies.

### Conformational Stability

For isocyanocyclopentane *Ax*, *Eq*, *twist (Tw)*, and *planar (Pl)* forms are possible conformers. For predictions of the most stable conformer, the MP2(full) and B3LYP calculations with utilization of 18 basis sets from 6-31G(d) to aug-cc-p-VTZ were used. From MP2(full)/6-31G(d) frequency calculations, the *Ax* and *Eq* conformers are predicted to have only positive frequencies whereas the *Tw* and *Pl* forms are predicted to have one or more negative frequency. From these calculations, it was predicted that the *Ax* and *Eq* forms are stable conformers whereas the *Tw* and *Pl* forms are not stable conformers. This prediction was confirmed by the lack of unassigned bands that should be present if a *Tw* or *Pl* form is present in the sample.

For estimating the more stable conformer between the *Ax* and *Eq* forms, the electronic energy was calculated (Table 18). From the MP2(full) basis sets calculations it

is predicted that the *Ax* form is the more stable conformer, whereas calculations from the DFT method by the basic sets B3LYP6-31G(d), 6-31+G(d), 6-311+G(2df,2pd) and aug-cc-pVTZ predict that the *Eq* form is the more stable conformer. Thus, from these energy calculations, it is difficult to state which of the two stable conformers is the more stable form.

In order to determine the more stable conformer along with the enthalpy differences between the *Ax* and *Eq* forms of isocyanocyclopentane, the sample was dissolved in liquefied xenon, and the mid-infrared spectra were recorded as a function of temperature from -65 to -100 °C. Very small interactions are expected to occur between xenon and the sample even though the sample can associate with itself forming a dimer, trimer or higher order complexes. However, due to the very small concentration of the sample ( $\sim 10^{-4}$  molar), self-association is greatly reduced. Therefore, only small frequency shifts are anticipated to result from the xenon interactions when passing from the gas phase to the liquefied xenon solution, which is confirmed with an average frequency shift of  $1 \text{ cm}^{-1}$ . A significant advantage of this study is that the conformer bands are better resolved in the xenon solution in comparison to those observed in the infrared spectrum of the gas (Fig. 19). From *ab initio* calculations, the dipole moments of the two conformers are predicted to have similar values, and the molecular sizes of the two conformers are nearly the same, so the  $\Delta H$  value obtained from the temperature dependent FT-IR study from the xenon solution is expected to be near to that for the gas.<sup>27,29,49,65,66</sup>

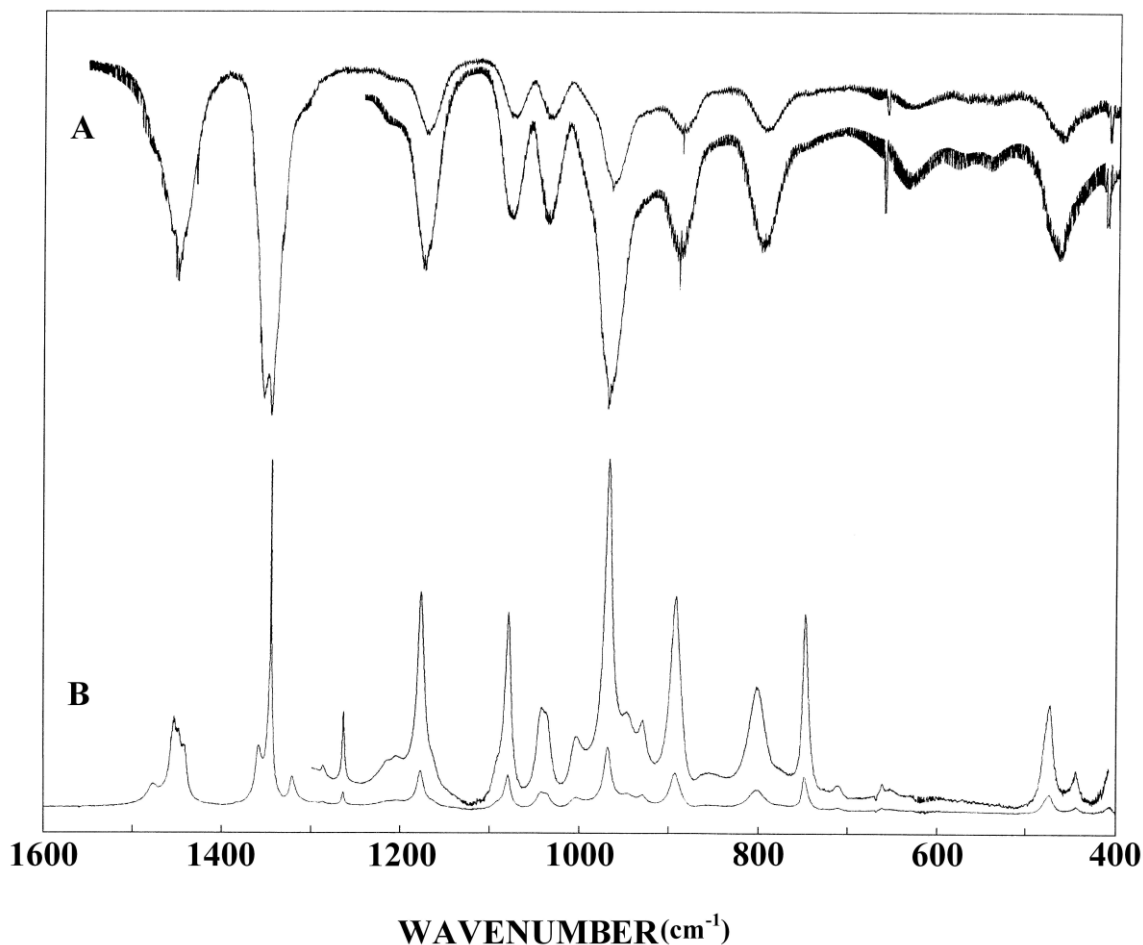


**Fig. 19** Infrared spectra of isocyanocyclopentane (A) gas; (B) Xe solution at  $-70\text{ }^{\circ}\text{C}$ .

Once confident assignments have been made for the fundamentals of the two observed conformers, the task was then to find pairs of bands from which the enthalpy difference could be obtained. The bands should be sufficiently resolved for determining their intensities. These bands should come from the region from  $1200$  to  $400\text{ cm}^{-1}$ , where there are a limited number of overtone and combination bands possible. The bands at  $407$ ,  $711$ ,  $803$ , and  $1080\text{ cm}^{-1}$  were assigned to the *A<sub>x</sub>* conformer, and  $444$ ,  $749$ , and  $1096$

$\text{cm}^{-1}$  were assigned to the *Eq* form (Fig. 17). These bands were well resolved and believed to be relatively free from combination and overtone bands. Thus they were used for the enthalpy difference determinations. The intensities of these individual bands were measured as a function of temperature (Fig. 20) and their ratios were determined (Table 22). By application of the van't Hoff equation  $-\ln K = \Delta H/(RT) - \Delta S/R$ , the enthalpy difference was determined from a plot of  $-\ln K$  versus  $1/T$ , where  $\Delta H/R$  is the slope of the line, and  $K$  is substituted with the appropriate intensity ratios, *i.e.*  $I_{\text{conf-1}} / I_{\text{conf-2}}$ , etc. It was assumed that  $\Delta S$  and van't Hoff factor  $\alpha$  are not functions of temperature in this relatively small temperature range utilized.

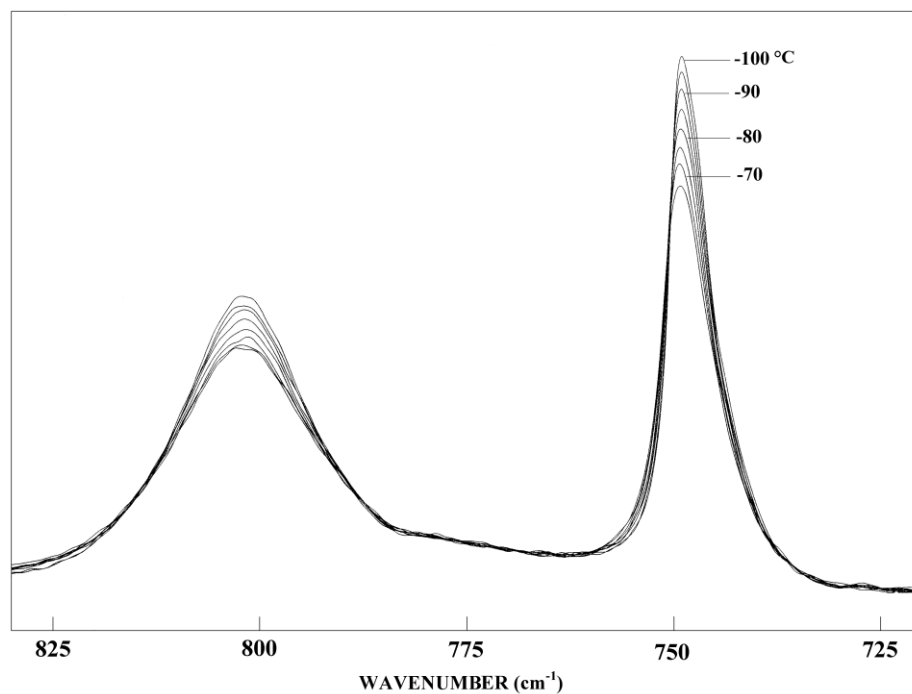


**Fig. 20** Temperature (-70 to -100 °C) dependent infrared spectrum of isocyanocyclopentane dissolved in liquid xenon solution.

These seven bands, with four from the *Ax* form and three from the *Eq* conformer, were utilized for the determination of the enthalpy difference by combining them to form 12 band pairs. By using these band pairs for the *Ax* and *Eq* conformers, the individually determined enthalpy differences ranged from the low value of  $84 \pm 4 \text{ cm}^{-1}$  to the highest value of  $138 \pm 8 \text{ cm}^{-1}$  (Table 22). However, an average value was obtained by taking the data from all twelve band pairs as a single data set. By this method, an average value of  $102 \pm 6 \text{ cm}^{-1}$  was obtained. The error limit was derived from the statistical standard deviation of two sigma ( $2\sigma$ ). These error limits do not take into account small associations with the liquid xenon or the interference of overtones and combination bands in near coincidence with the measured fundamentals. The variations in the individual values are undoubtedly due to these types of interferences, but by taking several pairs, the effect of such interferences should cancel. However, this  $6 \text{ cm}^{-1}$  statistical uncertainty is probably better than can be expected from this technique and, therefore, an uncertainty of about 10% in the enthalpy difference is probably more realistic, *i.e.*,  $102 \pm 10 \text{ cm}^{-1}$ . From these enthalpy differences the abundance of the *Ax* conformer at ambient temperature is estimated to be present at 62%, and  $38 \pm 1\%$  for the *Eq* form.

**Table 22.** Temperature and intensity ratios of the *Ax* and *Eq* bands of isocyanocyclopentane.

	T(°C)	1/T ( $\times 10^{-3}$ K $^{-1}$ )	I <sub>803</sub> / I <sub>444</sub>	I <sub>803</sub> / I <sub>749</sub>	I <sub>803</sub> / I <sub>1096</sub>	I <sub>1080</sub> / I <sub>444</sub>	I <sub>1080</sub> / I <sub>749</sub>	I <sub>1080</sub> / I <sub>1096</sub>
Liquid	-65	4.804	3.256	0.966	4.000	2.930	0.869	3.600
xenon	-70	4.922	3.326	0.987	4.123	2.989	0.887	3.705
	-75	5.047	3.370	1.006	4.212	3.022	0.903	3.777
	-80	5.177	3.426	1.025	4.271	3.064	0.917	3.820
	-85	5.315	3.464	1.031	4.352	3.134	0.933	3.938
	-90	5.460	3.500	1.048	4.430	3.160	0.946	4.000
	-95	5.613	3.608	1.070	4.554	3.255	0.965	4.109
	-100	5.775	3.695	1.096	4.697	3.314	0.983	4.213
$\Delta H^a$			85 $\pm$ 2	84 $\pm$ 4	107 $\pm$ 4	86 $\pm$ 3	86 $\pm$ 2	109 $\pm$ 3

	T(°C)	1/T ( $\times 10^{-3}$ K $^{-1}$ )	I <sub>407</sub> / I <sub>444</sub>	I <sub>407</sub> / I <sub>749</sub>	I <sub>407</sub> / I <sub>1096</sub>	I <sub>711</sub> / I <sub>444</sub>	I <sub>711</sub> / I <sub>749</sub>	I <sub>711</sub> / I <sub>1096</sub>
Liquid	-65	4.804	1.488	0.441	1.829	2.023	0.600	2.486
xenon	-70	4.922	1.528	0.453	1.894	2.067	0.613	2.563
	-75	5.047	1.543	0.461	1.929	2.109	0.630	2.636
	-80	5.177	1.617	0.484	2.016	2.170	0.650	2.706
	-85	5.315	1.629	0.485	2.047	2.247	0.669	2.824
	-90	5.460	1.640	0.491	2.076	2.280	0.683	2.886
	-95	5.613	1.667	0.494	2.104	2.333	0.692	2.946
	-100	5.775	1.695	0.503	2.155	2.362	0.701	3.002
$\Delta H^a$			91 $\pm$ 10	91 $\pm$ 12	113 $\pm$ 10	116 $\pm$ 7	116 $\pm$ 9	138 $\pm$ 8

<sup>a</sup>Average value  $\Delta H = 102 \pm 6$  cm $^{-1}$  ( $1.22 \pm 0.07$  kJ mol $^{-1}$ ) with the *Ax* conformer the more stable form and the statistical uncertainty ( $2\sigma$ ) obtained by utilizing all of the data as a single set.

## Structural Parameters

As there was no previous structural study reported on the *c*-C<sub>5</sub>H<sub>9</sub>NC, it was thought to be of interest to determine the structural parameters for this molecule. The adjusted  $r_0$  structure can be determined for the *Ax* conformer by utilizing the rotational constants reported herein from the microwave spectra. There are three rotational constants available for the determination of the structural parameter values of the *Ax* conformer of *c*-C<sub>5</sub>H<sub>9</sub>NC. It has been found that good structural parameters for hydrocarbons and many substituted ones can be determined by adjusting the structural parameters obtained from the *ab initio* MP2(full)/6-311+G(d,p) calculations to fit the rotational constants obtained from microwave experimental data by using the computer program “A&M” (*Ab initio* and Microwave) developed in our laboratory.<sup>32</sup>

*Ab initio* MP2(full)/6-311+G(d,p) calculations predict the carbon-hydrogen  $r_0$  structural parameters for more than fifty hydrocarbons to at least 0.002 Å compared to the experimentally determined<sup>34</sup> values from isolated CH stretching frequencies, which agree with previously determined values from earlier microwave studies. Therefore, all of the carbon-hydrogen parameters can be taken from the MP2(full)/6-311+G(d,p) predicted values for the *Ax* conformer. However, in order to further reduce the number of independent variables, the structural parameters are separated into sets according to their types, where bond distances in the same set keep their relative ratio and bond angles and torsional angles in the same set keep their difference in degrees. This assumption is based on the fact that errors from *ab initio* calculations are systematic. Therefore, it should be possible to obtain “adjusted  $r_0$ ” structural parameters for the twelve parameters

of the seven heavy atoms by adjusting the C-C distances as a single set and varying the  $\angle$ CCC angles as another set leaving eight parameters to adjust. However, this structure must be evaluated using parameters from similar molecules since there are a limited number of rotational constants available. By utilizing the experimentally determined rotational constants obtained from the microwave spectra reported in this study, we have obtained a complete set of structural parameters for the *Ax* form of *c*-C<sub>5</sub>H<sub>9</sub>NC.

The resulting adjusted  $r_0$  parameters with standard errors listed in Table 19. It is believed that the N $\equiv$ C, C-N, and C-C distances should be accurate to  $\pm 0.003$  Å, the C-H distances accurate to  $\pm 0.002$  Å, and the angles should be within  $\pm 0.5^\circ$ . The fit of the three determined rotational constants by the adjusted  $r_0$  structural parameters for the *Ax* conformer is excellent with the differences being 0.10, 0.15, and 0.07 MHz for the A, B and C rotational constants, respectively. Moreover, it is believed that the suggested uncertainties are realistic values and the determined structural parameters are probably as accurate as can be obtained for the molecule in the gas phase by either electron diffraction or microwave substitution methods.

Additionally, it has been shown that the differences in predicted distances and angles from the *ab initio* calculations for different conformers of the same molecule can usually be used as one parameter with the *ab initio* predicted differences except for some dihedral angles. Therefore, we have predicted structural parameters for the *Eq* form of isocyanocyclopentane by applying the corresponding adjustments from the *Ax* conformer to the MP2(full)/6-311+G(d,p) predicted parameters for the *Eq* form. These parameters should be close to the actual value except, possibly, for the dihedral angles.

## Discussion

Average and percent errors have been calculated between predicted and observed frequencies for the *Ax* and the *Eq* conformer of the isocyanocyclopentane. For both *Ax* and *Eq* conformers, *A'* modes have an average error of 6.64 and 6.19  $\text{cm}^{-1}$ , respectively, which represents percent errors of 0.38 and 0.40%, respectively. *A''* modes have an average error of 4.46 and 4.13  $\text{cm}^{-1}$ , respectively, which represents percent errors of 0.28 and 0.25%, respectively. Both the average and percent errors are reasonable and show that predicted frequencies are meaningful with respect to the vibrational assignments.

An interesting point to note is that A, B and C type band contours were not observed in the infrared spectra of gas of isocyanocyclopentane (Fig. 17). However, theoretical calculations show that there should be A, B and C type band contours. Predicted A, B, and C type band contours for both the *Ax* and *Eq* conformers are shown in Fig. 21. Exact reasons for this unusual behavior should be investigated. This has little effect on the experimental results in this study, as the bands are well resolved in the spectra of the xenon solutions.

The *Ax* fundamental  $\nu_{19}$  is assigned to the doublet at 711/661  $\text{cm}^{-1}$  in the infrared spectra of the xenon solutions and 683  $\text{cm}^{-1}$  in the infrared spectrum of the solid, and predicted to be at 709  $\text{cm}^{-1}$  from the *ab initio* calculations and 680  $\text{cm}^{-1}$  with scaling factors. This doublet, however, results from a Fermi resonance between of the *Ax* fundamental and a difference band. This band is consistent with an *Ax* band in the change in the band's intensity due to variation of the temperature and therefore an appropriate band for use in the enthalpy determination.

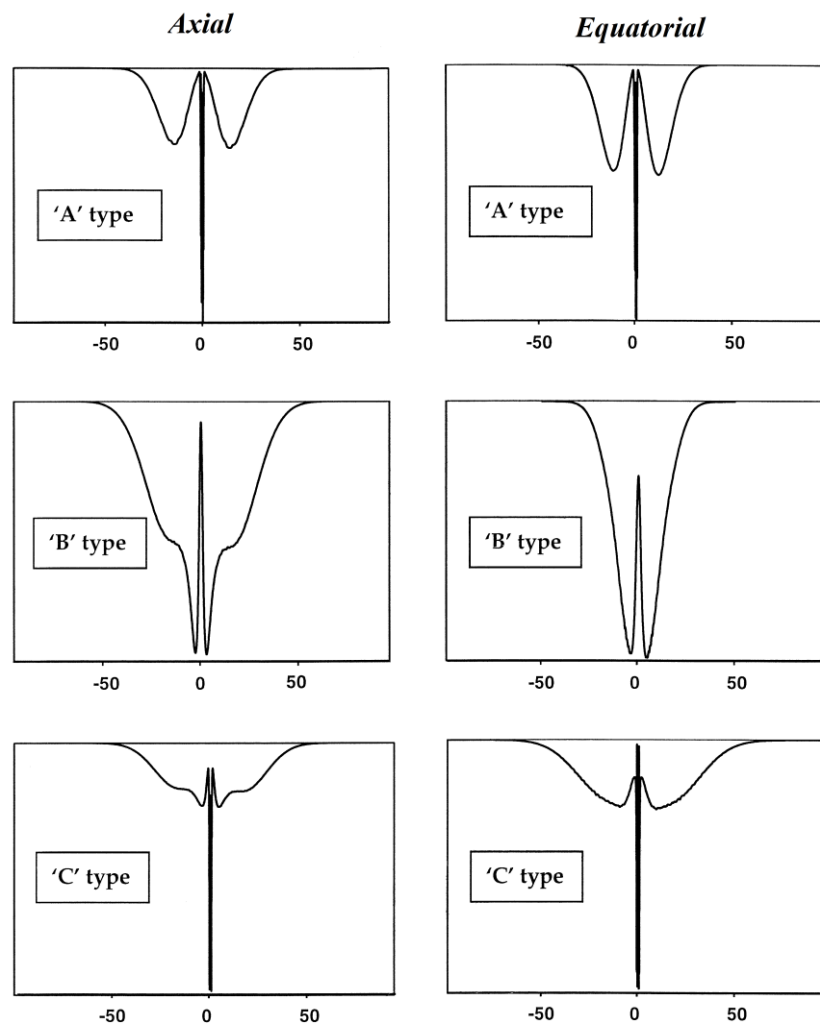


**Fig. 21** Band contour predictions for the *Ax* and *Eq* conformer of isocyanocyclopentane.

However, because of the somewhat ambiguous nature of the *Ax* band at  $711\text{ cm}^{-1}$ , which was used for the enthalpy determination, the enthalpy value was also determined without inclusion of the  $711\text{ cm}^{-1}$  band. This determination gives an enthalpy value of  $95 \pm 2\text{ cm}^{-1}$  ( $1.13 \pm 0.03\text{ kJ mol}^{-1}$ ) from 9 band pairs. This latter value is within the error

limits of the enthalpy value including the band at  $711\text{ cm}^{-1}$ , so the band at  $711\text{ cm}^{-1}$  does not appear to significantly change the enthalpy value. Therefore, the reported enthalpy value is thought to be accurate within its error limits and as accurate as what could be obtained from a dilute gas sample.

A natural population analysis (NPA) was carried out for the *Ax* and *Eq* conformers of isocyanocyclopentane and cyclopentane with the MP2(full) method using the 6-311+G(d,p) basis set. The C atoms for cyclopentane all carry a -0.34 charge. However the  $\text{-N}\equiv\text{C}$  substitution of cyclopentane gives a charge distribution for the *Ax* [*Eq*] form of  $C_\alpha = 0.01$  [0.00],  $C_\beta = -0.33$  [-0.33],  $C_\gamma = -0.35$  [-0.34],  $\text{-N}\equiv\text{C}^* = 0.34$  [0.35],  $\text{N} = -0.65$  [-0.64]. As might be expected, the  $\text{-N}\equiv\text{C}$  group has a large effect on the charge density of the  $\alpha$  carbon with a much reduced effect on the  $\beta$  and  $\gamma$  carbons. However, it is interesting to note that the *Ax*  $\gamma$  carbon, which is brought closer to the  $\text{-N}\equiv\text{C}$  electron orbitals due to the conformational geometry, is slightly more negative than the corresponding carbon in the *Eq* form.

Taking into account the low number of rotational constants, the structural parameters of *c*- $\text{C}_5\text{H}_9\text{NC}$  must be evaluated for their accuracy by comparing them with similar molecules. As can be seen from the data in Table 23, the  $\text{N}\equiv\text{C}$  distances and  $\text{C-N}\equiv\text{C}$  angles are consistent regardless of the substituent whereas the C-N distances change depending on the substituent. The predicted distances for the  $\text{N}\equiv\text{C}$  structural parameter values for the methyl-,<sup>67</sup> vinyl-,<sup>68</sup> ethynyl-,<sup>69</sup> and cyclopropyl<sup>70</sup> isocyanide compounds has an average difference of  $0.014\text{ \AA}$  of the structural parameter values obtained from the MP2(full)/6-311+G(d,p) calculations. The structures in this study were

determined for the *Ax* form of isocyanocyclopentane and the parameters were allowed to change in fitting the rotational constants. As can be seen from the information in Table 19, the differences between the values from the MP2(full)/6-311+G(d,p) calculation and the adjusted  $r_0$  structural parameter values for the N≡C bond distance is 0.010 Å which is similar to the distances in the molecular structure for similar bond distances as can be seen in Table 23. Due to the limited number of structural studies on molecules that contain the N≡C moiety, it would be of interest to obtain more molecular structures of such molecules.

Additionally, it would be of interest to compare the structural parameters of *c*-C<sub>5</sub>H<sub>9</sub>NC with the corresponding cyclopentanes with –C≡C or –C≡N moieties on them to see how the substitutions would affect the values of the molecular structures. As it can be seen from the data in Table 24, the *ab initio* MP2(full) calculation at the 6-311+G(d,p) basis set does a fairly good job predicting the bond distances and angles for these molecules. There is no significant difference between the cyano- and ethynylcyclopentane rings parameters as the differences are within the corresponding uncertainties. On the other hand, the C<sub>α</sub>-C<sub>β</sub>,C<sub>β</sub>' bond distances are ~0.008 Å shorter for the ring that is substituted with the –N≡C moiety as opposed to the rings that are substituted with –C≡C and –C≡N moieties. The <C<sub>β</sub>-C<sub>α</sub>-N is 1.1° smaller than both <C<sub>β</sub>-C<sub>α</sub>-C and <C<sub>β</sub>-C<sub>α</sub>-C angles. These differences are expected, and are reflected in the *ab initio* calculated values. The rest of the ring structural parameters of isocyanocyclopentane are within the errors associated with the parameters when it is compared to the other substituted ring molecules.

**Table 23.** Comparison of select structural parameters (Å and degrees) of molecules of the form C≡N-R.

Structural Parameters	C≡N-CH <sub>3</sub>		C≡N-C(H)=CH <sub>2</sub>		C≡N-C≡CH		<i>c</i> -C <sub>3</sub> H <sub>5</sub> -N≡C	
	Pred. <sup>a</sup>	Ref <sup>67, a</sup>	Pred. <sup>a</sup>	Ref <sup>68, b</sup>	Pred. <sup>a</sup>	Ref <sup>70, c</sup>	Pred. <sup>a</sup>	Ref <sup>70, d</sup>
rN≡C	1.183	1.1665	1.188	1.174(6)	1.192	1.176(1)	1.186	1.176(5)
rC <sub>α</sub> -N≡C	1.423	1.4266	1.386	1.379(6)	1.317	1.318(1)	1.400	1.377(8)
∠C <sub>α</sub> -N≡C	179.9	180.0	178.0	178.2(12)	180.0		179.8	180.0

<sup>a</sup>MP2(full) 6-311+ G(d,p)

<sup>b</sup>Electron Diffraction Structure

<sup>c</sup>r<sub>s</sub> structural parameters

<sup>d</sup>Adjusted r<sub>0</sub> structural parameters

<sup>e</sup>r<sub>s</sub> structural parameters

**Table 24.** Comparison of select structural parameters (Å and degrees) for the *Ax* conformer of molecules of the form *c*-C<sub>5</sub>H<sub>9</sub>-X≡Y.

Structural Parameters	<i>c</i> -C <sub>5</sub> H <sub>9</sub> -C≡C-H		<i>c</i> -C <sub>5</sub> H <sub>9</sub> -C≡N		<i>c</i> -C <sub>5</sub> H <sub>9</sub> -N≡C	
	MP2(full)/ 6-311+G(d,p)	Ref <sup>44, a</sup>	MP2(full)/ 6-311+G(d,p)	Ref <sup>47a</sup>	MP2(full)/ 6-311+G(d,p)	This Study <sup>a</sup>
rC <sub>α</sub> -C <sub>β</sub> , C <sub>β</sub> '	1.540	1.542(3)	1.539	1.542(3)	1.531	1.534 (3)
rC <sub>β</sub> -C <sub>γ</sub> , rC <sub>β</sub> '-C <sub>γ</sub> '	1.540	1.542(3)	1.540	1.542(3)	1.541	1.542 (3)
rC <sub>γ</sub> -C <sub>γ</sub> '	1.553	1.555(3)	1.553	1.559(3)	1.554	1.554 (3)
∠C <sub>β</sub> C <sub>α</sub> -X	111.0	111.5(5)	110.5	111.5(5)	109.4	110.4 (5)
∠C <sub>β</sub> C <sub>α</sub> C <sub>β</sub> '	101.4	102.1(5)	101.8	102.0(5)	102.4	102.9 (5)
∠C <sub>α</sub> C <sub>β</sub> C <sub>γ</sub>	103.8	103.7(5)	103.8	103.6(5)	103.7	103.6 (5)
∠C <sub>β</sub> C <sub>γ</sub> C <sub>γ</sub> '	105.6	105.9(5)	105.7	105.7(5)	105.7	105.9 (5)
τC <sub>α</sub> C <sub>β</sub> C <sub>γ</sub> C <sub>γ</sub> '	26.4	25.7(5)	25.9	25.8(5)	25.6	25.0 (5)
τC <sub>β</sub> C <sub>γ</sub> C <sub>γ</sub> 'C <sub>β</sub> '	0.0	0.0(5)	0.0	0.0	0.0	0.0 (5)

<sup>a</sup> Adjusted *r*<sub>0</sub> parameters.

Further, to examine the effect of substituting the isocyanide moiety on the cyclopentane ring, a comparison between the unsubstituted cyclopentane and isocyanocyclopentane would be of interest. The ring parameters are much more flexible where the ring distances, and angles for five membered rings are often relatively sensitive to substitution. The C-C distances of cyclopentane were reported to be 1.546(1) Å from an electron diffraction study.<sup>71</sup> It can be seen that the C<sub>α</sub>-C<sub>β</sub> bond distances are ~0.012 Å shorter for the cyclopentane ring with the -N≡C moiety on it as opposed to unsubstituted cyclopentane. The C<sub>β</sub>-C<sub>γ</sub> bond distances are longer and within the experimental error of the value from the cyclopentane r<sub>0</sub> structure. The C<sub>γ</sub>-C<sub>γ'</sub> bond distance is ~0.008 Å longer for the cyclopentane ring with the -N≡C moiety on it when compared to unsubstituted cyclopentane.

The electronegative -N≡C group as compared to cyclopentane causes a significant difference in the C<sub>α</sub> charge, which in turn appears to cause a significant difference in the C<sub>α</sub>-C<sub>β</sub> bond distance where the -N≡C molecule is 0.012 Å shorter. This effect is reduced in the β Carbon and the C<sub>β</sub>-C<sub>γ</sub> distance is closer to the unsubstituted cyclopentane where the -N≡C molecule is only 0.004 Å shorter, which is within the error limits. The C<sub>α</sub>-C<sub>β</sub> bond is also 0.008 Å shorter than the C<sub>β</sub>-C<sub>γ</sub> distance in the -N≡C molecule, which reinforces the idea that the charge on C<sub>α</sub> is the cause of the C<sub>α</sub>-C<sub>β</sub> bond shortening. There is a small 0.01 charge difference on the γ carbon charges between the Ax conformer of the -N≡C molecule and the cyclopentane carbons. However, this probably is not the cause of the difference in the C<sub>γ</sub>-C<sub>γ</sub> bond distance. Instead this difference is a common occurrence in substituted cyclopentane rings and is probably related to steric forces in the ring introduced by the substitution.

At the time this study was initiated there was some confusion regarding which conformer was the most stable form of many mono substituted cyclopentanes. It should be noted that cyanocyclopentane,<sup>47</sup> which belongs to this group of mono-substituted cyclopentanes, has the *Ax* conformer as the more stable form by  $109 \pm 37 \text{ cm}^{-1}$  determined from the infrared spectra of the xenon solutions. This is opposite to ethynylcyclopentane which has been reported<sup>44</sup> to have the *Eq* form more stable by  $94 \pm 9 \text{ cm}^{-1}$ . Thus from our current study of isocyanocyclopentane it was necessary to be absolutely sure which conformer was more stable. Therefore in addition to the enthalpy determinations from the infrared spectra of the xenon solution we obtained additional scientific evidence for the conformational stabilities.

The first step in this process was to obtain the stable conformer in the solid state. By utilizing *ab initio* predicted frequencies the spectra were predicted of the isolated molecules of the *Ax* and *Eq* forms, and they are shown in Fig. 17E and 15F. The infrared spectrum of the solid was thus obtained and it is shown in Fig. 17C. These spectra were then compared and, as can be observed from Fig. 17, the spectrum of the solid did not demonstrate a pure crystal of a single conformer. It is believed that spectrum is due to the sample being an amorphous mixture instead of a pure crystal. Nevertheless, from the spectra of the solid it is clearly observed that the band intensities of peaks attributable to the *Ax* form are significantly higher compared to that of the *Eq* form, especially in the spectral regions from 400 to  $1100 \text{ cm}^{-1}$ . Thus it appears that the *Ax* form is the more stable conformer in the solid as well. However, it should be noted that the *Ax* conformer need not be the more stable conformer in spectra of the gas and xenon solutions.

The *ab initio* calculations were carried out for this study, and the energy differences for the four possible forms were obtained with the *Ax* form as the most stable conformer followed by the *Eq*, *Tw* and *Pl* forms. From these *ab initio* calculations it was found that the other two possible conformers (*Tw* and *Pl* forms) are not stable conformers, but they represent transition states. The enthalpy differences obtained should be comparable to the *ab initio* predicted energy values, and also can be compared with other enthalpy differences obtained for other mono substituted cyclopentanes. The *ab initio* predicted energy difference from the MP2(full)/aug-cc-pVTZ calculations with 529 basis sets predicted the *Ax* conformer as the more stable form by  $372\text{ cm}^{-1}$  (4.45 kJ/mol) over the *Eq* form. The same basis set but with the B3LYP method gave instead the *Eq* form as the most stable conformer. Thus the MP2(full) calculation gives better results for conformational stability predictions in this study compared to the B3LYP method which was not able to predict a specific conformer as the more stable form.

The jet propulsion FT-microwave study provided conclusive conformational stability results. The rotational transitions that were assigned from the microwave study gave rotational constants that fit those for the *Ax* conformer alone. Thus, it was demonstrated that between the *Ax* and *Eq* forms, it is the *Ax* conformer that is the more stable form. Next to be considered was the variable temperature infrared spectrum of the sample in liquified xenon and those spectra were obtained and also confidently assigned. The determined  $\Delta H$  values conclusively showed that the *Ax* form was the more stable form by  $102 \pm 10\text{ cm}^{-1}$  compared to the *Eq* form. The lower wavenumber region is confidently assigned for both *Ax* and *Eq* conformers and so by using 12 band pairs the

value for enthalpy difference is conclusively determined. The uncertainty of the value for each individual band pair ranges from a high value of  $12\text{ cm}^{-1}$  to a low value of  $2\text{ cm}^{-1}$ . This relatively small spread in enthalpy differences indicates that there is little interference from overtone or combination bands.

The quadratic centrifugal distortion constants have been determined from the fit of the experimental rotational spectra and have been predicted by using the MP2(full) method with the 6-31G(d) and 6-311+G(d,p) basis sets. These data are given in Table 15 and as can be seen from the values of the CDCs, there is reasonable agreement with the predicted values for both calculations. Only the  $\Delta_K$  and  $\delta_K$  constants are relatively poorly predicted. However, this is probably due to the lack of high  $K_a$  energy levels with which to fit these constants, rather than an error in the predicted results. We have found in the past that the *ab initio* calculations usually predict fairly good distortion constants. The CDC's were also predicted by using the B3LYP method with the 6-311+G(d,p) basis set. However, only the  $\Delta_J$  is meaningful as the remaining values are either the wrong sign or multiples of magnitude in error (or both). This is interesting as this may be indicative of errors in the calculation of the force constants for this molecule. However, that is out of the scope of this study.

Since very few isocyano- molecules have been studied, in detail wider conclusions on this moiety's effects on molecular structures and conformational stabilities are limited. It would therefore be of interest to study additional isocyano- molecules in order to observe and interpret any trends so uncovered.

(This work has been published in *Spectrochimica Acta* A<sup>45</sup>.)

## CHAPTER 6

# MICROWAVE, $r_0$ STRUCTURAL PARAMETERS, CONFORMATIONAL STABILITY AND VIBRATIONAL ASSIGNMENT STUDIES OF CYCLOPROPYLCYANOSILANE

### Introduction

The determination of structural parameters and conformational stabilities are usually challenging for molecules like X-SiH<sub>2</sub>-Y (X = alkanes, cycloalkanes; Y = F, Cl, Br, CN, and CH<sub>3</sub>). Over the years, studies done on these molecules have been very limited. An investigation in our laboratories began with ethyl chlorosilane<sup>72</sup>, ethyl fluorosilane<sup>73</sup> and ethyl bromosilane.<sup>74</sup> For ethyl fluorosilane and ethyl chlorosilane both *gauche* and *trans* conformers were observed in fluid phases and only the *gauche* conformer was observed in the solid phase. However, for ethyl bromosilane, the *anti* and *gauche* conformers were observed in the vapor and liquid phases, and only the *gauche* form was observed in the solid phase.<sup>72, 73, 74</sup> By utilizing variable temperature studies of the infrared spectra of samples dissolved in xenon solutions, the enthalpy difference was determined to be  $54 \pm 16 \text{ cm}^{-1}$  ( $0.65 \pm 0.19 \text{ kJ/mol}$ ) for ethyl fluorosilane;  $204 \pm 23 \text{ cm}^{-1}$  ( $2.44 \pm 0.27 \text{ kJ/mol}$ ) for ethyl chlorosilane and  $140 \pm 25 \text{ cm}^{-1}$  ( $1.67 \pm 0.3 \text{ kJ/mol}$ ) for ethyl bromosilane with the *gauche* conformer being the more stable form in all three compounds.<sup>72,73,74</sup>

Further investigations included cyclopropylfluorosilane,<sup>75</sup> cyclopropylchlorosilane<sup>76</sup> and cyclopropylbromosilane.<sup>77</sup> The enthalpy difference was determined to be  $109 \pm 9 \text{ cm}^{-1}$  ( $1.30 \pm 0.1 \text{ kJ/mol}$ ) for cyclopropylfluorosilane with the *gauche* form the more stable conformer, whereas for cyclopropylchlorosilane and

cyclopropylbromosilane, the *cis* conformer was the more stable form, with the enthalpy differences of  $98 \pm 10 \text{ cm}^{-1}$  ( $1.2 \pm 0.12 \text{ kJ/mol}$ ) and  $126 \pm 25 \text{ cm}^{-1}$  ( $1.51 \pm 0.30 \text{ kJ/mol}$ ), respectively,<sup>75,76,77</sup> It is interesting to note that in cyclopropylchlorosilane and cyclopropylbromosilane both the *gauche* and *cis* conformers were present in the liquid phase and only the *gauche* conformer was present in the solid phase.<sup>76,77</sup> At ambient temperature,  $23 \pm 2 \%$  of cyclopropylfluorosilane was in the *cis* form, whereas for the cyclopropylbromosilane, the ratio of *gauche* to *cis* conformers was almost equal<sup>75,76</sup>. For these cyclopropylsilane derivatives, their conformational stability changes with respect to substitution of different halogens on the silane moiety. The study of cyclopropylmethylsilane<sup>78</sup> showed that the *gauche* form was the more stable conformer with an enthalpy difference of  $98 \pm 13 \text{ cm}^{-1}$  ( $1.17 \pm 0.16 \text{ kJ/mol}$ ), and at ambient temperature, the amount of *cis* conformer was  $23 \pm 6 \%$ . However, these data are not sufficient for establishing the relationship between conformational stability and substituted cyclopropylsilane derivatives. Studies of additional similar molecules would thus be useful for arriving at a firmer conclusion. There has been no previous study reported in the literature for cyclopropylcyanosilane, which is a pseudohalogen derivative of cyclopropylsilane and, hence, as a logical progression, it was decided to investigate this molecule. In this study, the aim was to determine structural parameters, enthalpy differences between conformers, and the more stable conformer of cyclopropylcyanosilane.

In order to determine structural parameters, we began by obtaining FT-microwave spectral data of cyclopropylcyanosilane, *c*-C<sub>3</sub>H<sub>5</sub>SiH<sub>2</sub>CN. For identifying fundamental vibrational modes of cyclopropylcyanosilane, the Raman spectrum of the liquid and

infrared spectrum of the gas were investigated. For determining the enthalpy difference between the two possible staggered conformers, variable temperature infrared spectra of the sample dissolved in xenon solution were investigated. To support the vibrational study, *ab initio* calculations with basis sets up to aug-cc-pVTZ as well as those with diffuse functions, *i.e.*, 6-311+G(2df,2pd) have been carried out. Density functional theory (DFT) calculations by the B3LYP method with the same basis sets have also been carried out. Optimized geometries, conformational stabilities, harmonic force fields, infrared intensities, Raman activities and depolarization ratios were also calculated. The results of these spectroscopic, structural and theoretical studies of cyclopropylcyanosilane are reported herein.

### Methods

The cyclopropylcyanosilane molecule,  $c\text{-C}_3\text{H}_5\text{SiH}_2\text{CN}$  was prepared from cyclopropylbromosilane and silver cyanide in solvent at 40 °C for 24 hours.(Fig. 22) However, cyclopropylbromosilane was prepared by the cycloprotonation of trimethoxysilane by using a slightly modified Simmons-Smith reaction.<sup>79</sup> A stirred slurry of Zn-Cu and vinyltrimethoxysilane in hexane was sonicated while methylene iodide was added. After the solvent was evaporated, the middle fraction of the distillate at 68-70 °C and 37.5 torr contained trimethoxycyclopropylsilane. It was reduced with lithium aluminum hydride in dry dibutyl ether under dry nitrogen gas to produce cyclopropylsilane which was brominated with an equivalent amount of boron tribromide at 0 °C for 18 hrs under vacuum. The bromo compound was first separated from diborane by using liquid nitrogen-alcohol slush at -80 °C. The sample was further purified using a trap-to-trap distillation several times before the reaction with silver cyanide.

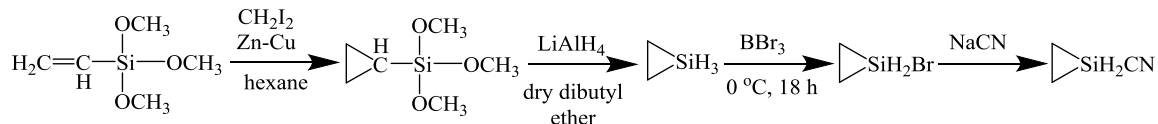


**Fig. 22** Synthesis of cyclopropylcyanosilane.

The rotational spectrum of cyclopropylcyanosilane was studied using a CP-FTMW spectrometer developed at the University of Virginia, and operating in the 6.5 to 18 GHz range. The chirped pulse methods used here have been described in detail previously<sup>80,81</sup> so only the brief details relevant to this experiment are necessary here.

The microwave source was a 24 GS/s arbitrary waveform generator, producing a 12-0.5 GHz linear frequency sweep in 1  $\mu$ s. The pulse was upconverted to 6.5-18 GHz by a 18.95 GHz phase-locked resonant dielectric oscillator (PRDO), and then amplified by a pulsed 300 W traveling wave tube amplifier. The amplified pulse is then transmitted through free space between two standard-gain microwave horns, where it interacts with a molecular beam generated by five pulsed nozzles (General Valve Series 9) operating perpendicular to the propagation direction of the microwave pulse. On the detection end, the receiver is protected from the high power pulse by a combination of a PIN diode limiter and single-pole microwave switch. The resulting molecular free induction decay (FID) was then amplified and digitized directly on a 100 GS/s oscilloscope with 33 GHz of hardware bandwidth, with a 20  $\mu$ s detection time per FID. Due to the speed of this excitation and detection process, a sequence of 10 excitation/detection cycles is possible per gas pulse, and all ten detected FIDs are collected and averaged together before the

next valve injection cycle begins. Phase stability of this experiment over the course of many valve injection cycles is enabled by locking all the frequency sources and the oscilloscope to a 10 MHz Rb-disciplined quartz oscillator. For this experiment, approximately 78,000 valve injection cycles of the sample gas were completed at 3.3 Hz to create a time-averaged spectrum of 780,000 molecular FIDs (approximately 6.5 hours of averaging). Additionally, the time domain resolution afforded by a 20  $\mu$ s FID generates an average Doppler broadened linewidth of approximately 130 kHz at FWHM.

For this experiment, approximately 25,000 valve injection cycles of the sample gas, using five pulsed nozzles, were completed at 4 Hz to create a time-averaged spectrum of 250,000 molecular FIDs (approximately 2.5 hours of averaging). Additionally, the time domain resolution afforded by a 20  $\mu$ s FID generates an average Doppler broadened linewidth of approximately 130 KHz at FWHM.

The sample was prepared by balancing cyclopropylcyanosilane vapor with approximately 3.4 atm of Ne gas (GTS Welco) for a total sample concentration of approximately 0.2%. This afforded a frequency-domain dynamic range of approximately 6,000:1 at 250,000 averages, which enabled assignment of all common heavy atom single isotopologues ( $^{13}\text{C}$ ,  $^{29}\text{Si}$ ,  $^{30}\text{Si}$ ) in natural abundance. The rotational temperature for the species detected in this experiment is roughly 1.5 K. Comparison between the observed frequencies and those from a least-squares fit for the *cis* conformer are listed in Tables 25 and 26, whereas for the *gauche* conformer, transitions are listed in Tables 27 and 28.

The experimental analysis of the cyclopropylcyanosilane spectrum was supplemented with *ab initio* electronic structure calculations to predict rotational,

centrifugal distortion and quadrupole coupling constants. All calculations were performed using the Gaussian 09 suite of programs<sup>82</sup> at the MP2/6-311++G(d,p) level of theory. Initial microwave fits were performed using Autofit, an automated triples fitting program for microwave spectra developed at the University of Virginia. Autofit is a front end for the freely available SPCAT and SPFIT fitting programs<sup>83</sup>. Details of the Autofit routine are to be published in a future article, but a current version is freely available at the Pate group website.<sup>84</sup> Using the *cis*-conformer as an example, the broadband spectrum was scanned using Autofit by automating the fitting of a number of strong predicted  $\mu_b$  and  $\mu_a$  type transitions, specifically the  $3_{03} - 2_{02}$ ,  $3_{12} - 2_{11}$  transitions, which together give a strong starting prediction for the values B+C and B-C, and the  $2_{21} - 1_{110}$   $\mu_b$  type transition, which determines the value of A when coupled with the two  $\mu_a$  type transition determinations of B&C. A/B/C triplets found in the spectrum, using these three fit transitions, were then checked for overall goodness of fit by adding an additional set of 8 transitions that were predicted to be of similar intensity to the chosen triple. This process was also used to identify the *gauche* conformer in the broadband microwave spectrum. Additionally, all final fits for all assigned species were performed using the AABS package.<sup>85</sup>

**Table 25.** Rotational transition frequencies (MHz) of the ground vibrational state of *cis*-cyclopropylcyanosilane, *c*-C<sub>3</sub>H<sub>5</sub>SiH<sub>2</sub>CN.

<i>c</i> -C <sub>3</sub> H <sub>5</sub> SiH <sub>2</sub> CN									
Transitions	F''	F'	$\nu_{\text{obs}}$ (MHz)	$\Delta\nu^a$	Transitions	F''	F'	$\nu_{\text{obs}}$ (MHz)	$\Delta\nu^a$
4 <sub>22</sub> ← 4 <sub>13</sub>	3	4	6046.1193	-0.0133	7 <sub>25</sub> ← 7 <sub>16</sub>	1	2	8273.7440	-0.0061
	5	4	6045.4984	-0.0025		3	2	8274.1709	0.0041
	5	5	6046.1184	-0.0032		1	0	8274.8692	0.0156
	4	5	6046.7001	0.0038		7 <sub>25</sub> ← 7 <sub>16</sub>	7	7	8276.1850
1 <sub>11</sub> ← 0 <sub>00</sub>	4	3	6046.8617	0.0058	3 <sub>22</sub> ← 3 <sub>13</sub>	2	2	8921.5324	-0.0021
	1	1	6071.5481	-0.0058	4	4	8921.8399	-0.0003	
	2	1	6072.2512	-0.0029	3	3	8922.7107	-0.0030	
5 <sub>23</sub> ← 5 <sub>14</sub>	0	1	6073.3000	-0.0045	8 <sub>35</sub> ← 8 <sub>26</sub>	9	9	9175.0405	-0.0061
	4	5	6235.9639	-0.0190	7 <sub>34</sub> ← 7 <sub>25</sub>	7	7	9400.1424	0.0081
	6	5	6236.1307	0.0029	8	8	9400.3594	0.0179	
3 <sub>21</sub> ← 3 <sub>12</sub>	6	6	6236.6144	0.0062	2 <sub>12</sub> ← 1 <sub>01</sub>	2	1	9441.0355	0.0127
	5	5	6236.8344	-0.0048	3	2	9441.7730	-0.0025	
	2	3	6244.8352	0.0054	3 <sub>03</sub> ← 2 <sub>12</sub>	2	1	9577.8821	-0.0012
2 <sub>20</sub> ← 2 <sub>11</sub>	4	3	6244.9450	-0.0195	4	3	9578.1740	0.0014	
	3	3	6245.3492	-0.0005	3	2	9578.5380	0.0017	
	4	4	6245.6698	-0.0045	2	2	9579.1063	-0.0032	
	2	2	6245.7983	0.0104	4 <sub>23</sub> ← 4 <sub>14</sub>	3	3	10021.2051	0.0031
5 <sub>24</sub> ← 5 <sub>15</sub>	3	4	6246.0596	0.0000	5	5	10021.4389	0.0043	
	3	2	6246.2855	-0.0223	4	4	10022.3431	0.0042	
	1	2	6651.5472	-0.0096	6 <sub>15</sub> ← 6 <sub>16</sub>	5	5	10143.4671	0.0130
	3	2	6651.6776	0.0121	7	7	10143.7004	0.0076	
	2	2	6651.8644	0.0031	6	6	10145.1109	0.0040	
	3	3	6652.4167	0.0010	3 <sub>22</sub> ← 3 <sub>03</sub>	4	4	10173.2727	-0.0055
	2	3	6652.6100	-0.0014	3	3	10173.6992	-0.0035	
6 <sub>24</sub> ← 6 <sub>15</sub>	1	1	6652.7303	0.0065	6 <sub>15</sub> ← 6 <sub>06</sub>	5	5	10384.9722	0.0134
	2	1	6653.0297	0.0015	7	7	10385.1896	0.0058	
	6	5	6693.9424	0.0228	6	6	10386.5223	0.0055	
2 <sub>12</sub> ← 1 <sub>11</sub>	5	5	6950.7446	0.0190	4 <sub>13</sub> ← 3 <sub>22</sub>	5	4	10503.5785	-0.0004
	6	6	6951.2830	-0.0089	4	3	10504.2083	0.0085	
	2	2	7249.9730	-0.0045	5 <sub>32</sub> ← 5 <sub>23</sub>	5	5	10769.4346	0.0148
	1	0	7250.1480	-0.0053	4 <sub>23</sub> ← 4 <sub>04</sub>	5	5	10813.0536	-0.0093
5 <sub>14</sub> ← 5 <sub>15</sub>	3	2	7250.7442	-0.0215	4	4	10813.6720	-0.0064	
	1	2	7251.1989	-0.0048	3 <sub>13</sub> ← 2 <sub>12</sub>	3	3	10828.7389	0.0018
	1	1	7251.9030	-0.0009	4	3	10829.5953	-0.0152	
	4	4	7463.9277	-0.0015	2	3	10829.9174	0.0010	
2 <sub>02</sub> ← 1 <sub>01</sub>	6	6	7464.2359	-0.0040	2	2	10830.7037	-0.0008	
	5	5	7465.7623	-0.0028	3 <sub>03</sub> ← 2 <sub>02</sub>	3	3	11336.6805	-0.0019
	2	1	7682.6952	0.0144	3	2	11336.8797	0.0014	
5 <sub>14</sub> ← 5 <sub>05</sub>	3	2	7682.8395	-0.0014	4	3	11337.0937	-0.0133	
	4	4	7917.5502	-0.0004	2	2	11337.4477	-0.0038	
2 <sub>21</sub> ← 2 <sub>12</sub>	6	6	7917.8275	-0.0009	5 <sub>24</sub> ← 5 <sub>15</sub>	4	4	11400.7397	0.0017
	5	5	7919.2063	0.0136	6	6	11400.9307	0.0058	
	1	1	8107.2940	0.0048	5	5	11401.8355	-0.0076	
2 <sub>11</sub> ← 1 <sub>10</sub>	3	3	8107.7418	-0.0062	4 <sub>31</sub> ← 4 <sub>22</sub>	4	4	11447.4761	0.0126
	2	2	8108.5752	0.0008	4	3	11448.1930	0.0073	
	1	1	8273.0099	-0.0044	3 <sub>22</sub> ← 2 <sub>21</sub>	4	3	11643.7222	0.0195

<sup>a</sup>  $\Delta\nu = \nu_{\text{obs}} - \nu_{\text{calc}}$  in MHz

**Table 25.- - Continued.**

Transitions	F''	F'	$\nu_{\text{obs}}$ (MHz)	$\Delta\nu^a$	Transitions	F''	F'	$\nu_{\text{obs}}$ (MHz)	$\Delta\nu^a$
$5_{24} \leftarrow 5_{05}$	6	6	11854.4990	-0.0144		1	0	14848.0698	0.0003
	5	5	11855.2641	-0.0066	$7_{26} \leftarrow 7_{17}$	6	6	14899.2492	-0.0035
$3_{30} \leftarrow 3_{21}$	3	3	11901.5528	0.0092		8	8	14899.3726	-0.0088
	4	4	11901.8565	0.0354		7	7	14900.2748	0.0004
$3_{21} \leftarrow 2_{20}$	2	2	11949.8113	0.0016		8	8	15021.4717	-0.0079
	4	3	11950.1442	0.0039		7	7	15022.3335	-0.0006
	3	2	11950.3328	0.0031	$5_{14} \leftarrow 4_{23}$	6	5	15292.3454	-0.0189
	3	3	11950.5142	-0.0113	$2_{20} \leftarrow 1_{11}$	1	0	15436.9377	-0.0127
	4	4	12280.0286	0.0292		3	2	15438.1127	0.0032
$3_{12} \leftarrow 2_{11}$	2	2	12355.8776	-0.0054		1	1	15438.7018	0.0008
	4	3	12356.9204	0.0387		2	1	15439.0038	-0.0015
	2	1	12357.0212	-0.0288	$4_{23} \leftarrow 3_{22}$	5	4	15462.4056	-0.0283
	3	3	12357.5902	-0.0012		5	4	15614.2773	-0.0003
$3_{13} \leftarrow 2_{01}$	3	2	12587.8667	-0.0005		3	3	15614.9631	0.0140
	4	3	12588.5489	0.0038	$4_{32} \leftarrow 3_{31}$	4	3	15663.4022	0.0226
	2	1	12588.7455	0.0033		5	4	15709.7040	-0.0055
	2	2	12589.0501	0.0035	$4_{22} \leftarrow 3_{21}$	5	4	16163.6449	-0.0227
$5_{33} \leftarrow 5_{24}$	5	5	12859.3074	-0.0098		4	3	16163.8757	0.0188
$6_{25} \leftarrow 6_{16}$	7	7	13039.0386	0.0032		4	4	16164.2061	-0.036
	6	6	13039.9661	0.0165	$7_{35} \leftarrow 7_{16}$	8	8	16295.9015	-0.0087
$7_{16} \leftarrow 7_{07}$	6	6	13064.2525	0.0074	$4_{13} \leftarrow 3_{12}$	3	3	16362.3442	-0.0066
	8	8	13064.4287	0.0072		5	4	16363.2384	0.0182
	7	7	13065.6296	-0.0151		4	4	16363.8202	-0.0207
$6_{25} \leftarrow 6_{06}$	6	6	13281.3461	-0.0133	$5_{41} \leftarrow 5_{32}$	5	5	16774.5573	-0.0143
$6_{34} \leftarrow 6_{25}$	5	5	13465.8506	-0.0156		6	6	16774.6797	-0.0351
	6	6	13466.2599	-0.0238	$4_{04} \leftarrow 3_{31}$	4	4	16950.4095	0.0322
$4_{04} \leftarrow 3_{13}$	4	4	13570.5466	0.0065		4	3	16950.5696	-0.0276
	3	2	13571.0594	-0.0187	$5_{42} \leftarrow 5_{33}$	6	6	16979.7063	-0.0226
	5	4	13571.2264	0.0151	$6_{43} \leftarrow 6_{34}$	7	7	16989.6793	-0.0105
	4	3	13571.4242	0.0107	$4_{41} \leftarrow 3_{32}$	5	5	17004.0205	-0.0068
	3	3	13572.2639	0.0065	$7_{44} \leftarrow 7_{35}$	8	8	17081.7879	0.0162
$7_{35} \leftarrow 7_{26}$	6	6	14338.7893	0.0000	$8_{45} \leftarrow 8_{36}$	7	7	17314.1804	0.0122
$4_{14} \leftarrow 3_{13}$	4	4	14361.8853	0.0055		8	8	17314.3021	0.0049
	3	2	14362.7907	0.0099	$5_{05} \leftarrow 4_{14}$	5	5	17395.0615	-0.0251
	3	3	14363.9676	0.0075		4	3	17395.9183	0.0147
$4_{04} \leftarrow 3_{03}$	4	4	14821.9706	-0.0073		5	4	17396.0753	0.0288
	4	3	14822.3990	-0.0035		4	4	17397.0990	-0.0113
	5	4	14822.6590	0.0097	$2_{20} \leftarrow 1_{01}$	3	2	17629.1342	0.0150
	3	3	14823.2463	-0.0001	$9_{46} \leftarrow 9_{37}$	10	10	17745.8146	0.0034
$2_{22} \leftarrow 1_{10}$	2	1	14846.3025	0.0132	$5_{15} \leftarrow 4_{14}$	5	4	17849.4569	-0.0172
	3	2	14846.9812	-0.0057		6	5	17849.5639	0.0050

<sup>a</sup>  $\Delta\nu = \nu_{\text{obs}} - \nu_{\text{calc}}$  in MHz

**Table 26.** Rotational transition frequencies (MHz) of the ground vibrational state of six isotopomers of *cis*-cyclopropylcyanosilane,  $c\text{-C}_3\text{H}_5^{29}\text{SiH}_2\text{CN}$ .

$c\text{-C}_3\text{H}_5^{29}\text{SiH}_2\text{CN}$									
Transitions	F''	F'	$\nu_{\text{obs}}$ (MHz)	$\Delta\nu^a$	Transitions	F''	F'	$\nu_{\text{obs}}$ (MHz)	$\Delta\nu^a$
$1_{11} \leftarrow 0_{00}$	1	1	6011.9241	-0.0009		4	3	11293.2722	-0.0203
	2	1	6012.6324	-0.0023		2	2	11293.6341	-0.0007
	0	1	6013.6983	-0.0009	$5_{24} \leftarrow 5_{15}$	5	5	11323.5173	-0.0019
$3_{21} \leftarrow 3_{12}$	3	3	6106.2778	-0.0001	$3_{22} \leftarrow 2_{21}$	4	3	11613.3876	0.0158
	4	4	6106.5936	-0.0054	$3_{00} \leftarrow 3_{21}$	3	3	11656.9018	-0.0050
	2	2	6106.7272	0.0158	$3_{00} \leftarrow 3_{21}$	4	4	11657.2112	0.0028
$5_{23} \leftarrow 5_{14}$	5	5	6154.5651	0.0002	$3_{21} \leftarrow 2_{20}$	2	2	11932.9600	-0.0007
	6	6	6154.3114	-0.0011		4	3	11933.3031	0.0105
$2_{20} \leftarrow 2_{11}$	2	2	6507.0244	-0.0020		3	2	11933.5074	0.0079
	3	3	6507.5949	0.0003	$3_{12} \leftarrow 2_{11}$	2	2	12333.2754	-0.0003
	1	1	6507.9061	-0.0041		4	3	12334.3268	0.0386
$6_{24} \leftarrow 6_{15}$	7	7	6922.1965	0.0013		3	3	12335.0113	0.0030
$2_{12} \leftarrow 1_{11}$	2	2	7222.7939	-0.0022		3	3	12492.0675	-0.0078
	1	0	7222.9506	-0.0076		3	2	12492.2729	0.0053
	3	2	7223.5608	-0.0239		4	3	12492.9469	-0.0014
	1	1	7224.7299	-0.0026		2	1	12493.1469	-0.0002
$5_{14} \leftarrow 5_{05}$	6	6	7552.1226	0.0102		2	2	12493.4460	-0.0001
	5	5	7553.6464	0.0068	$4_{04} \leftarrow 3_{13}$	3	2	13555.0127	-0.0015
$2_{02} \leftarrow 1_{01}$	2	1	7658.7581	0.0061		5	4	13555.1437	-0.0013
	3	2	7658.9209	0.0031		4	3	13555.3531	0.0148
$5_{14} \leftarrow 5_{05}$	4	4	7973.1170	0.0000	$4_{14} \leftarrow 3_{13}$	4	4	14301.7172	0.0018
	6	6	7973.4002	0.0033		5	4	14302.6547	-0.0209
	5	5	7974.7560	-0.0147		3	3	14303.7946	-0.0010
$2_{21} \leftarrow 2_{12}$	3	3	7980.0948	-0.0073	$2_{21} \leftarrow 1_{10}$	2	1	14684.4969	0.0033
	2	2	7980.9685	0.0496		3	2	14685.2023	0.0010
$2_{11} \leftarrow 1_{10}$	1	1	8259.7423	-0.0042		1	0	14686.2865	-0.0032
	3	2	8260.9025	-0.0022	$4_{04} \leftarrow 3_{03}$	4	4	14754.1534	0.0323
	1	0	8261.5998	0.0134		4	3	14754.5599	0.0106
$3_{22} \leftarrow 3_{13}$	2	2	8806.3883	-0.0004		5	4	14754.8278	0.0270
	3	4	8806.6873	-0.0069		3	3	14755.3996	-0.0041
	3	3	8807.5611	-0.0061	$2_{20} \leftarrow 1_{11}$	1	0	15285.8054	-0.0084
$2_{12} \leftarrow 1_{01}$	2	1	9364.3296	0.0053		3	2	15286.9735	-0.0114
	3	2	9365.0832	-0.0032		1	1	15287.5764	-0.0115
	1	0	9365.5066	0.0215		2	1	15287.8776	-0.0092
$3_{03} \leftarrow 2_{12}$	2	1	9586.8377	0.0018	$4_{14} \leftarrow 3_{03}$	5	4	15502.3228	-0.0085
	4	3	9587.1238	-0.0001		3	2	15502.4329	0.0045
	3	2	9587.4828	-0.0014		4	3	15501.8251	0.0257
$4_{23} \leftarrow 4_{14}$	5	5	9923.0880	-0.0036	$4_{22} \leftarrow 3_{21}$	5	4	16147.6185	-0.0183
	4	4	9923.9985	-0.0003	$4_{13} \leftarrow 3_{12}$	5	4	16327.1390	-0.0292
$4_{14} \leftarrow 3_{22}$	5	4	10623.7965	0.0084	$5_{05} \leftarrow 4_{14}$	6	5	17349.5120	-0.0189
$3_{13} \leftarrow 2_{12}$	3	3	10785.9083	0.0015					
	4	3	10786.7621	-0.0176	$c\text{-C}_3\text{H}_5^{30}\text{SiH}_2\text{CN}$				
	2	2	10787.8608	-0.0129	$5_{23} \leftarrow 5_{14}$	6	6	6079.4163	-5.2
$4_{31} \leftarrow 4_{22}$	4	4	11187.9447	-0.0072		5	5	6079.6770	-17.4
	5	5	11188.3823	0.0133	$2_{20} \leftarrow 2_{11}$	2	2	6369.4620	-7.1
$3_{03} \leftarrow 2_{02}$	3	3	11292.8484	-0.0159		3	3	6370.0391	1.9
	3	2	11293.0551	-0.0014		1	1	6370.3651	12.2
					$2_{12} \leftarrow 1_{11}$	2	2	7196.4514	11.8

<sup>a</sup>  $\Delta\nu = \nu_{\text{obs}} - \nu_{\text{calc}}$  in kHz

**Table 26.** - - Continued.

Transitions	F''	F'	$\nu_{\text{obs}}$ (MHz)	$\Delta\nu^a$	Transitions	F''	F'	$\nu_{\text{obs}}$ (MHz)	$\Delta\nu^a$
	3	2	7197.1985	-28.1		3	2	12400.6072	-5.7
	1	1	7198.3602	-15.1		4	3	12401.2859	-5.0
$2_{02} \leftarrow 1_{01}$	2	1	7635.3674	-6.6		2	1	12401.4910	2.6
	3	2	7635.5461	1.2		2	2	12401.7826	-7.6
$2_{21} \leftarrow 2_{12}$	1	1	7858.4430	-2.4	$4_{04} \leftarrow 3_{13}$	3	2	13537.4947	-9.8
	3	3	7858.8999	3.4		5	4	13537.6598	27.5
	2	2	7859.7085	0.0		4	3	13537.7891	-25.0
$5_{14} \leftarrow 5_{05}$	4	4	8026.9271	-0.3	$4_{14} \leftarrow 3_{13}$	4	4	14243.2602	13.2
	6	6	8027.2052	-2.1		3	3	14245.3525	26.1
	5	5	8028.5899	8.1	$2_{21} \leftarrow 1_{10}$	3	2	14530.9548	0.5
$2_{11} \leftarrow 1_{10}$	1	1	8246.7470	-9.4		2	1	14530.2425	-2.0
	3	2	8247.8888	-25.6		1	0	14532.0461	3.7
	1	0	8248.5891	-3.7	$4_{04} \leftarrow 3_{03}$	4	3	14688.2725	-4.3
	2	2	8248.6863	9.7		5	4	14688.5491	17.8
$3_{22} \leftarrow 3_{13}$	2	2	8697.2573	-5.5	$2_{20} \leftarrow 1_{11}$	1	0	15141.9344	-11.3
	3	4	8697.5705	2.5		3	2	15143.1202	-0.2
	2	3	8698.4385	-1.5		1	1	15143.7215	-2.6
$2_{12} \leftarrow 1_{01}$	3	2	9291.6424	-1.8		2	1	15144.0239	-1.9
	1	0	9292.0275	-19.1	$4_{14} \leftarrow 3_{03}$	4	3	15394.6002	18.6
	1	1	9292.1352	30.2	$4_{22} \leftarrow 3_{21}$	5	4	16132.2493	24.7
$3_{03} \leftarrow 2_{12}$	2	1	9594.0045	-3.3	$4_{13} \leftarrow 3_{12}$	5	4	16291.5903	-9.9
	4	3	9594.2948	2.2	$5_{05} \leftarrow 4_{14}$	6	5	17302.4863	-3.7
	3	2	9594.6478	3.8	$5_{15} \leftarrow 4_{14}$	6	5	17694.2701	-9.4
	2	2	9595.2230	-9.2	$3_{22} \leftarrow 2_{11}$	3	2	17866.1700	29.4
$4_{23} \leftarrow 4_{14}$	3	3	9829.9424	5.6		4	3	17866.9129	10.0
	5	5	9830.1671	-2.9		2	1	17867.3061	-20.1
	4	4	9831.0741	-3.4	$5_{05} \leftarrow 4_{04}$	5	4	18008.8430	-9.5
$4_{13} \leftarrow 3_{22}$	3	3	10736.6356	7.6		6	5	18009.0646	-0.5
	5	4	10736.7816	-6.9	$5_{15} \leftarrow 4_{04}$	6	5	18400.8698	15.1
	4	3	10737.4204	7.5	$5_{24} \leftarrow 4_{23}$	6	5	19112.9462	-31.3
$3_{13} \leftarrow 2_{12}$	3	3	10744.3153	-4.1	<i>c</i> -C <sub>3</sub> H <sub>5</sub> SiH <sub>2</sub> CN <sup>15</sup>				
	4	3	10745.1743	-17.0	$4_{22} \leftarrow 4_{13}$			6022.2951	-2.4
	2	2	10746.2721	-11.6	$3_{21} \leftarrow 3_{12}$			6229.5297	6.3
$4_{31} \leftarrow 4_{22}$	4	4	10940.5080	-3.6	$2_{12} \leftarrow 1_{11}$			7097.4746	2.1
	5	5	10940.9455	8.1	$2_{02} \leftarrow 1_{01}$			7521.1275	-6.1
$3_{03} \leftarrow 2_{02}$	3	3	11249.9658	9.6	$5_{14} \leftarrow 5_{05}$			7767.4729	2.5
	3	2	11250.1463	-4.0	$2_{21} \leftarrow 2_{12}$			8056.9222	-8.9
	4	3	11250.3723	-19.6	$2_{11} \leftarrow 1_{10}$			8097.6882	2.0
$3_{22} \leftarrow 2_{21}$	4	3	11583.8611	-1.7	$2_{12} \leftarrow 1_{01}$			9282.9946	-17.8
$3_{21} \leftarrow 2_{20}$	2	2	11916.8389	-0.4	$3_{03} \leftarrow 2_{12}$			9339.8155	-9.4
	4	3	11917.1964	19.6	$4_{23} \leftarrow 4_{14}$			9925.4312	4.1
	3	2	11917.4067	14.0	$3_{13} \leftarrow 2_{12}$			10601.5448	6.3
	3	3	11917.5969	10.0	$3_{03} \leftarrow 2_{02}$			11101.7092	5.4
$3_{12} \leftarrow 2_{11}$	4	3	12312.1036	12.4	$3_{22} \leftarrow 2_{21}$			11396.4097	14.4
	2	1	12312.2497	-12.5	$3_{21} \leftarrow 2_{20}$			11690.9081	2.6
	3	3	12312.8174	5.5	$3_{21} \leftarrow 2_{11}$			12094.3983	2.5
$3_{13} \leftarrow 2_{02}$	3	3	12400.4179	-1.0	$3_{13} \leftarrow 2_{02}$			12363.4201	2.8

<sup>a</sup>  $\Delta\nu = \nu_{\text{obs}} - \nu_{\text{calc}}$  in kHz

**Table 26.** - - Continued.

Transitions	F''	F'	$v_{\text{obs}}$ (MHz)	$\Delta v^a$	Transitions	F''	F'	$v_{\text{obs}}$ (MHz)	$\Delta v^a$
$4_{04} \leftarrow 3_{13}$			13256.7677	-7.8	$3_{12} \leftarrow 2_{11}$	2	2	12198.6522	12.5
$4_{14} \leftarrow 3_{13}$			14061.6075	15.2		4	3	12199.6798	11.6
$4_{04} \leftarrow 3_{03}$			14518.5014	12.3	$3_{13} \leftarrow 2_{02}$	3	2	12459.0173	-3.0
$2_{21} \leftarrow 1_{10}$			14654.2867	2.4		4	3	12459.7195	7.0
$4_{23} \leftarrow 3_{22}$			15135.2164	-14.8		2	1	12459.9201	0.8
$2_{20} \leftarrow 1_{11}$			15230.8179	-1.3		2	2	12460.1910	3.2
$4_{14} \leftarrow 3_{03}$			15323.2953	-10.5	$4_{04} \leftarrow 3_{13}$	3	2	13403.3240	-3.0
$4_{31} \leftarrow 3_{03}$			15372.0835	-5.6		5	4	13403.4799	17.1
$5_{05} \leftarrow 4_{14}$			17011.1027	-8.5		4	3	13403.6753	-3.1
$5_{15} \leftarrow 4_{14}$			17476.5361	4.1	$4_{14} \leftarrow 3_{13}$	5	4	14201.6676	-18.6
$5_{05} \leftarrow 4_{04}$			17815.9341	6.1	$4_{04} \leftarrow 3_{03}$	4	3	14656.7915	-2.3
<i>c</i> -C <sub>3</sub> H <sub>5</sub> SiH <sub>2</sub> CN (C <sup>13</sup> <sub>(4,5)</sub> )									
$1_{11} \leftarrow 0_{00}$	1	1	6009.5263	-6.0	$2_{21} \leftarrow 1_{10}$	2	1	14695.9369	-9.5
	2	1	6010.2521	0.5		1	0	14697.7521	-4.1
$3_{21} \leftarrow 3_{12}$	3	3	6202.7288	11.4	$2_{20} \leftarrow 1_{11}$	1	0	15272.0982	-3.1
	4	4	6203.0761	7.3		3	2	15273.2805	4.6
	2	2	6203.1907	-0.9		2	1	15274.1726	4.8
$2_{20} \leftarrow 2_{11}$	3	3	6605.3704	8.0	$4_{14} \leftarrow 3_{03}$	4	3	15454.7136	-4.2
	1	1	6605.6825	-12.1	$4_{32} \leftarrow 3_{31}$	5	4	15469.3726	-4.3
$2_{21} \leftarrow 1_{11}$	2	2	7167.0149	12.7	$4_{22} \leftarrow 3_{21}$	5	4	15953.2748	1.2
	3	2	7167.7682	-19.3		4	3	15953.4569	-17.6
	1	1	7168.9454	2.1	$4_{13} \leftarrow 3_{12}$	5	4	16157.9746	-9.0
$2_{02} \leftarrow 1_{01}$	2	1	7591.0185	2.9	$5_{05} \leftarrow 4_{14}$	6	5	17190.6597	-12.7
	3	2	7591.1726	-1.6		5	4	17190.7807	23.7
$2_{21} \leftarrow 2_{12}$	1	1	8028.3637	5.7	$5_{15} \leftarrow 4_{14}$	5	4	17651.2902	-9.0
	3	3	8028.8056	3.0	$5_{05} \leftarrow 4_{04}$	5	4	17988.6759	-5.0
	2	2	8029.6014	-1.3		6	5	17988.8974	1.4
$2_{11} \leftarrow 1_{10}$	1	1	8166.8161	-11.0	<i>c</i> -C <sub>3</sub> H <sub>5</sub> SiH <sub>2</sub> CN(C <sup>13</sup> <sub>(2)</sub> )				
	3	2	8167.9669	-21.3	$1_{11} \leftarrow 0_{00}$	1	1	6052.3565	-3.4
	1	0	8168.6471	-12.7		2	1	6053.0453	-8.0
	2	2	8168.7516	-7.2	$4_{22} \leftarrow 4_{13}$	3	3	6060.0093	-6.6
$3_{22} \leftarrow 3_{13}$	2	2	8823.5374	6.3	$2_{20} \leftarrow 2_{11}$	3	3	6672.4265	9.5
	3	4	8823.8207	-12.9	$2_{12} \leftarrow 1_{11}$	1	0	7202.5379	6.4
	3	3	8824.6993	1.0	$2_{02} \leftarrow 1_{01}$	3	2	7631.6776	-9.5
$2_{12} \leftarrow 1_{01}$	2	1	9343.3077	-5.1	$2_{22} \leftarrow 2_{12}$	1	1	8113.1937	3.4
	3	2	9344.0856	1.1		2	2	8114.4866	-6.5
$3_{03} \leftarrow 2_{12}$	2	1	9452.9278	0.4	$2_{11} \leftarrow 1_{10}$	1	1	8214.8144	8.2
	4	3	9453.2269	3.5		3	2	8215.9577	1.4
	3	2	9453.6138	6.1		1	0	8216.6423	-7.7
$4_{23} \leftarrow 4_{24}$	5	5	9897.7166	5.6	$3_{22} \leftarrow 3_{13}$	2	2	8918.5165	6.7
	4	4	9898.6143	0.5		4	4	8918.8277	10.9
$3_{13} \leftarrow 2_{12}$	3	3	10705.9372	-0.4	$2_{12} \leftarrow 1_{01}$	3	2	9401.3957	-5.6
	2	2	10707.9014	10.9		1	0	9401.7489	-25.1
$3_{03} \leftarrow 2_{02}$	3	2	11205.9101	5.1		1	1	9401.8972	12.5
	4	3	11206.1239	-9.5		2	1	9400.6576	2.3
	2	2	11206.4423	-4.2	$3_{03} \leftarrow 2_{12}$	2	1	9494.2735	6.9
$3_{22} \leftarrow 3_{13}$	4	3	11501.8363	2.8		4	3	9494.5603	4.7
$3_{21} \leftarrow 2_{20}$	4	3	11797.4042	29.7		3	2	9494.9253	8.1
$3_{30} \leftarrow 3_{21}$	3	3	11810.6924	-3.0	$3_{13} \leftarrow 2_{12}$	3	3	10758.2738	-6.9

<sup>a</sup>  $\Delta v = v_{\text{obs}} - v_{\text{calc}}$  in kHz

**Table 26.** - - Continued

Transitions	F''	F'	$\nu_{\text{obs}}$ (MHz)	$\Delta\nu^a$	Transitions	F''	F'	$\nu_{\text{obs}}$ (MHz)	$\Delta\nu^a$
	4	3	10759.1454	-12.5		1	0	8192.4130	-4.7
	2	2	10760.2467	-8.5	$3_{22}\leftarrow 3_{13}$	3	4	8938.9892	12.1
$3_{03}\leftarrow 2_{02}$	3	2	11264.0485	4.7		2	3	8939.8493	-0.7
	4	3	11264.2656	-4.1	$2_{12}\leftarrow 1_{01}$	2	1	9396.1220	15.7
	2	2	11264.6313	8.8		3	2	9396.8492	-1.4
$3_{23}\leftarrow 2_{22}$	4	3	11564.3150	-4.1		1	0	9397.2155	-8.6
$3_{21}\leftarrow 2_{20}$	4	3	11864.2159	13.3	$3_{03}\leftarrow 2_{12}$	2	1	9454.0036	-2.6
	3	2	11864.3805	1.0		4	3	9454.2895	-6.3
$3_{12}\leftarrow 2_{11}$	2	2	12269.8334	-6.7		3	2	9454.6571	-3.7
	3	3	12271.5377	8.8	$4_{23}\leftarrow 4_{14}$	5	5	10018.1198	4.0
$3_{13}\leftarrow 2_{01}$	3	2	12528.1984	0.9	$3_{13}\leftarrow 2_{12}$	3	3	10733.6300	5.2
	4	3	12528.8698	-2.3		4	3	10734.4707	-26.9
	2	1	12529.0568	-9.9		2	2	10735.5884	-1.7
$4_{04}\leftarrow 3_{13}$	3	2	13465.8506	-15.2	$3_{03}\leftarrow 2_{02}$	3	3	11238.2010	-9.4
	5	4	13465.9939	-5.8		3	2	11238.4115	2.4
$4_{14}\leftarrow 3_{13}$	5	4	14270.4237	-7.9		4	3	11238.6167	-15.6
$4_{04}\leftarrow 3_{13}$	4	3	14730.3807	23.0	$5_{24}\leftarrow 5_{15}$	6	6	11372.6384	-9.5
	5	4	14730.6222	20.0	$3_{22}\leftarrow 2_{21}$	4	3	11533.4371	20.7
$2_{12}\leftarrow 1_{10}$	2	1	14809.8322	-25.4	$3_{21}\leftarrow 2_{20}$	4	3	11828.0390	6.3
	1	2	14810.5396	17.8		3	2	11828.2175	8.8
	1	0	14811.6223	-5.7	$3_{12}\leftarrow 2_{11}$	2	2	12234.5267	1.3
$2_{10}\leftarrow 1_{11}$	1	0	15393.4436	-17.2		3	2	12235.4641	-6.9
	3	2	15394.6227	9.3		4	3	12235.5238	11.9
	2	1	15395.5133	4.0	$3_{13}\leftarrow 2_{02}$	3	2	12518.1650	5.1
$4_{14}\leftarrow 3_{03}$	4	3	15534.5116	12.8		4	3	12518.8395	5.4
	5	4	15535.0628	28.7		2	1	12519.0392	9.8
$4_{32}\leftarrow 3_{31}$	5	4	15554.6271	-11.2	$4_{04}\leftarrow 3_{13}$	3	2	13420.0547	5.6
$4_{22}\leftarrow 3_{21}$	5	4	16045.4394	10.1		5	4	13420.2062	22.5
$4_{13}\leftarrow 3_{12}$	5	4	16251.2075	-9.8		4	3	13420.4195	27.5
$5_{15}\leftarrow 4_{14}$	5	4	17735.8232	-3.9	$4_{14}\leftarrow 3_{13}$	5	4	14238.7428	-19.9
$5_{05}\leftarrow 4_{04}$	6	5	18076.5499	-17.2	$4_{04}\leftarrow 3_{03}$	4	4	14699.7277	6.8
<i>c</i> -C <sub>3</sub> H <sub>5</sub> SiH <sub>2</sub> CN(C <sup>13</sup> <sub>(10)</sub> )						4	3	14700.1482	5.4
$1_{11}\leftarrow 0_{00}$	1	1	6054.4827	-1.4		5	4	14700.4147	29.3
	2	1	6055.1724	-3.7	$2_{12}\leftarrow 1_{10}$	3	2	14823.5993	-4.9
$4_{22}\leftarrow 4_{13}$	5	5	6088.8106	-4.0		1	0	14824.6852	4.4
$3_{21}\leftarrow 3_{12}$	3	3	6300.4656	-2.5	$2_{02}\leftarrow 1_{11}$	1	0	15401.4772	11.2
	4	4	6300.7897	-4.4		3	2	15402.6043	-9.9
$2_{20}\leftarrow 2_{11}$	2	2	6707.7369	6.3		1	1	15403.2059	9.8
	3	3	6708.2681	-5.2	$4_{32}\leftarrow 3_{31}$	5	4	15511.1532	9.2
$2_{12}\leftarrow 1_{11}$	2	2	7185.3569	-14.9	$4_{14}\leftarrow 3_{03}$	4	3	15518.4364	8.5
	1	0	7185.5468	-11.3	$4_{22}\leftarrow 3_{21}$	5	4	15994.3706	-7.0
	3	2	7186.1453	-13.4	$4_{13}\leftarrow 3_{12}$	5	4	16206.3423	-14.8
$2_{02}\leftarrow 1_{01}$	2	1	7612.3620	3.8	$5_{15}\leftarrow 4_{14}$	5	4	17697.6670	-25.6
	3	2	7612.4953	-18.9	$5_{05}\leftarrow 4_{04}$	5	4	18041.4836	-15.5
	1	1	7612.6763	9.2		6	5	18041.7174	6.8
$2_{11}\leftarrow 1_{11}$	1	1	8190.5665	-15.0					
	3	2	8191.7206	-7.2					

<sup>a</sup>  $\Delta\nu = \nu_{\text{obs}} - \nu_{\text{calc}}$  in kHz

**Table 27.** Rotational transition frequencies (MHz) of the ground vibrational state of *gauche* *c*-C<sub>3</sub>H<sub>5</sub>SiH<sub>2</sub>CN.

<i>c</i> -C <sub>3</sub> H <sub>5</sub> SiH <sub>2</sub> CN									
Transitions	F''	F'	$\nu_{\text{obs}}$ (MHz)	$\Delta\nu^a$	Transitions	F''	F'	$\nu_{\text{obs}}$ (MHz)	$\Delta\nu^a$
2 <sub>11</sub> ← 1 <sub>10</sub>	2	1	6078.3766	0.0037	4 <sub>04</sub> ← 3 <sub>03</sub>	3	3	11392.6275	-0.0058
	3	2	6079.1777	-0.0103		4	4	11730.0741	0.0117
	1	0	6080.3341	-0.0134		5	4	11731.0207	-0.0205
3 <sub>12</sub> ← 3 <sub>03</sub>	2	2	6146.0643	0.0000	4 <sub>23</sub> ← 3 <sub>22</sub>	3	3	11732.2432	0.0179
	4	4	6146.2916	0.0057		4	3	11775.5344	0.0084
	3	3	6146.9183	-0.0004		5	4	11775.9122	0.0147
4 <sub>13</sub> ← 4 <sub>04</sub>	3	3	6563.1424	0.0127	4 <sub>22</sub> ← 3 <sub>21</sub>	4	3	11823.7140	0.0088
	5	5	6563.2486	-0.0087		5	4	11824.0712	0.0205
	4	4	6563.8288	-0.0027		4 <sub>13</sub> ← 3 <sub>12</sub>	4	4	12147.6084
4 <sub>04</sub> ← 3 <sub>13</sub>	5	4	6720.4701	0.0065		3	2	12147.9977	-0.0142
5 <sub>14</sub> ← 5 <sub>05</sub>	4	4	7110.2458	-0.0094		3	3	12148.4119	-0.0042
	6	6	7110.3801	0.0079	6 <sub>06</sub> ← 5 <sub>15</sub>	7	6	13229.4726	0.0189
	5	5	7110.9312	0.0004	3 <sub>13</sub> ← 2 <sub>02</sub>	3	2	13825.5760	-0.0119
6 <sub>15</sub> ← 6 <sub>06</sub>	7	7	7803.2227	-0.0183		4	3	13825.7900	0.0228
	6	6	7803.8059	0.0006		2	2	13827.0269	0.0078
1 <sub>11</sub> ← 0 <sub>00</sub>	2	1	8407.4334	0.0167		3	3	13824.7089	0.0017
3 <sub>13</sub> ← 2 <sub>12</sub>	3	2	8547.3939	0.0035	5 <sub>15</sub> ← 4 <sub>14</sub>	5	5	14229.1431	-0.0006
	4	3	8547.6331	-0.0159		5	4	14230.3105	-0.0153
	2	2	8548.8172	-0.0041		4	4	14231.8521	0.0162
7 <sub>16</sub> ← 7 <sub>07</sub>	8	8	8658.1909	-0.0250	5 <sub>05</sub> ← 4 <sub>04</sub>	5	5	14627.0497	-0.0169
3 <sub>03</sub> ← 2 <sub>02</sub>	3	3	8814.2453	0.0080		6	5	14628.0742	-0.0180
	2	1	8814.9877	-0.0186	5 <sub>24</sub> ← 4 <sub>23</sub>	6	5	14713.6223	0.0068
	4	3	8815.1607	-0.0088	5	4	14713.4244	0.0065	
	2	2	8816.3716	-0.0051	5 <sub>23</sub> ← 4 <sub>22</sub>	5	4	14809.1614	-0.0151
3 <sub>22</sub> ← 2 <sub>21</sub>	3	2	8834.0688	0.0043		6	5	14809.3587	0.0171
	4	3	8834.9150	-0.0182	4 <sub>22</sub> ← 4 <sub>13</sub>	5	5	15806.4224	-0.0026
	2	1	8835.4125	-0.0046	3 <sub>21</sub> ← 3 <sub>12</sub>	3	3	16130.7401	0.0223
3 <sub>21</sub> ← 2 <sub>20</sub>	3	2	8853.4085	0.0079		4	4	16130.3707	-0.0164
	4	3	8854.2443	-0.0057		2	2	16130.2497	-0.0216
	2	1	8854.7197	-0.0088	2 <sub>20</sub> ← 2 <sub>11</sub>	3	3	16391.6194	-0.0221
3 <sub>12</sub> ← 2 <sub>11</sub>	3	2	9115.2721	-0.0005	4 <sub>14</sub> ← 3 <sub>03</sub>	5	4	16401.8487	-0.0183
	4	3	9115.5189	0.0144	7 <sub>07</sub> ← 6 <sub>16</sub>	8	7	16517.2234	-0.0058
8 <sub>17</sub> ← 8 <sub>08</sub>	9	9	9690.4943	-0.0036	2 <sub>21</sub> ← 2 <sub>12</sub>	3	3	16954.6532	0.0123
	8	8	9691.1230	0.0221	6 <sub>16</sub> ← 5 <sub>15</sub>	7	6	17064.1761	-0.0010
5 <sub>05</sub> ← 4 <sub>14</sub>	6	5	9957.2406	-0.0259	3 <sub>22</sub> ← 3 <sub>12</sub>	2	2	17241.5713	0.0172
2 <sub>12</sub> ← 1 <sub>01</sub>	3	2	11163.0207	0.0073		4	4	17241.9426	0.0176
	1	1	11164.2678	-0.0015		3	3	17242.9780	-0.0068
	4	4	11390.0998	0.0124	6 <sub>06</sub> ← 5 <sub>05</sub>	7	6	17502.5988	0.0134
	4	3	11391.1268	-0.0204	6 <sub>25</sub> ← 5 <sub>24</sub>	7	6	17647.2186	-0.0177
	5	4	11391.2838	0.0144					

<sup>a</sup>  $\Delta\nu = \nu_{\text{obs}} - \nu_{\text{calc}}$  in MHz

**Table 28.** Rotational transition frequencies (MHz) of the ground vibrational state of seven isotopomers of *gauche*-cyclopropylcyanosilane,  $c\text{-C}_3\text{H}_5\text{SiH}_2\text{CN}$ .

$c\text{-C}_3\text{H}_5^{29}\text{SiH}_2\text{CN}$					$c\text{-}^{13}\text{C}_3\text{H}_5\text{SiH}_2\text{CN}$ (C5)				
Transitions	F''	F'	$\nu_{\text{obs}}$ (MHz)	$\Delta\nu^a$	Transitions	F''	F'	$\nu_{\text{obs}}$ (MHz)	$\Delta\nu^a$
$1_{11} \leftarrow 0_{00}$	2	1	8330.0043	-8.1	$6_{06} \leftarrow 5_{15}$	7	6	12877.0531	-3.9
$1_{11} \leftarrow 0_{00}$	2	1	8330.0035	-8.9	$5_{23} \leftarrow 4_{22}$	6	5	14550.9392	-23.4
$3_{13} \leftarrow 2_{12}$	3	2	8531.5712	6.7	$5_{14} \leftarrow 4_{13}$	6	5	14908.4180	20.3
	4	3	8531.8011	-22.1	$6_{16} \leftarrow 5_{15}$	7	6	16782.5933	2.9
	2	2	8532.9832	-11.3	$c\text{-C}_3\text{H}_5^{30}\text{SiH}_2\text{CN}$				
$7_{16} \leftarrow 7_{07}$	6	6	8640.9056	-12.2	$2_{11} \leftarrow 1_{10}$	2	1	6068.2007	63.0
	8	8	8641.0350	14.8		3	2	6068.9845	32.0
$3_{03} \leftarrow 2_{02}$	2	1	8802.4643	-12.6	$1_{11} \leftarrow 0_{00}$	1	1	8257.4257	0.9
	4	3	8802.6452	5.3	$3_{13} \leftarrow 2_{12}$	3	2	8516.1532	40.8
	2	2	8803.8396	-7.5		4	3	8516.4010	-51.8
	3	3	8801.7247	17.4	$3_{03} \leftarrow 2_{02}$	2	1	8790.2363	-19.4
$3_{22} \leftarrow 2_{21}$	3	2	8822.3530	0.0		4	3	8790.4096	-8.8
	3	3	8823.2078	-13.5		2	2	8791.6102	-16.1
$3_{21} \leftarrow 2_{20}$	3	2	8842.4943	0.7		3	3	8789.4933	8.1
	4	3	8843.3218	-21.8	$3_{21} \leftarrow 2_{20}$	3	2	8831.8866	37.6
	2	1	8843.8164	-5.3		4	3	8832.7089	11.9
$3_{12} \leftarrow 2_{11}$	3	2	9107.4037	-0.1		2	1	8833.1968	21.8
	4	3	9107.6498	14.1	$3_{12} \leftarrow 2_{11}$	3	2	9099.7208	57.4
$8_{17} \leftarrow 8_{08}$	9	9	9693.8422	-3.8		4	3	9099.9666	71.4
$2_{12} \leftarrow 1_{01}$	3	2	11079.0399	-7.9	$2_{12} \leftarrow 1_{01}$	3	2	10999.9978	-43.3
$4_{14} \leftarrow 3_{13}$	4	3	11369.8121	-16.3	$4_{14} \leftarrow 3_{13}$	4	3	11349.0252	-84.5
	5	4	11369.9537	3.0		5	4	11349.1808	-51.2
$4_{04} \leftarrow 3_{03}$	4	3	11713.3791	12.2	$4_{04} \leftarrow 3_{03}$	4	3	11696.1509	-3.9
$4_{22} \leftarrow 3_{21}$	4	3	11809.9684	11.5	$4_{23} \leftarrow 3_{22}$	4	4	11744.3607	15.3
	5	4	11810.3016	19.3		5	4	11744.7556	28.7
$4_{13} \leftarrow 3_{12}$	5	4	12137.2594	-17.1	$4_{22} \leftarrow 3_{21}$	4	3	11796.5513	56.3
$3_{13} \leftarrow 2_{02}$	4	3	13734.0211	26.1		5	4	11796.9048	65.7
$5_{15} \leftarrow 4_{14}$	6	5	14203.4318	15.5	$4_{13} \leftarrow 3_{12}$	3	2	12126.7632	56.7
$5_{05} \leftarrow 4_{04}$	6	5	14604.6381	15.7	$3_{13} \leftarrow 2_{02}$	4	3	13647.3032	-131.2
$5_{14} \leftarrow 4_{13}$	5	4	15161.3238	7.7	$5_{15} \leftarrow 4_{14}$	5	4	14177.0183	-81.4
$6_{16} \leftarrow 5_{15}$	7	6	17031.3152	-20.3	$5_{05} \leftarrow 4_{04}$	6	5	14581.6375	-43.3
$6_{06} \leftarrow 5_{05}$	7	6	17472.4261	-7.2	$5_{24} \leftarrow 4_{23}$	6	5	14674.1284	-11.2
$6_{24} \leftarrow 5_{23}$	6	5	17795.3187	4.8	$5_{23} \leftarrow 4_{22}$	6	5	14777.7625	73.0
$c\text{-}^{13}\text{C}_3\text{H}_5\text{SiH}_2\text{CN}$ (C5)					$5_{14} \leftarrow 4_{13}$	5	4	15147.7998	11.23
$3_{13} \leftarrow 2_{12}$	3	2	8405.5582	4.9	$6_{16} \leftarrow 5_{15}$	5	4	16999.2405	-8.91
$3_{13} \leftarrow 2_{12}$	4	3	8405.7982	-13.4	$6_{06} \leftarrow 5_{05}$	6	5	17442.8524	-28.3
$3_{03} \leftarrow 2_{02}$	2	1	8664.8001	-10.3	$c\text{-}^{13}\text{C}_3\text{H}_5\text{SiH}_2\text{CN}$ (C4)				
$3_{03} \leftarrow 2_{02}$	4	3	8664.9784	4.7	$3_{13} \leftarrow 2_{12}$	3	2	8453.3956	22.3
$3_{12} \leftarrow 2_{11}$	3	2	8954.4492	-10.8		4	3	8453.6351	1.2
$3_{12} \leftarrow 2_{11}$	4	3	8954.7087	17.0	$3_{03} \leftarrow 2_{02}$	4	3	8721.8498	-4.1
$2_{12} \leftarrow 1_{01}$	3	2	11094.0203	-3.9		2	1	8721.6737	-11.6
$4_{14} \leftarrow 3_{13}$	5	4	11202.5504	18.2	$3_{12} \leftarrow 2_{11}$	3	2	9023.6142	3.1
$4_{04} \leftarrow 3_{03}$	5	4	11532.3135	-17.6		4	3	9023.8583	6.5
$4_{22} \leftarrow 3_{21}$	5	4	11618.9588	15.4	$2_{12} \leftarrow 1_{01}$	3	2	10986.6919	5.2
$4_{13} \leftarrow 3_{12}$	5	4	11934.0077	-2.6	$4_{14} \leftarrow 3_{13}$	4	3	11265.6267	-21.9

<sup>a</sup>  $\Delta\nu = \nu_{\text{obs}} - \nu_{\text{calc}}$  in kHz

**Table 28.** - - Continued.

Transitions	F''	F'	$\nu_{\text{obs}}$ (MHz)	$\Delta\nu^a$	Transitions	F''	F'	$\nu_{\text{obs}}$ (MHz)	$\Delta\nu^a$
	5	4	11265.7868	17.0	$3_{12} \leftarrow 2_{11}$			8894.7235	-16.7
$4_{04} \leftarrow 3_{03}$	4	3	11605.9461	1.7	$4_{14} \leftarrow 3_{13}$			11123.7170	-10.9
$4_{23} \leftarrow 3_{22}$	5	4	11652.1630	9.9	$4_{04} \leftarrow 3_{03}$			11452.8167	10.1
$4_{22} \leftarrow 3_{21}$	4	3	11701.3555	6.6	$4_{22} \leftarrow 3_{21}$			11539.7941	19.3
	5	4	11701.6900	-19.8	$4_{13} \leftarrow 3_{12}$			11854.0905	0.4
$6_{06} \leftarrow 5_{15}$	7	6	13154.6196	5.3	$5_{15} \leftarrow 4_{14}$			13896.5575	16.5
$5_{15} \leftarrow 4_{14}$	6	5	14073.3024	1.9	$5_{05} \leftarrow 4_{04}$			14282.5753	0.2
$5_{05} \leftarrow 4_{04}$	6	5	14470.7915	5.9	$5_{14} \leftarrow 4_{13}$			14808.4698	8.5
$5_{14} \leftarrow 4_{13}$	6	5	15021.9839	0.2	$c\text{-}^{13}\text{C}_3\text{H}_5\text{SiH}_2\text{CN}$ (C10)				
$6_{16} \leftarrow 5_{15}$	7	6	16875.3552	3.9	$3_{13} \leftarrow 2_{12}$	3	2	8461.1113	19.2
$6_{06} \leftarrow 5_{05}$	7	6	17312.4525	-11.9	$3_{13} \leftarrow 2_{12}$	4	3	8461.3516	-37.4
$c\text{-}^{13}\text{C}_3\text{H}_5\text{SiH}_2\text{CN}$ (C2)					$3_{13} \leftarrow 2_{12}$	3	3	8460.3106	19.4
$1_{11} \leftarrow 0_{00}$	2	1	8358.5233	-19.0	$3_{03} \leftarrow 2_{02}$	4	3	8723.8366	-21.9
$3_{13} \leftarrow 2_{12}$	3	2	8518.8346	30.8		2	1	8723.6652	-30.2
	4	3	8519.0633	0.9	$3_{12} \leftarrow 2_{11}$	3	3	9017.4821	25.2
$3_{03} \leftarrow 2_{02}$	2	1	8782.7576	45.3		4	3	9017.7500	-6.1
	4	3	8782.9281	52.8	$5_{05} \leftarrow 4_{14}$	4	3	9776.2241	-41.0
$3_{12} \leftarrow 2_{11}$	3	2	9078.6175	34.6	$5_{05} \leftarrow 4_{14}$	6	5	9776.3520	-8.4
	4	3	9078.8703	55.8	$4_{14} \leftarrow 3_{13}$	5	4	11276.4484	-36.6
$2_{12} \leftarrow 1_{01}$	3	2	11105.9311	13.2		4	3	11276.3231	-40.1
$4_{14} \leftarrow 3_{13}$	4	3	11353.1738	-6.0	$4_{04} \leftarrow 3_{03}$	5	4	11610.2170	-24.0
	5	4	11353.3162	26.4	$4_{23} \leftarrow 3_{22}$	5	4	11653.2323	18.0
$4_{13} \leftarrow 3_{12}$	3	2	12099.2753	2.0	$4_{13} \leftarrow 3_{12}$	4	3	12017.8743	45.2
$5_{15} \leftarrow 4_{14}$	6	5	14183.1297	-4.9	$5_{15} \leftarrow 4_{14}$	6	5	14087.2299	-41.5
$5_{14} \leftarrow 4_{13}$	6	5	15114.5445	35.7	$5_{05} \leftarrow 4_{04}$	6	5	14478.5717	-5.2
$6_{16} \leftarrow 5_{15}$	7	6	17007.7159	-38.5	$5_{23} \leftarrow 4_{22}$	6	5	14652.2474	40.4
$c\text{-C}_3\text{H}_5\text{SiH}_2\text{CN}^{15}$					$5_{14} \leftarrow 4_{13}$	6	5	15013.0490	19.4
$1_{11} \leftarrow 0_{00}$			8317.8739	-0.0	$6_{16} \leftarrow 5_{15}$	6	5	16892.8286	-37.4
$3_{13} \leftarrow 2_{12}$			8346.6694	-12.3	$6_{06} \leftarrow 5_{05}$	6	5	17325.1826	-12.1
$3_{03} \leftarrow 2_{02}$			8605.3756	-19.2					
$3_{22} \leftarrow 2_{21}$			8623.7431	-8.9					

<sup>a</sup>  $\Delta\nu = \nu_{\text{obs}} - \nu_{\text{calc}}$  in kHz

The mid-infrared spectrum of cyclopropylcyanosilane in the gas phase was obtained from 3,500 to 220  $\text{cm}^{-1}$  on a Perkin-Elmer model 2,000 Fourier transform spectrometer. The mid-infrared spectra (3,500 to 400  $\text{cm}^{-1}$ ) of the sample dissolved in liquefied xenon (Fig. 23) at ten different temperatures (-55°C to -100 °C) were recorded on a Bruker model IFS-66 Fourier transform spectrometer. The Raman spectra (Fig. 24) were recorded on a

Spex model 1403 spectrophotometer. All of the observed bands in the Raman spectrum of the liquid, along with their proposed assignments and depolarization values, are listed in Tables 29 and 30. The predicted conformational energy differences calculated from *ab initio* calculations by using the Møller-Plesset perturbation method to the second order (MP2) with full electron correlation, as well as with density functional theory by the B3LYP method with different basis sets are listed in Table 31. The experimental methods of recording infrared and Raman spectra are provided in detail in Chapter 2.

In order to obtain a description of the molecular motions involved in the fundamental modes of *c*-C<sub>3</sub>H<sub>5</sub>SiH<sub>2</sub>CN, a normal coordinate analysis has been carried out. The force field in Cartesian coordinates was obtained with the Gaussian 03 program at the MP2(full) level with the 6-31G(d) basis set. The internal coordinates used to calculate the **B** and **G** matrices are given in Table 32 with the atomic numbering shown in Fig. 25. By using the **B** matrix,<sup>26</sup> the force field in Cartesian coordinates was converted to a force field in internal coordinates. Subsequently, scaling factors of 0.88 for CH and SiH stretches and CH deformations, and 0.9 for other coordinates were applied except for the heavy atom bends and torsions, along with the geometric average of the scaling factors for the interaction force constants, to obtain the fixed scaled force field and resultant wavenumbers. A set of symmetry coordinates was used (Table 32) to determine the corresponding potential energy distributions (P.E.D.s). A comparison between the observed and calculated wavenumbers, along with the calculated infrared intensities, Raman activities, depolarization ratios and potential energy distributions for the *cis* and the *gauche* conformers are listed in Tables 29 and 30, respectively.

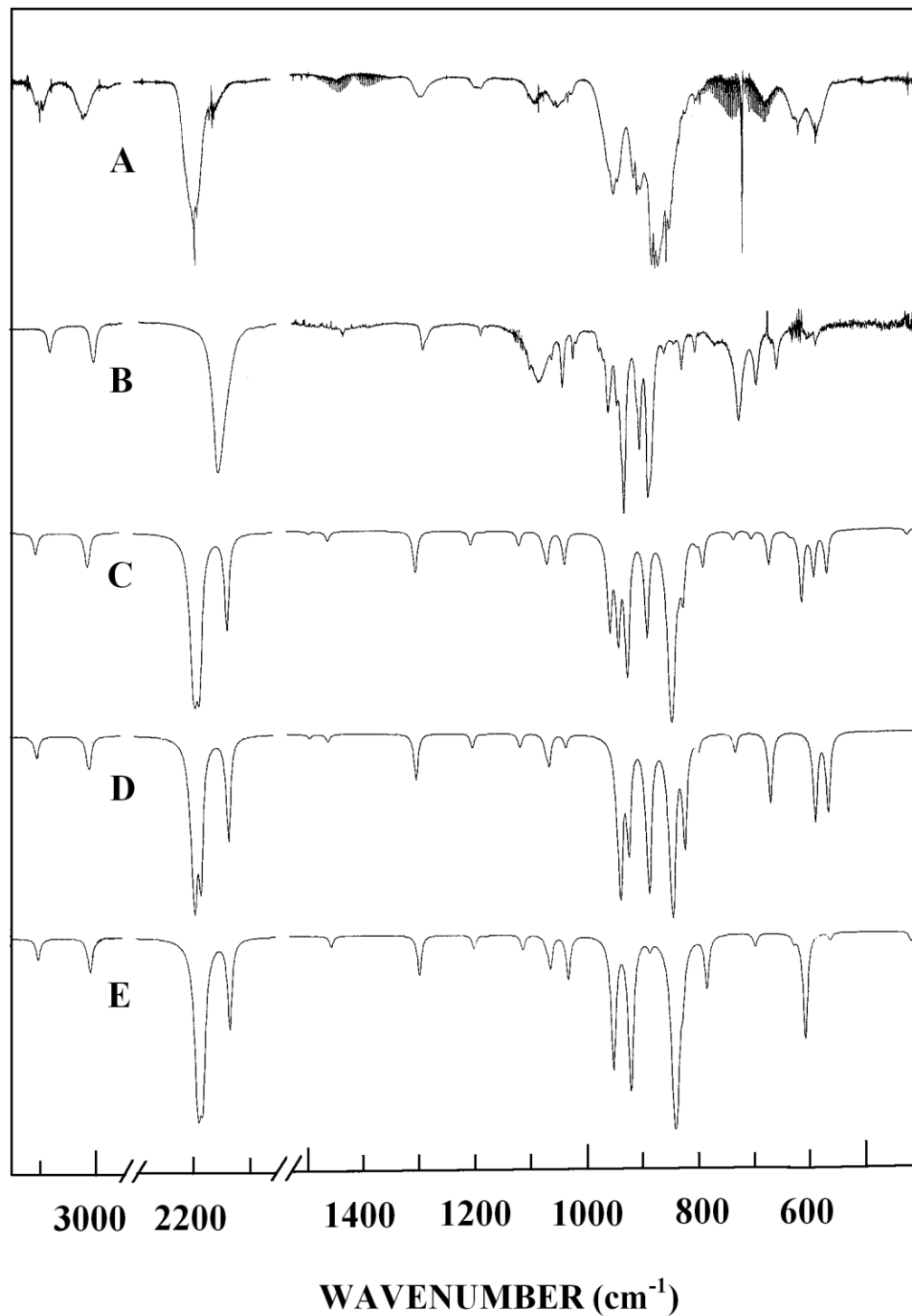


**Fig. 23** Comparison of experimental and calculated infrared spectra of cyclopropylcyanosilane: (A) observed spectrum of the gas; (B) observed spectrum in the xenon solution at  $-70\text{ }^{\circ}\text{C}$ ; (C) simulated spectrum of a mixture of *gauche* and *cis* conformers at  $-100\text{ }^{\circ}\text{C}$  with  $\Delta H = 123\text{ cm}^{-1}$ ; (D) simulated spectrum of the *gauche* conformer; (E) simulated spectrum of the *cis* conformer.

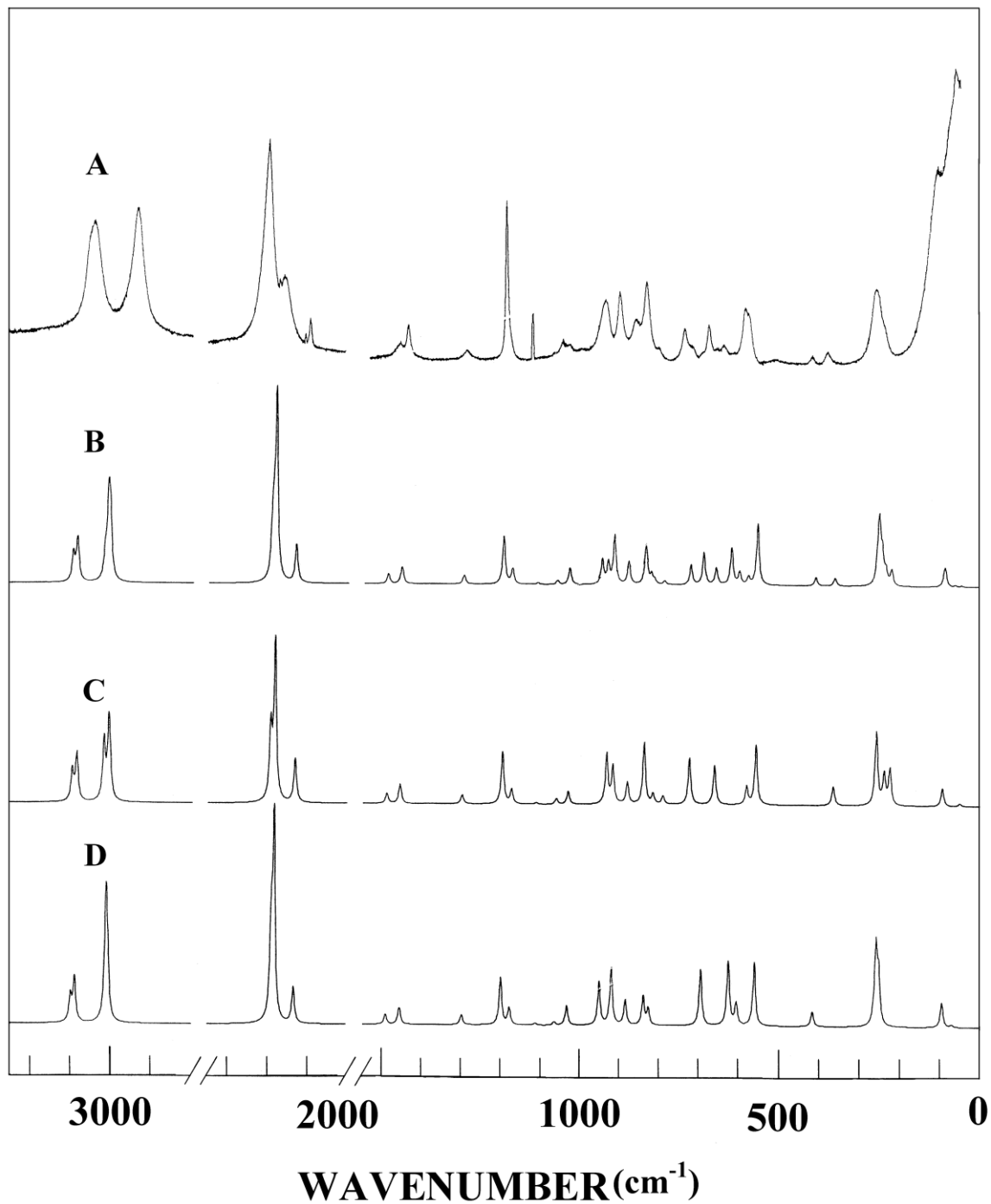


**Fig. 24** Comparison of experimental and calculated Raman spectra of cyclopropylcyanosilane: (A) observed spectrum of the liquid; (B) simulated spectrum of a mixture of *gauche* and *cis* conformers at 25 °C with  $\Delta H = 123 \text{ cm}^{-1}$ ; (C) simulated spectrum of the *gauche* conformer; (D) simulated spectrum of the *cis* conformer.

**Table 29.** Calculated<sup>a</sup> and observed frequencies (cm<sup>-1</sup>) for *cis* conformer of cyclopropylcyanosilane, *c*-C<sub>3</sub>H<sub>5</sub>SiH<sub>2</sub>CN

Sym. block	Vib. No.	Approx. Description	MP2 6-31G(d)	scaled <sup>b</sup>	IR int.	Raman Act.	dp	infrared		Raman liquid	P.E.D. <sup>c</sup>	Band Contour		
								gas	xenon			A	B	C
A'	v <sub>1</sub>	CH <sub>2</sub> antisymmetric stretch	3304	3100	7.3	42.0	0.50	3091	3075	3038	99S <sub>1</sub>	98	2	-
	v <sub>2</sub>	CH <sub>2</sub> symmetric stretch	3212	3013	1.7	192.5	0.10	3016	3000	2926	53S <sub>2</sub> , 46S <sub>3</sub>	79	21	-
	v <sub>3</sub>	CH stretch	3207	3008	4.7	39.3	0.45	3010	3000	2926	53S <sub>3</sub> , 47S <sub>2</sub>	1	99	-
	v <sub>4</sub>	SiH <sub>2</sub> symmetric stretch	2328	2183	108.8	181.6	0.07	2189	2152	2189	100S <sub>4</sub>	15	85	-
	v <sub>5</sub>	C≡N stretch	2140	2133	38.6	31.2	0.17	2154	2152	2193	94S <sub>5</sub>	37	63	-
	v <sub>6</sub>	CH <sub>2</sub> deformation	1575	1490	0.1	5.2	0.75	-	-	-	90S <sub>6</sub>	1	99	-
	v <sub>7</sub>	CH bend (in-plane)	1368	1298	14.6	4.4	0.64	1291	1289	1286	45S <sub>7</sub> , 24S <sub>8</sub> , 12S <sub>10</sub>	3	97	-
	v <sub>8</sub>	ring breathing	1264	1200	4.7	18.6	0.10	1190	1186	1189	59S <sub>8</sub> , 11S <sub>10</sub>	43	57	-
	v <sub>9</sub>	CH <sub>2</sub> wag	1121	1064	11.5	1.2	0.25	1047	1038	1043	84S <sub>9</sub>	1	99	-
	v <sub>10</sub>	CH <sub>2</sub> twist	1087	1032	16.1	6.5	0.73	1020	1019	1024	25S <sub>10</sub> , 29S <sub>7</sub> , 24S <sub>14</sub> , 11S <sub>9</sub>	90	10	-
	v <sub>11</sub>	SiH <sub>2</sub> deformation	1002	951	70.8	12.8	0.68	955	954	955	91S <sub>11</sub>	16	84	-
	v <sub>12</sub>	ring deformation	969	920	96.4	16.3	0.71	902	904	899	78S <sub>12</sub>	16	84	-
	v <sub>13</sub>	SiH <sub>2</sub> wag	885	840	236.1	7.4	0.75	838	837	831	74S <sub>13</sub> , 17S <sub>14</sub>	99	1	-
	v <sub>14</sub>	CH <sub>2</sub> rock	825	783	19.8	0.1	0.53	788	789	798	46S <sub>14</sub> , 40S <sub>10</sub> , 11S <sub>13</sub>	100	-	-
	v <sub>15</sub>	Si-C (ring) stretch	660	627	2.5	11.2	0.57	621	626	636	47S <sub>15</sub> , 18S <sub>16</sub>	74	26	-
	v <sub>16</sub>	Si-C (≡N) stretch	591	562	2.4	9.6	0.11	567	572	574	70S <sub>16</sub> , 20S <sub>15</sub>	20	80	-
	v <sub>17</sub>	CSiC bend	427	417	3.1	1.5	0.28	414	-	413	24S <sub>17</sub> , 41S <sub>19</sub> , 23S <sub>18</sub>	80	20	-
	v <sub>18</sub>	Ring-Si bend (in-plane)	262	254	4.0	2.3	0.67	-	-	255	52S <sub>18</sub> , 40S <sub>17</sub>	100	-	-
v <sub>19</sub>	Si-C≡N bend (in-plane)	99	97	6.1	2.7	0.75	-	-	104	52S <sub>19</sub> , 35S <sub>17</sub> , 13S <sub>18</sub>	97	3	-	
A''	v <sub>20</sub>	CH <sub>2</sub> antisymmetric stretch	3293	3090	0.3	70.8	0.75	3091	3075	3038	100S <sub>20</sub>	-	100	-
	v <sub>21</sub>	CH <sub>2</sub> symmetric stretch	3205	3007	7.2	24.2	0.75	3010	3000	2926	100S <sub>21</sub>	-	100	-
	v <sub>22</sub>	SiH <sub>2</sub> antisymmetric stretch	2335	2190	135.7	74.2	0.75	2195	2152	2189	100S <sub>22</sub>	-	100	-
	v <sub>23</sub>	CH <sub>2</sub> deformation	1534	1455	3.8	8.5	0.75	1442	1437	1438	100S <sub>23</sub>	-	100	-
	v <sub>24</sub>	CH <sub>2</sub> twist	1241	1178	0.6	6.6	0.75	1178	1173	1174	41S <sub>24</sub> , 49S <sub>28</sub>	-	100	-
	v <sub>25</sub>	CH bend (out-of-plane)	1173	1113	5.0	0.8	0.75	1098	1097	-	50S <sub>25</sub> , 37S <sub>24</sub>	-	100	-
	v <sub>26</sub>	CH <sub>2</sub> wag	1129	1071	2.6	0.0	0.75	1070	1080	1069	94S <sub>26</sub>	-	100	-
	v <sub>27</sub>	ring deformation	932	885	3.4	6.8	0.75	868	880	867	70S <sub>27</sub>	-	100	-

**Table 29.** - - Continued.

Sym. block	Vib. No.	Approx. Description	MP2 6-31G(d)	scaled <sup>b</sup>	IR int.	Raman Act.	dp	infrared		Raman liquid	P.E.D. <sup>c</sup>	Band Contour		
								gas	xenon			A	B	C
	v <sub>28</sub>	CH <sub>2</sub> rock	872	827	15.8	4.0	0.75	826	823	827	29S <sub>28</sub> , 26S <sub>27</sub>	-	100	-
	v <sub>29</sub>	SiH <sub>2</sub> twist	733	696	4.3	11.3	0.75	-	688	688	83S <sub>29</sub>	-	100	-
	v <sub>30</sub>	SiH <sub>2</sub> rock	637	607	48.4	3.7	0.75	612	-	608	77S <sub>30</sub>	-	100	-
	v <sub>31</sub>	Ring-Si bend (out-of-plane)	261	261	4.2	4.0	0.75	-	-	265	85S <sub>31</sub>	-	100	-
	v <sub>32</sub>	Asymmetric torsion	225	224	0.0	0.0	0.75	-	-	-	89S <sub>32</sub>	-	100	-
	v <sub>33</sub>	Si-C≡N bend (out-of-plane)	72	72	0.7	0.5	0.75	-	-	-	98S <sub>33</sub>	-	100	-

<sup>a</sup> MP2(full)/6-31G(d) *ab initio* calculations, scaled frequencies, infrared intensities (km mol<sup>-1</sup>), Raman activities (Å<sup>4</sup> u<sup>-1</sup>), depolarization ratios (dp) and potential energy distributions (P.E.D.s)

<sup>b</sup> Scaled *ab initio* calculations with factors of 0.88 for CH and SiH stretches, 0.9 for all other modes except torsions and heavy atom bends using MP2/6-31G(d) basis set

<sup>c</sup> Symmetry coordinates with P.E.D. contributions less than 10% are omitted.

**Table 30.** Calculated<sup>a</sup> and observed frequencies (cm<sup>-1</sup>) for *gauche* conformer of cyclopropylcyanosilane, *c*-C<sub>3</sub>H<sub>5</sub>SiH<sub>2</sub>CN

Vib. No.	Approx. Description	MP2 6- 31G(d)	scaled <sup>b</sup>	IR Int.	Raman Act.	dp	infrared		Raman liquid	P.E.D. <sup>c</sup>	Band Contour		
							gas	xenon			A	B	C
v <sub>1</sub>	CH <sub>2</sub> antisymmetric stretch	3303	3099	7.6	49.5	0.52	3091	3075	3038	98S <sub>1</sub>	18	20	62
v <sub>20</sub>	CH <sub>2</sub> antisymmetric stretch	3291	3088	0.1	75.5	0.75	3091	3075	3038	99S <sub>20</sub>	9	9	82
v <sub>3</sub>	CH stretch	3220	3021	0.3	92.2	0.25	3023	3000	2926	96S <sub>3</sub>	4	-	96
v <sub>2</sub>	CH <sub>2</sub> symmetric stretch	3208	3009	5.9	115.3	0.03	3016	3000	2926	95S <sub>2</sub>	53	6	41
v <sub>21</sub>	CH <sub>2</sub> symmetric stretch	3204	3005	8.6	27.6	0.69	3010	3000	-	99S <sub>21</sub>	30	67	3
v <sub>22</sub>	SiH <sub>2</sub> antisymmetric stretch	2339	2194	132.8	66.5	0.66	2195	2152	2189	99S <sub>22</sub>	4	29	67
v <sub>4</sub>	SiH <sub>2</sub> symmetric stretch	2328	2183	86.7	145.1	0.05	2189	2152	2189	99S <sub>4</sub>	1	84	15
v <sub>5</sub>	C≡N stretch	2139	2132	47.3	38.5	0.23	2154	2152	2151	94S <sub>5</sub>	68	31	-
v <sub>6</sub>	CH <sub>2</sub> deformation	1571	1490	1.4	5.3	0.74	-	-	-	90S <sub>6</sub>	60	19	21
v <sub>23</sub>	CH <sub>2</sub> deformation	1535	1457	2.5	9.9	0.75	-	1457	1456	100S <sub>23</sub>	18	75	7
v <sub>7</sub>	CH bend (in-plane)	1370	1300	16.9	3.9	0.60	1291	1291	1286	46S <sub>7</sub> , 23S <sub>8</sub> , 12S <sub>10</sub>	75	9	16
v <sub>8</sub>	Ring breathing	1263	1199	4.9	20.9	0.09	1190	1186	1187	60S <sub>8</sub> , 16S <sub>7</sub> , 11S <sub>10</sub>	75	14	11
v <sub>28</sub>	CH <sub>2</sub> rock	1239	1176	0.3	5.5	0.75	1176	1173	1174	49S <sub>28</sub> , 40S <sub>24</sub> , 10S <sub>25</sub>	3	81	17
v <sub>25</sub>	CH bend (out-of-plane)	1174	1114	4.7	0.6	0.69	1098	1097	-	53S <sub>25</sub> , 39S <sub>24</sub>	33	59	8
v <sub>26</sub>	CH <sub>2</sub> wag	1126	1068	4.4	0.1	0.75	1066	1063	1069	94S <sub>26</sub>	40	60	-
v <sub>9</sub>	CH <sub>2</sub> wag	1119	1062	10.5	2.0	0.43	1045	1043	1043	76S <sub>9</sub>	33	4	63
v <sub>10</sub>	CH <sub>2</sub> twist	1087	1032	4.5	4.3	0.75	1026	1023	1024	23S <sub>10</sub> , 27S <sub>7</sub> , 23S <sub>14</sub> , 19S <sub>9</sub>	32	8	60
v <sub>11</sub>	SiH <sub>2</sub> deformation	987	936	112.3	14.7	0.75	932	932	936	95S <sub>11</sub>	5	90	5
v <sub>12</sub>	Ring deformation	969	920	54.4	10.7	0.70	895	899	899	82S <sub>12</sub>	84	2	14
v <sub>27</sub>	Ring deformation	930	884	103.3	6.0	0.74	875	880	892	49S <sub>27</sub> , 27S <sub>13</sub>	94	5	1
v <sub>13</sub>	SiH <sub>2</sub> wag	888	842	163.2	15.8	0.74	849	853	853	44S <sub>13</sub> , 47S <sub>27</sub>	95	1	3
v <sub>24</sub>	CH <sub>2</sub> twist	862	819	51.6	2.5	0.69	820	822	818	13S <sub>24</sub> , 29S <sub>28</sub> , 25S <sub>13</sub> , 24S <sub>25</sub>	87	12	1
v <sub>14</sub>	CH <sub>2</sub> rock	836	794	5.0	2.0	0.69	798	798	798	62S <sub>14</sub> , 27S <sub>10</sub>	50	12	38
v <sub>29</sub>	SiH <sub>2</sub> twist	766	728	6.7	9.9	0.75	714	719	716	76S <sub>29</sub>	33	61	6
v <sub>15</sub>	Si-C (ring) stretch	699	665	28.4	7.4	0.42	664	661	674	42S <sub>15</sub> , 23S <sub>30</sub> , 11S <sub>10</sub>	30	-	70
v <sub>16</sub>	Si-C (≡N) stretch	614	585	38.2	2.9	0.62	579	581	581	73S <sub>16</sub> , 13S <sub>30</sub>	71	27	1
v <sub>30</sub>	SiH <sub>2</sub> rock	589	562	32.4	9.1	0.29	567	572	574	44S <sub>30</sub> , 18S <sub>15</sub> , 11S <sub>16</sub>	2	82	16

**Table 30.** - - Continued.

Vib. No.	Approx. Description	MP2 6-31G(d)	scaled <sup>b</sup>	IR Int.	Raman Act.	dp	infrared		Raman liquid	P.E.D. <sup>c</sup>	Band Contour		
							gas	xenon			A	B	C
v <sub>17</sub>	Si-C≡N bend (in-plane)	381	370	1.6	1.6	0.27	-	-	375	33S <sub>17</sub> , 37S <sub>19</sub> , 13S <sub>32</sub>	15	83	2
v <sub>31</sub>	Si-C≡N bend (out-of-plane)	264	264	3.5	3.8	0.75	-	-	264	87S <sub>31</sub>	3	9	88
v <sub>18</sub>	Ring-Si bend (in-plane)	250	245	0.9	1.4	0.38	-	-	248	66S <sub>18</sub> , 12S <sub>17</sub>	28	3	69
v <sub>32</sub>	Ring-Si bend (out-of-plane)	235	231	2.8	1.5	0.66	-	-	234	53S <sub>32</sub> , 27S <sub>17</sub> , 14S <sub>18</sub>	11	60	29
v <sub>19</sub>	CSiC bend	102	100	4.0	1.8	0.74	-	-	104	48S <sub>19</sub> , 23S <sub>17</sub> , 20S <sub>32</sub>	71	29	-
v <sub>33</sub>	Asymmetric torsion	56	56	1.8	0.8	0.72	-	-	-	87S <sub>33</sub>	-	87	12

<sup>a</sup>MP2(full)/6-31G(d) *ab initio* calculations, scaled frequencies, infrared intensities (km mol<sup>-1</sup>), Raman activities (Å<sup>4</sup> u<sup>-1</sup>), depolarization ratios (dp) and potential energy distributions (P.E.D.s)

<sup>b</sup>Scaled *ab initio* calculations with factors of 0.88 for CH and SiH stretches, 0.9 for all other modes except torsions and heavy atom bends using MP2/6-31G(d) basis set

<sup>c</sup>Symmetry coordinates with P.E.D. contributions less than 10% are omitted.

**Table 31.** Calculated electronic energies (Hartrees, H) and energy differences (cm<sup>-1</sup>) for cyclopropylcyanosilane, *c*-C<sub>3</sub>H<sub>5</sub>SiH<sub>2</sub>CN

Basis set	MP2(full)		B3LYP	
	<i>cis</i> <sup>a</sup>	<i>gauche</i> <sup>b</sup>	<i>cis</i> <sup>a</sup>	<i>gauche</i> <sup>b</sup>
6-31G(d)	-0.6724940	166	-1.8469537	0
6-31G(d,p)	-0.7303823	162	-1.8566482	2
6-31+G(d)	-0.6884991	160	-1.8573961	-34
6-31+G(d,p)	-0.7459130	162	-1.8670281	-29
6-311G(d,p)	-1.0123454	233	-1.9296877	6
6-311+G(d,p)	-1.0194749	203	-1.9332027	-26
6-311G(2d,2p)	-1.0867537	248	-1.9402307	3
6-311+G(2d,2p)	-1.0920849	207	-1.9433652	-35
6-311G(2df,2pd)	-1.1819737	272	-1.9497180	10
6-311+G(2df,2pd)	-1.1862035	221	-1.9525907	-32
MP2(full)/aug-cc-pVTZ	-1.1270799	261	-1.9591636	-30

<sup>a</sup> Energy of *cis* conformer is given as  $-(E + 499)$  H.

<sup>b</sup> Energy of *gauche* conformer is relative to *cis* form.

**Table 32.** Symmetry coordinates for cyclopropylcyanosilane, *c*-C<sub>3</sub>H<sub>5</sub>SiH<sub>2</sub>CN

Description		Symmetry Coordinate <sup>a</sup>	
A'	CH <sub>2</sub> antisymmetric stretch	S <sub>1</sub>	= r <sub>2</sub> - r <sub>3</sub> + r <sub>4</sub> - r <sub>5</sub>
	CH <sub>2</sub> symmetric stretch	S <sub>2</sub>	= r <sub>2</sub> + r <sub>3</sub> + r <sub>4</sub> + r <sub>5</sub>
	CH stretch	S <sub>3</sub>	= r <sub>1</sub>
	SiH <sub>2</sub> symmetric stretch	S <sub>4</sub>	= r <sub>6</sub> + r <sub>7</sub>
	C≡N stretch	S <sub>5</sub>	= r <sub>8</sub>
	CH <sub>2</sub> deformation	S <sub>6</sub>	= 4φ <sub>1</sub> - σ <sub>1</sub> - π <sub>1</sub> - η <sub>1</sub> - ε <sub>1</sub> + 4φ <sub>2</sub> - σ <sub>2</sub> - π <sub>2</sub> - η <sub>2</sub> - ε <sub>2</sub>
	CH bend (in-plane)	S <sub>7</sub>	= 2γ - α <sub>1</sub> - α <sub>2</sub>
	ring breathing	S <sub>8</sub>	= R <sub>2</sub> + R <sub>3</sub> + R <sub>4</sub>
	CH <sub>2</sub> wag	S <sub>9</sub>	= σ <sub>1</sub> - π <sub>1</sub> + η <sub>1</sub> - ε <sub>1</sub> + σ <sub>2</sub> - π <sub>2</sub> + η <sub>2</sub> - ε <sub>2</sub>
	CH <sub>2</sub> twist	S <sub>10</sub>	= σ <sub>1</sub> - π <sub>1</sub> - η <sub>1</sub> + ε <sub>1</sub> + σ <sub>2</sub> - π <sub>2</sub> - η <sub>2</sub> + ε <sub>2</sub>
	SiH <sub>2</sub> deformation	S <sub>11</sub>	= 4φ - μ <sub>1</sub> - μ <sub>2</sub> - ρ <sub>1</sub> - ρ <sub>2</sub>
	ring deformation	S <sub>12</sub>	= 2R <sub>4</sub> - R <sub>2</sub> - R <sub>3</sub>
	SiH <sub>2</sub> wag	S <sub>13</sub>	= μ <sub>1</sub> + μ <sub>2</sub> - ρ <sub>1</sub> - ρ <sub>2</sub>
	CH <sub>2</sub> rock	S <sub>14</sub>	= σ <sub>1</sub> + π <sub>1</sub> - η <sub>1</sub> - ε <sub>1</sub> + σ <sub>2</sub> + π <sub>2</sub> - η <sub>2</sub> - ε <sub>2</sub>
	Si-C (ring) stretch	S <sub>15</sub>	= R <sub>1</sub>
	Si-C (≡N) stretch	S <sub>16</sub>	= R <sub>5</sub>

**Table 32. - - Continued.**

Description		Symmetry Coordinate <sup>a</sup>	
	CSiC bend	S <sub>17</sub>	= $\omega$
	Ring-Si bend (in-plane)	S <sub>18</sub>	= $\beta_1 + \beta_2$
	Si-C $\equiv$ N bend (in-plane)	S <sub>19</sub>	= $\sigma$
A''	CH <sub>2</sub> antisymmetric stretch	S <sub>20</sub>	= $r_2 - r_3 - r_4 + r_5$
	CH <sub>2</sub> symmetric stretch	S <sub>21</sub>	= $r_2 + r_3 - r_4 - r_5$
	SiH <sub>2</sub> antisymmetric stretch	S <sub>22</sub>	= $r_6 - r_7$
	CH <sub>2</sub> deformation	S <sub>23</sub>	= $4\phi_1 - \sigma_1 - \pi_1 - \eta_1 - \varepsilon_1 - 4\phi_2 + \sigma_2 + \pi_2 + \eta_2 + \varepsilon_2$
	CH <sub>2</sub> twist	S <sub>24</sub>	= $\sigma_1 - \pi_1 - \eta_1 + \varepsilon_1 + \sigma_2 - \pi_2 - \eta_2 + \varepsilon_2$
	CH bend (out-of-plane)	S <sub>25</sub>	= $\alpha_1 - \alpha_2$
	CH <sub>2</sub> wag	S <sub>26</sub>	= $\sigma_1 - \pi_1 + \eta_1 - \varepsilon_1 - \sigma_2 + \pi_2 - \eta_2 + \varepsilon_2$
	ring deformation	S <sub>27</sub>	= $R_2 - R_3$
	CH <sub>2</sub> rock	S <sub>28</sub>	= $\sigma_1 + \pi_1 - \eta_1 - \varepsilon_1 - \sigma_2 - \pi_2 + \eta_2 + \varepsilon_2$
	SiH <sub>2</sub> twist	S <sub>29</sub>	= $\mu_1 - \mu_2 - \rho_1 + \rho_2$
	SiH <sub>2</sub> rock	S <sub>30</sub>	= $\mu_1 - \mu_2 + \rho_1 - \rho_2$
	Ring-Si bend (out-of-plane)	S <sub>31</sub>	= $\beta_1 - \beta_2$
	Asymmetric torsion	S <sub>32</sub>	= $\tau_1$
	Si-C $\equiv$ N bend (out-of-plane)	S <sub>33</sub>	= $\tau_2$

<sup>a</sup> Not normalized.

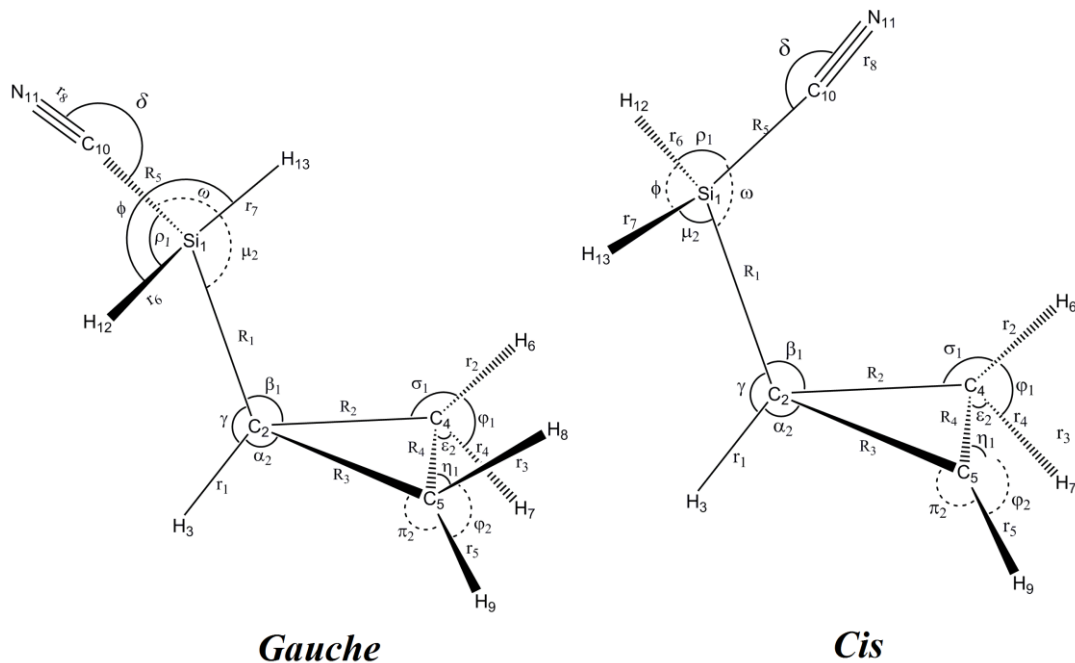


**Fig. 25** *Gauche* and *cis* conformers of cyclopropylcyanosilane showing atom numbering and internal coordinates.

The infrared spectrum of the gas and the predicted infrared spectra for the pure *gauche* and *cis* conformers, as well as the mixture of the two conformers with relative concentrations calculated for the equilibrium mixture at 25 °C by using the experimentally determined enthalpy difference, are shown in Fig. 23. The predicted spectrum is in good agreement with the experimental spectrum, which shows the utility of the scaled predicted frequencies and predicted intensities for supporting the vibrational assignment.

Raman spectra for the pure *gauche* and *cis* conformers, as well as the mixture of the two conformers with relative concentrations calculated for the equilibrium mixture at 25 °C by using the experimentally determined enthalpy difference (123 cm<sup>-1</sup>) are shown

in Fig. 24. The spectrum of the mixture should be compared to that of the Raman spectrum of the liquid at room temperature. The predicted spectrum is in reasonable agreement with the experimental spectrum, which also indicates the utility of the predicted Raman spectra for the supporting vibrational assignments.

### Microwave Results

Two conformers of cyclopropylcyanosilane, *cis*- and *gauche*-, were detected in the CP-FTMW spectrum. The *cis* conformer was calculated at the MP2/6-311++g(d,p) level of theory to be only 200 cm<sup>-1</sup> (2.4 kJ/mol) lower in energy than the *gauche*. Factoring in the differences in dipole moments between conformers, where  $\mu_a = 3.1 / 3.9$  D and  $\mu_b = 2.2 / 1.3$  D for the *cis* / *gauche* conformers, respectively, both conformers were detected in roughly equal abundance.

All single heavy atom isotopologues for both conformers were detected in their natural abundance. This includes three <sup>13</sup>C (the carbons at the 4- & 5- positions are equivalent by symmetry), <sup>29</sup>Si, <sup>30</sup>Si, and <sup>15</sup>N isotopologues. This large number of isotopic determinations enables direct determination of the heavy atom structure via Kraitchman's equations<sup>86</sup>. Rotational constants and other spectroscopic parameters determined by the least-squares method for all detected species can be found in Table 33.

The Kraitchman substitution structure ( $r_s$ ), calculated using the freely available KRA program<sup>87</sup>, is in excellent agreement with the *ab initio* structure. Although the  $|c|$  coordinates of the silicon and nitrogen atoms were forced to zero for the *cis* conformer, since Kraitchman's equations have a tendency to output non-real solutions to atomic coordinates near the principal axes due to vibrational averaging<sup>88</sup>, the *ab initio*  $|c|$  coordinates are well within the approximate error of 10<sup>-3</sup> Å found on the Kraitchman

determination of the other real-valued  $|c|$  coordinates. All *gauche* coordinates were determined with real values, with similar precisions as the *cis* conformer. The *cis* and *gauche* Kraitchman coordinates have RMS errors with respect to the MP2/6-311++g(d,p) geometries of 0.068 and 0.033 Å, respectively.

A potential complication of the rotational spectrum for the *gauche* conformer is a splitting due to tunneling between the two equivalent conformers. An MP2/6-311++g(d,p) scan of this double-well potential (with a trajectory through the local maximum, where the cyano group points directly away from the ring) has a calculated barrier of 640  $\text{cm}^{-1}$ . In order to predict the splitting associated with tunneling across this torsional barrier, the Pitzer-Gwinn 1-D hindered rotor approximation<sup>89</sup> was used. This method approximates the torsional potential energy surface as a Fourier series, in order to directly extract eigenvalues from a torsional Hamiltonian (which, under the assumption of a rigid frame, is uncoupled from the overall rotation). This method gives an tunneling splitting  $\Delta E = 337 \text{ kHz}$ , and a fundamental torsional frequency of 15.5  $\text{cm}^{-1}$ .

Experimentally, some high  $J$  lines of the *gauche* conformer with values of  $J' = 5, 6$ , are observed with some resolvable splitting not described by the hyperfine splitting arising from the nitrogen nucleus. Sometimes transitions observed near the end of the band in the 6-18 GHz CP-FTMW experiment can be found with a resolvable splitting, due to inhomogeneities in the Doppler profile of the molecular beam caused by clustering with the buffer gas. However, the profile of this splitting is generally asymmetric (where each component of the transition is not equally weighted in the transition), and the predicted center frequency of the transition is found at the midpoint of the splitting. In the case of the *gauche* splitting, the splitting is approximately 1:1 in intensity weighting, and

the predicted line center falls on a single peak of the split line, which is suggestive of a quantum mechanical effect such as this tunneling. This splitting can additionally be found on multiple hyperfine components of a single transition, and is not seen in transitions for the *cis* conformer with comparable center frequency or J.

However, due to the large Doppler broadening associated with the perpendicular expansion geometry of the CP-FTMW experiment, the splitting is only observed on a small set of transitions and the linewidths are such that a detailed quantitative analysis is difficult. Additionally, the ultimate determination of the splitting frequency,  $\Delta E$ , requires detection of electric dipole-forbidden transitions,  $\mu_c$ -type in this case, that are populated by tunneling across the gap. However, the predicted  $\mu_c$  dipole at the potential maximum is 0.2 D, which in the case of this molecule is far below the detection limit of the experiment (the most intense transitions in this spectrum arise from an MP2-calculated  $\mu_a$  dipole of approximately 4.0 D).

**Table 33.** Experimental and predicted rotational and centrifugal distortion constants of cyclopropylcyanosilane isotopomers,  $c\text{-C}_3\text{H}_5\text{SiH}_2\text{CN}$ .

	$A$ (MHz)	$B$ (MHz)	$C$ (MHz)	$\Delta_J$ (kHz)	$\Delta_{JK}$ (kHz)	$\Delta_K$ (kHz)	$\delta_J$ (kHz)	$\delta_K$ (kHz)	$N^a$
MP2(full)/6-311+G(d,p)	4297.9590	2221.5654	1687.1481	1.70496	-6.45635	9.87735	0.59672	-0.33360	
B3LYP/6-311+G(d,p)	4464.0199	2074.0715	1624.0378	1.58802	-6.51279	11.33687	0.53249	0.09655	
Experimental	4387.40278(84)	2196.50693(68)	1684.73866(60)	1.794(17)	-6.295(29)	10.429(47)	0.6035(37)	-0.688(48)	175
MP2(full)/6-311+G(d,p)	4247.3822	2220.0110	1678.3993	1.80453	-6.85840	10.17207	0.64434	-0.23247	
B3LYP/6-311+G(d,p)	4412.5282	2072.5075	1616.2213	1.58028	-6.48053	11.23777	0.53585	0.07621	
$^{29}\text{Si}$	4336.3163(18)	2194.9331(24)	1676.2027(18)	1.808(58)	-6.37(28)	10.08(45)	0.617(27)	-0.27(36)	87
MP2(full)/6-311+G(d,p)	4199.1034	2218.3939	1669.8921	1.79142	-6.80036	10.04363	0.64572	-0.22719	
B3LYP/6-311+G(d,p)	4363.4640	2070.9497	1608.6523	1.56898	-6.43902	11.11770	0.53754	0.08035	
$^{30}\text{Si}$	4287.6546(19)	2193.3559(14)	1667.9425(10)	1.760(31)	-6.35(19)	10.27(34)	0.599(16)	-0.33(29)	83
MP2(full)/6-311+G(d,p)	4289.7484	2205.3278	1.6765031	1.77600	-6.79336	10.19164	0.62686	-0.21213	
B3LYP/6-311+G(d,p)	4454.8513	2059.7725	1.6140557	1.55573	-6.40333	11.23596	0.52113	0.08968	
$^{13}\text{C}$ (2)	4378.7908(60)	2180.6356(28)	1674.1490(22)	1.874(47)	-6.55(40)	11.6(11)	0.645(37)	-0.72(45)	52
MP2(full)/6-311+G(d,p)	4255.2586	2191.7780	1669.4118	1.77484	-6.66352	9.90096	0.62278	-0.26116	
B3LYP/6-311+G(d,p)	4419.3634	2045.7024	1606.3194	1.55603	-6.30136	10.95860	0.51773	0.04352	
$^{13}\text{C}$ (4/5)	4343.2402(20)	2167.0676(18)	1666.8925(13)	1.911(44)	-6.51(23)	10.21(33)	0.636(25)	-0.63(35)	64
MP2(full)/6-311+G(d,p)	4295.4316	2198.4652	1673.3974	1.77205	-6.76317	10.18165	0.62274	-0.21542	
B3LYP/6-311+G(d,p)	4460.6438	2052.3638	1610.2669	1.55190	-6.38634	11.22665	0.51700	0.11065	
$^{13}\text{C}$ (10)	4384.2485(56)	2173.6720(23)	1670.8128(16)	1.923(59)	-6.64(18)	10.3(12)	0.635(30)	-0.52(32)	61
MP2(full)/6-311+G(d,p)	4246.0642	2173.9166	1651.7189	1.78507	-6.95374	10.43602	0.63062	-0.18157	
B3LYP/6-311+G(d,p)	4410.2821	2029.4281	1589.6187	1.55127	-6.49539	11.38997	0.51961	0.13244	
$^{15}\text{N}$	4335.0040(93)	2149.4641(29)	1649.340(18)	1.828(48)	-6.22(15)	10.4(14)	0.525(38)	-0.42	27

<sup>a</sup> Number of frequencies fitted.

**Table 33.** - - Continued.

	A (MHz)	B (MHz)	C (MHz)	$\Delta_I$ (kHz)	$\Delta_{JK}$ (kHz)	$\Delta_K$ (kHz)	$\delta_J$ (kHz)	$\delta_K$ (kHz)	<i>N</i>
MP2(full)/6-311+G(d,p)	6818.4779	1573.5298	1374.3846	0.70401	-10.33515	65.47481	0.20016	2.00245	
B3LYP/6-311+G(d,p)	7039.8442	1527.1073	1346.3113	0.64929	-9.96831	64.78186	0.18379	1.03587	
Experimental	7029.7244(45)	1567.1001(48)	1377.7489(45)	0.866(24)	-11.93(15)	73.39(93)	0.2499(38)	3.40(22)	80
MP2(full)/6-311+G(d,p)	6737.4659	1574.0330	1371.5060	0.80811	-11.26650	64.53863	0.23752	2.03910	
B3LYP/6-311+G(d,p)	6966.9968	1525.9845	1342.8824	0.64385	-9.86464	64.18921	0.18456	1.01886	
<sup>29</sup> Si	6955.5999(73)	1566.4729(17)	1374.4671(14)	0.827(16)	-12.40(24)	[73.39]	0.256(10)	[3.40]	33
MP2(full)/6-311+G(d,p)	6666.7153	1573.4077	1368.1596	0.80369	-11.20279	64.12256	0.23924	2.00343	
B3LYP/6-311+G(d,p)	6895.6552	1525.3315	1339.7943	0.64053	-9.79613	63.83413	0.18594	1.00375	
<sup>30</sup> Si	6886.1280(32)	1565.8541(31)	1371.2705(27)	0.846(24)	-12.41(24)	[73.39]	0.272(31)	[3.40]	31
MP2(full)/6-311+G(d,p)	6781.9095	1567.6633	1370.7491	0.79458	-11.17994	64.75210	0.22856	2.05380	
B3LYP/6-311+G(d,p)	7012.0322	1520.0987	1341.9620	0.63661	-9.75818	63.48276	0.17880	0.93968	
<sup>13</sup> C (2)	6984.967(26)	1560.3060(36)	1373.6546(29)	0.762(37)	-9.3(17)	[73.39]	0.195(33)	[3.40]	14
MP2(full)/6-311+G(d,p)	6810.0881	1545.7559	1352.7927	0.76738	-10.94280	64.26138	0.22006	2.00266	
B3LYP/6-311+G(d,p)	7038.8716	1499.0292	1324.4439	0.61130	-9.56571	63.66849	0.17099	1.00178	
<sup>13</sup> C (4)	6900.961(33)	1552.0327(28)	1361.8969(26)	0.759(30)	-12.32(30)	[73.39]	0.213(34)	[3.40]	19
MP2(full)/6-311+G(d,p)	6688.0970	1559.9481	1359.3756	0.82159	-11.17761	62.24582	0.23902	2.11854	
B3LYP/6-311+G(d,p)	6913.3606	1511.5407	1330.3235	0.65412	-9.82263	61.99082	0.18572	1.13247	
<sup>13</sup> C (5)	7027.050(47)	1538.6804(48)	1355.6570(39)	0.837(41)	-12.00(41)	[73.39]	0.258(45)	[3.4]	15
MP2(full)/6-311+G(d,p)	6810.1117	1557.3568	1361.6723	0.79891	-11.12174	63.87534	0.23026	1.99753	
B3LYP/6-311+G(d,p)	7039.7357	1509.7958	1332.8677	0.63317	-9.81228	64.35031	0.17759	1.02480	
<sup>13</sup> C (10)	7029.184(24)	1549.8303(39)	1364.2991(26)	0.794(27)	-12.94(32)	[73.39]	0.229(34)	[3.40]	20
MP2(full)/6-311+G(d,p)	6755.6363	1535.9845	1343.1868	0.78439	-11.13988	65.02118	0.22561	2.05651	
B3LYP/6-311+G(d,p)	6985.4295	1489.4067	1315.0643	0.62385	-9.80711	64.65918	0.17501	1.01389	
<sup>15</sup> N	6972.030(16)	1528.6305(17)	1345.8895(16)	[0.866]	[-11.93]	[73.39]	[0.2499]	[3.40]	12

<sup>a</sup> Number of frequencies fitted.

## Structural Parameters

We have found that good structural parameters for hydrocarbons and many substituted ones can be determined by adjusting the structural parameters obtained from the *ab initio* MP2(full)/6-311+G(d,p) calculations to fit the rotational constants obtained from microwave experimental data by using a computer program “A&M” (*Ab initio* and Microwave) developed<sup>32</sup> in our laboratory. In order to reduce the number of independent variables, the structural parameters are separated into sets according to their types where bond distances in the same set keep their relative ratio, and bond angles and torsional angles in the same set keep their difference in degrees. This assumption is based on the fact that errors from *ab initio* calculations are systematic. It has been shown<sup>33</sup> that *ab initio* MP2(full)/6-311+G(d,p) calculations have predicted the  $r_0$  structural parameters for more than fifty hydrocarbons, with the C-H distances predicted to better than 0.002 Å when compared to the experimentally determined values from isolated C-H stretching frequencies. In another study, C-H bond distances determined from isolated C-H stretching frequencies were observed to be in good agreement with the same parameters determined from earlier microwave studies.<sup>34</sup> Therefore, all of the carbon-hydrogen distances can be taken from the MP2(full)/6-311+G(d,p) predicted values for cyclopropylcyanosilane.

**Table 34.** Structural parameters (Å and degrees), rotational constants (MHz) and dipole moments for *cis* and *gauche* rotamers of cyclopropylcyanosilane, *c*-C<sub>3</sub>H<sub>5</sub>SiH<sub>2</sub>CN

Structural Parameters	Internal Coordinates	MP2(full)/6-311+G(d,p)		B3LYP/6-311+G(d,p)		Adjusted r <sub>0</sub>	
		<i>cis</i>	<i>gauche</i>	<i>cis</i>	<i>gauche</i>	<i>cis</i>	<i>gauche</i>
r(Si <sub>1</sub> C <sub>2</sub> )	R <sub>1</sub>	1.847	1.844	1.849	1.854	1.841 (3)	1.844 (3)
r(C <sub>2</sub> C <sub>4</sub> )	R <sub>2</sub>	1.522	1.524	1.517	1.528	1.518 (3)	1.517 (3)
r(C <sub>2</sub> C <sub>5</sub> )	R <sub>3</sub>	1.522	1.521	1.517	1.521	1.518 (3)	1.522 (3)
r(C <sub>4</sub> C <sub>5</sub> )	R <sub>4</sub>	1.499	1.499	1.494	1.500	1.494 (3)	1.500 (3)
r(Si <sub>1</sub> C <sub>10</sub> )	R <sub>5</sub>	1.860	1.860	1.862	1.867	1.857 (3)	1.840 (3)
r(C <sub>10</sub> N <sub>11</sub> )	r <sub>8</sub>	1.179	1.179	1.152	1.156	1.160 (3)	1.160 (3)
r(C <sub>2</sub> H <sub>3</sub> )	r <sub>1</sub>	1.087	1.087	1.085	1.086	1.087 (2)	1.087 (2)
r(C <sub>4</sub> H <sub>6</sub> )	r <sub>2</sub>	1.085	1.085	1.081	1.084	1.085 (2)	1.085 (2)
r(C <sub>4</sub> H <sub>7</sub> )	r <sub>3</sub>	1.083	1.083	1.081	1.083	1.083 (2)	1.083 (2)
r(C <sub>5</sub> H <sub>8</sub> )	r <sub>4</sub>	1.085	1.085	1.081	1.084	1.085 (2)	1.085 (2)
r(C <sub>5</sub> H <sub>9</sub> )	r <sub>5</sub>	1.083	1.083	1.081	1.083	1.083 (2)	1.083 (2)
r(Si <sub>1</sub> H <sub>12</sub> )	r <sub>6</sub>	1.473	1.472	1.477	1.481	1.478 (3)	1.479 (3)
r(Si <sub>1</sub> H <sub>13</sub> )	r <sub>7</sub>	1.473	1.474	1.477	1.482	1.478 (3)	1.478 (3)
∠Si <sub>1</sub> C <sub>2</sub> H <sub>3</sub>	γ	115.8	116.9	113.3	115.2	115.8 (5)	116.9 (5)
∠C <sub>2</sub> C <sub>4</sub> C <sub>5</sub>	A <sub>1</sub>	60.5	60.4	60.5	60.4	60.5 (5)	60.6 (5)
∠C <sub>2</sub> C <sub>5</sub> C <sub>4</sub>	A <sub>2</sub>	60.5	60.6	60.5	60.6	60.5 (5)	60.2 (5)
∠C <sub>4</sub> C <sub>2</sub> C <sub>5</sub>	A <sub>3</sub>	59.0	59.0	59.0	59.0	58.9 (5)	59.1 (5)
∠Si <sub>1</sub> C <sub>2</sub> C <sub>4</sub>	β <sub>1</sub>	120.3	119.3	122.4	120.1	120.5 (5)	119.1 (5)
∠Si <sub>1</sub> C <sub>2</sub> C <sub>5</sub>	β <sub>2</sub>	120.3	119.0	122.4	121.1	120.5 (5)	118.8 (5)
∠C <sub>2</sub> Si <sub>1</sub> C <sub>10</sub>	ω	105.5	108.8	108.2	110.0	106.6 (5)	110.7 (5)
∠Si <sub>1</sub> C <sub>10</sub> N <sub>11</sub>	δ	177.3	178.2	178.6	179.5	177.3 (5)	178.2 (5)
∠H <sub>6</sub> C <sub>4</sub> H <sub>7</sub>	φ <sub>1</sub>	115.1	114.8	114.3	114.1	115.1 (5)	114.8 (5)
∠H <sub>8</sub> C <sub>5</sub> H <sub>9</sub>	φ <sub>2</sub>	115.1	114.8	114.3	114.1	115.1 (5)	114.8 (5)
∠C <sub>2</sub> Si <sub>1</sub> H <sub>12</sub>	μ <sub>1</sub>	113.5	113.8	113.0	113.3	113.5 (5)	113.8 (5)
∠C <sub>2</sub> Si <sub>1</sub> H <sub>13</sub>	μ <sub>2</sub>	113.5	109.6	113.0	110.6	113.5 (5)	109.6 (5)
∠C <sub>10</sub> Si <sub>1</sub> H <sub>12</sub>	ρ <sub>1</sub>	107.0	106.6	106.3	105.8	106.4 (5)	105.5 (5)
∠C <sub>10</sub> Si <sub>1</sub> H <sub>13</sub>	ρ <sub>2</sub>	107.0	106.9	106.3	106.3	106.4 (5)	105.9 (5)
∠H <sub>12</sub> Si <sub>1</sub> H <sub>13</sub>	φ	109.9	110.8	110.0	110.5	109.9 (5)	110.8 (5)
τH <sub>3</sub> C <sub>2</sub> Si <sub>1</sub> C <sub>10</sub>	τ <sub>1</sub>	180.0	66.0	180.0	63.7	180.0 (5)	66.0 (5)
τN <sub>11</sub> C <sub>10</sub> Si <sub>1</sub> C <sub>2</sub>	τ <sub>2</sub>	0.0	3.5	0.0	5.2	0.0 (5)	3.5 (5)
A		4298.0	6811.6	4442.8	7041.6	4387.4	7029.5
B		2221.6	1574.7	2078.0	1526.6	2196.5	1567.1
C		1687.1	1375.0	1623.8	1346.6	1684.7	1377.7
μ <sub>a</sub>		3.329	4.208	3.391	4.167		
μ <sub>b</sub>		2.436	1.510	2.210	1.326		
μ <sub>c</sub>		0.000	0.073	0.000	0.082		
μ <sub>t</sub>		4.125	4.471	4.048	4.374		

It has also been shown that SiH distances can be obtained from isolated SiH stretching frequencies.<sup>90</sup> Therefore, we have obtained values of 1.478 Å for the  $r_6$  and  $r_7$  distances of the *cis* conformer and, 1.479 and 1.478 Å for the  $r_6$  and  $r_7$  distances of the *gauche* conformer (Table 34) which are 0.005 Å longer than values for the corresponding distances from the MP2(full)/6-311+G(d,p) predicted parameters. These longer distances are similar to the differences found for many SiH distances in other organosilanes.<sup>91,92</sup> Also the C≡N distance is nearly constant, irrespective of the substitutions near by it<sup>93</sup>. Thus, there are only four heavy atom distances and three heavy atom angles to be determined. For the *cis* conformer, two CCC angles ( $\angle C_2C_4C_5$  and  $\angle C_2C_5C_4$ ) can be treated as a single set and two of the CC distances ( $R_2$  and  $R_3$ ) can be treated as a single set, which leaves five independent parameters to be determined. However, for the *gauche* conformer all heavy atom distances and bond angles were treated as independent parameters, mainly due to its lack of symmetry.

From the microwave spectrum of cyclopropylcyanosilane and its isotopologues 21 and 24, rotational constants were obtained for the *cis* and *gauche* conformers, respectively (Table 35). These rotational constants were utilized to determine structural parameters of cyclopropylcyanosilane for both conformers. The resulting adjusted parameters obtained for both conformers are listed in Table 34. It is expected that the C-C, Si-C, and Si-H distances should be accurate to  $\pm 0.003$  Å, the C-H distances should be accurate to  $\pm 0.002$  Å, and the angles should be within  $\pm 0.5$  degree. The fits of all determined rotational constants (Table 34) by the structural parameters for both conformers are remarkably good, with most differences smaller than 0.3 MHz. Therefore, the suggested uncertainties are realistic values and the determined values are probably as

accurate as can be obtained for the parameters for this molecule in the gas phase.

For the *cis* conformer of cyclopropylcyanosilane, the  $r(\text{Si}_1\text{C}_2)$  bond distance was decreased by 0.006 Å,  $\angle\text{C}_2\text{Si}_1\text{C}_{10}$  was increased by 1.1° and  $\angle\text{C}_{10}\text{Si}_1\text{H}_{12,13}$  were decreased by 0.6° compared to predicted values calculated from MP2(full)/6-311+G(d,p) calculation (Table 34), whereas for the *gauche* conformer, the  $r(\text{Si}_1\text{C}_{10})$  bond distance was decreased by 0.020 Å and  $\angle\text{C}_2\text{Si}_1\text{C}_{10}$  bond angle was increased by 1.9° compared to predicted values obtained from the MP2(full) 6-311+G(d,p) calculation. (Table 34). However, the  $\angle\text{C}_2\text{Si}_1\text{C}_{10}$  bond angle was well predicted by B3LYP/6-311+G(d,p) calculation.

**Table 35.** Comparison of rotational constants (MHz) obtained from *ab initio* MP2(full)/6-311+G(d,p) predictions, experimental values from microwave spectra, and from the adjusted  $r_0$  structural parameters for cyclopropylcyanosilane, *c*-C<sub>3</sub>H<sub>5</sub>SiH<sub>2</sub>CN.

Isotopomer	Rotational constant	MP2(full)/6-311+G(d,p)	Experimental	Adjusted $r_0$	$ \Delta $
<i>c</i> - C <sub>3</sub> H <sub>5</sub> <sup>28</sup> SiH <sub>2</sub> CN	A	4298.0	4387.4	4387.5	0.1
	B	2221.6	2196.5	2196.6	0.1
	C	1687.1	1684.7	1684.8	0.0
<i>c</i> - C <sub>3</sub> H <sub>5</sub> <sup>29</sup> SiH <sub>2</sub> CN	A	4293.6	4336.3	4336.2	0.1
	B	2225.1	2194.9	2195.0	0.1
	C	1688.5	1676.2	1676.2	0.0
<i>c</i> - C <sub>3</sub> H <sub>5</sub> <sup>30</sup> SiH <sub>2</sub> CN	A	4296.9	4287.7	4287.3	0.3
	B	2222.9	2193.4	2193.4	0.0
	C	1687.7	1667.9	1668.0	0.0
<i>cis</i> <i>c</i> - <sup>13</sup> C <sub>3</sub> H <sub>5</sub> SiH <sub>2</sub> CN (C2)	A	4289.7	4378.8	4378.7	0.1
	B	2205.3	2180.6	2180.7	0.0
	C	1676.5	1674.2	1674.1	0.0
<i>c</i> - <sup>13</sup> C <sub>3</sub> H <sub>5</sub> SiH <sub>2</sub> CN	A	4255.3	4343.2	4343.6	0.3
	B	2191.8	2167.1	2167.0	0.1
	C	1669.4	1666.9	1666.9	0.0
<i>c</i> - <sup>13</sup> C <sub>3</sub> H <sub>5</sub> SiH <sub>2</sub> CN	A	4295.4	4384.2	4384.6	0.4
	B	2198.5	2173.7	2173.5	0.1
	C	1673.4	1670.8	1670.8	0.0
<i>c</i> -C <sub>3</sub> H <sub>5</sub> SiH <sub>2</sub> C <sup>15</sup> N	A	4246.1	4335.0	4334.8	0.2
	B	2173.9	2149.5	2149.5	0.0

**Table 35.** - - Continued.

Isotopomer	Rotational constant	MP2(full)/6-311+G(d,p)	Experimental	Adjusted $r_0$	$ \Delta $
<i>c</i> - C <sub>3</sub> H <sub>5</sub> <sup>28</sup> SiH <sub>2</sub> CN	C	1651.7	1649.3	1649.4	0.0
	A	6811.6	7029.6	7029.5	0.2
	B	1574.7	1567.1	1567.1	0.0
<i>c</i> - C <sub>3</sub> H <sub>5</sub> <sup>29</sup> SiH <sub>2</sub> CN	C	1375.0	1377.8	1377.7	0.0
	A	6737.5	6955.5	6955.8	0.2
	B	1574.0	1566.5	1566.4	0.1
<i>c</i> - C <sub>3</sub> H <sub>5</sub> <sup>30</sup> SiH <sub>2</sub> CN	C	1371.5	1374.5	1374.5	0.0
	A	6666.7	6886.1	6885.2	0.8
	B	1573.4	1565.9	1565.8	0.1
<i>gauche</i> <i>c</i> - <sup>13</sup> C <sub>3</sub> H <sub>5</sub> SiH <sub>2</sub> CN (C2)	C	1368.2	1371.3	1371.3	0.0
	A	6781.9	6984.9	6973.1	1.2
	B	1567.7	1560.3	1528.8	0.2
<i>gauche</i> <i>c</i> - <sup>13</sup> C <sub>3</sub> H <sub>5</sub> SiH <sub>2</sub> CN (C4)	C	1370.7	1373.7	1346.0	0.1
	A	6688.1	6900.9	6900.2	0.6
	B	1559.9	1552.0	1552.2	0.1
<i>gauche</i> <i>c</i> - <sup>13</sup> C <sub>3</sub> H <sub>5</sub> SiH <sub>2</sub> CN (C5)	C	1359.4	1361.9	1361.9	0.0
	A	6810.1	7026.9	7027.2	0.3
	B	1545.8	1538.7	1538.6	0.1
<i>gauche</i> <i>c</i> - <sup>13</sup> C <sub>3</sub> H <sub>5</sub> SiH <sub>2</sub> CN	C	1352.8	1355.7	1355.6	0.1
	A	6810.1	7029.1	7029.5	0.2
	B	1557.4	1549.8	1567.1	0.0
<i>c</i> -C <sub>3</sub> H <sub>5</sub> SiH <sub>2</sub> C <sup>15</sup> N	C	1361.7	1364.3	1377.7	0.0
	A	6755.6	6972.0	6955.8	0.2
	B	1536.0	1528.6	1566.4	0.1
	C	1343.2	1345.9	1374.5	0.0

### Vibrational Assignment

The microwave spectrum of cyclopropylcyanosilane showed bands belonging to both the *cis* and *gauche* conformers. However, this spectrum has no information regarding the stability of the conformers. This information can be obtained by determining the enthalpy difference between the two conformers, but for calculating the enthalpy difference, it is important to make confident vibrational assignments for both the

*cis* and *gauche* forms of cyclopropylcyanosilane. For this purpose, significant assistance was obtained from the *ab initio* MP2(full)/6-31G(d) calculations with two scaling factors to obtain the force constants. From these data the frequencies, infrared intensities, Raman activities, band contours and depolarization ratios were predicted. The “fingerprint” region of the spectra for this study, which is below 1,100 cm<sup>-1</sup>, is mainly used for providing suitable fundamentals for the  $\Delta H$  determination. Most of the fundamentals associated with the cyclopropyl ring are expected to have similar frequencies for the two conformers, as well as to those previously reported for the corresponding halides, *i.e.* *c*-C<sub>3</sub>H<sub>5</sub>SiH<sub>2</sub>Cl<sup>76</sup> and *c*-C<sub>3</sub>H<sub>5</sub>SiH<sub>2</sub>Br.<sup>77</sup> Hence, the ring modes will not be discussed in detail, but instead the emphasis will be on the SiH<sub>2</sub> bends and the CSi(CN) modes.

For both the *cis* and *gauche* conformers (Tables 29 and 30), the CN stretching fundamental was predicted at about 2,133 cm<sup>-1</sup> with medium infrared intensity. However, a big and broad band observed at 2,201 cm<sup>-1</sup> in the infrared spectrum of the gas is assigned for this mode. Strong fundamental peaks observed at 2,195 and 2,189 cm<sup>-1</sup> in the infrared spectrum of the gas are assigned to the SiH<sub>2</sub> antisymmetric and SiH<sub>2</sub> symmetric stretch.

The *cis* form of cyclopropylcyanosilane has C<sub>s</sub> symmetry and the vibrational modes are divided in to two (A' and A'') blocks (Table 29). The SiH<sub>2</sub> deformation, Si-C stretch, C-Si-C bend, ring Si bend (in-plane), and Si-C≡N bend (in-plane) fundamentals are in the A' block, whereas the SiH<sub>2</sub> twist, SiH<sub>2</sub> rock, ring Si bend (out-of-plane), asymmetric torsion and Si-C≡N (out-of-plane) fundamentals are in the A'' block. A shoulder peak of medium height observed at 955 cm<sup>-1</sup> in the infrared spectrum of the gas is assigned to the SiH<sub>2</sub> deformation ( $\nu_{11}$ ) mode. However, in the infrared spectrum of the sample dissolved in xenon solution, a broad and strong fundamental peak is observed at

955  $\text{cm}^{-1}$ . A medium, wide peak observed at 621  $\text{cm}^{-1}$  in the infrared spectrum of the gas and a small peak observed at 636  $\text{cm}^{-1}$  in the Raman spectrum of the liquid is assigned as the Si-C (ring) stretch ( $\nu_{15}$ ) mode. For the Si-C( $\equiv$ N) stretch ( $\nu_{16}$ ) mode, a shoulder peak is observed at 567  $\text{cm}^{-1}$  in the infrared spectrum of the gas and a medium peak is observed at 574  $\text{cm}^{-1}$  in the Raman spectrum of the liquid. A small peak observed at 413  $\text{cm}^{-1}$  in the Raman spectrum of the liquid and at 414  $\text{cm}^{-1}$  in the infrared spectrum of the gas is assigned to the CSiC ( $\nu_{17}$ ) mode. Peaks observed at 255  $\text{cm}^{-1}$  and 104  $\text{cm}^{-1}$  in the Raman spectrum of the liquid are assigned as the ring-Si bend (in-plane) ( $\nu_{18}$ ) and Si-C( $\equiv$ N) stretch ( $\nu_{19}$ ), respectively. A fundamental peak observed at 688  $\text{cm}^{-1}$  in both the infrared spectrum of the sample dissolved in liquid xenon and the Raman spectrum of the liquid is assigned for SiH<sub>2</sub> twist ( $\nu_{24}$ ). A sharp, medium peak observed at 612  $\text{cm}^{-1}$  in the infrared spectrum of the gas is assigned to the SiH<sub>2</sub> rocking ( $\nu_{30}$ ) mode. A shoulder peak observed at 265  $\text{cm}^{-1}$  in the Raman spectrum of the liquid is assigned as the ring-Si bend (out-of-plane) ( $\nu_{31}$ ) mode.

The *gauche* conformer of the cyclopropylcyanosilane has C<sub>1</sub> symmetry and all of the vibration modes are in one block (Table 30). In the infrared spectrum of the gas and the Raman spectrum of the liquid, medium intense bands observed at 932  $\text{cm}^{-1}$  and 936  $\text{cm}^{-1}$ , respectively, are assigned for the SiH<sub>2</sub> deformation ( $\nu_{11'}$ ) mode. The SiH<sub>2</sub> twist ( $\nu_{29'}$ ) mode was predicted at 728  $\text{cm}^{-1}$  with moderate infrared intensity and Raman activity; instead, a small shoulder peak was observed at 716  $\text{cm}^{-1}$  in the Raman spectrum of the liquid is assigned to this mode. A sharp, medium peak observed at 674  $\text{cm}^{-1}$  in the Raman spectrum of the liquid is assigned for the Si-C (ring) stretch. The Si-C( $\equiv$ N) ( $\nu_{16'}$ ) stretch was predicted at 585  $\text{cm}^{-1}$ , a medium and sharp peak observed at 579  $\text{cm}^{-1}$  in the

infrared spectrum of the gas, and at  $581\text{ cm}^{-1}$  in the Raman spectrum of the liquid are assigned to this mode. Similarly, a peak observed at  $567\text{ cm}^{-1}$  in the infrared spectrum of the gas is assigned for the  $\text{SiH}_2$  rock ( $\nu_{30'}$ ) mode. A small peak observed at  $375\text{ cm}^{-1}$  and a shoulder peak observed at  $265\text{ cm}^{-1}$  in the Raman spectrum of the liquid are assigned as  $\text{Si-C}\equiv\text{N}$  (in-plane) ( $\nu_{17'}$ ) and (out-of-plane) ( $\nu_{31'}$ ) bending modes, respectively. In the Raman spectrum of the liquid, a peak observed at  $248\text{ cm}^{-1}$  is assigned to the ring-Si (in-plane) ( $\nu_{18'}$ ) bending mode and the peak observed at  $234\text{ cm}^{-1}$  is assigned to ring-Si (out-of-plane) ( $\nu_{32'}$ ) bending mode. Additionally, a peak observed at  $104\text{ cm}^{-1}$  in the Raman spectrum of the liquid is assigned as the  $\text{CSiC}$  bend ( $\nu_{33'}$ ) mode.

The mixing of the vibrations is indicated by the potential energy distributions, and practically all modes have major contributions from two or more symmetry coordinates and their approximate descriptions are given in Tables 29 and 30. For the *cis* conformer (Table 29), the mixing was extensive for the  $\nu_7$ ,  $\nu_{10}$ ,  $\nu_{14}$ ,  $\nu_{17}$ , and  $\nu_{19}$  fundamentals. Most fundamentals have extensive contributions from three or more modes. The *gauche* conformer (Table 30) is similar, with extensive mixing occurring with the vibration at  $1295\text{ cm}^{-1}$  and below. On the other hand, the *gauche* form shows a significant increase in mixing with most of the modes having contributions of 10% or more from at least three modes. In the *cis* conformer, the descriptions of the  $\nu_{10}$ ,  $\nu_{17}$ , and  $\nu_{28}$  fundamentals are largely for bookkeeping purposes and the mixing is extensive for the  $\nu_{10}$  fundamental with contributions of more than 10% from 4 different modes. In the *gauche* form, descriptions of the  $\nu_{10'}$  and  $\nu_{24'}$  fundamental are also primarily for bookkeeping purposes. The *gauche* conformer has extensive mixing for the  $\nu_{10'}$  and  $\nu_{24'}$  fundamentals with contributions of more than 10% from 4 different modes. For the *cis* form,  $\nu_{10}$  has been

assigned as  $S_{10}$  ( $\text{CH}_2$  twist), with a 25% contribution, whereas the  $\nu_{17}$  fundamental has been assigned as  $S_{17}$  ( $\text{CSiC}$  bend), with a 24% contribution, and the  $\nu_{28}$  fundamental has been assigned as  $S_{28}$  ( $\text{CH}_2$  rock), with a 29% contribution. For the *gauche* form,  $\nu_{10'}$  has been assigned as  $S_{10}$  ( $\text{SiH}_2$  deformation), with a 23% contribution and  $\nu_{24'}$  fundamental has been assigned as  $S_{24}$  ( $\text{CH}_2$  twist), with a 13% contribution. With these assignments, the remaining vibrational modes are easily assigned, and the assignments for the fundamentals for this molecule are thus made with confidence.

### Conformational Stability

The electronic energy for both the *cis* and *gauche* conformers of cyclopropylcyanosilane were calculated by utilizing 22 basis sets from the MP2(full) and B3LYP calculations, along with utilization of 18 basis sets from 6-31G(d) to aug-cc-p-VTZ (Table 31). In MP2(full) calculations, the *cis* conformer was observed to be the more stable form and the electronic energy difference between the two conformers varies from 160 to 272  $\text{cm}^{-1}$ , whereas in the B3LYP calculations, both the *cis* and *gauche* conformers were observed to be stable forms with an electronic energy difference between -35 to +10  $\text{cm}^{-1}$  (Table 31). Hence, from theoretical calculations, it is difficult to draw a confident conclusion about the conformational stability and energy difference between the *cis* and the *gauche* conformers of cyclopropylcyanosilane.

To determine the more stable conformer and the enthalpy difference between the *cis* and *gauche* forms of cyclopropylcyanosilane, the sample was dissolved in liquefied xenon and the mid-infrared spectra were recorded as a function of temperature from -60 to -100 °C. Very small interactions are expected to occur between xenon and the sample, although though the sample can associate with itself forming dimers, trimmers, or higher

order complexes. However, due to the very small concentration of the sample ( $\sim 10^{-4}$  molar), self-association is greatly reduced. Therefore, only small frequency shifts are anticipated for the xenon interactions when passing from the gas phase to the liquefied xenon solution, which is confirmed with an average frequency shift of  $1\text{ cm}^{-1}$ . A significant advantage of this study is that the conformer bands are better resolved in the xenon solution in comparison to those observed in the infrared spectrum of the gas (Fig. 26). From *ab initio* calculations, the dipole moments of the two conformers are predicted to have similar values and the molecular sizes of the two conformers are nearly the same, so the  $\Delta H$  value obtained from the temperature dependent FT-IR study from the xenon solution is expected to be near to that for the gas.<sup>65,66,28,29,27</sup>

Once confident assignments have been made for the fundamentals of both observed conformers, then the task was to find pairs of bands from which the enthalpy difference could be obtained. The bands should be sufficiently resolved for determining their intensities. They should be in the region from  $1,200$  to  $400\text{ cm}^{-1}$ , where only a limited number of overtone and combination bands are possible. For the *cis* conformer, the  $\text{SiH}_2$  deformation ( $\nu_{11}$ ) observed at  $954\text{ cm}^{-1}$  and the  $\text{SiH}_2$  twist ( $\nu_{29}$ ) observed at  $688\text{ cm}^{-1}$  (Table 29), and for the *gauche* conformer, the  $\text{SiH}_2$  deformation ( $\nu_{11}'$ ) fundamental observed at  $932\text{ cm}^{-1}$  and the  $\text{SiH}_2$  twist ( $\nu_{29}$ ) fundamental observed at  $719\text{ cm}^{-1}$  (Table 30) were used for the enthalpy difference calculation (Fig. 26). These bands are well resolved and believed to be relatively free from combination and overtone bands, and thus were used for the enthalpy difference determinations. The intensities of these individual bands were measured in absorption as a function of temperature (Fig. 27) and their ratios were determined (Table 36). By application of the van't Hoff equation

$-\ln K = \Delta H/(RT) - \Delta S/R$ , the enthalpy difference was determined from a plot of  $-\ln K$  versus  $1/T$ , where  $\Delta H/R$  is the slope of the line and  $K$  is substituted with the appropriate intensity ratios, *i.e.*  $I_{conf-1} / I_{conf-2}$ , etc. It was assumed that  $\Delta S$  and van't Hoff factor  $\alpha$  are not functions of temperature in this small temperature range utilized.

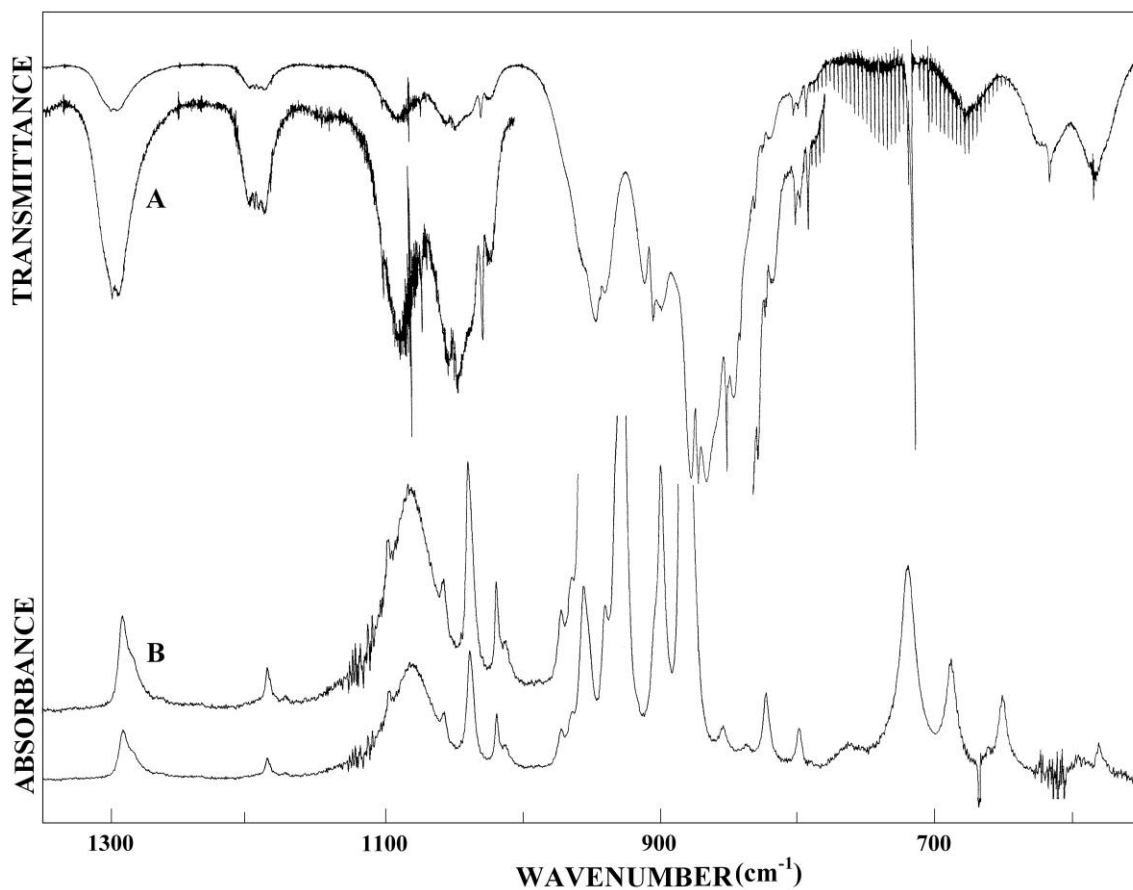


**Fig. 26** Mid-infrared spectra of cyclopropylcyanosilane: (A) gas in transmittance; (B) liquid xenon solution at -70 °C in absorbance.

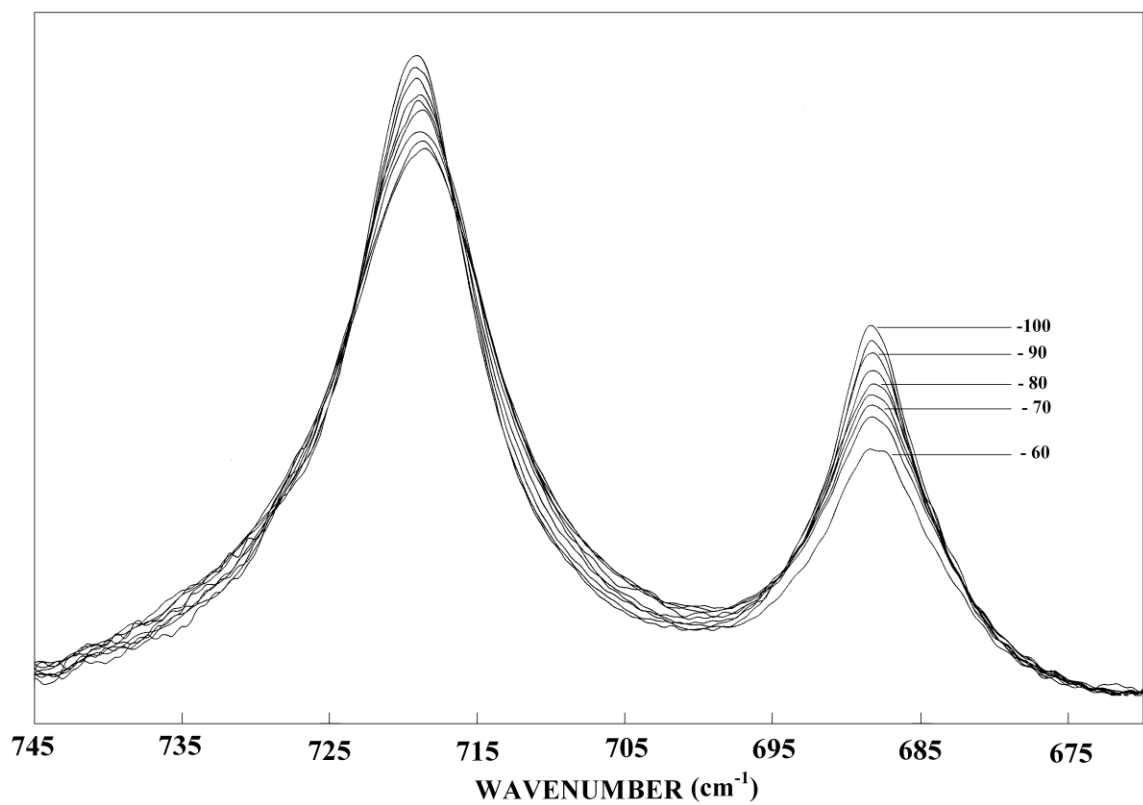


**Fig. 27** Temperature (- 60 to -100 °C) dependent mid-infrared spectrum of cyclopropylcyanosilane dissolved in liquid xenon.

**Table 36.** Temperature and intensity ratios of the conformational bands of cyclopropylcyanosilane,  $c\text{-C}_3\text{H}_5\text{SiH}_2\text{CN}$  from the infrared spectra of the liquid xenon solution phase.

T(°C)	1/T ( $\times 10^3 \text{ K}^{-1}$ )	$I_{688} / I_{719}$	$I_{954} / I_{719}$	$I_{688} / I_{932}$	$I_{954} / I_{932}$
-60.0	4.692	2.4727	1.5339	1.4180	0.8796
-65.0	4.804	2.2527	1.5227	1.2940	0.8747
-70.0	4.923	2.2011	1.4580	1.3669	0.9054
-75.0	5.047	2.1063	1.4366	1.3083	0.8923
-80.0	5.177	2.0666	1.4372	1.2220	0.8498
-85.0	5.315	1.9826	1.4408	1.1574	0.8411
-90.0	4.460	1.9710	1.3914	1.1570	0.8168
-95.0	5.613	1.9288	1.3914	1.1189	0.8071
-100.0	5.775	1.8505	1.3952	1.0384	0.7829
$\Delta H^a \text{ (cm}^{-1}\text{)}$		$161 \pm 17$	$62 \pm 10$	$184 \pm 19$	$85 \pm 14$

<sup>a</sup> Average value:  $\Delta H = 123 \pm 13 \text{ cm}^{-1}$  ( $1.47 \pm 0.16 \text{ kJ mol}^{-1}$ ) with the *cis* conformer the more stable form and the statistical uncertainty ( $2\sigma$ ) obtained by utilizing all of the data as a single set.

These four bands, with two each from the *cis* and the *gauche* conformers, were utilized for the determination of the enthalpy difference by combining them to form four band pairs. By using these band pairs for the *cis* and *gauche* conformers, the individually determined enthalpy differences ranged from  $62 \pm 10 \text{ cm}^{-1}$  to  $184 \pm 19 \text{ cm}^{-1}$  (Table 36). However, an average value was obtained by taking the data from all four band pairs as a single data set. By this method an average value of  $123 \pm 11 \text{ cm}^{-1}$  was obtained. The error limit was derived from the statistical standard deviation of two sigma. These error limits do not take into account small associations with the liquid xenon or the interference of overtones and combination bands in near coincidence with the measured fundamentals. The variations in the individual values are undoubtedly due to these types of

interferences, but by taking several band pairs, the effect of such interferences should cancel. However, this statistical uncertainty is probably better than can be expected from this technique and, therefore, an uncertainty of about 10% in the enthalpy difference is probably more realistic *i.e.*,  $123 \pm 13 \text{ cm}^{-1}$ . From these enthalpy differences the abundance of the *cis* conformer at ambient temperature is estimated to be present at 48 % and  $52 \pm 2 \%$  for *gauche* form. The abundance of *gauche* conformer is observed more than the *cis* conformer because of the double degeneracy of the *gauche* conformer.

### Discussion

From the microwave spectrum, a total of 773 transitions were assigned for cyclopropylcyanosilane and its isotopologue, of which 549 transitions were assigned for the *cis* conformer and 224 transitions were assigned for the *gauche* conformer. A, B and C rotational constants, along with  $\Delta_J$ ,  $\Delta_{JK}$ ,  $\Delta_K$ ,  $\delta_J$ , and  $\delta_K$  centrifugal distortion and quadrupole coupling constants were obtained for both conformers of cyclopropylcyanosilane (Table 33). Additionally, rotational, distortion and coupling constants predicted from MP2(full)/6-31+G(d,p) and B3LYP/6-31+G(d,p) calculations for both conformers of cyclopropylcyanosilane were also reported in Table 33. All corresponding experimental constants obtained from the microwave spectrum are close to predicted values obtained from these calculations.

Average and percent errors have been calculated between the predicted and the observed frequencies for the *cis* and the *gauche* conformer of the cyclopropylcyanosilane. The *cis* and the *gauche* conformers have average errors of 9.75 and 8.05  $\text{cm}^{-1}$ , which represent percent error of 0.64 and 0.50%, respectively. Both the average and percent errors are reasonable and show that predicted frequencies are meaningful with respect to

the vibrational assignments.

The enthalpy difference and conformational stability of cyclopropylcyanosilane may be compared with those for similar molecules in order to study the effect of different substituents on the cyclopropyl moiety. The enthalpy difference of  $123 \pm 13 \text{ cm}^{-1}$  ( $1.47 \pm 0.16 \text{ kJ mol}^{-1}$ ) for cyclopropylcyanosilane with the *cis* conformer as the more stable form is well predicted by the MP2(full) calculations from all the basis sets utilized in the current study, with average values of  $209 \text{ cm}^{-1}$  ( $2.5 \text{ kJ mol}^{-1}$ ). However, B3LYP calculations from all the basis sets utilized predicted the *gauche* conformer as the more stable form by an average value of  $15 \text{ cm}^{-1}$  ( $0.18 \text{ kJ mol}^{-1}$ ). For cyclopropyl fluoro, chloro and bromo silanes (*c*-C<sub>3</sub>H<sub>5</sub>SiH<sub>2</sub>-X; X = F, Cl, and Br) the enthalpy difference between the two conformers were determined to be  $109 \pm 19 \text{ cm}^{-1}$ ,  $98 \pm 13 \text{ cm}^{-1}$  and  $126 \pm 15 \text{ cm}^{-1}$  with the *gauche* conformer the more stable form for cyclopropylfluorosilane - whereas for both cyclopropylchlorosilane and cyclopropylbromosilane, the *cis* conformer was observed to be more stable conformer.<sup>75,76,77</sup> For cyanomethylcyclopropane, the enthalpy difference between the *cis* and the *gauche* conformer was determined to be  $54 \pm 4 \text{ cm}^{-1}$  with the *gauche* conformer being the more stable form.<sup>94</sup> In case of substitution of halogen group on the cyclopropylsilane moiety, chloro and bromo atoms have *cis* as the most stable form due to their large atomic size. For cyclopropylfluorosilane the *gauche* form is the more stable conformer because of small size of fluorine atom. However, the enthalpy difference is higher for cyclopropylfluorosilane compared to cyclopropylchlorosilane, probably due to the high electronegativity of the fluoro group. The enthalpy differences of cyclopropylbromosilane and cyclopropylcyanosilane are almost the same and, for both molecules the *cis* form is the more stable conformer. For

cyclopropylcyanosilane and cyanomethylcyclopropane, with the carbon atom of the methyl group substituted with a silicon atom, the conformational stability switched from the *gauche* to the *cis* form.

Structural parameters of cyclopropylcyanosilane can be compared with structural parameters of other, similar molecules (Table 37). As expected, as the Si-X distance increases as the size of the substituent increases. The  $r(\text{Si-CN})$  bond distance of cyclopropylcyanosilane is in between the  $r(\text{Si-F})$  bond distance of cyclopropylfluorosilane and the  $r(\text{Si-Cl})$  bond distance of cyclopropylchlorosilane and, less than the  $r(\text{Si-C})$  bond distance of cyclopropylmethylsilane. Similarly, the  $r(\text{Si-C})$  bond distance of cyclopropylcyanosilane is in between  $r(\text{Si-C})$  distance of cyclopropyl chloro and fluoro silane, and less than the  $r(\text{Si-C})$  distance of cyclopropylmethylsilane. Different substituents did not show significant effects on the structural parameters of the cyclopropane ring; hence  $r(\text{C-C})$  bond distances and  $\angle\text{CCC}$  bond angles remained within a fairly small range throughout different substitution. In the case of halogen substituted cyclopropylsilane compounds, as the atomic size increases,  $\angle\text{SiCH}$  decreases. The  $\angle\text{CSiX}$  bond angles also decrease as the atomic size increases. The  $\angle\text{CSiX}$  bond angle of the *gauche* conformer of cyclopropylcyanosilane is smaller than the  $\angle\text{CSiX}$  bond angle of *gauche* cyclopropylfluorosilane and cyclopropylmethylsilane. Similarly, the  $\angle\text{CSiX}$  bond angle of the *cis* conformer of cyclopropylcyanosilane is smaller than the  $\angle\text{CSiX}$  bond angle of the *cis* conformer of cyclopropyl chloro and bromo silane. Overall, the structural parameters obtained for both *cis* and *gauche* conformers of cyclopropylcyanosilane are generally reasonable and follow the trends for halogen substituted molecules reasonably well.

**Table 37.** Comparison of select structural parameters (Å and degrees) of molecules of the form C<sub>3</sub>H<sub>5</sub>SiH<sub>2</sub>X.

	<i>gauche-</i> cyclopropylfluorosilane 75,a	<i>cis-</i> cyclopropylchlorosilane 76,b	<i>cis-</i> cyclopropylbromosilane 77,b	<i>gauche-</i> cyclopropylmethylsilane 78,a
r(Si <sub>1</sub> X)	1.594 (3)	2.066	2.230	1.871 (3)
r(Si <sub>1</sub> C <sub>2</sub> )	1.836 (3)	1.845	1.842	1.852 (3)
r(C <sub>2</sub> C <sub>4</sub> )	1.524 (3)	1.520	1.520	1.518 (3)
r(C <sub>2</sub> C <sub>5</sub> )	1.518 (3)	1.520	1.520	1.519 (3)
r(C <sub>4</sub> C <sub>5</sub> )	1.500 (3)	-	1.500	1.500 (3)
r(Si <sub>1</sub> H <sub>12</sub> )	1.480 (3)	1.472	1.480	1.489 (3)
r(Si <sub>1</sub> H <sub>13</sub> )	1.482 (3)	1.472	1.480	1.489 (3)
∠Si <sub>1</sub> C <sub>2</sub> H <sub>3</sub>	117.7 (5)	114.7	113.9	117.1 (5)
∠C <sub>2</sub> C <sub>4</sub> C <sub>5</sub>	60.3 (5)	60.4	60.4	60.5 (5)
∠C <sub>2</sub> C <sub>5</sub> C <sub>4</sub>	60.7 (5)	60.4	60.4	60.5 (5)
∠C <sub>4</sub> C <sub>2</sub> C <sub>5</sub>	59.1 (5)	59.2	59.2	59.1 (5)
∠Si <sub>1</sub> C <sub>2</sub> C <sub>4</sub>	117.6 (5)	121.4	112.0	119.9 (5)
∠Si <sub>1</sub> C <sub>2</sub> C <sub>5</sub>	119.2 (5)	121.4	112.0	119.2 (5)
∠C <sub>2</sub> Si <sub>1</sub> H <sub>12</sub>	112.4 (5)	112.0	111.9	110.6 (5)
∠C <sub>2</sub> Si <sub>1</sub> H <sub>13</sub>	108.4 (5)	112.0	111.9	106.5 (5)
∠C <sub>2</sub> Si <sub>1</sub> X	111.2 (5)	107.8	108.3	111.5 (5)

<sup>a</sup> adjusted parameters<sup>b</sup> estimated parameters

The barriers and potential function governing the asymmetric rotor motion were predicted from the MP2(full)/6-31G(d) calculations, where the energy difference was predicted to be 166 cm<sup>-1</sup> between the *gauche* and *cis* conformers. The *gauche-gauche* barrier was predicted to be 668 cm<sup>-1</sup> and the *gauche* to *cis* barrier to be 903 cm<sup>-1</sup> (Fig. 28). It is possible to obtain values for four terms of the potential constants of the potential function governing the internal rotation of the SiH<sub>2</sub>CN moiety, which has the form:

$$V(\theta) = \frac{1}{2} \sum_{i=1}^4 V_i (1 - \cos i\theta)$$

The series coefficients,  $V_i$ , in the above equation, were determined by a non-linear least-squares fitting of the predicted energy differences and the torsional dihedral angles for the *gauche* (117.9°) and *cis* (0.0°) conformers and the two transition states (63.9° and -64.2°). The potential is nearly a three-fold rotation (barrier 903 cm<sup>-1</sup>), with the following values for the first four terms of the potential function:  $V_1 = -268.53$ ,  $V_2 = -43.90$ ,  $V_3 = -637.64$ , and  $V_4 = 7.35$  cm<sup>-1</sup>. These predicted values are expected to be reasonably near the unknown experimental ones that could be obtained from the frequencies of the asymmetric torsional modes from the two conformers. The potential function results obtained for cyclopropylcyanosilane are consistent with previously reported potential function values for cyclopropyl fluoro, chloro, bromo and methyl silane.<sup>75,76,77,78</sup>

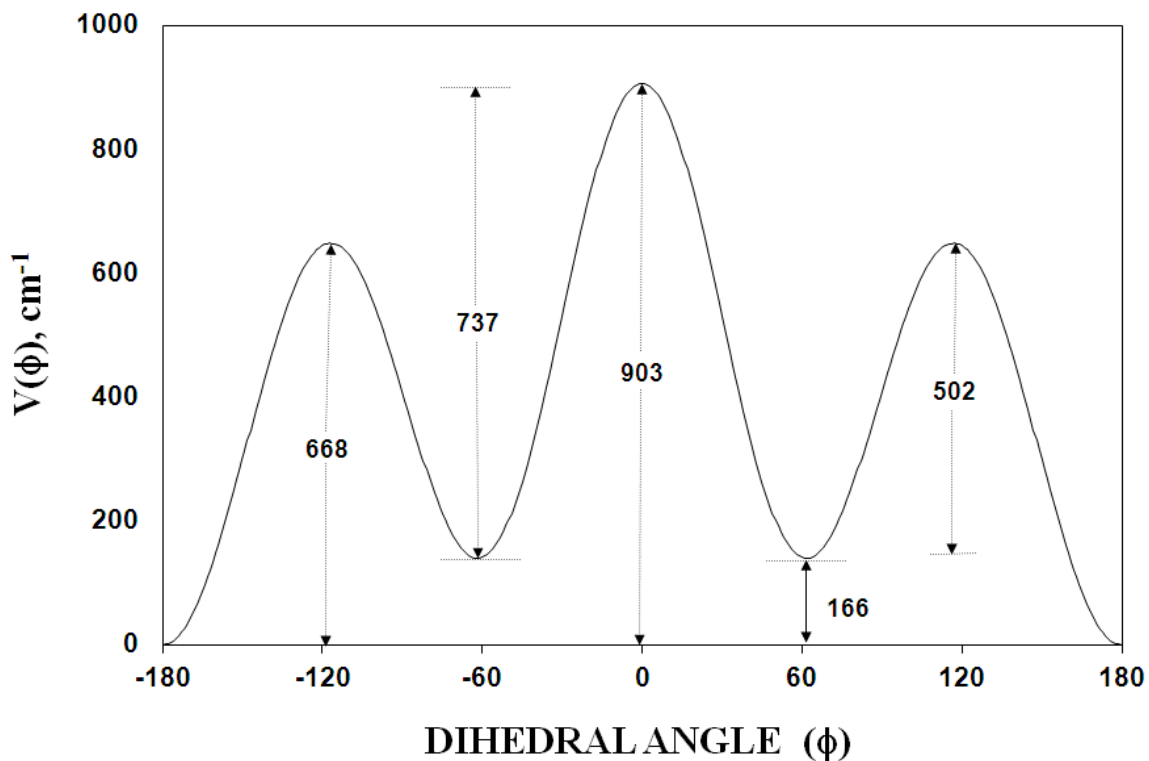


**Fig. 28** Potential energy function (MP2(full)) governing the internal rotation of the  $-\text{SiH}_2\text{CN}$  moiety from the *gauche* to the *cis* form for cyclopropylcyanosilane

A natural population analysis (NPA) was carried for the *cis* conformers of cyclopropylsilane derivatives. The NPA was calculated with the MP2(full) method using the 6-311+G(d,p) set. For cyclopropylcyanosilane, the silicon atom ( $\text{Si}_1$ ) carries a charge of 1.26, the carbon atom of the cyano group ( $\text{C}_{10}$ ) carries a charge of -0.13 and the carbon atoms of the cyclopropane ring ( $\text{C}_{2,4,5}$ ) carry charges of -0.72, -0.34 and -0.34 respectively. The F, Cl, Br atoms on the cyclopropylsilane moiety carry charges of -0.68 on fluorine, -0.42 on chlorine and -0.36 on bromine, while for cyclopropylmethylsilane, the carbon atom of the methyl group has charge of -1.03. Similarly the silicon atom of

cyclopropyl fluoro, chloro, bromo, and methyl silane has a charge of 1.67, 1.29, 1.21 and 1.32, respectively. The charge on the carbon atom on which Si is attached to cyclopropane ring varies from -0.71 to -0.76. The remaining two carbons of the cyclopropyl ring did not show significant effects on the charge by different substituent on the cyclopropylsilane moiety. From NPA, cyclopropylcyanosilane and cyclopropylchlorosilane have approximately equal charges on Si and on the carbon atom of the cyclopropane ring on which the silicon atom is attached to the cyclopropane ring.

In this study the conformational stability, enthalpy difference and structural parameters of cyclopropylcyanosilane have been determined and discussed. The effect of the cyano group on the cyclopropylsilane moiety was also studied. In the future, it would be of interest to study molecules like cyclopropylisocyanosilane, or cyclopropylcyanogermane, where the effect of the isocyano group on cyclopropylsilane moiety and the effect of the substitution of the silicon atom by a germanium atom can be studied in detail.

(This work has been published in the Chemical Physics journal<sup>95</sup>.)

## CHAPTER 7

### MICROWAVE, $r_0$ STRUCTURAL PARAMETERS, CONFORMATIONAL STABILITY AND VIBRATIONAL ASSIGNMENT STUDIES OF (CHLOROMETHYL)FLUOROSILANE

#### Introduction

Computational chemists have determined structural parameters, conformational stability, the enthalpy difference between two or more conformers and rotational barrier heights of (halomethyl)halosilanes ( $XCH_2SiH_2Y$  where  $X, Y = H, F, Cl, Br,$  and  $I$ ) by using different theoretical methods. The molecular mechanics approach was used to calculate structural parameters, energies, rotational barrier heights and torsional force constants of halogenated methyl silane ( $XCH_2SiH_2X$ ;  $X = F, Cl,$  and  $Br$ ) derivatives.<sup>96</sup> The calculated energy differences between the *trans* and *gauche* conformers were observed to be small with the *trans* conformer being the most stable form for (halomethyl)halosilanes, (halomethyl)dihalosilanes, and (dihalomethyl)dihalosilanes.<sup>96</sup> However, when excess charges on the atoms were neglected, the *gauche* conformer was calculated to be most stable form.<sup>96</sup> Density functional theory (DFT) and second order Møller-Plesset theory (MP2) were used for calculating structural parameters and energy differences between the *gauche* and *trans* conformers of (halomethyl)halosilane derivatives.<sup>97</sup> According to these calculations for all (halomethyl)halosilane derivatives, the *trans* conformer was predicted to be the most stable form. The energy differences between the two conformers and the rotational barrier height of (halomethyl)halosilane compounds increases as the size of the halogen increases.<sup>97</sup> These theoretical studies have helped to understand the conformational stability, structural parameters,

enthalpy differences and the rotational barrier heights of (halomethyl)halosilanes, but experimental data is necessary to confirm or contradict the prediction.

For (chloromethyl)chlorosilane ( $\text{ClCH}_2\text{SiH}_2\text{Cl}$ ) the *trans* to *gauche* and *gauche* to *gauche* barriers were determined to be 875 and 765  $\text{cm}^{-1}$ . The conformational stabilities of (chloromethyl)chlorosilane and (chloromethyl)bromosilane ( $\text{ClCH}_2\text{SiH}_2\text{Br}$ ) were determined by utilizing variable temperature FT-IR spectra of the sample dissolved in a krypton solution, whereas the conformational stability was only predicted for (chloromethyl)fluorosilane ( $\text{ClCH}_2\text{SiH}_2\text{F}$ ).<sup>98</sup> For (chloromethyl)chlorosilane and (chloromethyl)bromosilane, the enthalpy difference between the two most stable conformers was determined to be 175  $\text{cm}^{-1}$ . In a later study, the enthalpy difference for (chloromethyl)bromosilane was corrected to be 216  $\text{cm}^{-1}$ .<sup>99</sup> For both molecules, the *trans* conformer was observed to be the most stable form. In the case of (chloromethyl)fluorosilane, according to theoretical calculations, the enthalpy difference between the *trans* and *gauche* conformer was expected to be 300  $\text{cm}^{-1}$ ; however, based on the relative intensity of the peaks the authors suggested the enthalpy difference between the two conformers should be approximately 150  $\text{cm}^{-1}$ ,<sup>100</sup> but did not mention a specific value for the enthalpy difference. The vibrational assignment was reported only for the *trans* conformer of (chloromethyl)fluorosilane. To date, there is no information regarding the structural parameters and potential function of (chloromethyl)fluorosilane. Therefore it is desirable to determine the conformational stability, structural parameters and potential function of (chloromethyl)fluorosilane. This data will be useful for studying the effect of different halogen atoms on methyl silane derivatives.

In order to determine the structural parameters, FT-microwave spectral data of (chloromethyl)fluorosilane were obtained. For identifying the fundamental vibrational modes of (chloromethyl)fluorosilane, the Raman spectrum of the sample dissolved in liquefied krypton, and infrared spectra of the gas, amorphous and annealed solid were investigated. For determination of the enthalpy difference between *trans* and *gauche* conformers (Fig. 29), variable temperature infrared spectra of the sample dissolved in xenon solution was investigated. The variable temperature Raman spectra were also used to determine the enthalpy difference. To support the vibrational study, *ab initio* calculations with basis sets up to aug-cc-pVTZ, as well as those with diffuse functions, *i.e.* 6-311+G(2df,2pd), have been carried out. Density functional theory (DFT) calculations, using the B3LYP method with the same basis sets have also been carried out. Optimized geometries, conformational stabilities, harmonic force fields, infrared intensities, Raman activities and depolarization ratios are also calculated. The results of these spectroscopic, structural and theoretical studies of (chloromethyl)fluorosilane are reported herein and compared with those obtained for other, similar molecules.

### **Experimental Methods**

The sample of (chloromethyl)fluorosilane was prepared using the following steps (Fig. 30). First, (chloromethyl)trichlorosilane was treated with lithium aluminum hydride

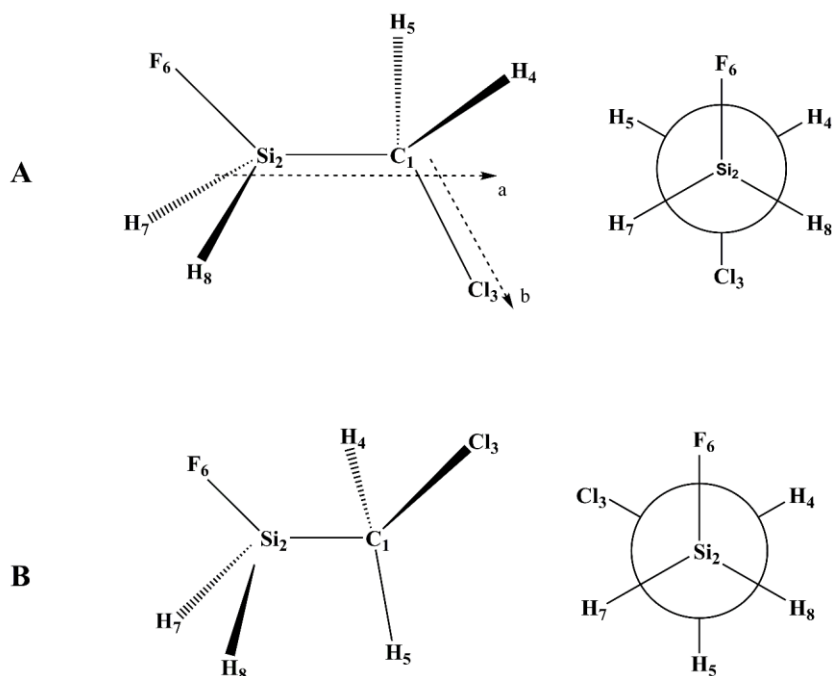


**Fig. 29** Conformers of (chloromethyl)fluorosilane (A) *trans*; (B) *gauche*.

in dry dibutyl ether for 2 h at room temperature (RT). The product, (chloromethyl)silane, was brominated with boron tribromide at 0 °C for 18 h and the product, (chloromethyl)bromosilane was separated from the unreacted material as well as the dibromo analogue using trap-to-trap distillation. The purified (chloromethyl)bromosilane was fluorinated by freshly sublimed antimony trifluoride at RT for 15 min. The final product was purified twice using a low pressure low temperature sublimation column. The fraction collected at -90 °C and 80 – 90 mTorr was used for further study.

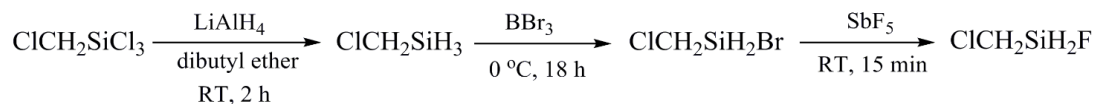


**Fig. 30** Synthesis of (chloromethyl)fluorosilane.

The rotational spectrum of (chloromethyl)fluorosilane was studied using a CP-FTMW spectrometer developed at the University of Virginia, operating in the 6.5 to 18 GHz and 18 to 26 GHz ranges. The chirped pulse methods used here have been described in detail previously, so only the brief details relevant to this experiment will be given.<sup>101,102,84</sup> The sample was prepared by balancing (chloromethyl)fluorosilane vapor with approximately 3.4 atm of neon gas (GTS Welco) for a total sample concentration of approximately 0.2%. The resulting mixture was pulsed into the chamber at a backing pressure of approximately 1 atm for all experiments.

For the 6.5-18 GHz measurement, approximately 25,000 valve injection cycles of the sample gas, using five pulsed nozzles, were completed at 3.3 Hz to generate a directly detected, time-averaged, 50 GS/s spectrum of 250,000 molecular FIDs (approximately 2 hours of signal averaging). Additionally, the time domain resolution afforded by a 20  $\mu\text{s}$  record length generates an average Doppler broadened FWHM linewidth of approximately 130 KHz (with point spacing of 24 kHz). For the 18-26 GHz measurement, approximately 29,000 valve injection cycles of the sample gas, using four pulsed nozzles, were completed at 3.3 Hz to generate a directly detected, 100 GS/s, time-averaged spectrum of 290,000 molecular FIDs. Due to the shortened Doppler decay

timescale and the more stringent Nyquist sampling limits, only a 10  $\mu$ s record length for molecular FID detection was used, which affords an average Doppler broadened linewidth of 260 kHz (with a 50 kHz point spacing).

These measurements afford a frequency-domain dynamic range of approximately 1000:1, which enabled assignment of all common heavy atom single isotopologues ( $^{13}\text{C}$ ,  $^{37}\text{Cl}$ ,  $^{29}\text{Si}$ ,  $^{30}\text{Si}$ ) in natural abundance. The rotational temperature for the species detected in this experiment is roughly 1.5 K. Comparison between the observed frequencies and those from a least-squares fit for the *trans* conformer of (chloromethyl)fluorosilane are listed in Table 38.

**Table 38.** Rotational transition frequencies (MHz) of the ground vibrational state for parent species and isotopologues of *trans*-(chloromethyl)fluorosilane.

Parent species									
Transitions	F''	F'	$\nu_{\text{obs}}$ (MHz)	$\Delta\nu^a$	Transitions	F''	F'	$\nu_{\text{obs}}$ (MHz)	$\Delta\nu^a$
$6_{06} \leftarrow 5_{15}$	5	4	6562.1615	-0.0027	$4_{04} \leftarrow 3_{03}$	6	5	14438.5340	-0.0099
	8	7	6563.3839	-0.0017	$8_{08} \leftarrow 7_{17}$	7	6	14504.9142	-0.0019
	6	5	6564.6646	-0.0036		10	9	14505.7671	-0.0111
	7	6	6565.9307	-0.0037		8	7	14507.7809	-0.0075
$1_{11} \leftarrow 2_{02}$	2	1	8694.4903	0.0064		9	8	14508.6668	-0.0035
	3	4	8700.8563	-0.0023	$1_{10} \leftarrow 1_{01}$	1	1	16029.5490	-0.0076
	1	2	8702.7288	-0.0030		3	3	16046.3993	-0.0101
	3	2	8704.1223	-0.0040		2	1	16046.9118	-0.0058
	2	2	8705.9263	-0.0020		1	2	16050.1181	-0.0128
	3	3	8712.3226	-0.0001		2	3	16056.0513	-0.0122
	2	3	8714.1229	-0.0017		3	2	16057.8288	-0.0090
$7_{07} \leftarrow 6_{16}$	8	8	10499.9914	-0.0063		2	2	16067.4825	-0.0094
	6	5	10510.8108	0.0133	$2_{11} \leftarrow 2_{02}$	2	1	16164.0135	0.0044
	9	8	10511.8345	0.0125		1	1	16165.7633	-0.0037
	7	6	10513.5621	0.0077		3	4	16170.8793	-0.0028
	8	7	10514.6167	0.0096		4	4	16172.6579	-0.0012
$3_{03} \leftarrow 2_{02}$	5	4	10831.7772	0.0101		3	2	16174.1501	0.0001

**Table 38.** - - Continued.

Transitions	F''	F'	$v_{\text{obs}}$ (MHz)	$\Delta v^a$	Transitions	F''	F'	$v_{\text{obs}}$ (MHz)	$\Delta v^a$
	2	2	16175.4514	-0.0021		6	5	16627.3106	0.0073
	1	2	16177.2138	0.0021	$5_{14} \leftarrow 5_{05}$	4	4	16935.6907	0.0105
	3	3	16182.3478	0.0015		7	7	16937.2289	-0.0053
	2	3	16183.6498	0.0000		6	5	16939.1890	-0.0035
	4	3	16184.1206	-0.0026		5	5	16940.9647	-0.0118
$3_{12} \leftarrow 3_{03}$	3	2	16353.9153	0.0088		6	6	16942.4406	0.0067
	4	5	16357.0464	0.0150		5	6	16944.2405	0.0226
	2	2	16358.4932	0.0066		4	5	16947.4025	0.0017
	5	5	16361.7171	0.0105	$6_{15} \leftarrow 6_{06}$	8	8	17328.8648	0.0006
	4	3	16363.1476	0.0129		5	5	17327.6710	0.0057
	3	3	16365.3835	0.0121		6	6	17332.6459	-0.0123
	4	4	16368.5498	0.0011		7	7	17333.8274	-0.0128
	2	3	16369.9544	0.0028	$7_{16} \leftarrow 7_{07}$	6	6	17792.8250	-0.0165
	3	4	16370.7923	0.0069		9	9	17793.7950	-0.0153
	5	4	16373.2415	0.0177		8	8	17798.6565	-0.0080
$4_{13} \leftarrow 4_{04}$	4	3	16607.9081	-0.0012	$1_{11} \leftarrow 0_{00}$	3	2	19537.539	-0.0154
	5	6	16609.9513	0.0057		2	2	19539.3459	-0.0104
	3	3	16613.8194	0.0114	$6_{06} \leftarrow 5_{05}$	6	5	21642.1792	0.0130
	6	6	16615.7114	0.0152	$2_{12} \leftarrow 1_{01}$	2	1	23013.8356	0.0039
	5	4	16617.4581	0.0081		3	3	23016.0721	-0.0039
	4	4	16619.4135	0.0028		1	1	23023.4761	-0.0058
	5	5	16621.5635	0.0108		4	3	23025.7046	-0.0067
	4	5	16623.5189	0.0055		3	2	23027.4979	-0.0064
	3	4	16625.3171	0.0078		2	2	23034.3996	-0.0063

<sup>a</sup>  $\Delta v = v_{\text{obs}} - v_{\text{calc}}$  in MHz

<sup>13</sup>C

Transitions	F''	F'	$v_{\text{obs}}$ (MHz)	$\Delta v^b$	Transitions	F''	F'	$v_{\text{obs}}$ (MHz)	$\Delta v^b$
$1_{11} \leftarrow 2_{02}$	3	4	8289.1037	1.0		3	4	15755.1326	11.8
	1	2	8290.9724	3.9		4	4	15756.8578	-7.3
	2	2	8294.1258	7.2		3	2	15758.3615	-15.4
	3	3	8300.5252	-13.2		2	2	15759.6393	-10.3
	2	3	8302.2992	0.9		1	2	15761.3941	3.4
$1_{10} \leftarrow 1_{01}$	1	1	15609.6470	11.6		3	3	15766.5513	-5.3
	3	3	15626.4729	-1.0		2	3	15767.8312	1.8
	2	1	15627.0018	-0.1		4	3	15768.3094	8.3
	1	2	15630.1593	-1.3	$3_{12} \leftarrow 3_{03}$	4	5	15947.6147	-13.2
	2	3	15636.1374	9.6		3	3	15955.9369	4.6
	3	2	15637.8715	-2.0		4	4	15959.1113	-5.8
	2	2	15647.5373	9.9	$4_{13} \leftarrow 4_{04}$	5	6	16209.2787	13.5
$2_{11} \leftarrow 2_{02}$	1	1	15749.9575	-12.7					

<sup>b</sup>  $\Delta v = v_{\text{obs}} - v_{\text{calc}}$  in kHz

<sup>37</sup>Cl

Transitions	F''	F'	$v_{\text{obs}}$ (MHz)	$\Delta v^b$	Transitions	F''	F'	$v_{\text{obs}}$ (MHz)	$\Delta v^b$
$1_{11} \leftarrow 2_{02}$	1	1	8917.1471	0.3		1	2	8926.1964	1.4
	2	1	8919.7204	7.5		3	2	8927.3059	-9.6
	3	4	8924.7312	-1.1		2	2	8928.7638	2.6

**Table 38.** - - Continued.

Transitions	F''	F'	$v_{\text{obs}}$ (MHz)	$\Delta v^b$	Transition	F''	F'	$v_{\text{obs}}$ (MHz)	$\Delta v^b$
	3	3	8933.7957	2.9		4	4	16384.2560	0.0
	2	3	8935.2333	-4.9		2	3	16385.4000	-2.6
$7_{07} \leftarrow 6_{16}$	6	5	9772.8398	1.3		3	4	16386.0167	1.0
	9	8	9773.6483	-0.8		5	4	16387.9712	6.4
	7	6	9775.0114	-2.7	$4_{13} \leftarrow 4_{04}$	4	3	16613.8094	18.8
	8	7	9775.8453	2.2		5	6	16615.4118	-6.9
$1_{10} \leftarrow 1_{01}$	1	1	16066.3584	-5.5		3	3	16618.4854	2.3
	3	3	16079.6689	-2.3		6	6	16619.9809	0.5
	2	1	16080.0461	-4.1		4	4	16622.8828	-11.6
	1	2	16082.6244	-4.0		5	5	16624.5776	1.6
	2	3	16087.2791	-1.1		4	5	16626.1126	-11.5
	3	2	16088.7041	-1.6		3	4	16627.5788	-8.1
	2	2	16096.3128	-1.8		6	5	16629.1471	9.5
$2_{11} \leftarrow 2_{02}$	2	1	16192.5467	2.4	$5_{14} \leftarrow 5_{05}$	4	4	16923.8073	13.9
	1	1	16193.9588	-2.6		7	7	16925.0295	5.3
	3	4	16197.9681	-1.3		5	5	16927.9733	10.9
	4	4	16199.3961	0.0	$6_{15} \leftarrow 6_{06}$	5	5	17295.3450	-12.6
	3	2	16200.5472	-5.4		8	8	17296.2922	-2.8
	2	2	16201.5902	-2.3		6	6	17299.2650	-6.9
	1	2	16203.0151	5.4		7	7	17300.1948	-2.4
	3	3	16207.0267	-3.0	$1_{11} \leftarrow 0_{00}$	1	2	19482.7148	0.9
	2	3	16208.0695	-0.1		3	2	19483.8363	1.8
	4	3	16208.4558	-0.6		2	2	19485.2803	0.2
$3_{12} \leftarrow 3_{03}$	3	2	16372.6818	6.1	$2_{12} \leftarrow 1_{01}$	2	1	22876.2473	-10.9
	4	5	16375.1566	-1.0		3	3	22878.0379	-11.6
	2	2	16376.3462	8.1		1	1	22883.8797	14.5
	5	5	16378.8690	2.7		4	3	22885.6434	-3.2
	4	3	16379.9831	2.3		3	2	22887.0872	3.1
	3	3	16381.7459	5.5		2	2	22892.5284	5.7

<sup>b</sup>  $\Delta v = v_{\text{obs}} - v_{\text{calc}}$  in kHz

<sup>29</sup> Si									
Transitions	F''	F'	$v_{\text{obs}}$ (MHz)	$\Delta v^b$	Transitions	F''	F'	$v_{\text{obs}}$ (MHz)	$\Delta v^b$
$1_{11} \leftarrow 2_{02}$	1	1	8597.1333	5.6		1	1	16046.9089	-5.2
	2	1	8600.2286	-22.9		3	4	16052.0751	5.1
	3	4	8606.6469	11.1		4	4	16053.8083	0.1
	1	2	8608.5292	-5.5		3	2	16055.3318	3.4
	2	2	8611.6682	9.6		2	2	16056.6075	1.0
	3	3	8618.0668	3.3		1	2	16058.3173	-3.8
	2	3	8619.8266	-1.2		3	3	16063.4987	1.0
$1_{10} \leftarrow 1_{01}$	1	1	15910.3035	1.7		2	3	16064.7766	0.8
	3	3	15927.1236	-0.6		4	3	16065.2335	-2.3
	2	1	15927.6671	1.3	$3_{12} \leftarrow 3_{03}$	3	2	16235.7750	-12.3
	1	2	15930.8019	-6.1		4	5	16238.9141	7.1
	2	3	15936.7762	-4.8		2	2	16240.3145	6.3
	3	2	15938.5167	1.4		5	5	16243.5395	1.6
	2	2	15948.1674	-4.6		4	3	16244.9950	5.6
$2_{11} \leftarrow 2_{02}$	2	1	16045.2076	8.1		3	3	16247.2062	-5.9

**Table 38.** - - Continued.

Transitions	F''	F'	v <sub>obs</sub> (MHz)	Δv <sup>b</sup>	Transitions	F''	F'	v <sub>obs</sub> (MHz)	Δv <sup>b</sup>
	4	4	16250.3883	-1.1		5	5	16504.3382	-5.2
	2	3	16251.7386	5.5	5 <sub>14</sub> ← 5 <sub>05</sub>	5	4	16819.6889	14.4
	3	4	16252.6147	2.3		5	7	16821.2316	-7.7
	5	4	16255.0314	11.0		5	5	16825.0059	12.2
4 <sub>13</sub> ← 4 <sub>04</sub>	3	3	16496.5832	3.2		5	6	16826.4439	-11.9
	6	6	16498.4563	-3.7	1 <sub>11</sub> ← 0 <sub>00</sub>	2	2	19406.9927	0.0
	4	4	16502.1661	-18.1					

<sup>b</sup> Δv = v<sub>obs</sub> - v<sub>calc</sub> in kHz

<sup>30</sup> Si									
Transitions	F''	F'	v <sub>obs</sub> (MHz)	Δv <sup>b</sup>	Transitions	F''	F'	v <sub>obs</sub> (MHz)	Δv <sup>b</sup>
1 <sub>11</sub> ← 2 <sub>02</sub>	1	1	8507.5118	2.2		3	3	15949.8261	0.1
	3	4	8516.9517	1.7		2	3	15951.0774	4.8
	1	2	8518.8615	-11.0		4	3	15951.5133	-5.9
	2	2	8521.9118	-3.6	3 <sub>12</sub> ← 3 <sub>03</sub>	3	2	16122.7712	-18.6
	3	3	8528.3465	12.6		4	5	16125.9242	13.0
	2	3	8530.0511	-1.9		2	2	16127.2528	2.1
1 <sub>10</sub> ← 1 <sub>01</sub>	1	1	15796.2714	1.9		5	5	16130.4937	5.9
	3	3	15813.0602	3.8		4	3	16131.9623	-8.7
	2	1	15813.6340	-0.4		3	3	16134.1829	11.7
	1	2	15816.6959	0.2		4	4	16137.3508	0.0
	2	3	15822.7106	-3.2		2	3	16138.6396	7.6
	3	2	15824.4090	5.9		3	4	16139.5368	-14.0
	2	2	15834.0493	-11.2	5 <sub>14</sub> ← 5 <sub>05</sub>	4	4	16708.5995	-21.7
2 <sub>11</sub> ← 2 <sub>02</sub>	2	1	15931.5717	-0.2		7	7	16710.1858	-3.9
	1	1	15933.2376	-3.0		5	5	16713.9489	-10.4
	4	4	15940.1471	11.7		6	6	16715.4279	-1.2
	3	2	15941.6900	1.7	6 <sub>15</sub> ← 6 <sub>06</sub>	6	6	17108.6745	8.5
	2	2	15942.9423	7.4		7	7	17109.8755	15.8

<sup>b</sup> Δv = v<sub>obs</sub> - v<sub>calc</sub> in kHz

All final fits for all assigned species were performed using the AABS package<sup>85</sup> as a front end to SPFIT,<sup>83</sup> including all assigned values for the quartic centrifugal distortion and nuclear quadrupole hyperfine constants. For <sup>13</sup>C, <sup>29</sup>Si and <sup>30</sup>Si isotopologues, distortion and hyperfine parameters are fixed to their parent species' values, whereas for the <sup>37</sup>Cl isotopologues, distortion and hyperfine parameters were allowed to change. The experimental analysis of (chloromethyl)fluorosilane spectrum

was supplemented with *ab initio* electronic structure calculations to predict rotational, centrifugal distortion and quadrupole coupling constants. All calculations were performed using the Gaussian 09 suite of programs<sup>82</sup> at the MP2/6-311++G(d,p) level of theory.

The mid-infrared spectrum (3,100 to 400  $\text{cm}^{-1}$ ) of (chloromethyl)fluorosilane in the gas (Fig. 31) and solid (Fig. 32) were obtained using a Perkin-Elmer model 2,000 Fourier transform spectrometer. The mid-infrared spectra (3,100 to 400  $\text{cm}^{-1}$ ) of the sample dissolved in liquefied xenon (Fig. 31) at ten different temperatures (-60 to -100 °C) were recorded on a Bruker model IFS-66 Fourier transform spectrometer. The Raman spectra (3050 to 400  $\text{cm}^{-1}$ ) of (chloromethyl)fluorosilane dissolved in liquefied krypton (Fig. 33) were recorded at three different temperatures (-133 to -153 °C) on a Trivista 557 spectrometer consisting of a double ( $f = 50$ ) cm monochromator equipped with a 2000 lines  $\text{mm}^{-1}$  grating, a  $f = 70$  cm spectrograph equipped with a 2400 lines  $\text{mm}^{-1}$  grating, and a back-illuminated LN2-cooled PI Acton Spec-10:2 kB/LN 2048 x 512 pixel CCD detector. For all experiments, the 514.5 nm line of a 2017-Ar S/N 1665 Spectra-Physics argon ion laser was used for Raman excitation, with the power set to 0.8 Watt. Signals related to the plasma lines were removed by using an interference filter. The frequencies were calibrated using neon emission lines, and depending on the setup used, are expected to be accurate within 0.4  $\text{cm}^{-1}$ . The experimental set-up used to investigate the solutions has been described before.<sup>103,104</sup> A home-built liquid cell equipped with four quartz windows at right angles was used to record the spectra. All of the observed bands in the Raman spectra of the sample dissolved in liquefied krypton (Fig. 34) along with their proposed assignments and depolarization values are listed in Tables 39 and 40 for the two conformers. The predicted conformational energy differences calculated from *ab initio*

calculations by using the Møller-Plesset perturbation method to the second order (MP2) with full electron correlation as well as with density functional theory by the B3LYP method with different basis sets as listed in Table 41. The experimental methods of recording infrared and Raman spectra are provided in detail in Chapter 2.

In order to obtain a description of the molecular motions involved in the fundamental modes of (chloromethyl)fluorosilane, a normal coordinate analysis has been carried out. The force field in Cartesian coordinates was obtained with the Gaussian 03 program at the MP2(full) level with the 6-31G(d) basis set. The internal coordinates used to calculate the **B** and **G** matrices are given in Table 42 with the atomic numbering shown in Fig. 35. By using the **B** matrix,<sup>26</sup> the force field in Cartesian coordinates was converted to a force field in internal coordinates. Subsequently, scaling factors of 0.88 for CH and SiH stretches and CH deformations, and 0.9 for other coordinates were applied, except for the heavy atom bends and torsions, along with the geometric average of the scaling factors for the interaction force constants, to obtain the fixed scaled force field and resultant wavenumbers. A set of symmetry coordinates was used (Table 42) to determine the corresponding potential energy distributions (P.E.D.s). A comparison between the observed and calculated wavenumbers, along with the calculated infrared intensities, Raman activities, depolarization ratios and potential energy distributions for the *trans* and the *gauche* conformers are listed in Tables 39 and 40, respectively.

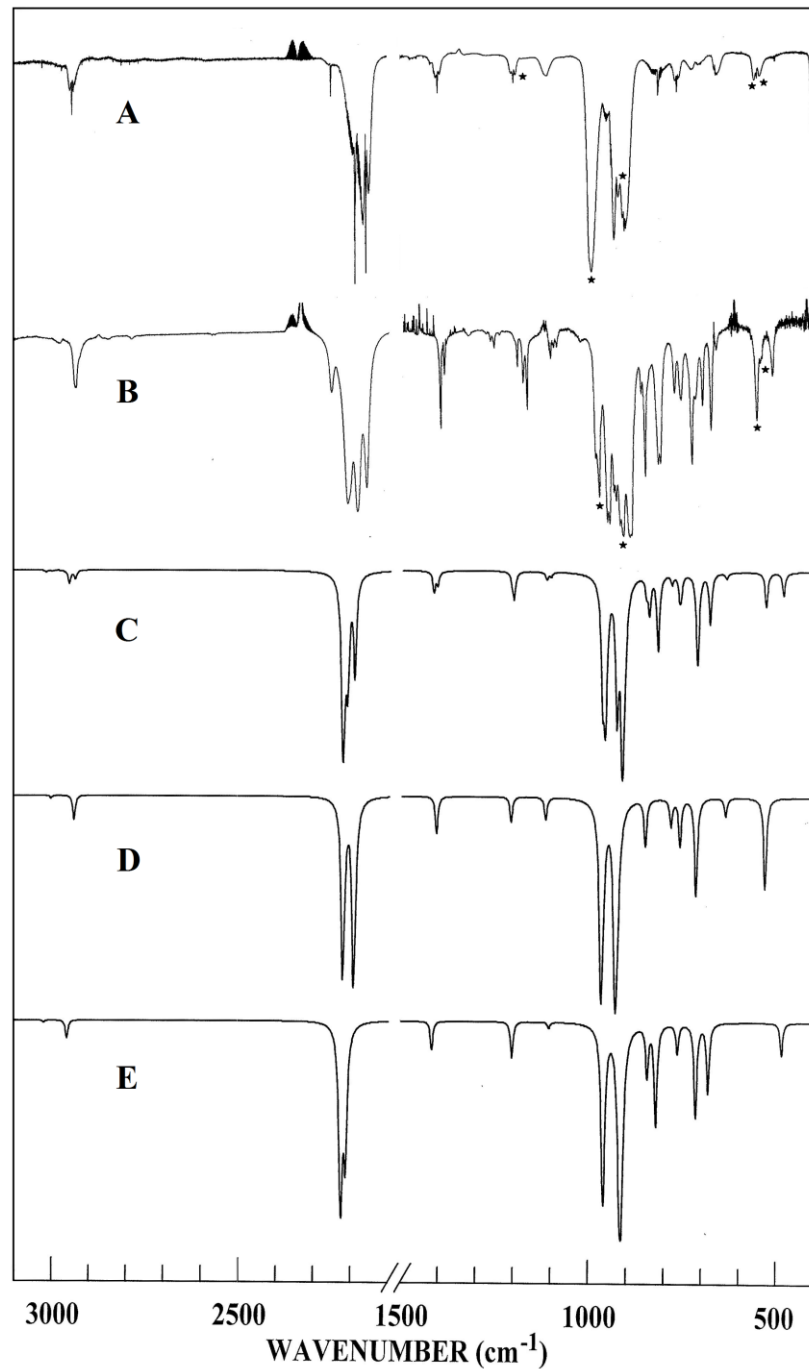


**Fig. 31** Comparison of the experimental and calculated infrared spectra of (chloromethyl)fluorosilane: (A) observed spectrum of the gas; (B) observed spectrum of the Xe solution at  $-70\text{ }^{\circ}\text{C}$ ; (C) simulated spectrum of a mixture of *trans* and *gauche* conformers ( $\Delta H = 109\text{ cm}^{-1}$ ) at  $25\text{ }^{\circ}\text{C}$ ; (D) simulated spectrum of the *gauche* conformer; (E) simulated spectrum of the *trans* conformer. (Peaks assigned for impurities were marked with star ‘★’ symbol).

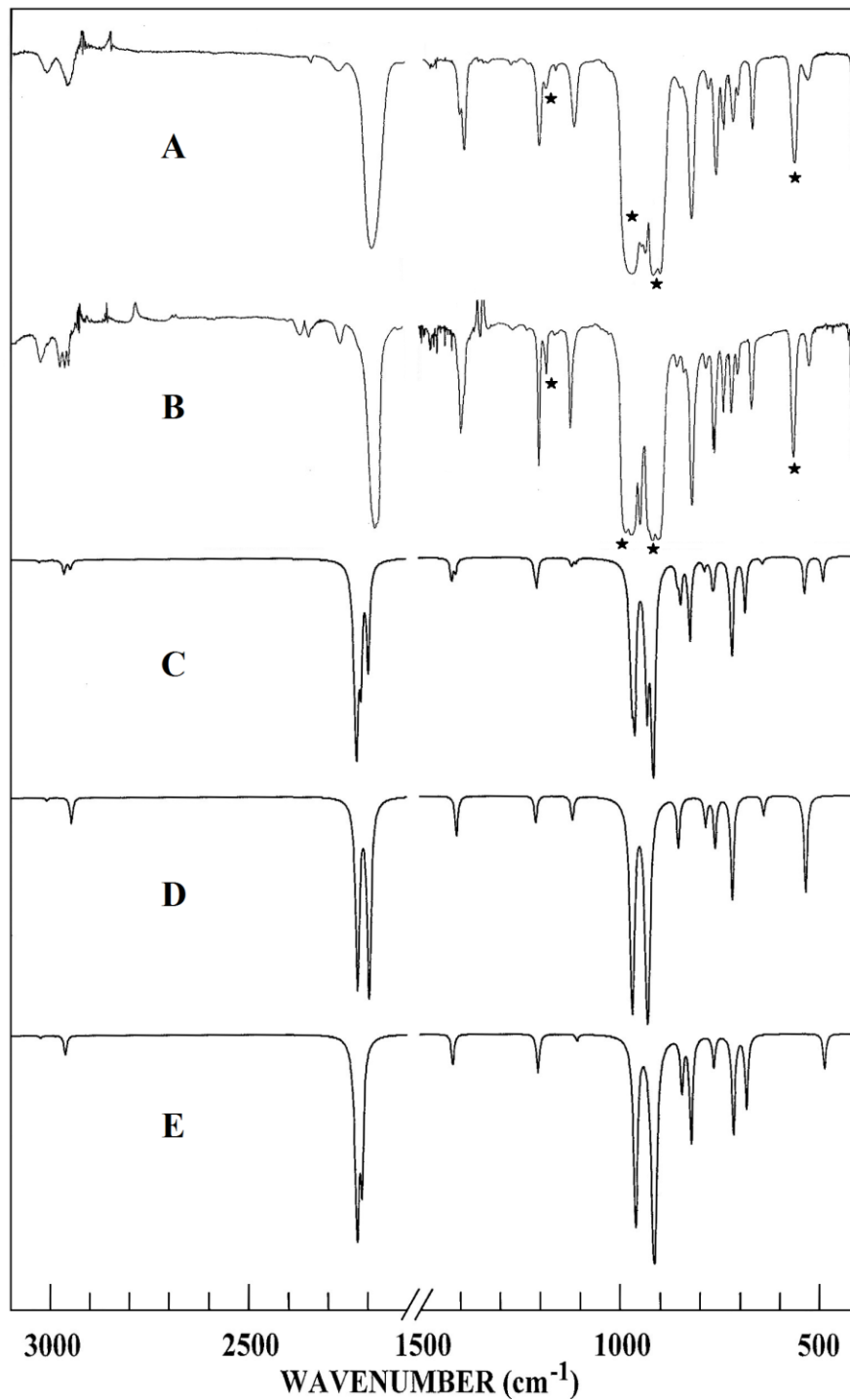


**Fig. 32** Comparison of experimental and calculated infrared spectra of (chloromethyl)fluorosilane: (A) observed spectrum of the amorphous solid; (B) observed spectrum of the annealed solid; (C) simulated spectrum of a mixture of *trans* and *gauche* conformers ( $\Delta H = 109 \text{ cm}^{-1}$ ) at  $25 \text{ }^\circ\text{C}$ ; (D) simulated spectrum of the *gauche* conformer; (E) simulated spectrum of the *trans* conformer. (Peaks assigned for impurities were marked with star '★' symbol).

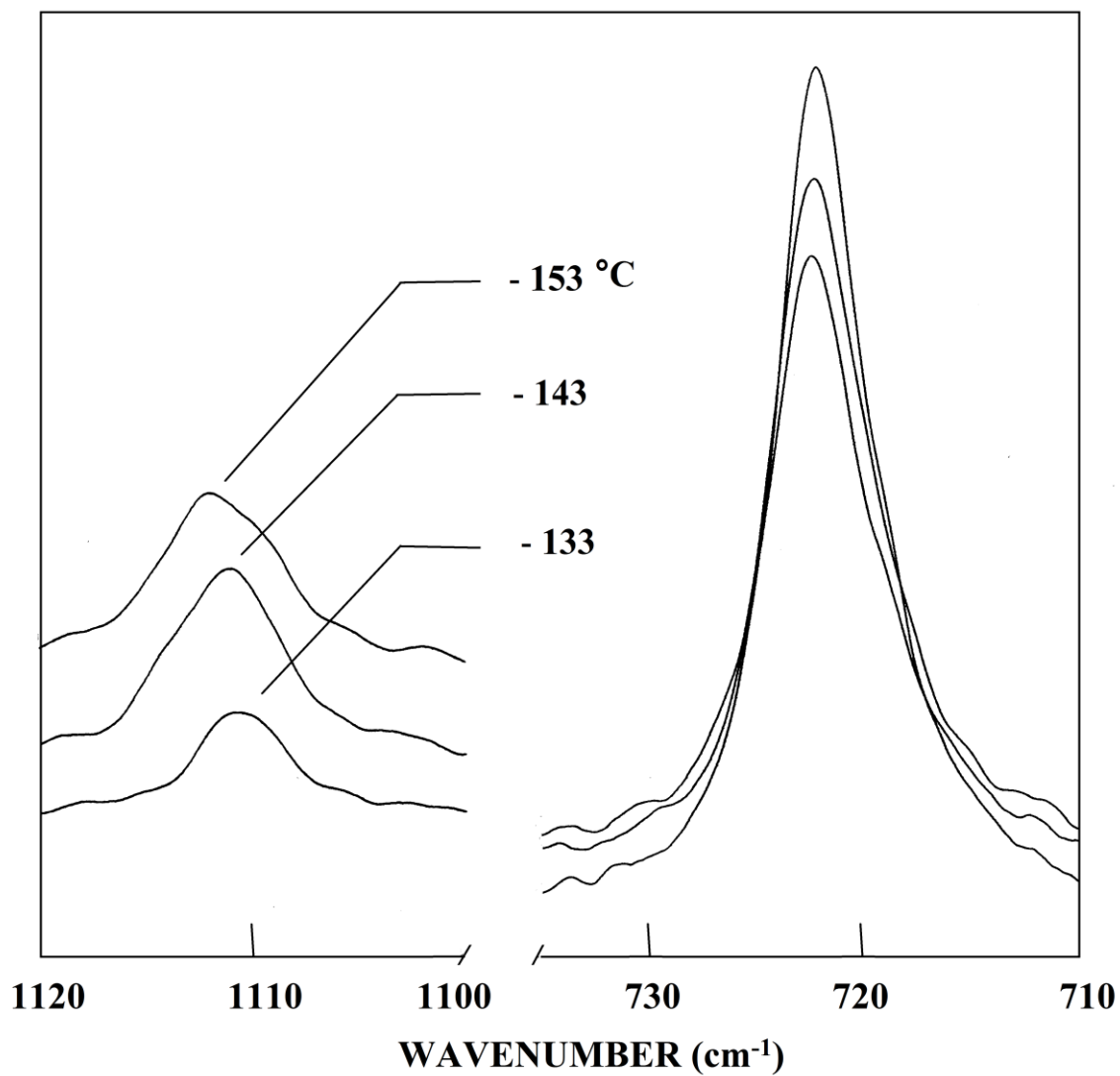


**Fig. 33** Temperature (-133 to -153 °C) dependent Raman spectrum of (chloromethyl)fluorosilane dissolved in liquid krypton solution.

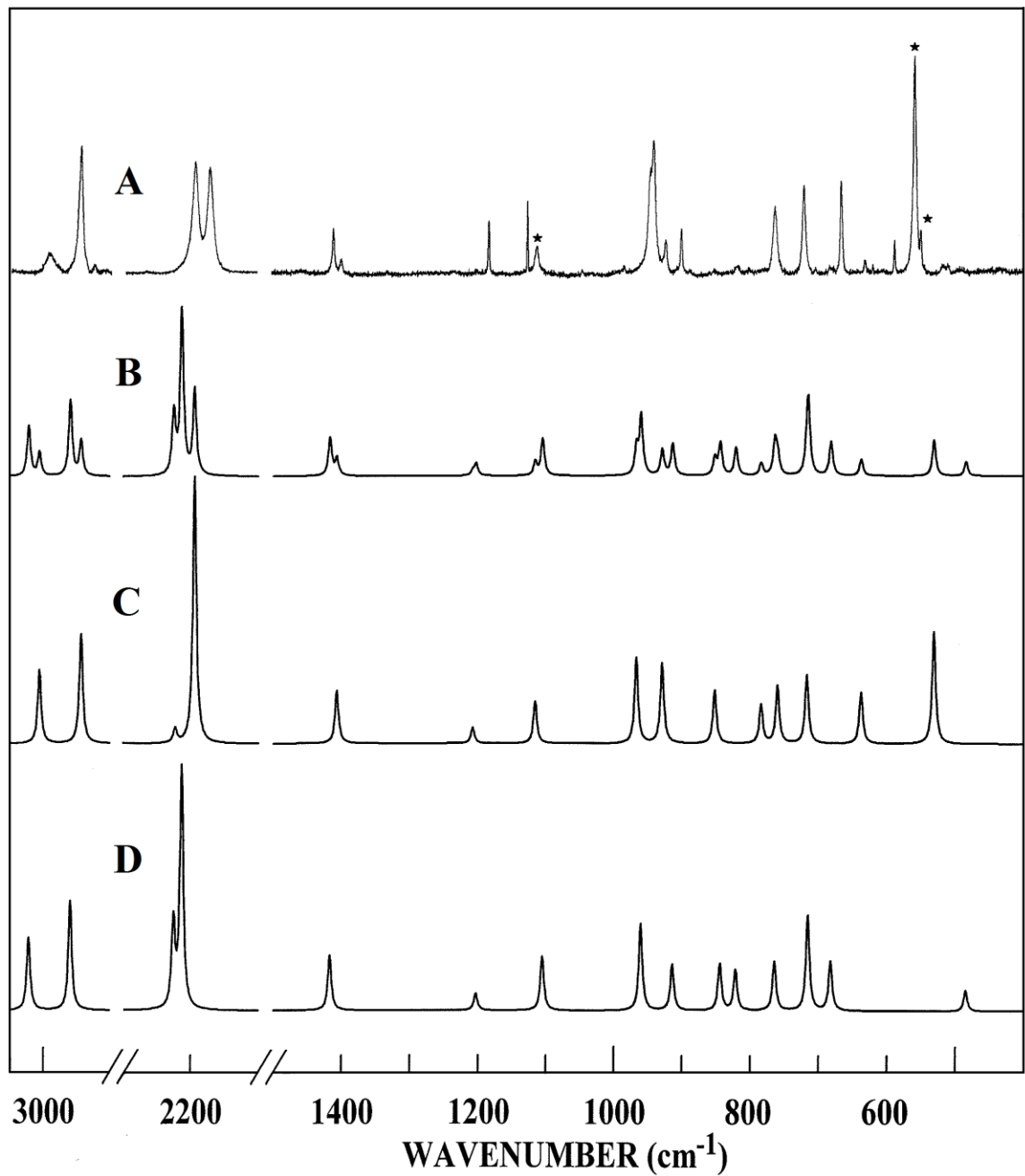


**Fig. 34** Comparison of experimental and calculated Raman spectra of (chloromethyl)fluorosilane: (A) observed spectrum of sample dissolved in the liquid krypton at 153 °C; (B) simulated spectrum of a mixture of *trans* and *gauche* conformers ( $\Delta H = 97 \text{ cm}^{-1}$ ) at 25 °C; (C) simulated spectrum of the *gauche* conformer; (D) simulated spectrum of the *trans* conformer. (Peaks assigned for impurities were marked with star '★' symbol.)

**Table 39.** Calculated<sup>a</sup> and observed frequencies (cm<sup>-1</sup>) for the *trans* form of (chloromethyl)fluorosilane.

Sym. block	Vib. No.	Approx. description	<i>ab initio</i>	fixed scaled <sup>b</sup>	IR int.	Raman act.	dp	IR				Raman Krypton	P.E.D. <sup>c</sup>	Band Contour	
								gas	xenon	Solid Amorphous	Solid Annealed			A	B
A'	v <sub>1</sub>	CH <sub>2</sub> symmetric stretch	3154	2959	7.0	94.1	0.10	2953	2941	2953	2956	2947	100S <sub>1</sub>	72	28
	v <sub>2</sub>	SiH <sub>2</sub> symmetric stretch	2359	2212	84.4	128.7	0.08	2164	2161	2180	2181	2167	100S <sub>2</sub>	1	99
	v <sub>3</sub>	CH <sub>2</sub> deformation	1511	1417	11.5	15.8	0.71	1405	1403	1400	1405	1408	99S <sub>3</sub>	54	46
	v <sub>4</sub>	CH <sub>2</sub> wag	1282	1203	14.8	3.9	0.40	1200	1197	1199	1199	1192	73S <sub>4</sub> , 25S <sub>8</sub>	53	47
	v <sub>5</sub>	SiH <sub>2</sub> deformation	1014	960	141.4	15.1	0.60	962	959	967	963	945	97S <sub>5</sub>	26	74
	v <sub>6</sub>	SiH <sub>2</sub> wag	965	914	310.5	7.5	0.64	899	899	900	898	899	62S <sub>6</sub> , 18S <sub>7</sub> , 10S <sub>10</sub>	92	8
	v <sub>7</sub>	Si-F stretch	891	844	22.1	6.9	0.58	847	-	844	850	848	74S <sub>7</sub> , 18S <sub>6</sub>	10	90
	v <sub>8</sub>	C-Cl stretch	806	764	12.2	6.4	0.71	768	762	760	761	763	60S <sub>8</sub> , 38S <sub>11</sub>	58	42
	v <sub>9</sub>	C-Si stretch	713	682	31.6	5.6	0.12	664	662	662	664	666	44S <sub>9</sub> , 34S <sub>8</sub> , 10S <sub>10</sub>	72	27
	v <sub>10</sub>	CSiF in-plane-bend	263	258	3.5	3.3	0.37	-	-	-	-	-	47S <sub>10</sub> , 22S <sub>9</sub> , 12S <sub>11</sub>	0	100
	v <sub>11</sub>	SiCCl in-plane-bend	148	146	10.1	0.3	0.26	-	-	-	-	-	44S <sub>11</sub> , 24S <sub>10</sub> , 19S <sub>4</sub> , 11S <sub>6</sub>	29	71
A''	v <sub>12</sub>	CH <sub>2</sub> antisymmetric stretch	3222	3022	0.8	65.0	0.75	2964	2983	3001	3017	2991	100S <sub>12</sub>	-	-
	v <sub>13</sub>	SiH <sub>2</sub> antisymmetric stretch	2372	2225	172.4	45.8	0.75	2190	2186	2180	2182	2189	100S <sub>13</sub>	-	-
	v <sub>14</sub>	CH <sub>2</sub> twist	1178	1105	2.2	11.2	0.75	-	-	-	-	-	77S <sub>14</sub> , 21S <sub>16</sub>	-	-
	v <sub>15</sub>	CH <sub>2</sub> rock	872	821	51.4	5.8	0.75	817	815	816	813	819	43S <sub>15</sub> , 39S <sub>17</sub> , 19S <sub>14</sub>	-	-
	v <sub>16</sub>	SiH <sub>2</sub> twist	763	715	46.2	11.4	0.75	713	719	711	714	721	98S <sub>16</sub>	-	-
	v <sub>17</sub>	SiH <sub>2</sub> rock	513	485	13.4	1.5	0.75	-	-	-	-	-	59S <sub>17</sub> , 34S <sub>16</sub>	-	-
	v <sub>18</sub>	torsion	86	86	6.3	1.2	0.75	-	-	-	-	-	99S <sub>18</sub>	-	-

<sup>a</sup> MP2(full)/6-31G(d) *ab initio* calculations, scaled frequencies, infrared intensities (km/mol), Raman activities ( $\text{\AA}^4/\text{u}$ ), depolarization ratios (dp) and potential energy distributions (P.E.D.s).

<sup>b</sup> Scaled frequencies with scaling factors of 0.88 for CH and SiH stretches and CH deformation, 0.90 for all other modes except torsion and heavy atom bends.

<sup>c</sup> Symmetry coordinates with P.E.D. contributions less than 10% are omitted.

**Table 40.** Calculated<sup>a</sup> and observed frequencies (cm<sup>-1</sup>) for the *gauche* form of (chloromethyl)fluorosilane.

Vib. No.	Approx. description	<i>ab initio</i>	fixed scaled <sup>b</sup>	IR int.	Raman act.	dp	IR				Raman Krypton	P.E.D. <sup>c</sup>	Band Contour		
							gas	Xen on	Solid Amorphous	Solid Annealed			A	B	C
v <sub>12</sub>	CH <sub>2</sub> antisymmetric stretch	3204	3006	1.1	64.3	0.72	2964	2983	3001	2997	2991	98S <sub>12</sub>	15	31	54
v <sub>1</sub>	CH <sub>2</sub> symmetric stretch	3137	2943	9.7	92.4	0.10	2949	2941	2953	2956	2947	99S <sub>1</sub>	44	50	6
v <sub>13</sub>	SiH <sub>2</sub> antisymmetric stretch	2370	2223	139.0	7.6	0.33	2195	2186	2180	2181	2190	69S <sub>13</sub> , 31S <sub>2</sub>	1	1	98
v <sub>2</sub>	SiH <sub>2</sub> symmetric stretch	2339	2194	157.5	140.5	0.15	2166	2161	2180	2181	2167	69S <sub>2</sub> , 31S <sub>13</sub>	53	46	1
v <sub>3</sub>	CH <sub>2</sub> deformation	1500	1407	15.3	15.0	0.71	1399	1392	1390	1397	1398	99S <sub>3</sub>	77	7	17
v <sub>4</sub>	CH <sub>2</sub> wag	1287	1208	9.8	3.6	0.33	1200	1197	1199	1199	1192	73S <sub>4</sub> , 25S <sub>9</sub>	29	46	25
v <sub>14</sub>	CH <sub>2</sub> twist	1189	1116	8.6	8.8	0.73	1114	1107	1112	1119	1124	74S <sub>14</sub> , 22S <sub>16</sub>	26	54	20
v <sub>5</sub>	SiH <sub>2</sub> deformation	1023	967	206.8	15.0	0.67	962	959	967	963	945	66S <sub>5</sub> , 13S <sub>7</sub>	8	77	15
v <sub>6</sub>	SiH <sub>2</sub> wag	979	929	269.9	13.3	0.73	931	929	927	923	922	48S <sub>6</sub> , 33S <sub>5</sub>	87	4	9
v <sub>7</sub>	Si-F stretch	900	852	19.7	7.9	0.63	847	855	844	850	848	70S <sub>7</sub> , 19S <sub>6</sub>	32	48	20
v <sub>8</sub>	C-Cl stretch	826	784	10.9	5.2	0.75	774	776	774	777	773	58S <sub>8</sub> , 29S <sub>11</sub>	5	-	95
v <sub>17</sub>	SiH <sub>2</sub> rock	803	760	20.2	7.4	0.68	761	759	753	756	763	39S <sub>17</sub> , 20S <sub>16</sub> , 11S <sub>15</sub>	51	-	49
v <sub>15</sub>	SiH <sub>2</sub> twist	763	717	48.3	8.2	0.72	727	728	735	734	722	85S <sub>15</sub>	2	14	84
v <sub>16</sub>	CH <sub>2</sub> rock	672	638	7.3	5.3	0.35	-	-	-	-	-	31S <sub>16</sub> , 27S <sub>11</sub> , 10S <sub>10</sub> , 10S <sub>17</sub>	86	1	13
v <sub>9</sub>	C-Si stretch	561	532	43.8	9.1	0.43	527	-	523	519	519	37S <sub>9</sub> , 21S <sub>10</sub> , 13S <sub>18</sub> , 14S <sub>4</sub>	48	31	21
v <sub>10</sub>	CSiF-in-plane-bend	276	272	11.9	1.4	0.47	-	-	-	-	-	43S <sub>10</sub> , 22S <sub>9</sub> , 14S <sub>6</sub>	71	-	28
v <sub>11</sub>	SiCCl in-plane-bend	167	167	0.1	0.6	0.24	-	-	-	-	-	25S <sub>11</sub> , 45S <sub>17</sub> , 24S <sub>8</sub>	6	1	93
v <sub>18</sub>	torsion	76	76	2.0	0.3	0.73	-	-	-	-	-	88S <sub>18</sub>	4	95	1

<sup>a</sup> MP2(full)/6-31G(d) *ab initio* calculations, scaled frequencies, infrared intensities (km/mol), Raman activities (Å<sup>4</sup>/u), depolarization ratios (dp) and potential energy distributions (P.E.D.s).

<sup>b</sup> Scaled frequencies with scaling factors of 0.88 for CH and SiH stretches and CH deformation, 0.90 for all other modes except torsion and heavy atom bends. .

<sup>c</sup> Symmetry coordinates with P.E.D. contributions less than 10% are omitted.

**Table 41.** Calculated electronic energies (Hartrees, H) and energy differences ( $\text{cm}^{-1}$ ) for (chloromethyl)fluorosilane.

Basis set	MP2(full)		B3LYP	
	<i>trans</i> <sup>a</sup>	<i>gauche</i> <sup>b</sup>	<i>trans</i> <sup>a</sup>	<i>gauche</i> <sup>b</sup>
6-31G(d)	0.6326327	318	2.1008633	300
6-31+G(d)	0.6514445	320	2.1147702	342
6-31G(d,p)	0.6659758	307	2.1060481	299
6-31+G(d,p)	0.6843526	311	2.1197753	337
6-311G(d,p)	0.9825008	310	2.2005730	301
6-311+G(d,p)	0.9922688	322	2.2061834	361
6-311G(2d,2p)	1.0826543	345	2.2157242	295
6-311+G(2d,2p)	1.0892120	399	2.2195446	359
6-311G(2df,2pd)	1.1731938	359	2.2227718	278
6-311+G(2df,2pd)	1.1796752	385	2.226983	329
MP2(full)/aug-cc-pVTZ	1.1151651	442	2.2387781	332

<sup>a</sup> Energy of *trans* conformer is given as  $-(E + 888)$  H.

<sup>b</sup> Energy of *gauche* conformer is relative to *trans* form.

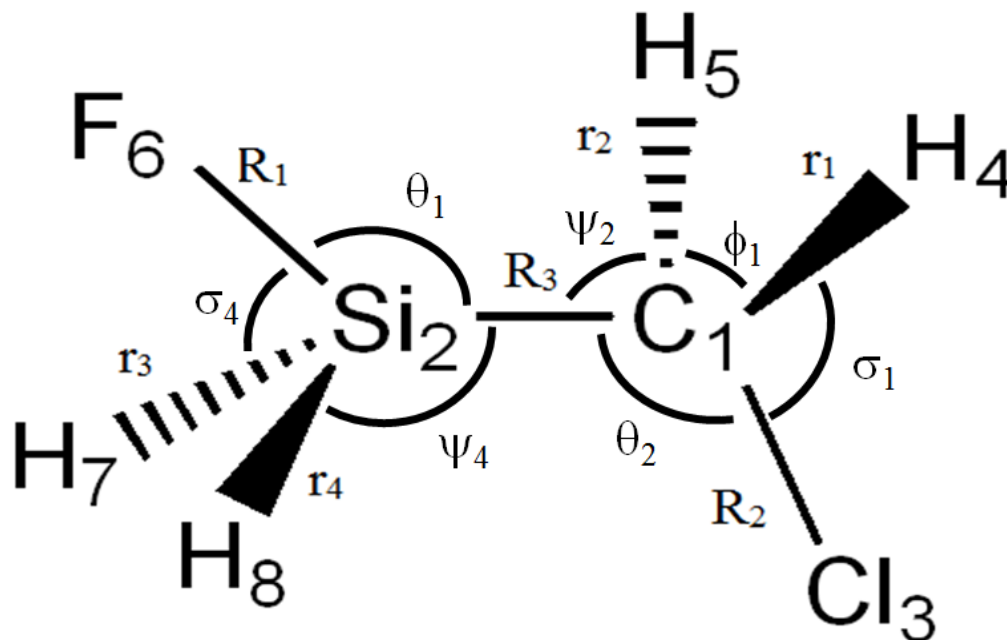


**Fig. 35** Internal coordinates for (chloromethyl)fluorosilane.

**Table 42.** Symmetry coordinates for the *trans* conformer of (chloromethyl)fluorosilane.

Description		Symmetry Coordinate <sup>a</sup>	
A'	CH <sub>2</sub> symmetric stretch	S <sub>1</sub>	= r <sub>1</sub> + r <sub>2</sub>
	SiH <sub>2</sub> symmetric stretch	S <sub>2</sub>	= r <sub>3</sub> + r <sub>4</sub>
	CH <sub>2</sub> deformation	S <sub>3</sub>	= φ <sub>1</sub>
	CH <sub>2</sub> wag	S <sub>4</sub>	= φ <sub>1</sub> + φ <sub>2</sub>
	SiH <sub>2</sub> deformation	S <sub>5</sub>	= φ <sub>2</sub>
	SiH <sub>2</sub> wag	S <sub>6</sub>	= φ <sub>3</sub> + φ <sub>4</sub>
	Si-F stretch	S <sub>7</sub>	= R <sub>1</sub>
	C-Cl stretch	S <sub>8</sub>	= R <sub>2</sub>
	C-Si stretch	S <sub>9</sub>	= R <sub>3</sub>
	CSiF in-plane-bend	S <sub>10</sub>	= 2θ <sub>1</sub> - φ <sub>3</sub> - φ <sub>4</sub>
	SiCCl in-plane-bend	S <sub>11</sub>	= 2θ <sub>2</sub> - φ <sub>1</sub> - φ <sub>2</sub>
A''	CH <sub>2</sub> antisymmetric stretch	S <sub>12</sub>	= r <sub>1</sub> - r <sub>2</sub>
	SiH <sub>2</sub> antisymmetric stretch	S <sub>13</sub>	= r <sub>3</sub> - r <sub>4</sub>
	CH <sub>2</sub> twist	S <sub>14</sub>	= σ <sub>1</sub> - σ <sub>2</sub>
	CH <sub>2</sub> rock	S <sub>15</sub>	= φ <sub>1</sub> - φ <sub>2</sub>
	SiH <sub>2</sub> twist	S <sub>16</sub>	= σ <sub>3</sub> - σ <sub>4</sub>
	SiH <sub>2</sub> rock	S <sub>17</sub>	= φ <sub>3</sub> - φ <sub>4</sub>
	torsion	S <sub>18</sub>	= σ

<sup>a</sup> Not normalized.

Comparison of the experimental Raman spectrum of the sample dissolved in liquefied krypton and the predicted Raman spectra for the pure *trans* and *gauche* conformers, as well as the mixture of the two conformers with relative concentrations calculated for the equilibrium mixture at 25 °C by using the experimentally determined enthalpy difference (97 cm<sup>-1</sup>) are shown in Fig. 34. The spectrum of the mixture is then compared to the Raman spectrum of the sample dissolved in krypton solution. The predicted spectrum is in reasonable agreement with the experimental spectrum, which indicates the utility of the predicted Raman spectra for the supporting vibrational assignments.

## Microwave Results

Upon consideration of the *trans* and *gauche* conformers of (chloromethyl)fluorosilane, transitions for only the *trans* conformer were detected in the CP-FTMW spectrum. By utilizing the MP2(full)/6-311+G(d,p) basis set, the energy difference between *trans* and *gauche* conformers was predicted to be  $203\text{ cm}^{-1}$  with the *trans* form as the more stable conformer (Table 41). Only 'B type' P, Q and R branch lines were observed in the microwave spectrum. All single heavy atom isotopologues for the *trans* conformer were detected in natural abundance. This includes  $^{13}\text{C}$ ,  $^{37}\text{Cl}$ ,  $^{29}\text{Si}$  and  $^{30}\text{Si}$  isotopologues (Table 38). For *trans* form of (chloromethyl)fluorosilane, 82 transitions were fitted for the parent species with an r.m.s. error of 8.6 kHz. Similarly for  $^{13}\text{C}$  and  $^{37}\text{Cl}$  isotopologues, 25 and 64 transitions were fitted with an r.m.s. error of 8.5 and 6.2 kHz, respectively. For the  $^{29}\text{Si}$  and  $^{30}\text{Si}$  isotopologues of (chloromethyl)fluorosilane, 43 and 36 transitions were fitted with an r.m.s. error of 7.6 and 8.7 kHz, respectively. Overall errors between observed and calculated frequencies are small and transitions are well fitted for the *trans* conformer of (chloromethyl)fluorosilane.

Rotational constants predicted by MP2(full)/6-311+G(d,p) and B3LYP/6-311+G(d,p) basis sets and experimental rotational constants for the *trans* conformer of (chloromethyl)fluorosilane are reported in Table 43. Rotational constants predicted by both methods are in good agreement with experimental rotational constants obtained for the parent species and isotopologues of (chloromethyl)fluorosilane. Among the A, B and C rotational constants, 'A' rotational constants calculated by the MP2(full)/6-311+G(d,p) method for the parent species and isotopologues of the *trans*

conformer of (chloromethyl)fluorosilane have higher values compared to experimental rotational constants, whereas rotational constants calculated by the B3LYP/6-311+G(d,p) method predicted lower values compared to the experimental rotational constants. B and C rotational constant values predicted by MP2(full) and B3LYP calculations by utilizing 6-311+G(d,p) basis set are both lower than the experimental rotational constants. Rotational constants predicted by the MP2(full)/6-311+G(d,p) basis set are more accurate than the rotational constants predicted by the B3LYP/6-311+G(d,p) basis set. Experimental rotational constants obtained for normal and isotopic species enable direct structure determination of the heavy atom skeleton. The nuclear quadrupole coupling constants predicted by *ab initio* calculations for the parent species and  $^{37}\text{Cl}$  isotopologues are in good agreement with the experimental values (Table 44). Additionally, the quadrupole coupling constants for other isotopologues are also reported in Table 44.

**Table 43.** Experimental and predicted rotational constants including centrifugal distortion constants for the *trans* conformer of (chloromethyl)fluorosilane.

	<i>A</i> (MHz)	<i>B</i> (MHz)	<i>C</i> (MHz)	$\Delta_J$ (kHz)	$\Delta_{Jk}$ (kHz)	<i>N</i> <sup>a</sup>
MP2(full)/6-311+G(d,p)	17910.7737	1820.5088	1703.3526	0.37661	-2.60284	
B3LYP/6-311+G(d,p)	17585.2216	1786.0668	1670.8424	0.37110	-2.61902	
Parent species	17794.2740(20)	1867.72449(64)	1743.66072(51)	0.587(10)	-1.27(18)	82
MP2(full)/6-311+G(d,p)	17511.1813	1819.4083	1698.7028	0.37292	-2.96340	
B3LYP/6-311+G(d,p)	17196.4118	1785.1156	1666.4319	0.36774	-2.93556	
<sup>13</sup> C	17369.2567(60)	1866.7240(14)	1738.5789(23)	[0.587]	[-1.27]	25
MP2(full)/6-311+G(d,p)	17902.6887	1772.4038	1661.0966	0.36167	-2.53677	
B3LYP/6-311+G(d,p)	17578.0049	1738.6808	1629.2402	0.35595	-2.55441	
<sup>37</sup> Cl	17783.5634(21)	1818.4850(11)	1700.57413(50)	0.512(22)	-2.40(36)	64
MP2(full)/6-311+G(d,p)	17773.8219	1814.4370	1696.7945	0.37680	-2.44118	
B3LYP/6-311+G(d,p)	17448.4666	1780.1019	1664.3857	0.37111	-2.47680	
<sup>29</sup> Si	17668.485(42)	1861.662(66)	1737.164(13)	[0.587]	[-1.27]	43
MP2(full)/6-311+G(d,p)	17642.7888	1808.5470	1690.4475	0.37698	-2.29023	
B3LYP/6-311+G(d,p)	17317.4426	1774.2677	1658.0913	0.37112	-2.34100	
<sup>30</sup> Si	17547.9341(44)	1855.5800(11)	1730.6916(16)	[0.587]	[-1.27]	36

<sup>a</sup> Number of frequencies fitted.**Table 44.** Nuclear quadrupole coupling constants for the parent species and isotopologues of *trans* (chloromethyl)fluorosilane.

	MP2(full)/6-311++G(d,p) Parent species	Parent species	<sup>13</sup> C	MP2(full)/6-311++G(d,p) <sup>37</sup> Cl	<sup>37</sup> Cl	<sup>29</sup> Si	<sup>30</sup> Si
$3/2(\chi_{aa})$ (MHz)	-70.2	-68.578(11)	-68.413(18)	-57.6	-54.2130(88)	-68.353(12)	-68.085(15)
$1/4(\chi_{bb}-\chi_{cc})$ (MHz)	-7.05	-7.8649(36)	-7.8970(60)	-8.05	-6.1742(28)	-7.9065(40)	-7.9520(54)
$\chi_{ab}$ (MHz)	45.2	47.36(80)	34.9(39)	29.5	36.76(70)	49.83(95)	50.1(12)

## Structural Parameters

The microwave study of the title molecule was performed using the  $^{13}\text{C}$ ,  $^{37}\text{Cl}$ ,  $^{29}\text{Si}$  and  $^{30}\text{Si}$  isotopologues as well as the parent species. The results indicated that only the *trans* conformer was present with no evidence of the *gauche* conformer. The rotational constants for each isotopologue of the *trans* conformer were determined experimentally and by *ab initio* methods using the MP2(full)/6-311+G(d,p) basis set, shown in Table 45. The structural parameters were then determined from both the MP2(full) and B3LYP methods using the 6-311+G(d,p) basis set. The 15 experimentally determined rotational constants and calculated structural parameters were then used to determine the adjusted  $r_0$  structural parameters for the *trans* conformer of (chloromethyl)fluorosilane in Table 46. The predicted  $r_0$  structural parameters for the *gauche* rotamer are also given in Table 46.

We have found that good structural parameters for hydrocarbons and many substituted ones can be determined by adjusting the structural parameters obtained from the *ab initio* MP2(full)/6-311+G(d,p) calculations to fit the rotational constants obtained from microwave experimental data by using a computer program "A&M" (*Ab initio* and Microwave) developed<sup>32</sup> in our laboratory. In order to reduce the number of independent variables, the structural parameters are separated into sets according to their types, where bond distances in the same set keep their relative ratio, and bond angles and torsional angles in the same set keep their difference in degrees. This assumption is based on the fact that errors from *ab initio* calculations are systematic. It has been shown<sup>33</sup> that *ab initio* MP2(full)/6-311+G(d,p) calculations have predicted the  $r_0$  structural parameters for more than fifty hydrocarbons, with the C-H distances predicted to better than 0.002 Å when compared to the experimentally determined values from isolated C-H stretching

**Table 45.** Comparison of rotational constants (MHz) obtained from *ab initio* MP2(full)/6-311+G(d,p) predictions, experimental values from microwave spectra, and from the adjusted  $r_0$  structural parameters for the *trans* form of (chloromethyl)fluorosilane (ClCH<sub>2</sub>SiH<sub>2</sub>F).

Isotopologue	Rotational constant	MP2(full)/6-311+G(d,p)	Experimental	Adjusted $r_0$	$ \Delta $
Parent species	A	17910.8	17794.3	17795.	0.8
	B	1820.5	1867.7	1867.7	0.0
	C	1703.4	1743.7	1743.6	0.0
<sup>13</sup> C	A	17511.2	17369.3	17369.	0.0
	B	1819.4	1866.7	1866.5	0.2
	C	1698.7	1738.6	1738.4	0.2
<sup>37</sup> Cl	A	17902.7	17783.6	17784.	0.0
	B	1772.4	1818.5	1818.8	0.5
	C	1661.1	1700.6	1700.8	0.2
<sup>29</sup> Si	A	17773.8	17668.5	17668.	0.2
	B	1814.4	1861.7	1861.6	0.1
	C	1696.8	1737.2	1737.1	0.1
<sup>30</sup> Si	A	17642.8	17547.9	17546.	1.0
	B	1808.5	1855.6	1855.6	0.0
	C	1690.4	1730.7	1730.7	0.0

frequencies. In another study, C-H bond distances determined from isolated C-H stretching frequencies were observed to be in good agreement with the same parameters determined from earlier microwave studies.<sup>34</sup> Therefore, all of the carbon-hydrogen distances can be taken from the MP2(full)/6-311+G(d,p) predicted values for (chloromethyl)fluorosilane. The same adjustment of the structural parameters using the MP2 method to get the adjusted  $r_0$  parameters for the *trans* conformer were applied to the *gauche* conformer's structural parameters using the MP2 method to get the predicted  $r_0$  structural parameters for the *gauche* conformer. Therefore the systematic adjustments made to that conformer's structural parameters were the same as the adjustments for the *trans* conformer for each given bond distance and bond angle.

**Table 46.** Structural parameters (Å and degrees), rotational constants (MHz) and dipole moment (Debye) for (chloromethyl)fluorosilane.

Structural Parameters	Internal Coordinates	MP2(full)/ 6-311+G(d,p)		B3LYP/ 6-311+G(d,p)		Adjusted $r_0$	Predicted $r_0$
		<i>Trans</i>	<i>Gauche</i>	<i>Trans</i>	<i>Gauche</i>	<i>Trans</i>	<i>Gauche</i>
r (Si-F)	R <sub>1</sub>	1.625	1.620	1.634	1.628	1.608 (3)	1.603
r (C-Cl)	R <sub>2</sub>	1.790	1.786	1.822	1.817	1.771 (3)	1.767
r (Si-C)	R <sub>3</sub>	1.875	1.873	1.885	1.883	1.884 (3)	1.888
r (C-H <sub>4</sub> )	r <sub>1</sub>	1.091	1.093	1.089	1.092	1.091 (2)	1.093
r (C-H <sub>5</sub> )	r <sub>2</sub>	1.091	1.092	1.089	1.091	1.091 (2)	1.092
r (Si-H <sub>7</sub> )	r <sub>3</sub>	1.467	1.467	1.477	1.477	1.469 (2)	1.469
r (Si-H <sub>8</sub> )	r <sub>4</sub>	1.467	1.472	1.477	1.482	1.469 (2)	1.474
∠ FSiC	θ <sub>1</sub>	108.2	108.7	107.4	109.2	108.9 (5)	109.4
∠ ClCSi	θ <sub>2</sub>	107.4	111.5	107.7	112.3	104.9 (5)	109.0
∠ H <sub>4</sub> CSi	ψ <sub>1</sub>	112.3	110.5	112.9	110.5	113.5 (5)	111.7
∠ H <sub>5</sub> CSi	ψ <sub>2</sub>	112.3	110.9	112.9	111.6	113.5 (5)	112.1
∠ H <sub>7</sub> SiC	ψ <sub>3</sub>	110.1	110.9	110.5	111.2	109.7 (5)	110.6
∠ H <sub>8</sub> SiC	ψ <sub>4</sub>	110.1	109.1	110.5	108.5	109.7 (5)	108.8
∠ H <sub>4</sub> CH <sub>5</sub>	φ <sub>1</sub>	108.3	107.6	108.7	108.0	108.3 (5)	107.6
∠ H <sub>7</sub> SiH <sub>8</sub>	φ <sub>2</sub>	112.1	112.1	112.3	112.1	112.1 (5)	112.1
∠ ClCH <sub>4</sub>	σ <sub>1</sub>	108.2	108.1	107.2	107.1	108.2 (5)	108.1
∠ ClCH <sub>5</sub>	σ <sub>2</sub>	108.2	108.1	107.2	107.1	108.2 (5)	108.1
∠ FSiH <sub>7</sub>	σ <sub>3</sub>	108.1	108.2	108.0	108.2	108.1 (5)	108.2
∠ FSiH <sub>8</sub>	σ <sub>4</sub>	108.1	107.7	108.0	107.5	108.1 (5)	107.7
τ ClCSiF	δ	180.0	65.5	180.0	67.8	180.0 (5)	65.5
A		17910.8	9285.4	17585.2	9315.0	17795.1	
B		1820.5	2295.5	1786.1	2204.6	1867.7	
C		1703.4	2017.3	1670.8	1953.8	1743.6	
μ <sub>a</sub>		0.071	0.592	0.102	0.495		
μ <sub>b</sub>		0.339	2.975	0.328	2.689		
μ <sub>c</sub>		0.000	0.289	0.000	0.297		
μ <sub>t</sub>		0.346	3.047	0.343	2.750		

The internal coordinates, basis set, conformer, and adjusted parameters have all been given in Table 46. The MP2(full) and B3LYP methods were used for general comparisons and to further increase the accuracy of the adjusted  $r_0$  parameters. The bond distances are given first, followed by bond angles, and then the one torsional angle. The resulting calculated and adjusted  $r_0$  parameters for the *trans* conformer are given in Table 46 where the heavy atom distances should be accurate to  $\pm 0.003$  Å, the C-H distances accurate to  $\pm 0.002$  Å, and uncertainties of angles should be within  $\pm 0.5^\circ$ . The differences between experimental and adjusted rotational constants are less than 1.0 MHz where the largest difference can be seen for the  $^{30}\text{Si}$  isotopologue (Table 45).

Most of the structural parameters predicted by *ab initio* calculations using the MP2 method are in good agreement with the adjusted  $r_0$  parameters for the *trans* conformer (Table 46). There are, however, some changes in bond distances and bond angles containing heavy atoms that are worth mentioning. Most of the calculated parameters either increased slightly or were not adjusted further. The  $r$  (C-Cl) bond distance decreased from 1.790 to 1.771 Å. The  $r$  (Si-F) bond distance and  $\angle$  ClCSi bond angle decreased from 1.625 Å to 1.608 Å and  $107.4^\circ$  to  $104.9^\circ$ , respectively. Additionally, there were other parameters that were adjusted by a significant amount. The  $r$  (Si-C) bond distance and  $\angle$  H<sub>4,5</sub>CSi bond angle increased from 1.875 Å to 1.884 Å and  $112.3^\circ$  to  $113.5^\circ$ , respectively. By using the Kraitchman equation, the  $r$  (C-Cl),  $r$  (Si-C) bond distances and the  $\angle$  ClCSi bond angle were calculated to be 1.808(9) Å, 1.853(5) Å and  $104.7(5)^\circ$ , respectively. The planar moments ( $P_{aa}$ ,  $P_{bb}$ ,  $P_{cc}$ ) obtained for all assigned species and MP2(full)/6-311++G(d,p) are reported in Table 47. The overestimation of calculated bond length and bond angles are mainly due to a calculated large  $P_{aa}$  value

from the MP2(full)/6-311++G(d,p) basis set calculation which is largely due to zero point effects. A vibrationally averaged structure using anharmonic corrections would likely alleviate these issues. It might be prudent to see how use of a larger basis set might compress this bond length theoretically.

**Table 47.** The three planar moments ( $P_{aa}$ ,  $P_{bb}$ ,  $P_{cc}$ ) for parent species and isotopologues of *trans*-(chloromethyl)fluorosilane with the *ab initio* values for the parent species.

	MP2(full)/6-311+G(d,p)	Parent Species	$^{13}\text{C}$	$^{37}\text{Cl}$	$^{29}\text{Si}$	$^{30}\text{Si}$
$P_{aa}$ (u $\text{\AA}^2$ )	273.04	266.011(15)	266.160(20)	273.338(50)	266.89(25)	267.7831(10)
$P_{bb}$ (u $\text{\AA}^2$ )	23.65	23.8269(52)	24.525(18)	23.8438(42)	24.029(21)	24.2267(89)
$P_{cc}$ (u $\text{\AA}^2$ )	4.566	4.5743(10)	4.5707(55)	4.57451(75)	4.5741(86)	4.5732(15)

### Vibrational Assignment

From both MP2(full) and B3LYP calculations for (chloromethyl)fluorosilane, the *trans* conformer was predicted as the more stable conformer compared to the *gauche* form (Table 41). In the microwave study, transitions were observed only for the *trans* conformer. Additionally, in the previous study there was no vibrational assignment reported for the *gauche* conformer of (chloromethyl)fluorosilane.<sup>100</sup> In order to determine the conformational stability and enthalpy difference between the *trans* and *gauche* form of (chloromethyl)fluorosilane, it is important to make confident vibrational assignments. For this purpose, significant assistance was obtained from the *ab initio* MP2(full)/6-31G(d) calculations with two scaling factors to obtain the force constants.

From these data the frequencies, infrared intensities, Raman activities, band contours and depolarization ratios were predicted (Tables 39 and 40).

The *trans* conformer of (chloromethyl)fluorosilane has  $C_s$  point group symmetry and its vibrational modes are divided into  $A'$  and  $A''$  blocks, whereas the *gauche* conformer has  $C_1$  point group symmetry and all vibrational modes are in one block. The  $A'$  block of the *trans* conformer has eleven vibrational modes and the  $A''$  block has seven vibrational modes. A peak observed with medium intensity at  $2953\text{ cm}^{-1}$  is assigned as the  $\text{CH}_2$  symmetric stretch ( $\nu_1$ ) fundamental mode and the peak observed with high intensity at  $2161\text{ cm}^{-1}$  is assigned to the  $\text{SiH}_2$  symmetric stretch ( $\nu_2$ ) fundamental mode in the infrared spectrum of the gaseous sample. The  $\text{CH}_2$  deformation ( $\nu_3$ ) fundamental mode is predicted at  $1417\text{ cm}^{-1}$  with medium intensity and observed at  $1405\text{ cm}^{-1}$  in the infrared spectrum of the gaseous sample. The same mode ( $\nu_3$ ) is observed at  $1408\text{ cm}^{-1}$  in the Raman spectrum of the sample dissolved in liquid krypton. Additionally, the peaks observed at  $1400\text{ cm}^{-1}$  in the infrared spectra of the amorphous solid and a shoulder peak observed at  $1405\text{ cm}^{-1}$  in the infrared spectrum of the annealed solid are assigned to the  $\text{CH}_2$  deformation ( $\nu_3$ ) mode. A small intensity peak observed at  $1200\text{ cm}^{-1}$  is assigned to the  $\text{CH}_2$  wag ( $\nu_4$ ) fundamental mode. The  $\text{SiH}_2$  deformation ( $\nu_5$ ) and the  $\text{SiH}_2$  wag ( $\nu_6$ ) fundamental modes are assigned to peaks observed at  $962$  and  $899\text{ cm}^{-1}$ , respectively, in the infrared spectrum of sample in gaseous phase. For the heavy atom stretches, the Si-F stretch ( $\nu_7$ ) and the C-Cl stretch ( $\nu_8$ ) fundamental modes are predicted at  $844$  and  $764\text{ cm}^{-1}$  respectively. These modes, however, are observed at  $847\text{ cm}^{-1}$  ( $\nu_7$ ) and  $768\text{ cm}^{-1}$  ( $\nu_8$ ) respectively. The C-Si stretch ( $\nu_9$ ) fundamental mode is predicted at  $764\text{ cm}^{-1}$  and observed at  $664\text{ cm}^{-1}$ .

In the  $A''$  block of the *trans* conformer, the  $\text{CH}_2$  antisymmetric stretch ( $\nu_{12}$ ) and  $\text{SiH}_2$  antisymmetric stretch ( $\nu_{13}$ ) fundamental modes are predicted at 3022 and 2225  $\text{cm}^{-1}$ . The corresponding peaks are observed at 2964  $\text{cm}^{-1}$  ( $\nu_{12}$ ) and 2190  $\text{cm}^{-1}$  ( $\nu_{13}$ ), respectively. The  $\text{CH}_2$  twist ( $\nu_{14}$ ) fundamental mode is predicted at 1105  $\text{cm}^{-1}$  with low infrared intensity and medium Raman activity. However in the spectra, no peak is observed near the predicted region in the infrared and Raman spectra of the sample. The  $\text{CH}_2$  rock ( $\nu_{15}$ ) fundamental mode is predicted at 821  $\text{cm}^{-1}$  and peak observed at 817  $\text{cm}^{-1}$  in the infrared spectrum of gaseous sample. The same ( $\nu_{15}$ ) fundamental mode is assigned for a peak observed at 819  $\text{cm}^{-1}$  in the Raman spectrum of the sample dissolved in liquid krypton. Additionally the  $\text{CH}_2$  rock ( $\nu_{15}$ ) fundamental mode is observed at 816  $\text{cm}^{-1}$  in the infrared spectra of the amorphous solid and 813  $\text{cm}^{-1}$  in the infrared spectrum of the annealed solid. The peak observed at 713  $\text{cm}^{-1}$  in the infrared spectra of gaseous sample is assigned to the  $\text{SiH}_2$  twist ( $\nu_{16}$ ) fundamental mode which is predicted at 715  $\text{cm}^{-1}$ . The same ( $\nu_{16}$ ) fundamental mode is observed at 719  $\text{cm}^{-1}$  in the infrared spectrum of the sample dissolved in liquid xenon, 711  $\text{cm}^{-1}$  in the infrared spectrum of the amorphous solid and 714  $\text{cm}^{-1}$  in the infrared spectrum of the annealed solid.

For the *gauche* conformer of (chloromethyl)fluorosilane, peaks observed at 2964 and 2949  $\text{cm}^{-1}$  in the infrared spectrum of the gaseous sample are assigned for the  $\text{CH}_2$  antisymmetric stretch ( $\nu_{12}$ ) and  $\text{CH}_2$  symmetric stretch ( $\nu_1$ ) fundamental modes, respectively. Similarly, strong peaks observed at 2195 and 2166  $\text{cm}^{-1}$  in the infrared spectrum of the gaseous sample are assigned as the  $\text{SiH}_2$  antisymmetric stretch ( $\nu_{13}$ ) and  $\text{SiH}_2$  symmetric stretch ( $\nu_2$ ) fundamental modes, respectively. The  $\text{CH}_2$  deformation ( $\nu_3$ ) fundamental mode is assigned to a peak observed at 1399  $\text{cm}^{-1}$  in

the infrared spectrum of the gaseous sample. The same ( $\nu_3$ ) mode is observed at 1390  $\text{cm}^{-1}$  in the infrared spectrum of the amorphous solid form and at 1397  $\text{cm}^{-1}$  in the infrared spectrum of the annealed solid. The  $\text{CH}_2$  wag ( $\nu_4$ ) fundamental mode is assigned to a low intensity peak observed at 1200  $\text{cm}^{-1}$ . The  $\text{CH}_2$  twist ( $\nu_{14}$ ) fundamental mode is assigned to a small peak observed at 1114  $\text{cm}^{-1}$  in the infrared spectrum of the gaseous sample and the same mode is assigned to the strong peak observed at 1124  $\text{cm}^{-1}$  in the Raman spectrum of sample dissolved in liquid krypton. The  $\text{SiH}_2$  deformation ( $\nu_5$ ) and the  $\text{SiH}_2$  wag ( $\nu_6$ ) fundamental modes are assigned to peaks observed at 962 and 931  $\text{cm}^{-1}$ , respectively. For the heavy atom stretches, the Si-F stretch ( $\nu_7$ ) fundamental mode is assigned to a peak observed at 847  $\text{cm}^{-1}$  in the infrared spectrum of the gaseous sample. The C-Cl stretch ( $\nu_8$ ) fundamental mode is observed at 774  $\text{cm}^{-1}$  in the infrared spectrum of the gaseous sample. A peak observed at 727  $\text{cm}^{-1}$  in the infrared spectrum of gaseous sample is assigned as the  $\text{SiH}_2$  twist ( $\nu_{15}$ ) fundamental mode. A peak observed at 761  $\text{cm}^{-1}$  is assigned as the  $\text{SiH}_2$  rock ( $\nu_{17}$ ) fundamental mode. The C-Si ( $\nu_9$ ) fundamental mode is assigned to peaks observed at 523 and 519  $\text{cm}^{-1}$  in the infrared spectra of the amorphous and annealed solids, respectively.

Prominent mixing is observed in the  $\nu_9$ ,  $\nu_{10}$ ,  $\nu_{11}$  and  $\nu_{15}$  fundamental modes, which have been assigned to the *trans* conformer. Similarly, for the *gauche* conformer, prominent mixing is observed in  $\nu_6$ ,  $\nu_9$ ,  $\nu_{10}$ ,  $\nu_{16}$  and  $\nu_{17}$  fundamental modes. In all the mentioned above fundamental modes, contributions from other vibrational modes are significant. The decomposition of (chloromethyl)fluorosilane leads to formation of hydrofluoric acid, along with other unknown impurities. However, the decomposition rate of (chloromethyl)fluorosilane is very slow. Peaks for impurities are observed

at 544, 553, 915, 979 and 1181  $\text{cm}^{-1}$  in all infrared and Raman spectra (Figs. 31, 32, and 34). Even though the sample contains impurities, the vibrational assignments have been successfully made for the *trans* and the *gauche* conformers of (chloromethyl)fluorosilane.

### Conformational Stability

In the infrared spectrum of the amorphous solid, peaks observed at 664, 713, 817 and 1405  $\text{cm}^{-1}$  are specifically assigned to the *trans* conformer of (chloromethyl)fluorosilane (Fig. 32, Table 39). Similarly peaks observed at 761, 1114 and 1399  $\text{cm}^{-1}$  are specifically assigned to the *gauche* conformer of (chloromethyl)fluorosilane (Fig. 32, Table 40). In the infrared spectrum of the annealed solid, intensities of peaks that are assigned to the *gauche* conformer decreased while the peak intensities for the *trans* conformer increased simultaneously. Overall for (chloromethyl)fluorosilane, the *trans* form was observed as the more stable conformer. To determine the enthalpy difference between the two conformers, the sample was dissolved in liquefied xenon and krypton solutions. The IR spectrum of the xenon solution and Raman spectrum of the krypton solution were collected at low temperature ranges of -100 to -60  $^{\circ}\text{C}$  and -153 to -133  $^{\circ}\text{C}$ , respectively (Figs. 31 and 34). Relatively small interactions are expected to occur between xenon or krypton and the sample, but the sample can associate with itself through van der Waals interactions. However, due to the very small concentration of sample ( $\sim 10^{-4}$  molar), self-association is greatly reduced. Therefore, only small wavenumber shifts are anticipated for the noble gas interactions when passing from the gas phase to the liquefied xenon/krypton (Fig. 36). A significant advantage of this study is that the conformer bands are better resolved in comparison with those in the infrared spectrum of the gas.

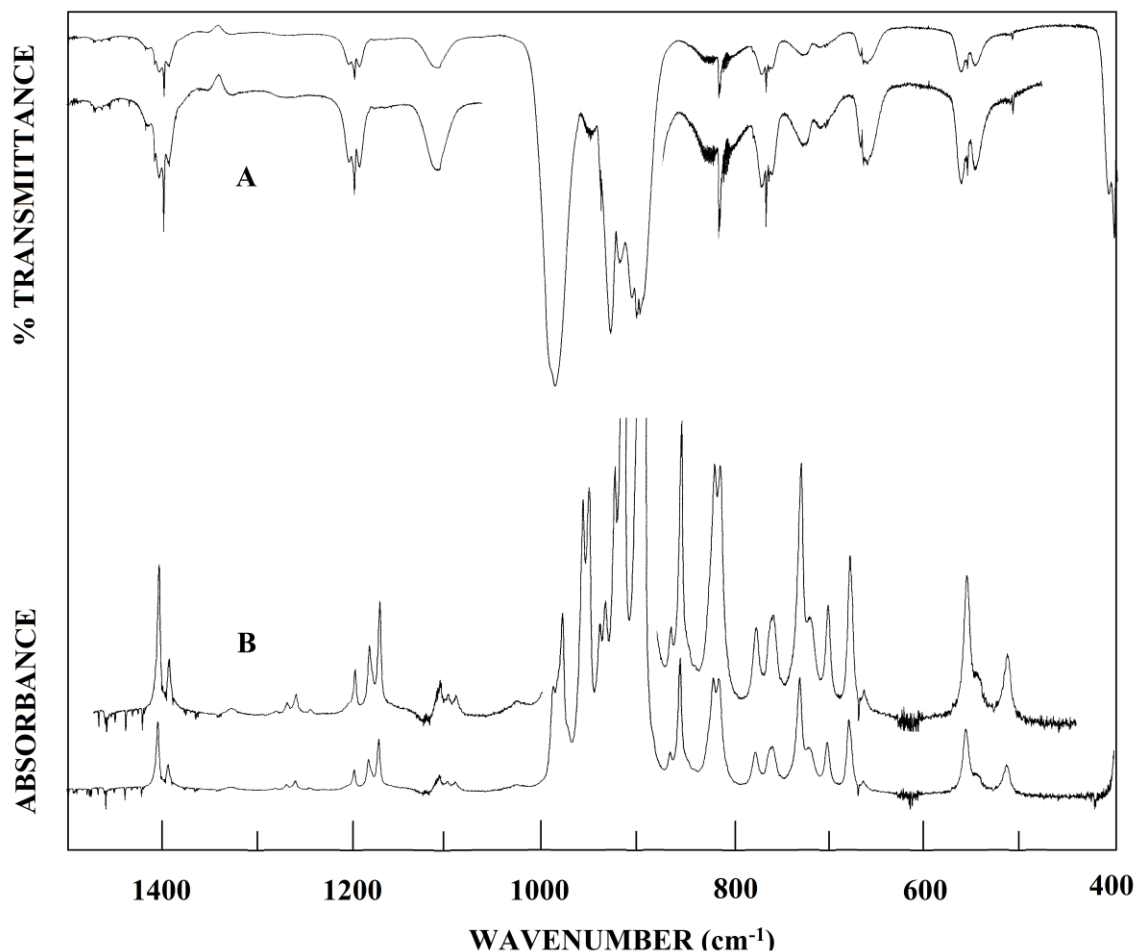


**Fig. 36** Infrared spectra of (chloromethyl)fluorosilane (A) gas; (B) Xe solution at  $-70\text{ }^{\circ}\text{C}$ .

The vibrational assignments for the two conformers (Table 39 and 40) were used to find pairs of bands from which the enthalpy determination could be obtained. To minimize the effect of combination and overtone bands in the enthalpy determination, it is desirable to have the lowest frequency pairs that are possible for the determination. The bands should also be sufficiently resolved so reproducible intensities can be obtained. Therefore all bands used in determining the enthalpy difference were below  $1500\text{ cm}^{-1}$ .

The intensities of the individual bands were measured as a function of temperature and their ratios were determined (Figs. 33 and 37). By application of the van't Hoff equation,  $-\ln K = \Delta H/(RT) - \Delta S/R$ , the enthalpy differences were determined from a plot of  $-\ln K$  versus  $1/T$ , where  $\Delta H/R$  is the slope of the line and  $K$  is substituted with the appropriate intensity ratios, *i.e.*  $I_{\text{conf-1}} / I_{\text{conf-2}}$ , etc. It was assumed that  $\Delta S$  and the van't Hoff factor ( $\alpha$ ) are not functions of temperature in the range studied.

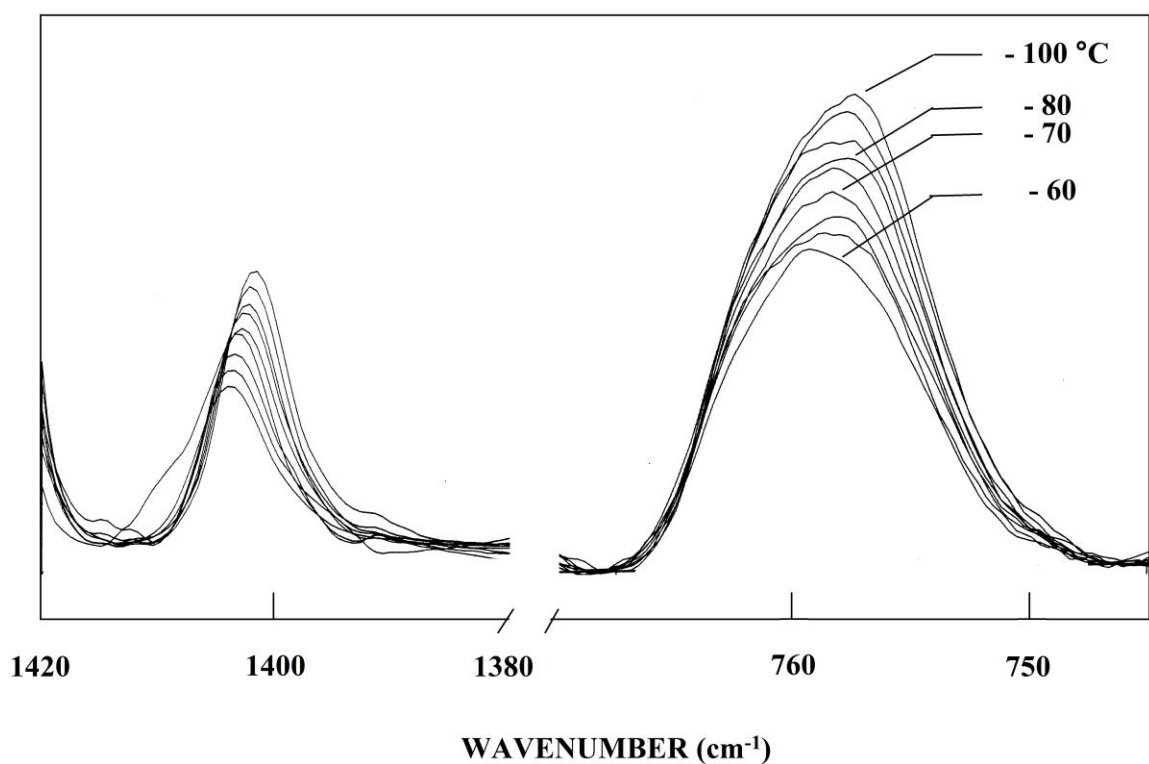


**Fig. 37** Temperature (-60 to -100 °C) dependent infrared spectrum of (chloromethyl)fluorosilane dissolved in liquid xenon solution.

In the IR spectra of the xenon solution, two bands at 719 cm<sup>-1</sup> and 1403 cm<sup>-1</sup> for the *trans* conformer and two bands at 759 cm<sup>-1</sup> and 1392 cm<sup>-1</sup> for the *gauche* conformer were used to determine the enthalpy difference. It is assumed that all four bands are free from impurities and have minimal interference from other vibrations. The four bands were chosen because they were among the well resolved bands in the spectra. The intensity of each band was measured for the temperature range -100 to -60 °C (Fig. 37) and recorded in Table 48. Individual enthalpy differences are determined from each band pair ratio. These enthalpy differences are then used to determine the average enthalpy ratio. The statistical average with standard deviation of two sigma was obtained by treating all the data as a single set which gives a value of 109 ± 15 cm<sup>-1</sup> and indicates the *trans* conformer is more stable than the *gauche* form.

**Table 48.** Temperature and intensity ratios of the conformational bands of (chloromethyl)fluorosilane from the infrared spectra of the liquid xenon solution phase.

T(°C)	1/T (×10 <sup>3</sup> K <sup>-1</sup> )	I <sub>719</sub> / I <sub>759</sub>	I <sub>719</sub> / I <sub>1392</sub>	I <sub>1403</sub> / I <sub>759</sub>	I <sub>1403</sub> / I <sub>1392</sub>
-60.0	4.692	0.3092	0.9216	0.9079	2.7059
-65.0	4.804	0.3439	1.0189	0.9427	2.7925
-70.0	4.923	0.3614	1.1111	0.9458	2.9074
-75.0	5.047	0.3815	1.2000	0.9422	2.9636
-80.0	5.177	0.3736	1.1724	0.9451	2.9655
-85.0	5.315	0.3874	1.2333	0.9529	3.0333
-90.0	4.460	0.3909	1.2419	0.9645	3.0645
-95.0	5.613	0.3816	1.2344	0.9662	3.1250
-100.0	5.775	0.4038	1.3030	0.9718	3.1364
$\Delta H^a$ (cm <sup>-1</sup> )		129 ± 30	184 ± 36	95 ± 18	89 ± 10

<sup>a</sup> Average value:  $\Delta H = 109 \pm 15$  cm<sup>-1</sup> (1.47 ± 0.16 kJ mol<sup>-1</sup>) with the *trans* conformer the more stable form and the statistical uncertainty (2σ) obtained by utilizing all of the data as a single set.

The variable temperature Raman spectra (-133 to -153 °C) of the krypton solution were used to supplement the information obtained from the IR spectra of the xenon solution. Due to impurities, there were only three bands used to determine the enthalpy difference between the conformers. The band at 819 cm<sup>-1</sup> was used for the *trans* conformer and the bands at 763 and 1124 cm<sup>-1</sup> were used for the *gauche*. Both band pair ratios and their enthalpies were used to obtain an average enthalpy (Table 49). The statistical average with standard deviation of two sigma was obtained by treating all the data as a single set which gives a value of 97 ± 16 cm<sup>-1</sup>. This result also verified that the *trans* conformer is more stable than the *gauche* form.

**Table 49.** Temperature and intensity ratios of the conformational bands of (chloromethyl)fluorosilane from the Raman spectra of the liquid krypton solution phase.

T(°C)	1/T (×10 <sup>3</sup> K <sup>-1</sup> )	I <sub>819</sub> / I <sub>763</sub>	I <sub>819</sub> / I <sub>1124</sub>
-133.0	7.144	0.3796	0.5714
-143.0	7.692	0.4080	0.6329
-153.0	8.333	0.4286	0.7059
ΔH <sup>a</sup> (cm <sup>-1</sup> )		71 ± 8	123 ± 31

<sup>a</sup> Average value: ΔH = 97 ± 16 cm<sup>-1</sup> (1.16 ± 0.19 kJ mol<sup>-1</sup>) with the *trans* conformer the more stable form and the statistical uncertainty (2σ) obtained by utilizing all of the data as a single set.

The Raman spectra of the krypton solution are in good agreement with the IR spectra of the xenon solution and were used to verify the results for the conformational stability. Approximately  $46 \pm 2$  % of the *trans* form is present at ambient temperature. Our predictions and experimentally determined energies are both in agreement that the *trans* form is the more stable conformer.

### Discussion

Average and percent errors have been calculated between the predicted and the observed frequencies for the *trans* and the *gauche* conformer of (chloromethyl)fluorosilane. The *trans* and *gauche* conformers have average errors of 16.23 and 11.43  $\text{cm}^{-1}$ , respectively, which represent percent errors of 1.13 and 0.81%, respectively. Both the average and percent errors indicate the predicted frequencies from *ab initio* calculations produced reasonably accurate results with respect to the vibrational assignments of the two conformers.

The *ab initio* calculations and experimental results both indicate that the *trans* form is the more stable conformer, but the values of the enthalpy difference between the *trans* and *gauche* conformers differ significantly. This study is in good agreement with previous studies<sup>98,99</sup> that determined the *trans* conformer to be the more stable conformer. Previous studies of (chloromethyl)chlorosilane determined the enthalpy difference between the two conformers to be 175  $\text{cm}^{-1}$  and 177  $\text{cm}^{-1}$  with the *trans* conformer being more stable.<sup>98,100</sup> Similarly the *trans* conformer was also found to be the more stable conformer for studies on (chloromethyl)bromosilane which determined the enthalpy difference to be 175  $\text{cm}^{-1}$  and 216  $\text{cm}^{-1}$ .<sup>99,100</sup> Collectively those studies,

along with this study, have a qualitative agreement in conformational stability. If the enthalpy difference for (chloromethyl)bromosilane was found to be higher than  $175\text{ cm}^{-1}$ , then it would confirm earlier theoretical predictions that the energy difference increases when the halogen atom on the silyl group becomes larger in size.<sup>97</sup>

The most probable reasons for not observing the high energy *gauche* conformer in the microwave spectra of the sample are mainly due to the conformational relaxation of (chloromethyl)fluorosilane due to supersonic expansion. The same pattern was observed for 1-hexanal where high energy conformers were also not detected.<sup>84</sup> Additionally the conformational relaxation can be minimized by using helium as a carrier gas, but due to the experimental limitations this experiment was not carried out. Additionally the acquired spectrum contains many small peaks with hyperfine-split contaminants (or lines from decomposition products) in that regions where one would expect transitions of the *gauche* conformer to be visible. It appears there are many chlorine-containing species in the region. Given the agreement between theory and experiment for the quadrupole coupling constants of the *trans* conformer, similar agreement is expected for the predictions of *gauche* conformer. However, the observed spectrum is not consistent with the predicted patterns of the *gauche* conformer.

The adjusted  $r_0$  structural parameters regarding the C, Cl and Si bond distances and angles from the *trans* conformer of (chloromethyl)fluorosilane can be compared to a previous study of chloromethylsilane.<sup>105</sup> The  $r$  (Si-C) bond distance for chloromethylsilane was determined to be  $1.886\text{ \AA}$ ,<sup>105</sup> which is almost same the determined value for (chloromethyl)fluorosilane. The  $r$  (C-Cl) bond distance for

chloromethylsilane was determined to be 1.791 Å which is 0.020 Å larger than (chloromethyl)fluorosilane. Additionally the  $\angle$  ClCSi bond angle decreases from 109.3° in chloromethylsilane to 104.9° for (chloromethyl)fluorosilane. It would be of interest in future studies to perform microwave studies for (chloromethyl)bromosilane and (chloromethyl)iodosilane to determine their adjusted  $r_0$  structural parameters for comparison.

The barriers and potential function governing the asymmetric rotor motion was predicted from the MP2(full)/6-31G(d) calculations, where the energy difference was predicted to be 313 cm<sup>-1</sup> between the *trans* and *gauche* conformers (Table 41). The *gauche-gauche* barrier was predicted to be 794 cm<sup>-1</sup> and the *gauche* to *trans* barrier to be 1288 cm<sup>-1</sup> (Fig. 38). It is possible to obtain values for four terms of the potential constants of the potential function governing the internal rotation of the (chloromethyl)fluorosilane which has the form:

$$V(\theta) = \frac{1}{2} \sum_{i=1}^4 V_i (1 - \cos i\theta)$$

The series coefficients,  $V_i$ , in the above equation, were determined by a non-linear least-squares fitting of the predicted energy differences and the torsional dihedral angles for the *gauche* (68.0°) and *trans* (180.0°) conformers and the two transition states (120.8° and -120.8°). The potential is nearly a three-fold internal rotation (barrier 1288 cm<sup>-1</sup>) with the following values for the first four terms of the potential function:  $V_1 = -562.97$ ,  $V_2 = -154.37$ ,  $V_3 = -724.71$ ,  $V_4 = 58.01$  cm<sup>-1</sup>. These predicted values are expected to be reasonably near the unknown experimental ones that would be obtained from the frequencies of the asymmetric torsional modes from the two conformers.

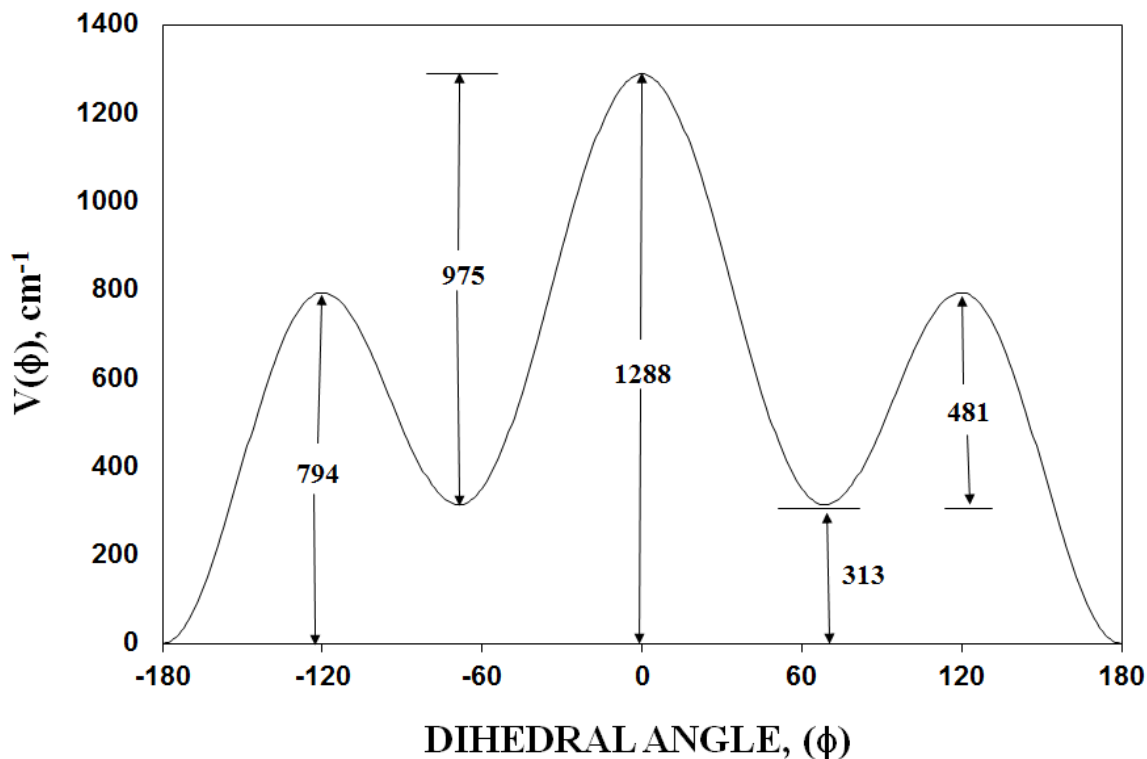


**Fig. 38** Potential energy function (MP2(full)) governing the internal rotation of (chloromethyl)fluorosilane from the *gauche* to the *trans* form.

Similarly, barriers and potential functions were predicted for (fluoromethyl)fluorosilane, (chloromethyl)chlorosilane, (chloromethyl)bromosilane and (bromomethyl)fluorosilane from the MP2(full)/6-31G(d) calculations (Figs. 39-42). For (fluoromethyl)fluorosilane, (chloromethyl)fluorosilane and (bromomethyl)fluorosilane ( $XCH_2-SiH_2F$ ;  $X = F, Cl$  and  $Br$ ) the *gauche-gauche* barriers were predicted to be 884, 794 and 1224  $cm^{-1}$  respectively. Similarly the *gauche to trans* barrier was predicted to be 1531  $cm^{-1}$  for (fluoromethyl)fluorosilane, 1288  $cm^{-1}$  for (chloromethyl)fluorosilane and 1609  $cm^{-1}$  for (bromomethyl)fluorosilane. The *gauche-gauche* and *gauche to trans* barriers were predicted low for (chloromethyl)fluorosilane compared to

(fluoromethyl)fluorosilane and (bromomethyl)fluorosilane. In the comparison of (chloromethyl)fluorosilane, (chloromethyl)chlorosilane and (chloromethyl)bromosilane ( $\text{ClCH}_2\text{-SiH}_2\text{Y}$ ;  $\text{Y} = \text{F}, \text{Cl}$  and  $\text{Br}$ ) both *gauche-gauche* and *gauche to trans* barriers increases as the halogen atom attached to the silicon atom changed from fluorine to bromine.

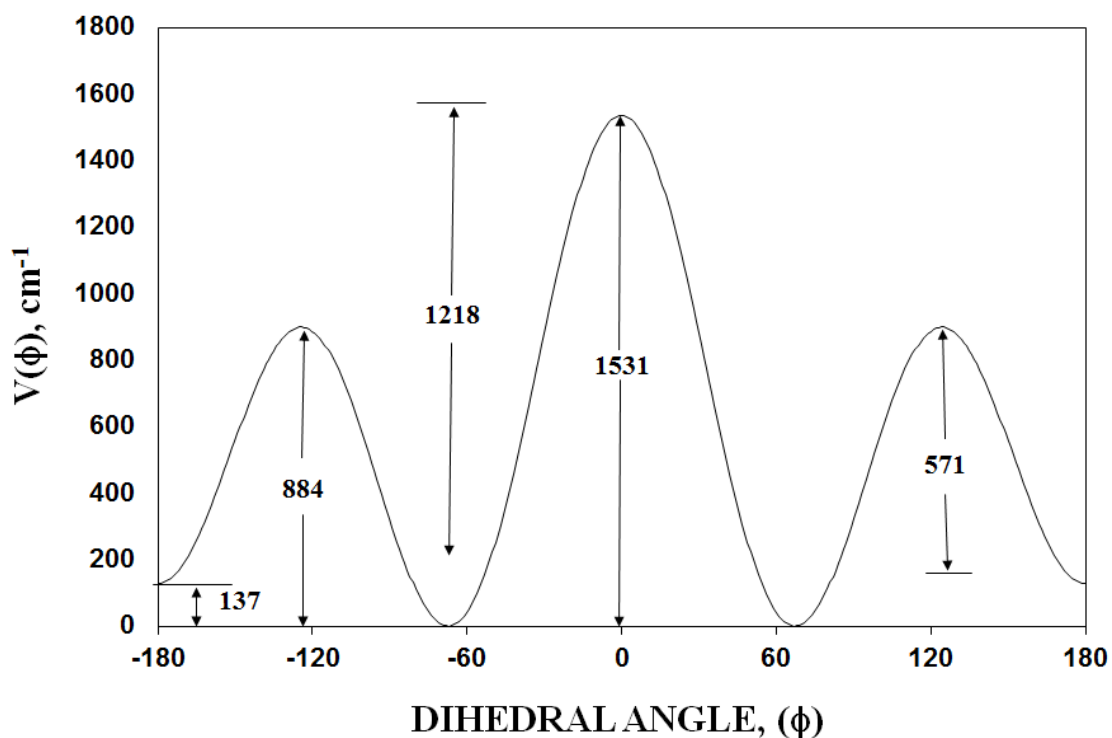


**Fig. 39** Potential energy function (MP2(full)) governing the internal rotation of (fluoromethyl)fluorosilane from the *trans* to the *gauche* form.

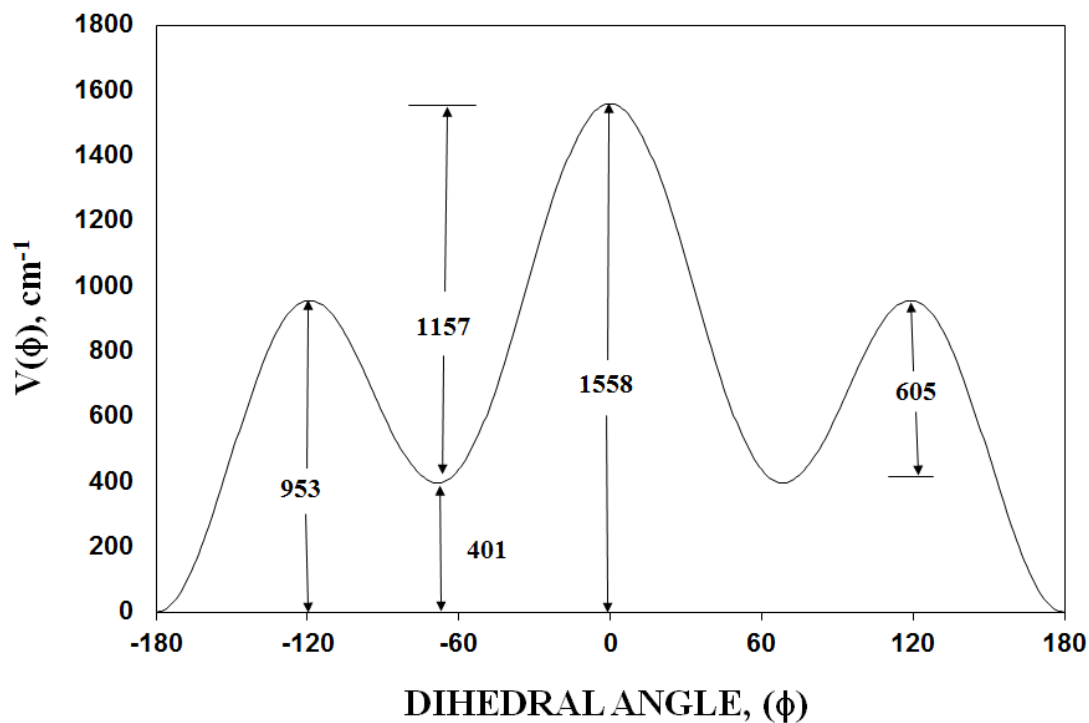


**Fig. 40** Potential energy function (MP2(full)) governing the internal rotation of (chloromethyl)chlorosilane from the *trans* to the *gauche* form.

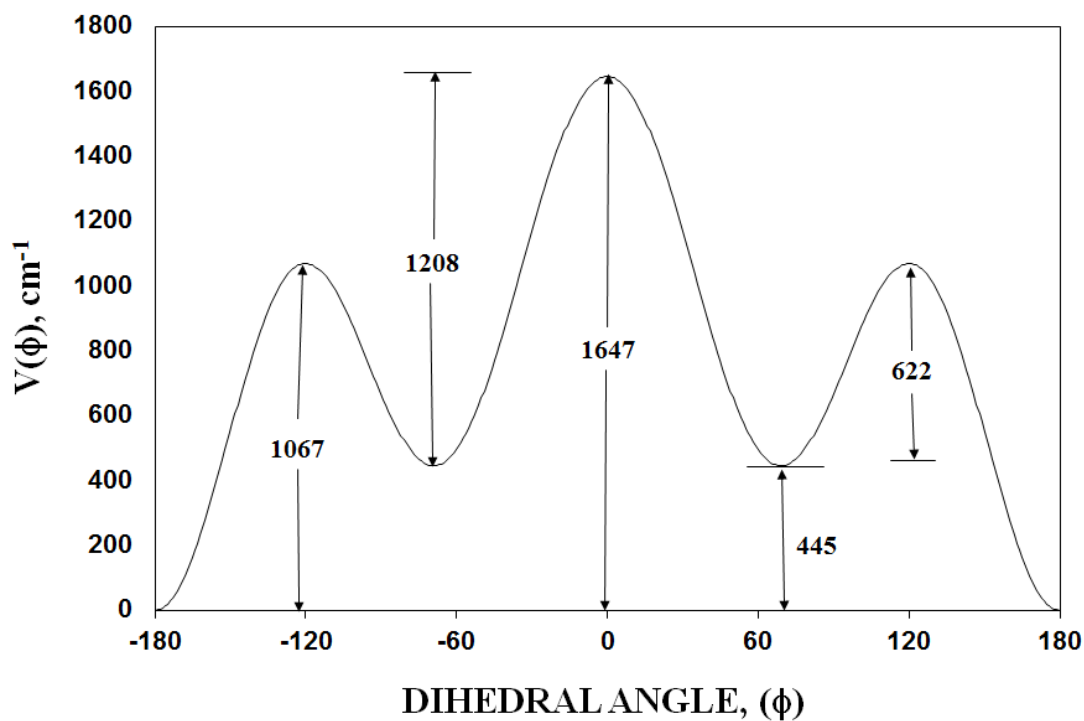


**Fig. 41** Potential energy function (MP2(full)) governing the internal rotation of (chloromethyl)bromosilane from the *trans* to the *gauche* form.

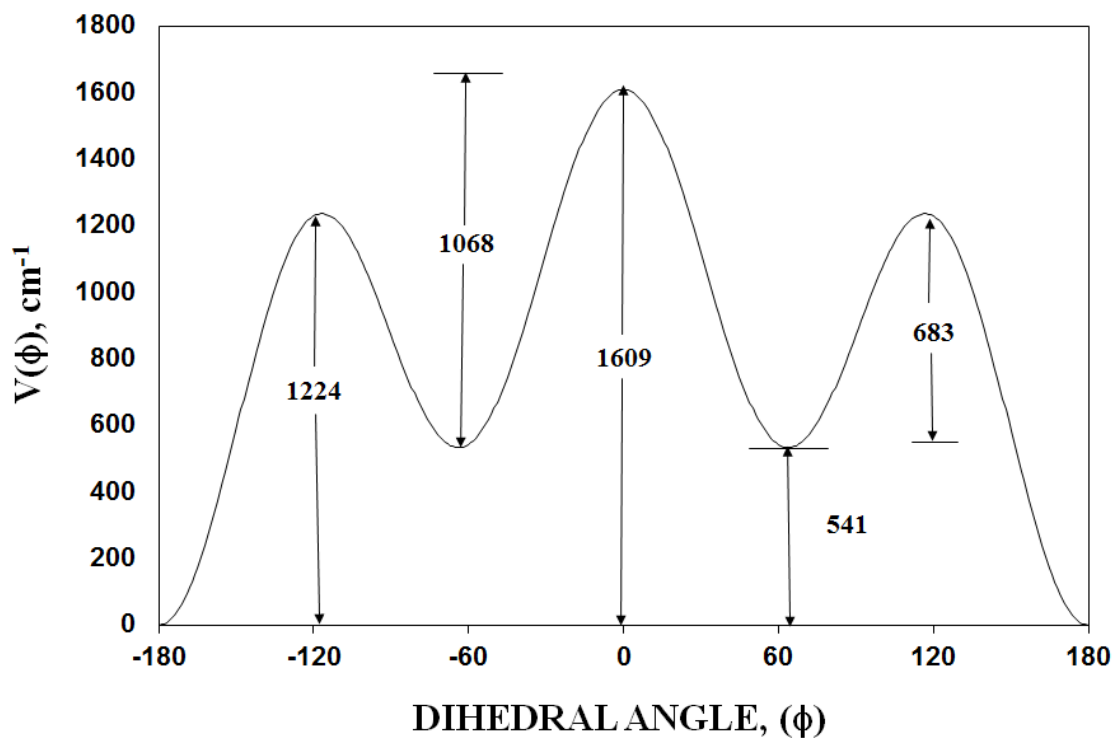


**Fig. 42** Potential energy function (MP2(full)) governing the internal rotation of (bromomethyl)fluorosilane from the *trans* to the *gauche* form.

The effects of different halogen (F, Cl and Br) groups on carbon and silicon atoms were studied by carrying out a Natural Population Analysis (NPA) for the *trans* and *gauche* conformers of (chloromethyl)fluorosilane, (fluoromethyl)fluorosilane, (chloromethyl)chlorosilane, (chloromethyl)bromosilane and (bromomethyl)fluorosilane ( $\text{XCH}_2\text{-SiH}_2\text{Y}$ ; X, Y = F, Cl and Br) by using the MP2(full)/6-311+G(d,p) basis set (Table 50).

**Table 50.** Natural population analysis for (halomethyl)halosilane derivatives

XCH <sub>2</sub> -SiH <sub>2</sub> Y	X	C	Si	Y
<i>Trans</i> ClCH <sub>2</sub> -SiH <sub>2</sub> F	-0.07626	-0.82852	1.64350	-0.68214
<i>Gauche</i> ClCH <sub>2</sub> -SiH <sub>2</sub> F	-0.06589	-0.83823	1.65026	-0.67748
<i>Trans</i> FCH <sub>2</sub> -SiH <sub>2</sub> F	-0.43706	-0.30686	1.59438	-0.68187
<i>Gauche</i> FCH <sub>2</sub> -SiH <sub>2</sub> F	-0.43185	-0.30977	1.59348	-0.67763
<i>Trans</i> ClCH <sub>2</sub> -SiH <sub>2</sub> Cl	-0.07200	-0.81005	1.25122	-0.40639
<i>Gauche</i> ClCH <sub>2</sub> -SiH <sub>2</sub> Cl	-0.06284	-0.81548	1.24962	-0.39466
<i>Trans</i> ClCH <sub>2</sub> -SiH <sub>2</sub> Br	-0.07067	-0.81098	1.16688	-0.34079
<i>Gauche</i> ClCH <sub>2</sub> -SiH <sub>2</sub> Br	-0.06132	-0.81597	1.16221	-0.32607
<i>Trans</i> BrCH <sub>2</sub> -SiH <sub>2</sub> F	-0.00576	-0.92328	1.64683	-0.68276
<i>Gauche</i> BrCH <sub>2</sub> -SiH <sub>2</sub> F	0.00633	-0.93686	1.65776	-0.67740

Halogens attached to silicon atoms are more electronegative compared to the same halogens attached to carbons atom. In comparing the electronegativities between the *trans* and *gauche* conformer of different compounds, halogens of *trans* conformers are observed to be more electronegative compared to halogens of *gauche* conformers. Similarly carbon atoms of *gauche* conformers are more electronegative than carbon atoms of *trans* conformers. Silicon atoms of the *trans* conformer are observed to be more electropositive compared to silicon atoms of the *gauche* conformer except for (chloromethyl)fluorosilane and (bromomethyl)fluorosilane, where the silicon atoms of the *gauche* conformers are observed to more electropositive compared to the silicon atoms of the *trans* conformers. For the *trans* and *gauche* conformers of (fluoromethyl)fluorosilane, (chloromethyl)fluorosilane and (bromomethyl)fluorosilane (XCH<sub>2</sub>-SiH<sub>2</sub>F; X = F, Cl and Br), as expected the electronegativity decreases from fluorine to bromine atoms, but the electronegativity of the carbon atom increases, and is observed to reach a minimum for the fluorine atom and maximum for the bromine atom.

The electropositivity of silicon atom increases from fluorine to bromine atoms for the *trans* and *gauche* conformers of (fluoromethyl)fluorosilane, (chloromethyl)fluorosilane and (bromomethyl)fluorosilane. The effects of a chlorine atom attached to carbon was also studied by comparing the NPA values obtained for *trans* and *gauche* conformers of (chloromethyl)fluorosilane, (chloromethyl)chlorosilane and (chloromethyl)bromosilane ( $\text{ClCH}_2\text{-SiH}_2\text{Y}$ ;  $\text{Y} = \text{F, Cl and Br}$ ). Halogens attached to the silicon atoms did not have a major effect on the electronegativity of the carbon atoms. For the silicon atoms however, electropositivity decreased from fluorine to bromine atoms, for the *trans* and *gauche* conformers of (chloromethyl)fluorosilane, (chloromethyl)chlorosilane and (chloromethyl)bromosilane. Overall when different halogens were substituted on  $\text{XCH}_2\text{-SiH}_2\text{Y}$  ( $\text{X, Y} = \text{F, Cl and Br}$ ), moiety-specific trends were observed for the charge on carbon and silicon atoms of (chloromethyl)fluorosilane, (fluoromethyl)fluorosilane, (chloromethyl)chlorosilane, (chloromethyl)bromosilane and (bromomethyl)fluorosilane.

In this study the conformational stability, enthalpy difference and structural parameters of (chloromethyl)fluorosilane were determined, and the effect of halogens on the carbon and silicon atoms were also studied. In the future, it would be of interest to study molecules like (difluoromethyl)difluorosilane, (dichloromethyl)difluorosilane and (dibromomethyl)difluorosilane, where the effects of the four halogen atoms could be explored in detail.

(This work has been published in the Journal of Physical Chemistry A<sup>106</sup>.)

## CHAPTER 8

### CONCLUSION

From the foregoing chapters, it should be clear that the combination of experimental methods of vibrational spectra, coupled with computational approaches indeed constitute powerful tools for molecular structure determination. For example, the following results of the present research are summarized with respect to the application of these methods. (1) The conformational stabilities and enthalpy differences between two or more conformers were successfully determined for 2-methylbutane, cyanocyclopentane, isocyanocyclopentane, cyclopropylcyanosilane and (chloromethyl)fluorosilane. (2) Infrared and Raman spectra were recorded for molecules in the vapor, liquid solution, amorphous and crystalline solid states, and in inert matrices at high pressures or low temperatures. (3) Vibrational assignments were obtained for all possible conformers. (4) Microwave spectra were also recorded for isocyanocyclopentane, cyclopropylcyanosilane and (chloromethyl)fluorosilane. (5) Rotational constants obtained from the microwave spectra were used for determining detailed structural parameters of the molecules studied in this investigation. Whenever possible, data obtained from the experimental and theoretical calculations were compared with results for other similar molecules. Changes in conformational stabilities, enthalpy differences and  $r_0$  structural parameters with respect to changes in functional groups, size of rings or chains were studied successfully.

The vibrational frequencies and energies of different conformers of all studied molecules were obtained with the Gaussian 03 program at the MP2(full) level using the 6-31G(d) basis set. However, calculated vibrational frequencies and energies of

molecules were always found to be higher than experimental values. Thus differences between the predicted and experimental frequencies were minimized with the help of scaling factors. Perhaps the newest version of the Gaussian software package (Gaussian 16, just released) might enable predictions closer to experimental enthalpy difference values, and frequencies may not need scaling factors.

The infrared and Raman spectra along with vibrational assignments reported for all observed conformers of the molecules herein will be useful to organic, pharmaceutical, and theoretical chemistry researchers. Additionally, structural parameters and conformational data obtained for these different molecules will be useful for understanding physicochemical properties and chemical reactivity of the molecules studied. The ribose structure of DNA and RNA, for example, has a five membered ring which is similar to the structure of the cyclopentane ring of cyano and isocyanocyclopentane. So a study of other, similar molecules along with furan containing molecules can be useful for understanding of different conformational structures of DNA and RNA. The study of isocyanocyclopentane is also helpful in solving the nature of the isocyano group. Similar to the cyano group, the isocyano group is also assumed to be a triple bond, but in the case of isocyanocyclopentane, the isocyano group is observed to have more double bond rather than triple bond character. Polyisocyanide compounds form helix-like structures.<sup>107</sup> Conformational and structural data of isocyanocyclopentane and other similar molecules will be useful for studying the structural and conformational behavior of polyisocyanides. Lastly, carbon-silicon (C-Si) bonds are larger, and while more polar are weaker than carbon-carbon (C-C) bonds.<sup>7</sup> This detailed study of cyclopropylcyanosilane and

(chloromethyl)fluorosilane will be useful for understanding physicochemical properties of organosilicon compounds in general. Overall this study gives significant contributions in the field of spectroscopy and other chemistry related fields.

Due to experimental and sample limitations, the determination of conformational stabilities and enthalpy differences of molecules were always restricted to volatile compounds. More recently, though, for recording the microwave spectra of non-volatile compounds, a laser ablation method has been successfully utilized for transferring the sample from the solid form into the gaseous phase.<sup>108,109</sup> Recently, the same method (laser ablation) has been successfully utilized for recording the infrared spectra of non-volatile samples.<sup>110</sup> In the future, this newly developed method may become more readily available to be utilized for the study of non-volatile compounds, and, hence, expand the range of compounds capable of being studied in detail by vibrational spectroscopy.

## REFERENCE LIST

- (1) McWade, M. A.; Sanders, M. E.; Broome, J. T.; Solórzano, C. C.; Mahadevan-Jansen, A. Establishing the Clinical Utility of Autofluorescence Spectroscopy for Parathyroid Detection. *Surgery* **2016**, *159* (1), 193–203.
- (2) Haka, A. S.; Sue, E.; Zhang, C.; Bhardwaj, P.; Sterling, J.; Carpenter, C.; Leonard, M.; Manzoor, M.; Walker, J.; Aleman, J. O.; Gareau, D.; Holt, P. R.; Breslow, J. L.; Zhou, X. K.; Giri, D.; Morrow, M.; Iyenger, N.; Berman, I.; Hudis, C. A.; Dannenberg, A. J.; Noninvasive Detection of Inflammatory Changes in White Adipose Tissue by Label-Free Raman Spectroscopy. *Anal. Chem.* **2016**, *88* (4), 2140–2148.
- (3) Shou-Yuan, T.; Zhi-Ning, X.; Yu-Jie, F.; Qian, G. Advances and Applications of Microwave Spectroscopy. *Chinese J. Anal. Chem.* **2008**, *36* (8), 1145–1151.
- (4) Ahlers, S. k. D.; Brett, R. A.; McTaggart, N. G. Infrared Study of the *Cis* and *Trans* Isomers of C<sub>18</sub> Fatty Acids. *J. Appl. Chem.* **1953**, *3*, 433–444.
- (5) Chalmers, J. M.; Griffiths, P. R. Classical Methods of Quantitative Analysis. *Handbook of Vibrational Spectroscopy*; John Wiley & Sons, Ltd., 2002; 2251–2257.
- (6) *Dictionary of Organic Compounds*, sixth.; Chapman and Hall electronic publishing, 1996.
- (7) *CRC Handbook of Chemistry and Physics*, 97<sup>th</sup> ed.; Hayes, W. M., Ed.; CRC press: Boca Raton, 2016.
- (8) Stangel, M.; Moharregg-Khiabani, D.; Linker, R.; Gold, R. Fumarate in the Treatment of Multiple Sclerosis. *Neurologist* **2008**, *79* (2), 212–217.
- (9) Voet, D.; Voet, J. *Biochemistry*, 3rd ed.; John Wiley & Sons, Ltd.: New Jersey, 2004.
- (10) Bakhle, Y. S. Drugs of Today. *Drugs Today* **1999**, *35* (4-5), 237.
- (11) Vane, J.; Botting, R. . The Mechanism of Action of Aspirin. *Thromb. Res.* **2003**, *110* (5-6), 255–258.
- (12) Moller, C.; Plesset, M. S. Note on an Approximation Treatment for Many-Electron Systems. *Phys. Rev.* **1934**, *46* (7), 618–622.
- (13) Frisch, M. J.; Trucks, G. W.; Schlegel, H. B.; Scuseria, G. E.; Robb, M. a; Cheeseman, J. R.; Montgomery, J. a; Vreven, T.; Kudin, K. N.; Burant, J. C.; Millam, J. M.; Iyengar, S. S.; Tomasi, J.; Barone, V.; Mennucci, B.; Cossi, M.; Scalmani, G.; Rega, N.; Petersson, G. A.; Nakatsuji, H.; Hada, M.; Ehara, M.; Toyota, K.; Fukuda, R.;

Hasegawa, J.; Ishida, M.; Nakajima, T.; Honda, Y.; Kitao, O.; Nakai, H.; Klene, M.; Li, X.; Knox, J. e.; Hratchian, H. P.; Cross, J. B.; Bakken, V.; Adamo, C.; Jaramillo, J.; Gomperts, R.; Stratmann, R. E.; Yazyev, O.; Austin, A. J.; Cammi, R.; Pomelli, C.; Ochterski, J. W.; Ayala, P. K.; MoroKuma, K.; Voth, G. A.; Salvador, P.; Dannenberg, J. J.; Zakrzewski, V. G.; Dapprich, S.; Daniels, A. D.; Strain, M. C.; Farkas, O.; Malick, D. K.; Rabuck, A. D.; Raghavachari, K.; Foresman, J. B.; Ortiz, J. V.; Cui, Q.; Baboul, A. G.; Clifford, S.; Cioslowski, J.; Stefanov, B. B.; Liu, G.; Liashenko, A.; Piskorz, P.; Komaromi, I.; Martin, R. L.; Fox, D. J.; Keith, T.; Al-Laham, M. A.; Peng, C. Y.; Nanayakkara, A.; Challacombe, M.; Gill, P. M. W.; Johnson, B.; Chen, W.; Wong, M. W.; Gonzalez, C.; and Pople, J. A.; Gaussian 03, Revision D.01. Gaussian, Inc.: Wallingford CT **2004**.

- (14) Frisch, M. J.; Trucks, G. W.; Schlegel, H. B.; Scuseria, G. E.; Robb, M. A.; Cheeseman, J. R.; Montgomery, J. A.; Vreven, T.; Kudin, K. N.; Burant, J. C.; Millam, J. M.; Iyengar S. S.; Tomasi, J.; Barone, V.; Mennucci, B.; Cossi, M.; Scalmani, G.; Rega, N.; Petersson, G. A.; Nakatsuji, H.; Hada, M.; Ehara, M.; Toyota, K.; Fukuda, R.; Hasegawa, J.; Ishida, M.; Nakajima, T.; Honda, Y.; Kitao, O.; Nakai, H.; Klene, M.; Li, X.; Knox, J. e.; Hratchian, H. P.; Cross, J. B.; Bakken, V.; Adamo, C.; Jaramillo, J.; Gomperts, R.; Stratmann, R. E.; Yazyev, O.; Austin, A. J.; Cammi, R.; Pomelli, C.; Ochterski, J. W.; Ayala, P. K.; MoroKuma, K.; Voth, G. A.; Salvador, P.; Dannenberg, J. J.; Zakrzewski, V. G.; Dapprich, S.; Daniels, A. D.; Strain, M. C.; Farkas, O.; Malick, D. K.; Rabuck, A. D.; Raghavachari, K.; Foresman, J. B.; Ortiz, J. V.; Cui, Q.; Baboul, A. G.; Clifford, S.; Cioslowski, J.; Stefanov, B. B.; Liu, G.; Liashenko, A.; Piskorz, P.; Komaromi, I.; Martin, R. L.; Fox, D. J.; Keith, T.; Al-Laham, M. A.; Peng, C. Y.; Nanayakkara, A.; Challacombe, M.; Gill, P. M. W.; Johnson, B.; Chen, W.; Wong, M. W.; Gonzalez, C.; and Pople, J. A.; Gaussian 03, Revision C.02. Gaussian, Inc.: Wallingford CT **2003**.
- (15) Pulay, P. *Ab Initio* Calculation of Force Constants and Equilibrium Geometries in Polyatomic Molecules. *Mol. Phys.* **1969**, *17*, 197–204.
- (16) Frisch, M. J.; Yamaguchi, Y.; Gaw, J. F.; Schaefer, H. F.; Binkley, J. S. Analytic Raman Intensities from Molecular Electronic Wave Functions. *J. Chem. Phys.* **1986**, *84* (1), 531.
- (17) Amos, R. D. Calculation of Polarizability Derivatives Using Analytic Gradient Methods. *Chem. Phys. Lett.* **1986**, *124* (4), 376–381.
- (18) Polavarapu, P. L. *Ab Initio* Vibrational Raman and Raman Optical Activity Spectra. *J. Phys. Chem.* **1990**, *94* (21), 8106–8112.
- (19) Chantry, G. W. *The Raman Effect*; Anderson, A., Ed.; Marcel Dekker Inc: New York, 1971

- (20) Rasmussen, R. S. Vibrational Frequency of Assignments for Paraffin Hydrocarbons; Infra-Red Absorption Spectra of Butanes and Pentanes. *J. Chem. Phys.* **1948**, *16* (7), 712–722.
- (21) Axford, D. W. E.; D. H. Rank. Spectroscopic Studies of Rotational Isomerism. V. The Infra-Red Absorption Spectra of Six Solid Hydrocarbons in the Region 1600–650  $\text{cm}^{-1}$ . *J. Chem. Phys.* **1950**, *18*, 51–54.
- (22) Sheppard, N.; Szasz, G. J. Spectroscopic Studies of Rotational Isomerism. III. The Normal Paraffins in the Liquid and Solid States. *J. Chem. Phys.* **1949**, *17* (1), 86–92.
- (23) Szasz, G. J.; Sheppard, N. Spectroscopic Studies of Rotational Isomerism. IV. 2-Methyl Butane and 2,3-Dimethyl Butane. *J. Chem. Phys.* **1949**, *17* (1), 93–97.
- (24) Verma, A. L.; Murphy, W. F.; Bernstein, H. J. Rotational Isomerism. XI. Raman Spectra of N-Butane, 2-Methylbutane, and 2,3-Dimethylbutane. *J. Chem. Phys.* **1974**, *60* (4), 1540–1544.
- (25) Churchill, G. B.; Dombrowski, J. P.; Ma, L.; Swana, K.; Bohn, R. K.; Montgomery, J. A. Microwave Spectroscopy and Conformations of 2-Methylbutane and 2,3-Dimethylbutane. *J. Mol. Struct.* **2010**, *978*, 11–13.
- (26) Guirgis, G. A.; Zhu, X.; Yu, Z.; Durig, J. R. Raman and Infrared Spectra, Conformational Stability, Normal Coordinate Analysis, Vibrational Assignment, and *Ab Initio* Calculations of 3,3-Difluorobutene. *J. Phys. Chem. A* **2000**, *104* (19), 4383–4393.
- (27) Herrebout, W. A.; van der Veken, B. J. Solute-Solvent Interactions in Liquid Noble Gases As Probed by the Conformational Equilibrium of Some 1,2-Distributed Ethane. *J. Phys. Chem.* **1996**, *100*, 9671–9677.
- (28) Herrebout, W. A.; van der Veken, B. J.; Wang, A.; Durig, J. R. Enthalpy Difference between Conformers of N-Butane and the Potential Function Governing Conformational Interchange. *J. Phys. Chem.* **1995**, *99*, 578–585.
- (29) Bulanin, M. O. Spectroscopy of Molecules in Liquid Noble Gases. *J. Mol. Struct.* **1995**, *347*, 73–82.
- (30) Van der Veken, B. J.; R., D. M. F. An Infrared Study of Monomeric and Oligomeric (n=2,3, and 4) Hydrogen Chloride in Liquidified Noble Gases. *J. Chem. Phys.* **1992**, *97*, 3060.
- (31) Bulanin, M. O. Infrared Spectroscopy in Liquified Gases. *J. Mol. Struct.* **1973**, *19*, 59–79.

- (32) Van der Veken, B. J.; Herrebout, W. A.; Durig, D. T.; Zhao, W.; Durig, J. R. Conformational Stability of 3-Fluoropropene in Rare Gas Solutions from Temperature-Dependent FT-IR Spectra and *Ab Initio* Calculations. *J. Phys. Chem. A* **1999**, *103* (13), 1976–1985.
- (33) Durig, J. R.; Kar, W. N.; Zheng, C.; Shen, S. Comparison of *Ab Initio* MP2/6-311+G(d,p) Predicted Carbon-Hydrogen Bond Distances with Experimentally Determined  $r_0$  (C-H) Distances. *Struct. Chem.* **2004**, *15* (2), 149–157.
- (34) McKean, D. C. New Light on the Stretching Vibrations, Lengths and Strengths of CH, SiH and GeH Bonds. *J. Mol. Struct.* **1984**, *113*, 251–266.
- (35) Boyd, R. H. The Molecular Structures and Thermodynamics Functions of 2-Methylbutane and 2,3-Dimethylbutane. *J. Am. Chem. Soc.* **1975**, *97* (19), 5353–5357.
- (36) Guirgis, G. A.; Yu, Z.; Durig, J. R. Infrared and Raman Spectra, Conformational Stability, Barrier to Internal Rotation, and *Ab Initio* Calculations of 1,1-Difluoropropane. *J. Mol. Struct.* **1999**, *509* (1-3), 307–328.
- (37) Mohamed, T. A.; Stidham, H. D.; Guirgis, G. A.; Afifi, M. S.; Durig, J. R. Infrared and Raman Spectra, Conformational Stability, Barrier to Internal Rotation, and *Ab Initio* Calculations of 1,1-Dichloropropane. *J. Mol. Struct.* **1993**, *299*, 111–140.
- (38) Wurrey, C. J.; Shen, S.; Gounev, T. K.; Durig, J. R. Conformational Stability of Ethylcyclopropane from Raman Spectra, Temperature Dependent FT-IR Spectra of Xenon Solutions and *Ab Initio* Calculations. *J. Mol. Struct.* **1997**, *406* (3), 207–218.
- (39) Durig, J. R.; Zheng, C.; Guirgis, G. A.; Nanaie, H. Microwave Spectrum,  $r_0$  Structure, Barriers to Internal Rotation and *Ab Initio* Calculations of *Gauche*-1,1-Difluoropropane. *J. Mol. Struct.* **2005**, *742* (1-3), 191–198.
- (40) Cremer, D.; Binkley, J. S.; Pople, J. A. Molecular Orbital Theory of the Electronic Structure of Organic Compounds. 25. Conformations of Methyl- and Fluoro- Substituted Cyclopentanes and Cyclohexanes. *J. Am. Chem. Soc.* **1976**, *98* (22), 6838–6839.
- (41) Badawi, H. M.; Herrebout, W. A.; Zheng, C.; Mohamed, T. A.; Van Der Veken, B. J.; Durig, J. R. Conformational Stability from Variable-Temperature Infrared Spectra of Krypton Solutions, *Ab Initio* Calculations, and  $r_0$  Structural Parameters of Chlorocyclopentane. *Struct. Chem.* **2003**, *14* (6), 617–635.
- (42) Badawi, H. M.; Herrebout, W. A.; Mohamed, T. A.; Van der Veken, B. J.; Sullivand, J. F.; Durig, D. T.; Zheng, C.; Kalasinsky, K. S.; Durig, J. R. Conformational Stability from Variable Temperature Infrared Spectra of Krypton Solutions, *Ab Initio*

- Calculations, and Vibrational Assignment of Bromocyclopentane. *J. Mol. Struct.* **2003**, *645* (2-3), 89–107.
- (43) Durig, J. R.; El Defrawy, A. M.; Ganguly, A.; Gounev, T. K.; Guirgis, G. A. Conformational Stability  $r_0$  Structural Parameters, *Ab Initio* Calculations, and Vibrational Assignment for Fluorocyclopentane. *J. Phys. Chem. A* **2009**, *113* (35), 9675–9683.
- (44) Durig, J. R.; Klaassen, J. J.; Deodhar, B. S.; Darkhalil, I. D.; Herrebout, W. A.; Dom, J. J. J.; Van Der Veken, B. J.; Purohita, S. S.; Guirgis, G. A. Conformational and Structural Studies of Ethynylcyclopentane from Temperature Dependent Raman Spectra of Xenon Solutions, Infrared Spectra, and *Ab Initio* Calculations. *J. Mol. Struct.* **2013**, *1044*, 10–20.
- (45) Durig, J. R.; Klaassen, J. J.; Sawant, D. K.; Deodhar, B. S.; Panikar, S. S.; Gurusinghe, R. M.; Darkhalil, I. D.; Tubergen, M. J. Microwave, Structural, Conformational, Vibrational Studies and *Ab Initio* Calculations of Isocyanocyclopentane. *Spectrochim. Acta - Part A Mol. Biomol. Spectrosc.* **2015**, *136* (PA), 3–15.
- (46) Choe, J. I.; Harmony, M. D. Microwave Spectral Study of the Axial and Equatorial Conformers of Cyanocyclopentane. *J. Mol. Spectrosc.* **1980**, *81* (2), 480–493.
- (47) Durig, J. R.; Ward, R. M.; Ganguly, A.; El Defrawy, A. M.; Nelson, K. G.; Gounev, T. K.; Soliman, M. S.; Guirgis, G. A. Conformational Stability,  $r_0$  Structural Parameters, *Ab Initio* Calculations, and Vibrational Assignment for Cyanocyclopentane. *Vib. Spectrosc.* **2010**, *53* (1), 45–53.
- (48) Guirgis, G. A.; Zhu, X.; Yu, Z.; Durig, J. R. Raman and Infrared Spectra, Conformational Stability, Normal Coordinate Analysis, Vibrational Assignment, and *Ab Initio* Calculations of 3,3-Difluorobutene. *J. Phys. Chem. A* **2000**, *104* (19), 4383–4393.
- (49) Herrebout, W. A.; van der Veken, B. J.; Wang, A.; Durig, J. R. Enthalpy Difference between Conformers of n-Butane and the Potential Function Governing Conformational Interchange. *J. Phys. Chem. A* **1995**, *99* (2), 578–585.
- (50) Hilderbrandt, R. L.; Leavitt, H.; Shen, Q. The Structure and Pseudorotation of Cyanocyclopentane as Determined by Gas Phase Electron Diffraction. *J. Mol. Struct.* **1984**, *116* (1-2), 29–37.
- (51) Caminati, W.; Vogelsanger, B.; Meyer, R.; Grassi, G.; Bauder, A. Rotational Spectrum, Dipole Moment, and Ring-Puckering Potential of Cyclobutane-1,1- $d_2$ . *J. Mol. Spectrosc.* **1988**, *131* (1), 172–184.

- (52) Durig, J. R.; Ganguly, A.; Klaassen, J. J.; Guirgis, G. A. The  $r_0$  Structural Parameters, Conformational Stability, and Vibrational Assignment of Equatorial and Axial Cyanocyclobutane. *J. Mol. Struct.* **2009**, *923* (1-3), 28–38.
- (53) Durig, J. R.; Ward, R. M.; Conrad, A. R.; Tubergen, M. J.; Nelson, K. G.; Groner, P.; Gounev, T. K. Microwave, Raman, and Infrared Spectra,  $r_0$  Structural Parameters, Conformational Stability, and Vibrational Assignment of Cyanocyclohexane. *J. Mol. Struct.* **2010**, *967* (1-3), 99–111.
- (54) Sawant, D. K.; Klaassen, J. J.; Gounev, T. K.; Durig, J. R.  $r_0$  Structural Parameters, Conformational, Vibrational Studies and *Ab Initio* Calculations of Cyanocyclopentane. *Spectrochim. Acta Part A Mol. Biomol. Spectrosc.* **2015**, *151*, 468–479.
- (55) Kilpatrick, J. E.; Pitzer, K. S.; Spitzer, R. The Thermodynamics and Molecular Structure of Cyclopentane. *J. Am. Chem. Soc.* **1947**, *69* (10), 2483–2488.
- (56) Pitzer, K. S.; Donath, W. E. Conformations and Strain Energy of Cyclopentane and Its Derivatives. *J. Am. Chem. Soc.* **1959**, *81* (13), 3213–3218.
- (57) Ekejiuba, I. O. C.; Hallam, H. E. Spectroscopic Studies of Cyclopentyl Compounds-I. Infra-Red and Raman Spectra of Cyclopentyl Mono-Halides. *Spectrochim. Acta Part A Mol. Spectrosc.* **1970**, *26* (1), 59–66.
- (58) Ekejiuba, I. O. C.; Hallam, H. E. Spectroscopic Studies of Cyclopentyl Compounds-II. Conformational Isomerism and  $\nu(\text{C-Hal})$  Frequencies of Cyclopentyl Mono-Halides. *Spectrochim. Acta Part A Mol. Spectrosc.* **1970**, *26* (1), 67–75.
- (59) Wertz, D. W.; Shasky, W. E. Vibrational Spectra and Conformation of the Cyclopentyl Fluoride Ring. *J. Chem. Phys.* **1971**, *55* (4), 2422–2425.
- (60) Carreira, L. A. CNDO Calculation of the Pseudorotational Potential Energy of Fluorocyclopentane. *J. Chem. Phys.* **1971**, *55* (1), 181–185.
- (61) Suenram, R. D.; Grabow, J. U.; Zuban, A.; Leonov, I. A Portable, Pulsed-Molecular-Beam, Fourier-Transform Microwave Spectrometer Designed for Chemical Analysis. *Rev. Sci. Instrum.* **1999**, *70* (4), 2127–2135.
- (62) Suenram, R. D.; Lovas, F. J.; Plusquellic, D. F.; Lesarri, A.; Kawashima, Y.; Jensen, J. O.; Samuels, A. C. Fourier Transform Microwave Spectrum and *Ab Initio* Study of Dimethyl Methylphosphonate. *J. Mol. Spectrosc.* **2002**, *211* (1), 110–118.
- (63) Conrad, A. R.; Teumelsan, N. H.; Wang, P. E.; Tubergen, M. J. A Spectroscopic and Computational Investigation of the Conformational Structural Changes Induced by Hydrogen Bonding Networks in the Glycidol-Water Complex. *J. Phys. Chem. A* **2010**, *114* (1), 336–342.

- (64) Watson, J. K. G.; Durig, J. R. (Ed. . *Vibrational Spectra and Structure, Vol. 6*; Durig, J. R., Ed.; Elsevier scientific publishing Company, 1978: Amsterdam, The Netherlands, 1977.
- (65) Bulanin, M. O. Infrared Spectroscopy in Liquefied Gases. *J. Mol. Struct.* **1973**, *19* (C), 59–79.
- (66) Van Der Veken, B. J.; De Munck, F. R. An Infrared Study of Monomeric and Oligomeric (n=2, 3, and 4) Hydrogen Chloride in Liquefied Noble Gases. *J. Chem. Phys.* **1992**, *97* (5), 3060–3071.
- (67) Kessler, M.; Ring, H.; Trambarulo, R.; Gordy, W. Microwave Spectra and Molecular Structures of Methyl Cyanide and Methyl Isocyanide. *Phys. Rev.* **1950**, *79* (1), 54–56.
- (68) Chang, T.; Harmony, M. D.; Staley, S. W. Microwave Spectrum and Molecular Structure of Vinyl Isocyanide: Experimental and Theoretical Evaluation of Conjugation. *J. Mol. Struct.* **1988**, *190* (C), 17–29.
- (69) Kruger, M.; Dreizler, H.; Pregschat, D.; Lentz, D. Synthesis and Structure of Ethynyl Isocyanide. *Angew. Chem. Int. Ed. Engl.* **1991**, *30*, 1644–1646.
- (70) Taylor, W. H.; Harmony, M. D.; Cassada, D. A.; Staley, S. W. Microwave Spectrum, Structure, and  $\Pi$  Conjugation of Isocyanocyclopropane. *J. Chem. Phys.* **1984**, *81* (12), 5379–5383.
- (71) Adams, W. J.; Geise, H. J.; Bartell, L. S. Structure, Equilibrium Conformation, and Pseudorotation in Cyclopentane. An Electron Diffraction Study. *J. Am. Chem. Soc.* **1970**, *92* (17), 5013–5019.
- (72) Mohamed, T. A.; Guirgis, G. A.; Nashed, Y. E.; Durig, J. R. Spectra and Structure of Silicon-Containing Compounds. XXV. Raman and Infrared Spectra,  $r_0$  Structural Parameters, Vibrational Assignment, and *Ab Initio* Calculations of Ethyl Chlorosilane-Si- $d_2$ . *Struct. Chem.* **1999**, *10* (5), 333–348.
- (73) Durig, J. R.; Nashed, Y. E.; Tao, J.; Guirgis, G. A. Conformational and Structural Studies of Ethyl Fluorosilane from Temperature Dependent FT-IR Spectra of Krypton Solutions and *Ab Initio* Calculations. *J. Mol. Struct.* **2001**, *560* (1-3), 39–55.
- (74) Guirgis, G. A.; Nashed, Y. E.; Tao, J.; Powell, D. L.; Gruodis, A.; Aleksa, V.; Nielsen, C. J.; Klaeboe, P.; Durig, J. R. Spectra and Structure of Silicon Containing Compounds. XXXI. Raman and Infrared Spectra, Conformational Stability, *Ab Initio* Calculations, and Vibrational Assignment of Ethyl Bromosilane and Ethyl Bromosilane-Si- $d_2$ . *J. Mol. Struct.* **2002**, *641* (2-3), 125–146.

- (75) Panikar, S. S.; Guirgis, G. A.; Eddens, M. T.; Dukes, H. W.; Conrad, A. R.; Tubergen, M. J.; Gounev, T. K.; Durig, J. R. Microwave, Infrared and Raman Spectra, Adjusted  $r_0$  Structural Parameters, Conformational Stability, and Vibrational Assignment of Cyclopropylfluorosilane. *Chem. Phys.* **2013**, *415*, 124–132.
- (76) Gounev, T. K.; Weston, J. W.; Shen, S.; Dakkouri, M.; Grunvogel-Hurst, A.; Durig, J. R. Infrared and Raman Spectra, Conformational Stability, *Ab Initio* Calculations, and Vibrational Assignments for Cyclopropylchlorosilane. *J. Phys. Chem. A* **1997**, *101* (46), 8614–8624.
- (77) Guirgis, G. A.; Pan, C.; Bragg, J.; Durig, J. R. Spectra and Structure of Silicon Containing Compounds. XLI. Infrared and Raman Spectra, Conformational Stability, Vibrational Assignment and *Ab Initio* Calculations of Cyclopropylbromosilane. *J. Mol. Struct.* **2003**, *657* (1-3), 239–254.
- (78) Durig, J. R.; Panikar, S. S.; Guirgis, G. A.; Gounev, T. K.; Ward, R. M.; Peebles, R. A.; Peebles, S. A.; Liberatore, R. J.; Bell, S.; Wurrey, C. J. Conformational Stability,  $r_0$  Structural Parameters, Barriers to Internal Rotation, Vibrational Spectra and *Ab Initio* Calculations of *c*-C<sub>3</sub>H<sub>5</sub>SiH<sub>2</sub>CH<sub>3</sub>. *J. Mol. Struct.* **2009**, *923* (1-3), 1–12.
- (79) Simmons, H. E.; Smith, R. D. A New Synthesis of Cyclopropanes<sup>1</sup>. *J. Am. Chem. Soc.* **1959**, *81* (16), 4256–4264.
- (80) Brown, G. G.; Dian, B. C.; Douglass, K. O.; Geyer, S. M.; Shipman, S. T.; Pate, B. H. A Broadband Fourier Transform Microwave Spectrometer Based on Chirped Pulse Excitation. *Rev. Sci. Instrum.* **2008**, *79* (5), 053103.
- (81) Pérez, C.; Lobsiger, S.; Seifert, N. A.; Zaleski, D. P.; Temelso, B.; Shields, G. C.; Kisiel, Z.; Pate, B. H. Broadband Fourier Transform Rotational Spectroscopy for Structure Determination: The Water Heptamer. *Chem. Phys. Lett.* **2013**, *571*, 1–15.
- (82) Frisch, M. J.; Trucks, G. W.; Schlegel, H. B.; Scuseria, G. E.; Robb, M. A.; Cheeseman, J. R.; Scalmani, G.; Barone, V.; Mennucci, B.; Petersson, G. A.; Nakatsuji, H.; Caricato, M.; Li, X.; Hratchian, H. P.; Izmaylov, A. F.; Bloino, J.; Zheng, G.; Sonnenberg, J. L.; Hada, M.; Ehara, M.; Toyota, K.; Fukuda, R.; Hasegawa, J.; Ishida, M.; Nakajima, T.; Honda, Y.; Kitao, O.; Nakai, H.; Vreven, T.; Montgomery, J. A., Jr.; Peralta, J. E.; Ogliaro, F.; Bearpark, M.; Heyd, J. J.; Brothers, E.; Kudin, K. N.; Staroverov, V. N.; Kobayashi, R.; Normand, J.; Raghavachari, K.; Rendell, A.; Burant, J. C.; Iyengar, S. S.; Tomasi, J.; Cossi, M.; Rega, N.; Millam, J. M.; Klene, M.; Knox, J. E.; Cross, J. B.; Bakken, V.; Adamo, C.; Jaramillo, J.; Gomperts, R.; Stratmann, R. E.; Yazyev, O.; Austin, A. J.; Cammi, R.; Pomelli, C.; Ochterski, J. W.; Martin, R. L.; Morokuma, K.; Zakrzewski, V. G.; Voth, G. A.; Salvador, P.; Dannenberg, J. J.; Dapprich, S.; Daniels, A. D.; Farkas, Ö.; Foresman, J. B.; Ortiz, J. V.; Cioslowski, J.; Fox, D. J. *Gaussian 09*, Gaussian, Inc., Wallingford CT, **2009**.

- (83) Pickett, H. M. The Fitting and Prediction of Vibration-Rotation Spectra with Spin Interactions. *J. Mol. Spectrosc.* **1991**, *148* (2), 371–377.
- (84) Seifert, N. A.; Finneran, I. A.; Perez, C.; Zaleski, D. P.; Neill, J. L.; Steber, A. L.; Suenram, R. D.; Lesarri, A.; Shipman, S. T.; Pate, B. H. AUTOFIT, an Automated Fitting Tool for Broadband Rotational Spectra, and Applications to 1-Hexanal. *J. Mol. Spectrosc.* **2015**, *312*, 13–21.
- (85) Kisiel, Z.; Pszczółkowski, L.; Medvedev, I. R.; Winnewisser, M.; De Lucia, F. C.; Herbst, E. Rotational Spectrum of *Trans-Trans* Diethyl Ether in the Ground and Three Excited Vibrational States. *J. Mol. Spectrosc.* **2005**, *233* (2), 231–243.
- (86) Kraitchman, J. Determination of Molecular Structure from Microwave Spectroscopic Data. *Am. J. Phys.* **1953**, *21* (1), 17.
- (87) Kisiel, Z. PROSPE – Programs for ROtational SPEctroscopy  
<http://www.ifpan.edu.pl/~kisiel/prospe.htm>.
- (88) Costain, C. C.; Bradley, W. F. (Ed); Hanson, H. P. (Ed). Machine Interpretations of Patterson Functions and Alternative Direct Approaches and The Austin Symposium on Gas Phase Molecular Structure. In *Trans. Am. Crystallogr. Assoc.*; 1966; p 157.
- (89) Pitzer, K. S.; Gwinn, W. D. Thermodynamic Functions for Molecules with Internal Rotation. *J. Chem. Phys.* **1941**, *9* (6), 485.
- (90) Duncan, J. L.; Harvie, J. L.; McKean, D. C.; Cradock, S. The Ground State Structures of Disilane, Methyl Silane and the Silyl Halides, and an SiH Bond Length Correlation with Stretching Frequency. *J. Mol. Struct.* **1986**, *145* (3-4), 225–242.
- (91) Durig, J. R.; Pan, C.; Guirgis, G. A. Spectra and Structure of Silicon Containing Compounds. XXXII. Raman and Infrared Spectra, Conformational Stability, Vibrational Assignment and *Ab Initio* Calculations of N-Propylsilane-d<sub>0</sub> and Si-d<sub>3</sub>. *Spectrochim. Acta - Part A Mol. Biomol. Spectrosc.* **2003**, *59* (5), 979–1002.
- (92) Durig, J. R.; Pan, C.; Guirgis, G. A. Spectra and Structure of Silicon Containing Compounds. XLII. Conformational Stability, *Ab Initio* Calculations, r<sub>0</sub> Structural Parameters, and Vibrational Assignments for Ethylmethylsilane and Ethylmethylsilane-Si-d<sub>2</sub>. *J. Mol. Struct.* **2004**, *688* (1-3), 95–109.
- (93) Pauling, L. N. *The Nature of The Chemical Bond*, Third.; Cornell University: Ithaca, NY, USA, 1960.
- (94) Wurrey, C. J.; Shen, S.; Zhu, X.; Zhen, H.; Durig, J. R. Conformational Studies of Cyanomethylcyclopropane from Temperature-Dependent FT-IR Spectra of Xenon Solutions and *Ab Initio* calculations<sup>1</sup>. *J. Mol. Struct.* **1998**, *449* (2–3), 203–217.

- (95) Durig, J. R.; Guirgis, G. A.; Sawant, D. K.; Seifert, N. A.; Deodhar, B. S.; Pate, B. H.; Panikar, S. S.; Groner, P.; Overby, J. S.; Askarian, S. M. Microwave,  $r_0$  Structural Parameters, Conformational Stability and Vibrational Assignment of Cyclopropylcyanosilane. *Chem. Phys.* **2014**, *445*, 68–81.
- (96) Stølevik, R.; Bakken, P. Conformational Structures, Energies, Rotational Barrier Heights and Torsional Force Constants in Halogenated Methyl-Silanes Obtained by Molecular-Mechanics Calculations. *J. Mol. Struct. {THEOCHEM}* **1985**, *124* (3–4), 335–341.
- (97) Bhonoah, B.; Ghoorun, A.; Abdallah, H. H.; Ramasami, P. Theoretical Study of the *Gauche* and *Trans* Conformers of  $\text{SiH}_2\text{X}-\text{CH}_2\text{X}$ ,  $\text{SiH}_2\text{F}-\text{CH}_2\text{Y}$ , and  $\text{SiH}_2\text{Y}-\text{CH}_2\text{F}$  (X = F, Cl, Br, I and Y = Cl, Br, I) in the Gas and Solution Phases. *J. Solution Chem.* **2011**, *40* (3), 430–446.
- (98) Guirgis, G. A.; Pan, C.; Shen, S.; Durig, J. R. Conformational Stability of Chloromethyl Silyl Chloride from Temperature-Dependent FT-IR Spectra of Krypton Solutions. *Struct. Chem.* **2001**, *12* (6), 445–458.
- (99) Guirgis, G. A.; Pan, C.; Durig, J. R. Spectra and Structure of Silicon-Containing Compounds. XXXIII — Raman and Infrared Spectra, Conformational Stability and Vibrational Assignment of Chloromethylsilyl Bromide. *J. Raman Spectrosc.* **2002**, *33* (9), 677–688.
- (100) Guirgis, G. A.; Pan, C.; Shen, S.; Durig, J. R. Variable Temperature FT-IR of Krypton Solutions and *Ab Initio* Calculations of  $\text{ClCH}_2\text{SiH}_2\text{X}$  (X=F, Cl, Br). *Asian J. Spectrosc.* **2001**, *5*, 113–122.
- (101) Brown, G. G.; Dian, B. C.; Douglass, K. O.; Geyer, S. M.; Shipman, S. T.; Pate, B. H. A Broadband Fourier Transform Microwave Spectrometer Based on Chirped Pulse Excitation. *Rev. Sci. Instrum.* **2008**, *79* (5), 1–14.
- (102) Pérez, C.; Lobsiger, S.; Seifert, N. A.; Zaleski, D. P.; Temelso, B.; Shields, G. C.; Kisiel, Z.; Pate, B. H. Broadband Fourier Transform Rotational Spectroscopy for Structure Determination: The Water Heptamer. *Chem. Phys. Lett.* **2013**, *571*, 1–15.
- (103) Herrebout, W. A.; Nagels, N.; van der Veken, B. J. On the  $\nu_1 \text{CO}_2/2\nu_2 \text{CO}_2$  Resonance in the Complex of Carbon Dioxide with Dimethyl Ether. *ChemPhysChem* **2009**, *10* (17), 3054–3060.
- (104) Michielsen, B.; Dom, J. J. J.; Veken, B. J. van der; Hesse, S.; Xue, Z.; Suhm, M. A.; Herrebout, W. A. The Complexes of Halothane with Benzene: The Temperature Dependent Direction of the Complexation Shift of the Aliphatic C–H Stretching. *Phys. Chem. Chem. Phys.* **2010**, *12* (42), 14034–14044.

- (105) Guirgis, G. A.; Panikar, S. S.; El Defrawy, A. M.; Kalasinsky, V. F.; Durig, J. R. Vibrational Spectra,  $r_0$  Structural Parameters, Barriers to Internal Rotation, and *Ab Initio* Calculations of  $\text{ClCH}_2\text{SiH}_3$ ,  $\text{Cl}_2\text{CHSiH}_3$ ,  $\text{ClCH}_2\text{SiF}_3$ , and  $\text{Cl}_2\text{CHSiF}_3$ . *J. Mol. Struct.* **2009**, 922 (1-3), 93–102.
- (106) Guirgis, G. A.; Sawant, D. K.; Brenner, R. E.; Deodhar, B. S.; Seifert, N. A.; Geboes, Y.; Pate, B. H.; Herrebout, W. A.; Hickman, D. V.; Durig, J. R. Microwave,  $r_0$  Structural Parameters, Conformational Stability, and Vibrational Assignment of (Chloromethyl)fluorosilane. *J. Phys. Chem. A* **2015**, 119 (47), 11532–11547.
- (107) Millich, F. Polyisocyanides. *J. Polym. Sci. Macromol. Rev.* **1980**, 15, 207–253.
- (108) Mata, S.; Peña, I.; Cabezas, C.; López, J. C.; Alonso, J. L. A Broadband Fourier-Transform Microwave Spectrometer with Laser Ablation Source: The Rotational Spectrum of Nicotinic Acid. *J. Mol. Spectrosc.* **2012**, 280, 91–96.
- (109) Lesarri, A.; Mata, S.; Lopez, J. C.; Alonso, J. L. A Laser-Ablation Molecular-Beam Fourier-Transform Microwave Spectrometer: The Rotational Spectrum of Organic Solids. *Rev. Sci. Instrum.* **2003**, 74, 4799.
- (110) Kawaguchi, K.; Sanechika, N.; Nishimura, Y.; Fujimori, R.; Oka, T. N.; Hirahara, Y.; Jaman, A. I.; Civiš, S. Time-Resolved Fourier Transform Infrared Emission Spectroscopy of Laser Ablation Products. *Chem. Phys. Lett.* **2008**, 463 (1–3), 38–41.

## VITA

Dattatray Kisan Sawant was born on July 07, 1983 in Pune, India to Kisan and Sunanda Sawant. He was educated at the M. H. High School in Thane and graduated from high school in 2000. He was admitted to the University Department of Chemical Technology in Mumbai, and he graduated in 2004 with a Bachelor of Technology (B.Tech.) degree in Technology of Intermediates and Dyes. After earning his bachelor's degree in Dyes, he decided to pursue a career in Research and Development (R&D), and began his career as an R&D chemist, where his job responsibilities included designing and developing syntheses and analytical methods for organic compounds. His desire to pursue innovative research brought him to the University of Kentucky in 2008 where he graduated with a Master of Science degree in Chemistry (non-thesis) in 2010.

Dattatray joined the Department of Chemistry at the University of Missouri-Kansas City in the Fall of 2011 for the interdisciplinary Ph.D. program. He has been working in the field of molecular spectroscopy with Prof. James R. Durig. In 2014, he received the Fong Wu Cheng scholarship for excellence in graduate research. He began publishing soon after joining the Durig group, and during the course of his Ph.D, he has co-authored the following peer-reviewed journal publications:

- Sawant, D. K.; Klaassen, J. J.; Gounev, T. K.; Durig, J. R.  $r_0$  Structural Parameters, Conformational, Vibrational Studies and *Ab Initio* Calculations of Cyanocyclopentane. *Spectrochim. Acta Part A Mol. Biomol. Spectrosc.* **2015**, *151*, 468–479.
- Sawant, D. K.; Klaassen, J. J.; Panikar, S. S.; Durig, J. R. Infrared and Raman Spectra, Adjusted  $r_0$  Structural Parameters, and Vibrational Assignment of Isopropyl Isocyanide. *J. Mol. Struct.* **2014**, *1073* (Supplement C), 112–118.

- Guirgis, G. A.; Sawant, D. K.; Brenner, R. E.; Deodhar, B. S.; Seifert, N. A.; Geboes, Y.; Pate, B. H.; Herrebout, W. A.; Hickman, D. V.; Durig, J. R. Microwave,  $r_0$  Structural Parameters, Conformational Stability, and Vibrational Assignment of (Chloromethyl)fluorosilane. *J. Phys. Chem. A* **2015**, *119* (47), 11532–11547.
- Durig, J. R.; Guirgis, G. A.; Sawant, D. K.; Seifert, N. A.; Deodhar, B. S.; Pate, B. H.; Panikar, S. S.; Groner, P.; Overby, J. S.; Askarian, S. M. Microwave,  $r_0$  Structural Parameters, Conformational Stability and Vibrational Assignment of Cyclopropylcyanosilane. *Chem. Phys.* **2014**, *445*, 68–81.
- Durig, J. R.; Klaassen, J. J.; Sawant, D. K.; Deodhar, B. S.; Panikar, S. S.; Gurusinghe, R. M.; Darkhalil, I. D.; Tubergen, M. J. Microwave, Structural, Conformational, Vibrational Studies and *Ab Initio* Calculations of Isocyanocyclopentane. *Spectrochim. Acta - Part A Mol. Biomol. Spectrosc.* **2015**, *136* (PA), 3–15.
- Panikar, S. S.; Deodhar, B. S.; Sawant, D. K.; Klaassen, J. J.; Deng, J.; Durig, J. R. Raman and Infrared Spectra,  $r_0$  Structural Parameters, and Vibrational Assignments of  $(\text{CH}_3)_2\text{PX}$  Where X=H, CN, and Cl. *Spectrochim. Acta Part A Mol. Biomol. Spectrosc.* **2013**, *103* (Supplement C), 205–215.
- Guirgis, G. A.; Klaassen, J. J.; Deodhar, B. S.; Sawant, D. K.; Panikar, S. S.; Dukes, H. W.; Wyatt, J. K.; Durig, J. R. Structure and Conformation Studies from Temperature Dependent Infrared Spectra of Xenon Solutions and *Ab Initio* Calculations of Cyclobutylgermane. *Spectrochim. Acta Part A Mol. Biomol. Spectrosc.* **2012**, *99* (Supplement C), 266–278.
- Deodhar, B. S.; Brenner, R. E.; Sawant, D. K.; Guirgis, G. A.; Geboes, Y.; Herrebout, W. A.; Durig, J. R. Vibrational Assignments and Conformer Stability Determination of Cyclobutyldichlorosilane by Variable Temperature Raman Spectra in Krypton Solution. *Vib. Spectrosc.* **2015**, *81* (Supplement C), 119–130.